LEVEL II

(12)

AD

Technical Memorandum 8-81

EXPERIMENTAL QUIET SPROCKET DESIGN AND NOISE REDUCTION IN TRACKED VEHICLES

Stephen A. Hammond
Curtis A. Aspelund
David C. Rennison
Thomas R. Norris
Georges R. Garinther

DTIC
ELECTE
AUG 14 1981
S
E

April 1981
AMCMS Code 612716.H700011
(Contract DAAK11-78-C-0131)

Approved for public release;
distribution unlimited.

AD A102842

DTIC FILE COPY

U. S. ARMY HUMAN ENGINEERING LABORATORY
Aberdeen Proving Ground, Maryland

81 8 14 056

Destroy this report when no longer needed.
Do not return it to the originator.

The findings in this report are not to be construed as an official Department of the Army position unless so designated by other authorized documents.

Use of trade names in this report does not constitute an official endorsement or approval of the use of such commercial products.

18 HEL

SECURITY CLASSIFICATION OF THIS PAGE *(When Data Entered)*

REPORT DOCUMENTATION PAGE

READ INSTRUCTIONS
BEFORE COMPLETING FORM

1. REPORT NUMBER: Technical Memorandum 8-81 (18) TM-
2. GOVT ACCESSION NO.: AD-A102 840
3. RECIPIENT'S CATALOG NUMBER:
4. TITLE *(and Subtitle)*: EXPERIMENTAL QUIET SPROCKET DESIGN AND NOISE REDUCTION IN TRACKED VEHICLES (9)
5. TYPE OF REPORT & PERIOD COVERED: Final rept.
6. PERFORMING ORG. REPORT NUMBER:
7. AUTHOR(s): (10)
Stephen A. Hammond
Curtis A. Aspelund
David C. Rennison
Thomas R. Norris
Georges R. Carinther
8. CONTRACT OR GRANT NUMBER(s): (15) DAAK11-78-C-0131
9. PERFORMING ORGANIZATION NAME AND ADDRESS:
FMC Corporation, Ordnance Engineering Division,
1105 Coleman Avenue, San Jose, CA 95108
10. PROGRAM ELEMENT, PROJECT, TASK AREA & WORK UNIT NUMBERS: AMCMS Code 612716.H700011
11. CONTROLLING OFFICE NAME AND ADDRESS:
US Army Human Engineering Laboratory
Aberdeen Proving Ground, MD 21005
12. REPORT DATE: (11) April 1981
13. NUMBER OF PAGES: 240
14. MONITORING AGENCY NAME & ADDRESS *(if different from Controlling Office)*: (12) 243
15. SECURITY CLASS. *(of this report)*: UNCLASSIFIED
15a. DECLASSIFICATION/DOWNGRADING SCHEDULE:
16. DISTRIBUTION STATEMENT *(of this Report)*:
Approved for public release; distribution unlimited.
17. DISTRIBUTION STATEMENT *(of the abstract entered in Block 20, if different from Report)*:
18. SUPPLEMENTARY NOTES:
19. KEY WORDS *(Continue on reverse side if necessary and identify by block number)*:

Tracked Vehicles
Noise Reduction
Mechanical Impedance Measurement
Noise Sources
Track and Suspension
Statistical Energy Analysis
Finite Element Modal Analysis

20. ABSTRACT *(Continue on reverse side if necessary and identify by block number)*

The noise produced by track-laying vehicles has historically been a problem in the US Army. Exterior noise provides enemy forces with a means of detection at great distances. Interior vehicle noise prevents accurate person-to-person or electrically-aided communication and is responsible for excessive hearing loss among exposed personnel.

This program provides the Army with advanced technology to reduce tracked-vehicle noise. The goals established were a 15 dB(A) reduction in interior

(Contined)

DD FORM 1 JAN 73 1473 EDITION OF 1 NOV 65 IS OBSOLETE

SECURITY CLASSIFICATION OF THIS PAGE *(When Data Entered)*

[illegible]

20. ABSTRACT (Continued)

noise to a level meeting the 100dB(A) limit of MIL-STD-1474B, and a 6 dB reduction in exterior noise, representing a 50% reduction in detection range.

The work presently being reported, which is the third phase of the program, involved the design and fabrication of a high compliance prototype idler and a high compliance experimental sprocket. The idler provided a reduction of 15 dB(A) of idler-contributed noise and the sprocket provided approximately 10 dB(A) of sprocket-contributed noise.

This report provides a comparison of the hull dynamics of the M113A1 and the AIFV in order to determine the reason for the significantly lower noise level of the AIFV.

A preliminary finite element analysis was made to determine if this technique could be used to predict the dynamic response of the hull with the ultimate aim of providing a method of predicting hull configuration to achieve significant noise reduction.

AMCMS Code 612716.H700011

Technical Memorandum 8-81

EXPERIMENTAL QUIET SPROCKET DESIGN AND NOISE REDUCTION IN TRACKED VEHICLES

Stephen A. Hammond[a]
Curtis A. Aspelund[a]
David C. Rennison[b]
Thomas R. Norris[c]
Georges R. Garinther

Accession For
NTIS GRA&I ☒
DTIC TAB ☐
Unannounced ☐
Justification

By
Distribution/
Availability Codes

Dist	Avail and/or Special
A	

April 1981

APPROVED: John Weisz
JOHN D. WEISZ
Director
U.S. Army Human Engineering Laboratory

[a]FMC Corporation
[b]Bolt Beranek & Newman Inc.
[c]Consultants in Engineering Acoustics

U. S. ARMY HUMAN ENGINEERING LABORATORY
Aberdeen Proving Ground, Maryland 21005

Approved for public release;
distribution unlimited.

CONTENTS

Page No

1. EXECUTIVE SUMMARY 1

2. OBJECTIVES AND GOALS. 5

3. DISCUSSION OF TRACKED VEHICLE INTERIOR NOISE. 3

- 3.1 General Discussion 3
- 3.2 M113A1 Interior Noise Levels 13

4. EXPERIMENTAL COMPARISON OF THE HULL DYNAMICS OF THE AIFV AND M113A1 VEHICLES 13

- 4.1 Conceptual Approach. 13
- 4.2 Vehicle Structural Characteristics 14
- 4.3 Power Flow Analysis. 21
  - 4.3.1 Review of Concepts. 21
  - 4.3.2 Measured Results. 23
    - 4.3.2.1 Hull Vibration Levels. 23
    - 4.3.2.2 Interior Noise Levels. 23
    - 4.3.2.3 Hull Radiation Efficiencies. 28
    - 4.3.2.4 Structural and Acoustic Loss Factor Data 28
    - 4.3.2.5 Power Flow Calculations. 35
  - 4.3.3 Discussion. 37
- 4.4 Hull Attachment Point Transfer Function Analysis 40
  - 4.4.1 General 40
  - 4.4.2 Noise-to-Force Transfer Functions 40
  - 4.4.3 Hull Inertance Transfer Functions 42
    - 4.4.3.1 Left/Right Asymmetries - AIFV. 42
    - 4.4.3.2 Left/Right Asymmetries - M113A1. 49
    - 4.4.3.3 Effect of the AIFV Turret. 49
    - 4.4.3.4 AIFV/M113A1 Comparisons. 56
  - 4.4.4 Discussion. 56

5. FINITE ELEMENT MODAL ANALYSIS OF AN M113A1 VEHICLE. 63

- 5.1 General. 63
- 5.2 Summary of Equations for Generalized Structural Vibration Response and Interior Acoustic Power Radiation 64
- 5.3 Modeling Procedure 65
- 5.4 Results. 67
  - 5.4.1 Initial Model Configuration 67
  - 5.4.2 Revised Hull Dynamic Model. 90
  - 5.4.3 Frequency and Space-Averaged Calculations 101
- 5.5 Discussion and Recommendations 109

6. PROTOTYPE COMPLIANT IDLER WHEEL DEVELOPMENT 110

- 6.1 Background 110
- 6.2 Experimental Idler Wheel 110
  - 6.2.1 Conceptual Approach 110
  - 6.2.2 Test Results 111

PRECEDING PAGE BLANK-NOT FILMED

6.2.2.1 Compliance 111
6.2.2.2 Interior Noise Reduction of the Experimental Idler Wheel. 115
6.2.2.3 Exterior Noise Reduction of the Experimental Idler Wheel. 115
6.2.2.4 Durability of the Experimental Idler Wheel 118
6.2.3 Further Investigations with the Experimental Idler Wheel. . 120
6.2.3.1 Sources of Rapid Noise Level Variations. 120
6.2.3.2 Shape of Experimental Idler Paddle Contact Surfaces 127
6.2.3.3 Effects of Combined Axial and Radial Compliance Changes. 127
6.2.3.4 Track Guide Scrub Noise. 131
6.2.3.5 Increased Diameter Idler 131
6.3 Prototype Idler Wheel. 134
6.3.1 Design Goals. 134
6.3.2 Design Criteria 134
6.3.3 Design Concepts 138
6.3.3.1 Sectional Idler Rim. 138
6.3.3.2 Thin Flexible Rim/Rubber in Compression 138
6.3.3.3 Thick Rigid Rim/Rubber in Compression 140
6.3.3.4 Rim of Rollers 140
6.3.3.5 Rigid Rim/Rubber-in-Shear 140
6.3.4 Results 143
6.3.4.1 Compliance 144
6.3.4.2 Interior Noise Reduction 144
6.3.4.3 Exterior Noise Reduction 144
6.3.4.4 Durability 148
6.3.4.5. Conclusions and Recommendations. 149

7. EXPERIMENTAL SPROCKET CARRIER DEVELOPMENT 149

7.1 Conceptual Approach. 149
7.2 Design Goals 150
7.3 Design Criteria. 150
7.4 Design Concepts. 151
7.4.1 Rubber in Radial Compression and Torsional Shear. 151
7.4.1.1 Solid Pair of Rubber Rings 152
7.4.1.2 Directionally Modified Compliance. 152
7.4.1.3 Three Concentric Ring Pairs. 154
7.4.1.4 Rubber in Radial Compression and Radial Shear. . . 154
7.4.2 Compliant Fabric Isolator 154
7.4.3 Overload Gear with Rubber Separators in Compression 158
7.4.4 Rubber in Shear 158
7.4.4.1 Single and Double Pairs of Annuli. 158
7.4.4.2 Triple Annuli Pairs. 161
7.5 Results. 161
7.5.1 Compliance. 161
7.5.2 Interior Noise Reduction of the Experimental Sprocket . . . 161
7.5.3 Exterior Noise Signature at the Experimental Sprocket . . . 164
7.5.4 Experimental Sprocket Clatter 164
7.5.5 Durability. 172
7.6 Recommendations. 174
References. 175

Appendices

A. Theory for Hull Vibrational Response and Interior Sound Levels. . . . 177
B. STARDYNE Input and Output Data for Original Hull Model. 189
C. STARDYNE Input and Output Data for Revised Hull Model 208

Figures

3.1 Schematic Diagram of Sources and Paths Responsible for Interior Noise in Tracked Vehicles 9

3.2 Noise Source Spectra at 15 mph At Center of Crew Compartment . . 10

3.3 Noise Source Spectra at 25 mph At Center of Crew Compartment . . 10

3.4 Noise Source Spectra at 32 mph At Center of Crew Compartment . . 11

3.5 Track System Source Contributions to M113A1 Crew Area Noise Levels At Various Speeds 11

3.6 Speed Dependence of Production M113A1 Noise At the Crew Position Operating On Paved Track 12

4.1 Comparison of Hull Vertical Sections, Taken Along Vehicle Length 15

4.2 Comparison of AIFV/M113A1 Hull Details -- Rear View. 16

4.3 Hull Section Views, Looking Forward. 17

4.4 Comparison of Horizontal Sections of Vehicles, Above Sponsons. . 18

4.5 Comparison of Left and Right Idler Pads for AIFV 19

4.6 Comparison of Left Idler Pad for AIFV and M113 20

4.7 Comparison of Hull Acceleration Levels on Left and Right Hand Sides of Tracked Vehicles at 32 km/hr (20 mph): (a) AIFV # SJ005, (b) M113A1 (on blocks [16]) 25

4.8 Comparison of Acceleration Levels on Similar Hull Surfaces on AIFV and M113A1 Tracked Vehicles Underway at 32 km/hr (20 mph) . 26

4.9 Dependence of A-Weighted Interior Sound Level on Vehicle Speed for the Vehicles Tested 27

4.10 Crew Position Interior Sound Level Spectra for Underway AIFV Vehicles at 32 km/hr (20 mph) 29

4.11 Interior Sound Level Spectra, AIFV NSJ0005, Showing the Effect of Forward Speed 30

4.12 Effect of Forward Speed on Interior Sound Level Spectra for AIFV NSJ0002 31

4.13 Calculated Radiation Efficiencies for Typical Hull Panels. . . . 32

4.14 Structural Loss Factor Data for AIFV (NSJ0005) 33

Figures (cont.)

4.15 Structural Loss Factor Data for M113A1 (SJ136). 34

4.16 Comparison of Hull Dissipated (L_{wd}), Hull Radiated (L_{wr}), and Acoustic Dissipated (L_{wa}) Power Levels; AIFV (NSJ0005) at 32 km/hr (20 mph), Test Track Data 36

4.17(a) Major Contributors to the Hull Radiated Power Levels; AIFV (NSJ0005) at 32 km/hr (20 mph), Test Track Data. 38

4.17(b) Major Contributors to the Hull Radiated Power Levels, M113A1 Vehicle at 32 km/hr (20 mph) supported on Jackstands. 39

4.18 Instrumentation for Hull Inertance and Transfer Function Measurements. 41

4.19 Noise-to-Force Transfer Functions for Horizontal Excitation of Idler Spindle (a) AIFV, (b) M113A1. 43

4.20 Noise-to-Force Transfer function for Vertical Excitation of Idler Spindle (a) AIFV, (b) M113A1. 44

4.21 Noise-to-Force Transfer Functions for (a) Vertical and (b) Horizontal Excitation of Idler Spindles (Average of Left and Right Idlers Presented; 50N Pink Noise Force Input) 45

4.22 Comparison of Left - and Right-side Horizontal Inertances on AIFV Idler Spindles (Turret on Vehicle) 46

4.23 Comparison of Left - and Right-side Vertical Inertances on AIFV Idler Spindles (Turret on Vehicle). 47

4.24 Comparison of Horizontal and Vertical Left Idler Spindle Inertances on AIFV Vehicle (Turret on Vehicle). 48

4.25 Comparison of Left - and Right-side Horizontal Final Drive Inertances on AIFV Vehicles (Turret on Vehicle) 50

4.26 Comparison of Left - and Right-side Vertical Final Drive Inertances on AIFV Vehicle (Turret on Vehicle). 51

4.27 Comparison of Left - and Right-side Horizontal Inertances on M113A1 Idler Spindles 52

4.28 Comparison of Left - and Right-side Vertical Inertances on M113A1 Idler Spindles 53

4.29 Comparison of Horizontal and Vertical Left Idler Spindle Inertances on M113A1 Vehicle. 54

4.30 Effect of Turret Mass on Horizontal Idler Inertance Function of AIFV (Right Side). 55

Figures (cont.)

4.31 Effect of Turret Mass on Vertical Idler Inertance Function of AIFV (Right Side). 57

4.32 Effect of Turret Mass on Vertical Final-drive Inertance Function of AIFV (Right Side) 58

4.33 Comparison of Vertical Inertance Functions for M113A1 and AIFV Vehicles (Left Side) 59

4.34 Comparison of Horizontal Inertance Functions for M113A1 and AIFV Vehicles (Left Side) 60

4.35 Comparison of AIFV and M113A1 Inertance Functions: Final Drive Attach. 61

4.36 Roadwheel Attach Inertance, Measured at Bottom of Attach. 62

5.1 Isometric View of Node Locations, Initial Hull Model
(a) Side Plate (b) Bottom Plate (c) Top Plate 68
(d) Element Projections 69

5.2 Isometric View of Hull Elements - Initial Hull Model. 70

5.3 Idler Pad Static Flexibilities. 72

5.4 Typical Vibration Mode Shapes for Initial Model of M113A1 Hull
(a) 19.6 Hz Antisymmetric (b) 30.3 Hz Symmetric
(c) 53.2 Hz Antisymmetric (d) 56.4 Hz Symmetric 75
(e) 62.7 Hz Antisymmetric (f) 66.8 Hz Symmetric
(g) 85.9 HzAntisymmetric (h) 93.7 Hz Symmetric 76
(i) 111.6 Hz Antisymmetric (j) 136.6 Hz Symmetric
(k) 156 Hz Antisymmetric (l) 176 Hz Symmetric. 77
(m) 207 Hz Antisymmetric (n) 219.7 Hz Symmetric
(o) 222 Hz Antisymmetric 78

5.5 Hull Modal Density. 80

5.6 (a) Horizontal Idler Response to Horizontal Idler Excitation . . 81
(b) Vertical Idler Response to Vertical Idler Excitation. 82
(c) Vertical Idler Response to Horizontal Idler Excitation. . . . 83

5.7 Comparison of Measured and Calculated Horizontal and Vertical Left Idler Spindle Inertances on M113A1 Vehicle 84

5.8 (a) Top Plate Response to Idler Force. 86
(b) Bottom Plate Response to Idler Force 87

5.9 Effect of Variation in Loss Factor on Calculated Horizontal and Vertical Left Idler Spindle Inertances on M113A1 Vehicle. 88

Figures (cont.)

5.10 Effect of Loss Factor Changes on Calculated Bottom Plate Transfer Function (Node 1001) for Vertical Idler Force. 89

5.11 Top Plate Transfer Functions for Vertical Idler Force 89

5.12 Representative Modes Shapes of Torsion Box Beam 91

5.13 (a) Isometric View of Hull Elements - Revised Hull Model 93
(b) Node Map of Revised Hull Model: Projection. 94

5.14 Typical Vibration Mode Shapes For Revised Model of M113 Hull
(a) 29.5 Hz Symmetric (b) 41.3 Hz Antisymmetric
(c) 55.0 Hz Symmetric (d) 62.6 Hz Antisymmetric. 97
(e) 103.0 Hz Antisymmetric (f) 105.0 Hz Symmetric
(g) 172.7 HzSymmetric (h) 213.3 Hz Antisymmetric 98
(i) 245.1 Hz Symmetric (j) 273.0 Hz Antisymmetric
(k) 296.0 Hz Symmetric 99

5.15 Comparison of Measured and Calculated, Horizontal and Vertical Inertances for M113A1 Left Idler Spindle: Revised Hull Model . . 100

5.16 Acceleration-to-Force Transfer Function for Hull Top Plate: Comparison of Calculations and Measured Data. 100

5.17(a) The Effect of Different Idlers and Their Locations on Horizontal Idler Inertance Functions. 102

5.17(b) The Effect of Different Idlers and Their Locations on Vertical Idler Inertance Functions. 102

5.18 Effect of Ilder Location on Roof Response: Vertical Excitation . 103

5.19 Vertical Idler Inertance (10) of M113 Vehicle 105

5.20 Contribution of Resonant and Nonresonant Modes to Top Plate Response for Vertical Excitation of Idler (10). 107

5.21 Comparison of Measured and Predicted Noise-to-Force Transfer Function for Vertical Excitation of Idler Spindle on M113A1 . . . 108

6.1 Schematic Diagram of the Experimental Compliant Idler Wheel . . . 112

6.2 Experimental Idler Wheel Mounted on Test Stand. 113

6.3 Experimental Idler Wheel Mounted on Test Stand (Closeup). 114

6.4 Interior Noise Reduction of the Experimental Compliant Idler. . . 116

6.5 Interior Noise Spectra at 30 mph Due to Right Idler Wheel Only. . 117

Figures (cont.)

6.6 Exterior Noise of M113A1 Standard Idler Pair Compared to M113A1 Exhaust Noise at 25 Feet to the Left 119

6.7 2,000 Hz Exterior Noise at 30-mph, 3 Feet from Experimental Idler 121

6.8 250 Hz Interior Noise at 30-mph, Due to Experimental Idler. . . . 122

6.9 Spectrum of Sound Level Meter "DC" Output which Corresponds to Interior Noise Level Fluctuations. 126

6.10 Effect of Metallic Track-Idler Impacts. Compliant Idler, Rounded Paddle vs Flat Tops 128

6.11 Triaxial Vibration Levels on the Experimental Idler Disc at 30 mph 129

6.12 Triaxial Vibration Levels on the Increased Compliance Experimental Idler at 30 mph. 130

6.13 The Effect of Increased Compliance in the Experimental Idler at 30 mph, Interior Noise 132

6.14 The Effect of Track Guide Scrubbing on Interior Noise 133

6.15 Interior Noise Reduction Due to a Large Diameter Idler Wheel. . . 135

6.16 Prototype Idler Wheel Mounted on an M113A1 Vehicle. 136

6.17 Schematic Diagram of the Prototype Compliant Idler Wheel. 137

6.18 Idler Concept: Thin Flexible Rim; Rubber in Compression. 139

6.19 Idler Concept: Thick Rigid Rim; Rubber in Compression. 141

6.20 Idler Concept: Rim Composed of Rollers 142

6.21 Interior Noise Reduction with the Prototype Compliant Idler Wheel 145

6.22 Interior Noise Spectra Comparison for the Standard and Prototype Idler Wheels. 146

6.23 Exterior Noise Spectra of M113A1 Standard Idler Pair, Prototype Idler and M113A1 Exhaust, at 25 feet to the Left of Hull. 147

7.1 Sprocket Concept: Solid Rubber Ring in Compression 153

7.2 Sprocket Concept: Segmented Rubber Ring in Compression with Circumferential Holes 155

7.3 Sprocket Concept: Three Rubber Ring Pairs in Compression 156

Figures (cont.)

7.4 Sprocket Concept: Rubber in Both Radial Compression and Radial Shear. 157

7.5 Sprocket Concept: Fabric Isolator. 159

7.6 Sprocket Concept: Overload Gear with Rubber Separators in Compression 160

7.7 Sprocket Concept: Rubber in Shear. The Design Chosen for Experimental Development and Test 162

7.8 Experimental Sprocket Mounted on Test Stand 163

7.9 Noise Reduction in Crew compartment Due to the Experimental Compliant Sprocket. 165

7.10 Noise Reduction in the Driver's Compartment Due to the Experimental Compliant Sprocket 166

7.11 Crew Area Noise Spectra of Standard and Experimental Sprocket Wheels at 30 mph 167

7.12 Drivers Compartment Noise Spectra of Standard and Experimental Sprocket Wheels at 30 mph. 168

7.13 Exterior Noise Levels 25 feet to the Right of the Vehicle Due to the Left Sprocket Only 169

7.14 Exterior Noise Spectra at 30 mph Due to the Left Sprocket Only. Measured 25 feet to the Right of the Hull. 170

Tables

4.1 Space-Averaged Mean Square Acceleration Level, dB re 1 g, for the AIFV NSJ0005 at 32 km/hr (20 mph). 24

4.2 Loss Factor Data for Hull Structure and Interior Acoustic Volume For the AIFV Vehicle. 35

5.1 Idler Attach Pad Flexibility 71

5.2 Modal Extraction Data: Initial Hull Model 74

5.3 Modal Extraction Data: Revised Hull Model 96

5.4 Equivalent Beam Properties (5-inch idler spindle). 101

5.5 Normalized Generalized Mass of Structural Elements 106

6.1 Variations of Interior Sound Levels. 124

6.2 Calculated Interior Noise Modulation Frequencies 125

ACKNOWLEDGEMENT

The Human Engineering Laboratory greatly appreciates the encouragement and funding provided by the U. S. Army Tank-Automotive Command. The success of this program would not have been possible without the effort of Don Rees of that organization.

1. EXECUTIVE SUMMARY

THIS STUDY SHOWED THAT CONVENTIONAL NOISE REDUCTION TECHNIQUES ARE ONLY MARGINALLY EFFECTIVE IN TRACKED VEHICLES. BASED ON A SPECIAL COMPUTER PROGRAM PREDICTION, IT SHOULD BE POSSIBLE TO ACHIEVE A 65% NOISE REDUCTION INSIDE AN M113 HULL BY REDESIGNING THE IDLER AND SPROCKET AND ISOLATING THE ROADWHEELS. THE ADDITIONAL NOISE REDUCTION TO MEET MIL-STD-1474B SHOULD COME ABOUT THROUGH HULL MODIFICATIONS. FULL SCALE SUSPENSION HARDWARE HAS DEMONSTRATED THAT THE ABOVE GOAL IS REALISTICALLY ACHIEVABLE.

The noise produced by track-laying vehicles has historically been a problem in the U.S. Army. Exterior vehicle noise provides enemy forces with a means of detection at great distances. Interior vehicle noise prevents accurate person-to-person or electrically aided communication and contributes to hearing loss among exposed Army personnel.

If the Army is to provide personnel with armored vehicles having maximum effectiveness, noise must be reduced to the limits prescribed by MIL-STD-1474B. To accomplish this end, a multiphase program has been conducted to develop a thorough understanding of the noise sources, the acoustical and vibratory paths through which energy enters the hull structure, and the mechanisms by which noise arrives at the various crew locations, and emanates from the exterior of the vehicle. Based upon the results of these analyses, the redesign of major noise-producing components and the application of new materials and coatings will then be undertaken. The vehicle chosen to develop this noise reduction technology is the M113A1. The goals set for the program were a 17 dB(A) reduction in interior noise to a level of 100 dB(A), and a 6 dB reduction in exterior noise representing a 50% reduction in detection range. This report describes the third phase of the program to reduce the noise of armored track-laying vehicles to the above goals.

Phase I of the program isolated and rank ordered the various noise sources responsible for overall noise, developed a computer program to predict changes in noise level produced by changes in track and suspension systems, and provided an understanding of the noise producing mechanism of vehicles such as the M113A1. This phase found that track-idler interaction was the major source of noise with the sprocket and roadwheels being the second and third sources, respectively.

Phase II developed the concepts necessary to reduce suspension system noise, and produced an experimental idler to verify the noise reduction capability of these concepts. The vibratory power flow of the M113A1 hull was analyzed and experimental damping, absorptive, and barrier treatments were evaluated along with experimental modifications.

The present phase (III) involved designing and fabricating a prototype quiet idler and an experimental quiet sprocket. Also the hull dynamics of the M113A1 and the AIFV (both of similar size and suspension) were compared to determine the reason for the significantly lower noise level of the AIFV. A preliminary finite element analysis was made to determine if this technique could be used to predict the vibrational mode shapes and dynamic response of the M113A1 vehicle with the ultimate aim of predicting the hull configuration required to achieve significant noise reduction.

Based upon the conclusion that the idler is the major noise contributor, a completely new design of the idler wheel was pursued. The design proceeded in two steps, the first being a verification of the concept that an increase in compliance of the wheel rim would indeed reduce noise. This idler wheel was designed to permit experimental variations of radial, tangential and axial compliance. The second step was a practical design which incorporated those features determined to be most appropriate in the experimental version of the idler. This prototype idler wheel was designed with the goal of being practical, increasing noise reduction potential, and being directly interchangeable with the standard idler wheel. It has a solid outer rim mounted on two rubber "doughnuts" acting in shear which isolate the rim from the axle. The maximum stroke of the rim when contacting the track is 3/4 inch, with a fail-safe stop in the event of a severe impact upon the idler. Measurements on the test stand indicate that this prototype idler wheel reduces interior idler generated noise by 15 dB(A) to a sound level of 95 dB(A) at a speed of 30 mph. Limited durability tests at 30 mph indicate that this idler wheel is both durable and practical.

The idler contribution to the exterior acoustic signature was reduced to well below the level of exhaust noise. If the sprockets and roadwheels can be quieted as much as the idler, then suspension-related noise would no longer lead to vehicle detection, even at high speeds, as the exhaust noise would then be dominant.

Based upon the concepts developed for the idler, an experimental sprocket has been developed using a number of rubber "doughnuts" to isolate the axle from the outer rim. However, a compliant sprocket is significantly more complicated since it must be capable of transmitting torque through the compliant element. Also, it must have fail-safe stops in the tangential as well as the radial direction. Tests of the experimental sprocket indicate that it is up to 10 dB(A) quieter than the noise produced by a standard sprocket. Although noise reduction is less than that provided by the prototype idler and the design is more complex, it is anticipated that the second generation sprocket design will be practical and will provide 12-15 dB(A) noise reduction.

The next subject which was addressed in Phase III was the comparison of the noise of the M113A1 with that of the AIFV. A-weighted noise levels inside the AIFV vehicles and structural vibration levels on the hull of the vehicle are on the average, 5 dB lower than for M113A1 vehicles. Although the track and suspension of both vehicles are essentially the same the upper hull shape and idler attachment are different. These differences were investigated using the concepts of statistical energy analysis for hull generated noise and the attachment transfer function to investigate idler generated noise. It was concluded from this analysis that the major hull radiating elements are the bottom plates and upper side plates at low frequencies for the AIFV vehicle. For the M113A1 vehicle the top plate is dominant and the side plates are still important. At higher frequencies (above 500 Hz), the sponsons dominate the acoustic radiation for both vehicles.

Inertance functions are measures of the power accepting and dissipating characteristics of the hull structure. In general, reductions in idler inertances will lead to reductions in structural response levels, which in turn will lead to reductions in interior noise levels, provided that the acoustic radiation efficiencies of the structural elements are not significantly altered.

At frequencies below 250 Hz, the vertical inertance of both M113A1 and AIFV hulls is greater than that in the horizontal direction. This indicates that if the horizontal and vertical idler input forces were equal, vertical forces would dominate the hull response. However, test track data show the horizontal forces can exceed vertical forces by up to 10 dB for at least one speed during normal operation.

Changes in idler attachment point configuration have no significant effect on vertical inertances. However, the raised idler location for the AIFV vehicle has a lower horizontal inertance (by about 5 dB) in the frequency range 125 Hz to 250 Hz. Therefore, at frequencies above 125 Hz (see Fig. 22, ref. 16), the idler attachment point will, to some extent, affect (by up to 5 dB) the vehicle interior noise levels, at least at a speed of 30 mph.

It was also concluded that changes in the idler stiffness by up to a factor of ten will have no significant effect on the hull structural response or vehicle interior noise levels. This is because power flow into the hull is controlled by relatively flexible hull members with long structural wavelengths. Additionally, the turret mass does not significantly impact the vehicle inertance functions and hence interior noise levels.

Appropriate structural modifications were not immediately obvious from the statistical energy and attachment transfer function analyses, so a finite element analysis was developed to guide the hull redesign process which aims to produce practical hull modifications providing 5 to 10 dB(A) noise reduction. In this analysis technique, the M113A1 is modeled by a number of individual structural components or elements which are interconnected at a number of joints, or nodal points. The simplicity of the M113A1 shape lends itself well to this type of analysis. This analysis technique provides accurate calculation of hull resonance frequencies and mode shapes which, in turn, provides an understanding of the hull power flow for noise control purposes.

The initial model which was made has some accuracy problems. A second model, which was constructed with a greater number of elements, is sufficiently detailed to allow reasonable predictions of mode shapes and resonance frequencies up to frequencies of about 300 Hz. Extension above

400 Hz using the current nodal arrangement is not recommended. Good predictions of the measured vertical idler inertance function have been made with the developed model, but the measured horizontal intertance function is underpredicted by about 10 dB.

A preliminary calculation using frequency and space averaging to predict interior noise levels was encouraging and showed reasonable agreement between measured data and results predicted using finite element analysis for the noise-to-force transfer function corresponding to one third octave band vertical excitation of the idler spindle on the M113A1 vehicle.

Frequency and space average calculations using finite element analysis results indicate that the interior noise levels at frequencies above 31.5 Hz are controlled by resonant response of the hull, rather than by stiffness controlled response as was considered a possibility at an earlier stage of the work. This suggests that, in theory at least, damping of the structure should be an effective means of interior noise control. In practice however it is difficult to effectively damp the important hull members due to the long structural wavelengths involved.

Statistical energy analysis provides a useful framework for understanding the power flow between the hull structure and vehicle interior space, even at low frequencies. This allows frequency averaged interior noise levels to be accurately calculated from frequency and space averaged structural response data which may be measured experimentally or calculated using the finite element model.

Frequency and space averaging of the modal output data (using statistical energy analysis) from the finite element model is the most efficient and useful means of evaluating the effects of hull structure modifications on structural response and hence interior noise levels. It is anticipated that this method will be used in the future to evaluate the effect of hull structural changes on interior noise levels, as evaluating the data mode by mode is tedious and the results are difficult to interpret.

To date, the entire noise reduction program has identified the idler as the major noise source, with the sprocket and roadwheels being 3-4 dB(A) less intense. A computer program has been written to predict the changes in sound level resulting from configuration changes in the track and suspension system. Idler noise has been reduced by the predicted amount of 15 dB(A), and the first generation sprocket design has produced up to a 10 dB(A) reduction. It is anticipated that roadwheel isolation will provide a 10-12 dB(A) reduction of roadwheel noise. A complete suspension system incorporating the above quieted wheels should provide an interior noise level at least 10 dB(A) (65% noise reduction) quieter than a standard M113 vehicle.

The additional 7 dB(A) of desired noise reduction will be achieved by modifications to the hull. Preliminary results indicate that simple, conventional noise reduction techniques provide only marginal results and may not be practical. Therefore, a more extensive approach is required to reduce hull generated noise. It is anticipated that hull noise can be reduced by 5-7 dB(A) which combined with the suspension noise reduction will provide the desired total of 17 dB(A). This reduction will produce a vehicle which meets the noise limit of 100 dB(A) prescribed by MIL-STD-1474B.

The fielding of light armored track-laying vehicles meeting this 100 dB(A) limit will provide a vehicle which is less detectable and operates more efficiently, and will permit the crew and cavalry personnel to perform their mission in a more effective manner.

2. OBJECTIVE AND GOALS

The basic objective of this program was to develop feasible noise control concepts to aid in construction of a lightweight tracked vehicle that will permit crew members to perform their duties without the additional use of hearing protectors. They are presently required to use hearing protectors in addition to the DH132 Combat Vehicle Crewman's Helmet. Reduction of the interior noise level also would improve communication between crew members.

Accordingly, the goal of an interior A-weighted noise level of 100dB has been set, in conformance with the guidelines of MIL-STD-1474B, Category B. Achievement of this goal requires a 17 dB(A) noise reduction in the M113A1, primarily at low frequencies. In a weight-critical machine designed for survivability in an extreme environment, this represents a major technical challenge.

The U.S. Army Human Engineering Laboratory (HEL) and the U.S. Army Tank-Automotive Command (TACOM) have recognized that practical design modifications required to achieve significant interior noise reductions were not available. It also was realized that the development of these noise controls must be based on experimental and analytical evaluations of both the noise sources and their transmission paths. Studies prior to the HEL sponsored work [2, 11, 18 and 19] had identified the major noise sources but had not quantified their contributions. Two preceding studies by FMC Corporation, sponsored by HEL, have been conducted. The first study identified the separate contributions to interior noise generated by the idlers, the sprockets, and the roadwheels. This work also identified several promising concepts for tracked vehicle noise reduction. The second study developed an experimental idler to prove and optimize noise reduction concepts. Concepts for reducing hull-generated noise also were explored.

Beginning with the third phase of this program, TACOM, which has recognized the operational advantages of reducing both interior and exterior noise, has provided funding for this joint HEL/TACOM effort. The M113A1 vehicle was chosen as the demonstration vehicle for this study because it was used in the previous HEL-sponsored studies, because of vehicle availability, and because of the relative availability and low cost of replacement parts. However, all noise reducing concepts developed in this study could be adapted to other tracked vehicles with suitable scaling changes.

Only suspension noise sources were considered in this study. Previous studies [3, 16] have shown that other noise sources are secondary; such as the engine, power train, and final drive gearing. Furthermore, suspension noise sources are common to high-speed tracked vehicle noise problems and the technology needed to successfully reduce the noise from these sources does not exist at present. Developing practical noise controls for these suspension noise sources is the fundamental purpose of this program.

This present phase of the work follows largely from the results of the previous two phases [16, 17]. The most important conclusions obtained from that research were:

1. The technology to reduce tracked vehicle noise does not exist and will require development.
2. Very careful control of testing parameters is necessary to accurately measure the incremental noise reductions obtained when evaluating potential noise reduction methods.
3. At and below 20 mph, both idler and sprocket noise must be reduced to meet the noise reduction goals.
4. Above 20 mph, roadwheel noise also must be controlled in addition to idler and sprocket noise.
5. Engine and power train noise is not significant compared to suspension induced noise.
6. Vehicle interior sound absorptive treatments are not practical.
7. Making the idler and sprocket wheel rims more compliant is an effective noise reduction technique.
8. The best spring material for compliant idlers and sprockets appears to be either natural or synthetic base "natural" rubber. Steel springs would be difficult to engineer into the limited space available.
9. A number of highly resilient elastomers were evaluated as spring materials, but were found to have inferior mechanical or damping properties.
10. In a compliant idler wheel, axial as well as radial and tangential compliance need to be investigated.

11. A very compliant experimental idler wheel was designed, fabricated, and found to be rugged enough for extensive acoustical testing. Measurements showed that the compliant wheel is 10-12 dB(A) quieter than the standard idler wheel.

12. Local stiffening of the hull at the roadarm and idler locations provided no significant changes to the mechanical impedances and, therefore, no noise reduction potential.

13. A damping treatment applied to both sponsons provided appreciable sponson vibration reduction at 500 Hz and higher frequencies. This treatment also gave a modest vibration reduction of other hull plates, and noise reduction of approximately 0-2 dB(A).

14. To achieve appreciable noise reduction by means of hull plate damping, a promising technique is constrained layer damping. (This was later found to be much less effective than initially expected.)

15. The computerized simulation of track dynamics, while producing promising results, would require incremental refinement before it should be used in designing lower noise suspension components.

The reported program extends the previous work. The purposes are to evaluate and optimize the noise reduction of the previously developed experimental compliant idler, to demonstrate a practical reduced noise idler, to demonstrate the feasibility of a compliant sprocket, and to gain a better understanding of how the suspension vibration is conveyed throughout the hull and can be reduced by hull changes. This research was divided into five independent tasks, each of which could help reduce noise. These tasks were to:

1. Measure noise and durability characteristics of the previously developed experimental idler. Determine the importance of axial, radial, and tangential compliance on idler noise reduction.

2. Based upon the results above, design, fabricate and test a prototype quiet idler with a goal of A-weighted interior noise level of 95dB and a service life of greater than 2000 miles. Exterior noise reduction will also be assessed.

3. Design, fabricate, and test an experimental sprocket carrier based upon concepts developed for the compliant idler.

4. Determine the source of differences in interior and exterior noise levels between M113A1 and AIFV vehicles. Consideration would be given to individual noise sources, the method of attachment of the suspension components, and the coupling and radiation properties of the hulls.

5. Construct and exercise a finite element model to predict the vibrational mode shapes and dynamic response of the M113A1 vehicle.

The first task validated the concept of a compliant-rimmed idler, and determined those features which were most important for noise reduction. The second task showed that the concept could be used in a practical, production-feasible idler that has the durability required of tracked vehicle suspension components, and will still lead to reduced interior A-weighted noise level produced by the idler of 95 dB. The third task showed that the concept proven on the idler also could be adapted to a practical sprocket design which could transmit torque through the compliant elements to the track. The fourth and fifth tasks compared the hull structures of two vehicles of similar design, one of which is, on the average, 5 dB(A) quieter than the other. The fourth task approached this problem with an experimental comparison, while the fifth task addressed the problem from an analytical approach.

In this project, FMC Corporation, the producer of the M113A1 vehicle, was the prime contractor responsible for the design, test, fabrication, and overall management of the program. Mr. Thomas Norris of Consultants in Engineering Acoustics produced the idler concepts and preliminary design, and assisted in the final hardware design and testing. The experimental comparison of the hull dynamics of the AIFV and M113A1 vehicles was conducted by Dr. David Rennison of Bolt Beranek and Newman Inc. of Canoga Park, California. The finite element modal analysis work was conducted by Dr. Rennison, with the computer modeling done by Dr. Kenneth Foster of Foster Engineering Company.

3. DISCUSSION OF TRACKED VEHICLE INTERIOR NOISE

3.1 General Discussion

Interior noise in tracked vehicles results from track interaction with the drive sprockets, idler wheels, and roadwheels. The engine and power train are secondary noise sources in most tracked vehicles. Some vehicles, such as the M60 tank and the Infantry Fighting Vehicle (IFV), have track support rollers which also may produce significant interior noise. The track-ground interaction was not found to be a significant source in any of the vehicles tested. Figure 3.1 is a schematic representation of tracked vehicle noise sources and vibration paths.

Noise in moving tracked vehicles results from vibration of the hull which is excited by suspension and engine-power train components. The interior noise levels at the driver and crew locations consist of direct and reverberant contributions. Due to space and other practical limitations, noise reduction in lightweight tracked vehicles can only be obtained by reducing hull vibration, rather than by installing barriers or absorbers. Consideration of "conventional" acoustic noise control barriers and absorbers showed that, because the entire hull radiates noise, the A-weighted noise goal of 100dB could not be met within practical weight, cost, durability, and size limits. Therefore, the noise control concepts addressed in this study were: (1) the reduction of vibration at the various sources, and (2) attenuation of vibration energy paths between sources and the hull.

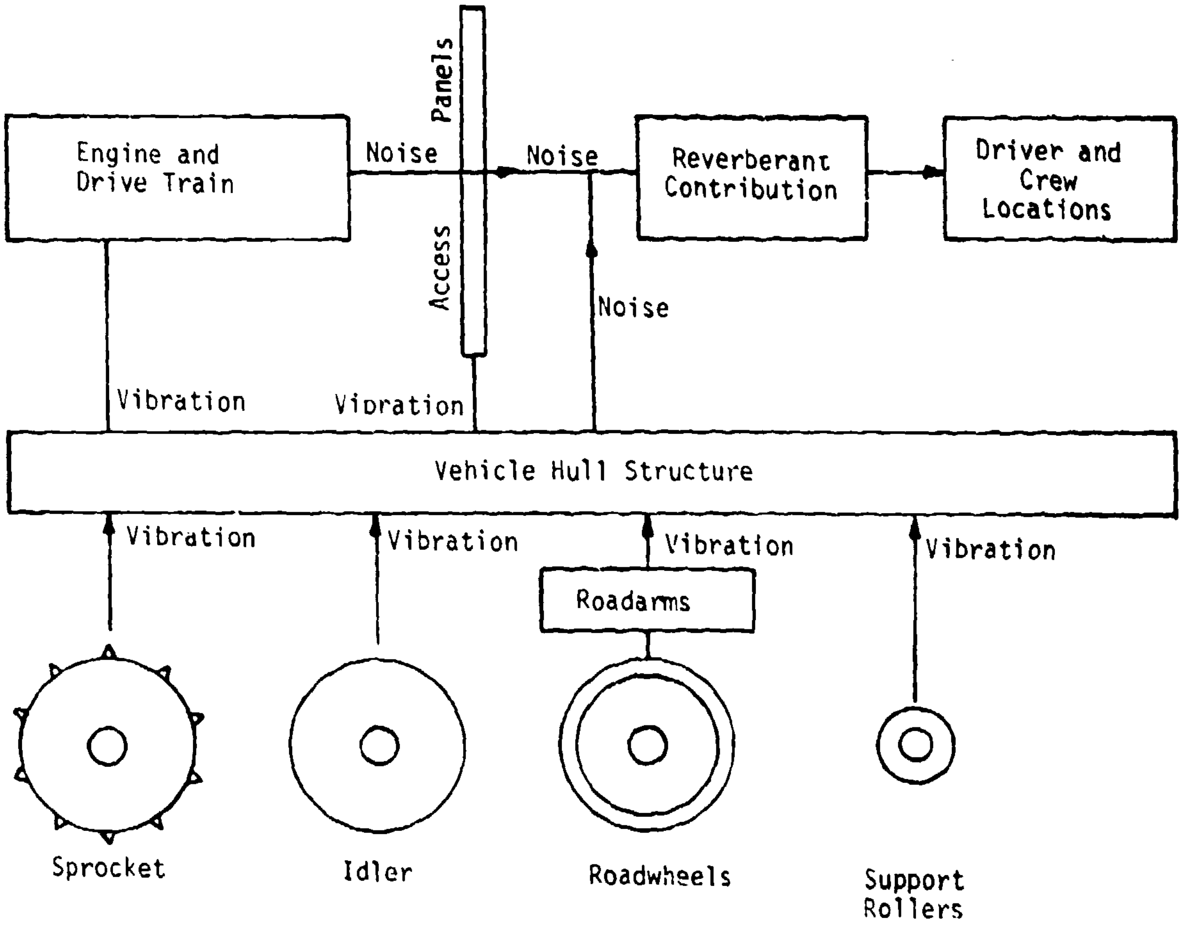
Panels
Engine and Drive Train
Noise
Noise
Reverberant Contribution
Driver and Crew Locations
Access
Noise
Vibration
Vibration
Vehicle Hull Structure
Vibration
Vibration
Vibration
Vibration
Roadarms
Sprocket
Idler
Roadwheels
Support Rollers

Figure 3.1 Schematic Diagram of Sources and Paths Responsible for Interior Noise in Tracked Vehicles.

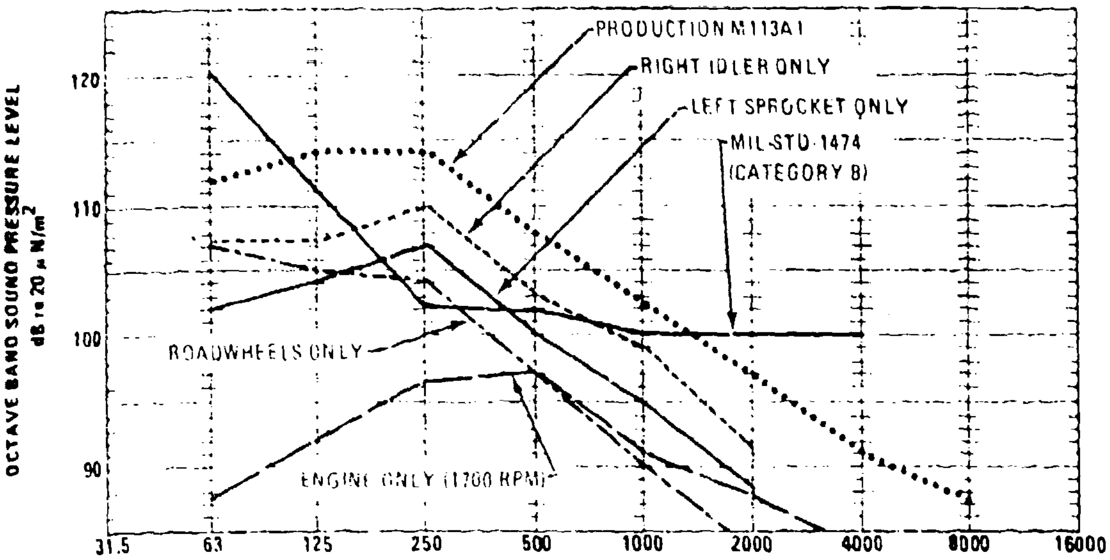

Figure 3.2 Noise Source Spectra at 15 mph at Center of Crew Compartment

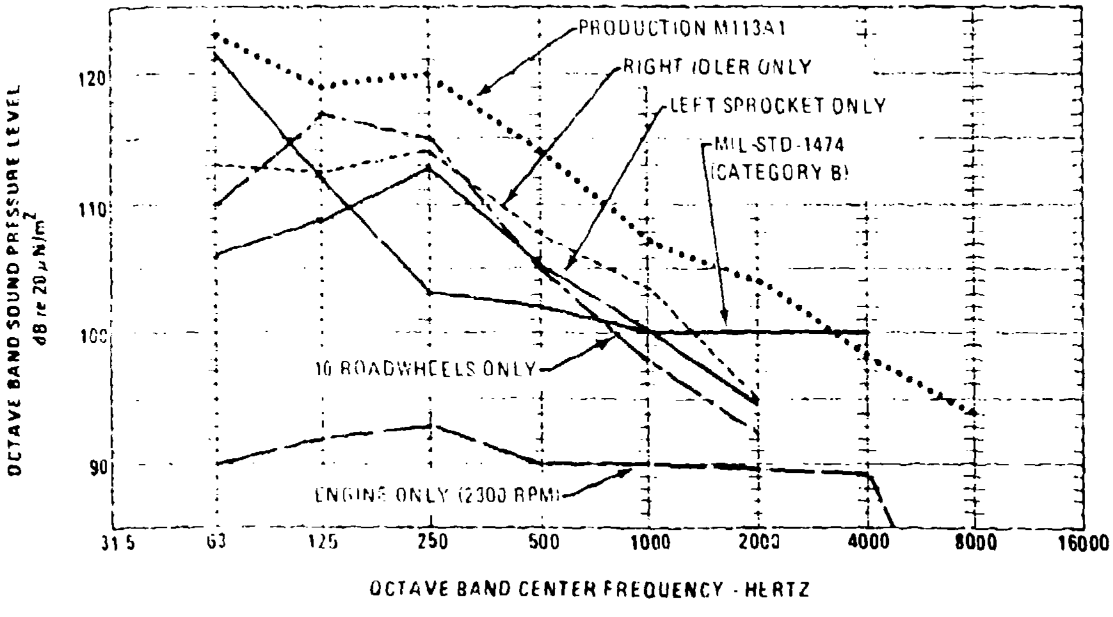

Figure 3.3 Noise Source Spectra at 25 mph at Center of Crew Compartment

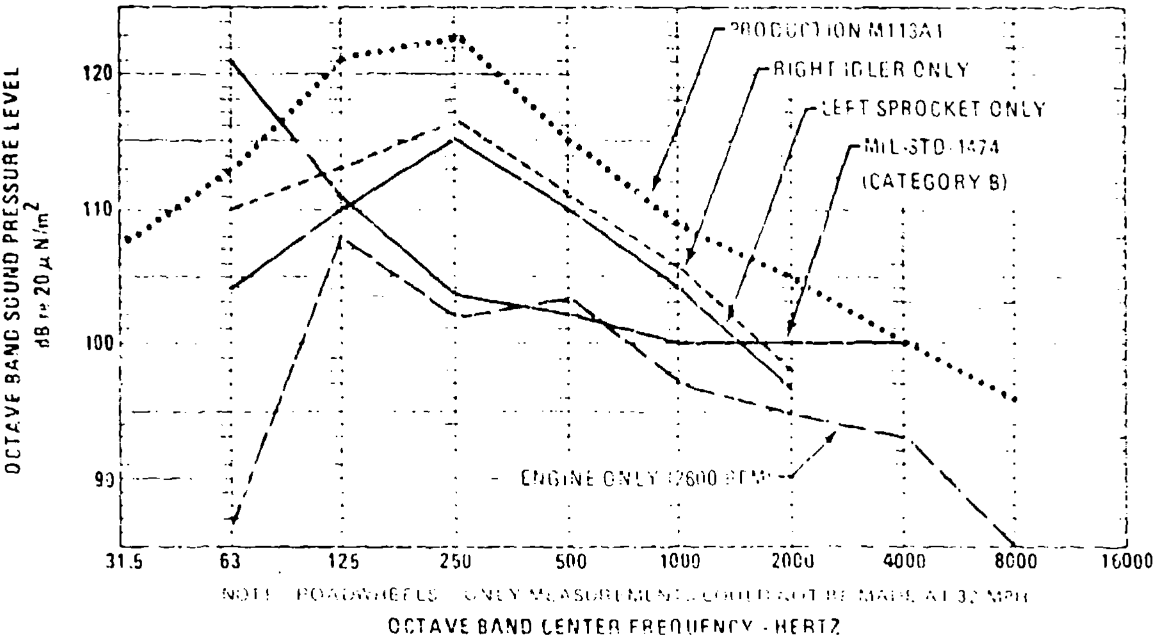

Figure 3.4 Noise Source Spectra at 32 mph at Center of Crew Compartment

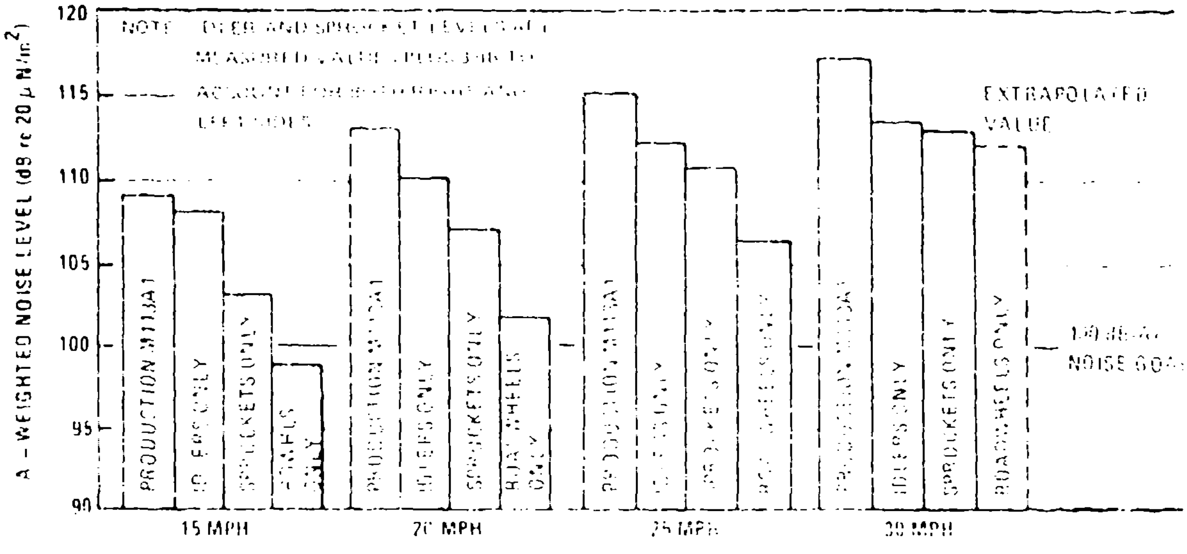

Figure 3.5 Track System Source Contributions to M113A1 Crew Area Noise Levels at Various Speeds.

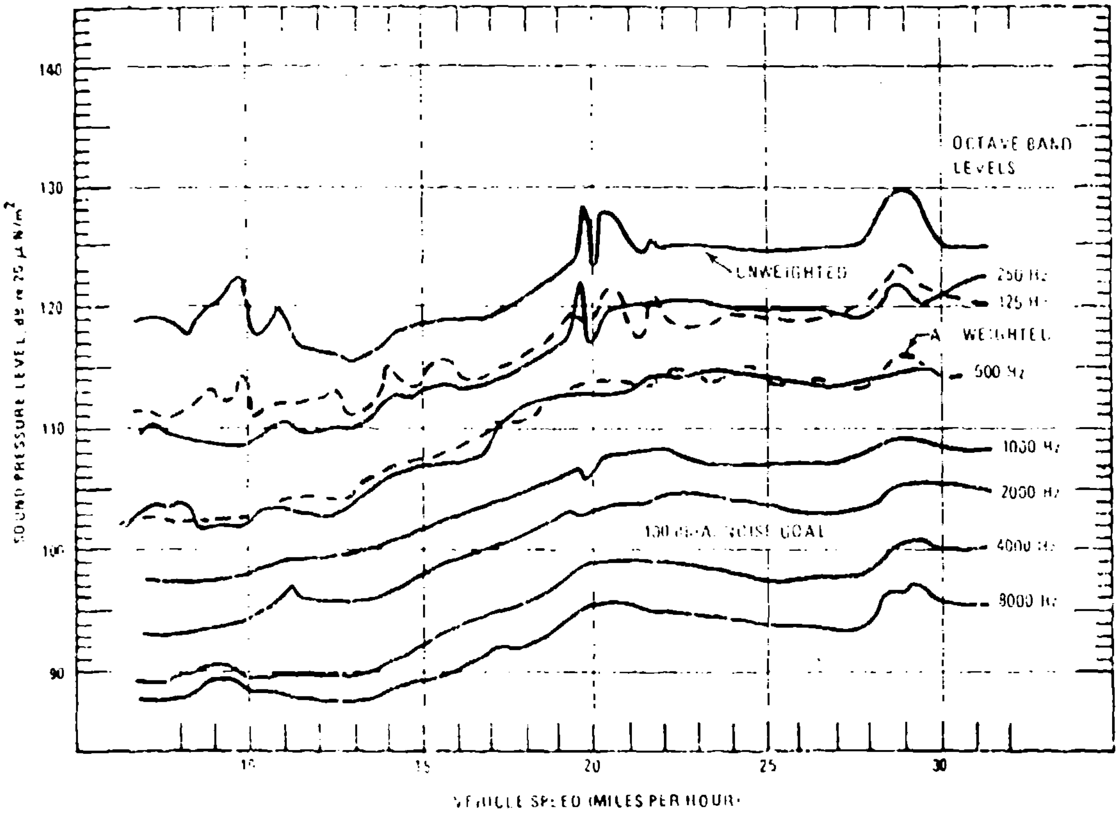

Figure 3.6 Speed Dependence of Production M113A1 Noise at the Crew Position Operating on Paved Track.

The basic phenomena responsible for tracked vehicle hull vibration at typical operating speeds are tension changes due to the geometry of track engagement with the idler and sprocket wheels, and forces resulting from impacts between track shoes and the idler and sprocket wheels. Both of these phenomena occur at track-laying rate. A further discussion of these phenomena appears in Reference [16].

3.2 M113A1 Interior Noise Levels

When under way, the airborne noise levels in both the crew area and driver space on the M113A1 armored personnel carrier exceed comfort, communication, and hearing conservation standards.

For example, at 30 miles per hour the A-weighted noise level near the driver's head location is 117 dB. At the same speed, the noise level is 124 dB in the 250 Hz octave band. These levels are, respectively, 17 and 21 dB above those noise levels specified as acceptable in MIL-STD-1474B, Category B, which is the maximum allowable level for systems requiring electrically-aided communication via an attenuating helmet or headset.

The octave band spectra for 15, 25 and 32 mph in the crew compartment are presented in Figures 3.2, 3.3, and 3.4. The noise levels of the production M113A1 exceed the specification goal by 12 to 19 dB at 250 Hz, depending on vehicle speed.

The relative noise contributions of the idlers, sprockets, and roadwheels are presented in Figure 3.5. The dependence on speed of both the A-weighted noise level and octave band noise levels is presented in Figure 3.6. A more complete discussion of these noise source levels appears in Reference [16].

4. EXPERIMENTAL COMPARISON OF THE HULL DYNAMICS OF THE AIFV AND M113A1 VEHICLES

4.1 Conceptual Approach

It has been observed that the A-weighted noise levels inside certain AIFV vehicles are on the average 5 dB lower than inside the similar M113A1 vehicles. The primary structural differences between these two vehicles of almost identical size are the upper hull shape and the idler attachment details, the track and suspension system being essentially the same for the two vehicles. An excellent opportunity was therefore available to explore the potential for interior noise reduction as a function of these hull design differences.

In an effort to develop an empirical understanding of the importance of these subtle structural differences, two studies were undertaken to examine energy flow within both vehicles. The first investigated noise and vibration characteristics by using the concepts of statistical energy analysis and the second contrasted the attachment point transfer functions of the vehicles' suspension systems. The results of these analyses were then used to guide the development of an analytical model, which is to be used to predict the effects of practical structural hull modifications on the vehicle interior noise levels.

4.2 Vehicle Structural Characteristics

The AIFV evolved from the baseline M113 concept insofar as the suspension, track, and lower structure are almost identical for the two classes of vehicles; in fact, many of the structural components are interchangeable. Various differences exist, some major and others rather subtle; this discussion will concentrate on these differences. Figures 4.1 to 4.6 present alternative views of the two hulls selected to highlight the major structural elements expected to have the greatest influence on the noise differences between the two vehicles. Emphasis has been placed on the vehicles' rear sections and the idler attachment areas. In each figure the M113A1 hull is used as the baseline and the AIFV appears on the overlay.

Figure 4.1 shows a section view looking from the vehicles' left sides. The largest differences at the vehicle front are the shallower slope of the AIFV nose and its relatively thinner hull thickness. The use of bolt-on armor protection mounted over buoyancy foam equalizes the hull surface density, but reduces 'panel' bending rigidity. The final drive mounting system, flooring configuration, box beam lower side plate, and sponson details appear the same for the two vehicles. Roadarms are mounted in the same positions in the box beams.

Major differences occur in the vehicle top surfaces and rear configurations. The AIFV has provision for a turret (mass about 1200 kg) and its rear half is composed of more and smaller plate elements, forming a stiffer hull in the circumferential direction (see Figure 4.2 for a rear view). Figure 4.3 contrasts the vehicle cross sections in the 'turret' plane: the added turret mass and the more rigid hull cross section might be expected to reduce the power accepting characteristics of the hull and thereby reduce the inflow of vibrational energy, at least at low frequency. A comparison of the details of the horizontal section toward the rear of the hull and at a plane above the sponsons is shown in Figure 4.4. The fuel tanks are relocated from an inboard left position on the M113A1 to a rear-mounted overhanging position on the AIFV (see Figure 4.1). A considerable difference in hull vertical inertance could result at the idler attachment position. In general, the thicknesses of the 'upper side' plates on the AIFV are some 30% less than on the M113A1, due to the use of space-laminate bolt-on armor. Ramp details for the two vehicles are similar.

Idler plate details are compared in Figures 4.5 and 4.6. The former compares the configuration of left and right idler plate shapes for the

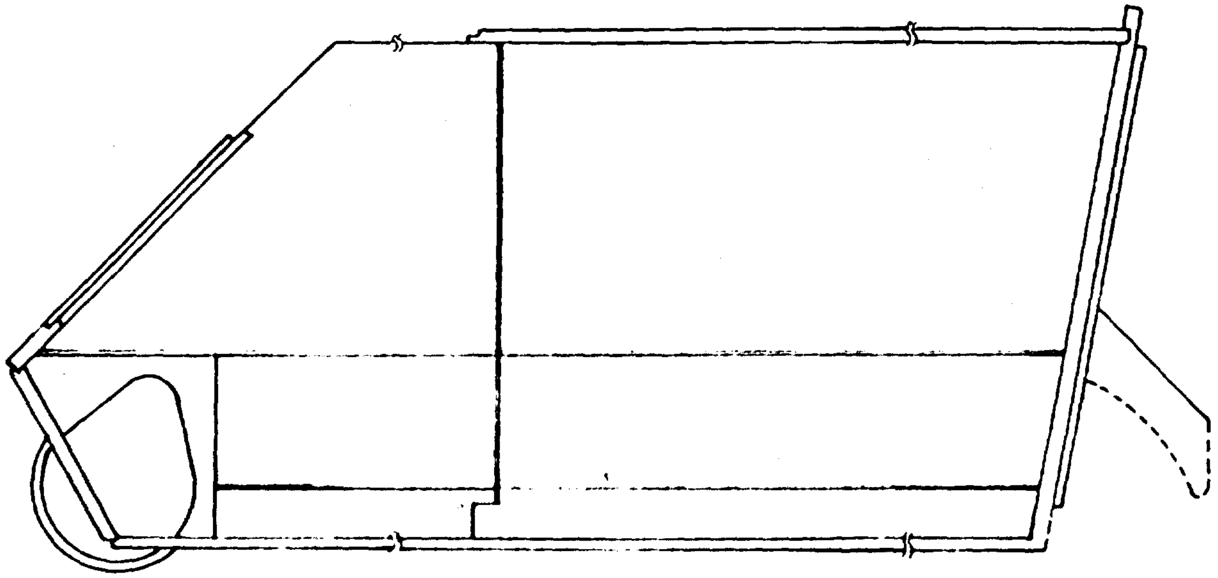

M113A1, FMC DWG 10932750

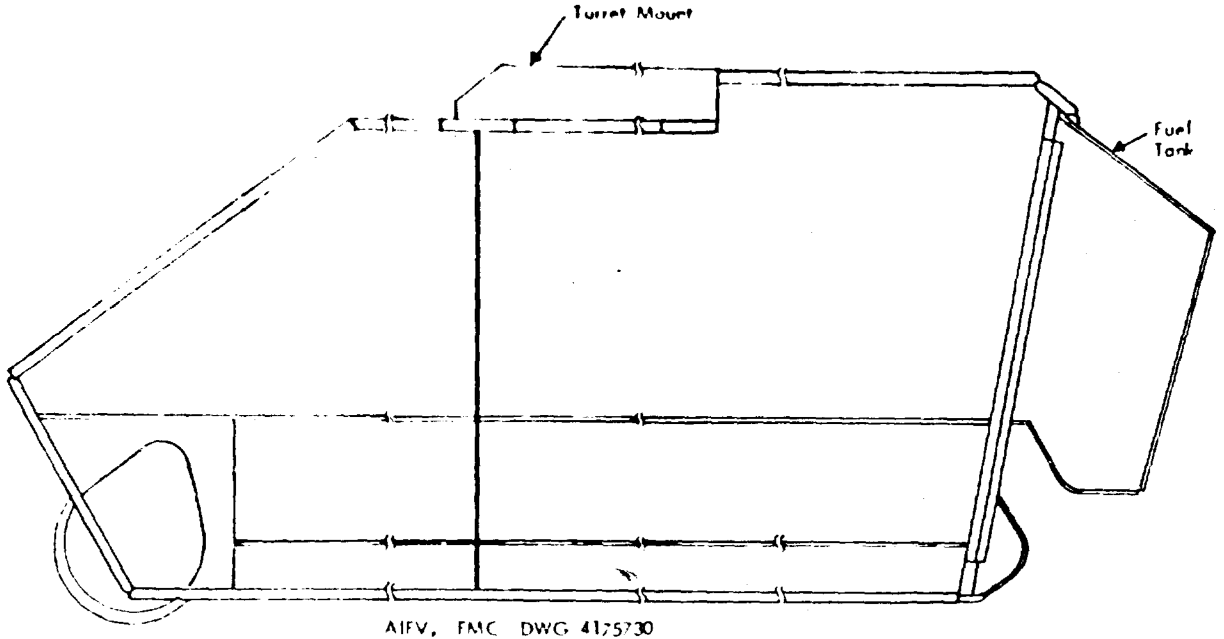
Turret Mount
Fuel Tank

AIFV, FMC DWG 4175730

Figure 4.1 Comparison of Hull Vertical Sections, Taken Along Vehicle Length

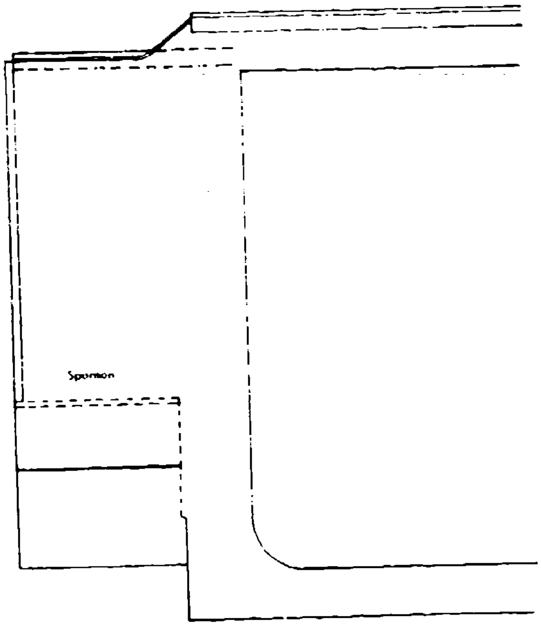

M113A1, FMC DWG 10932750

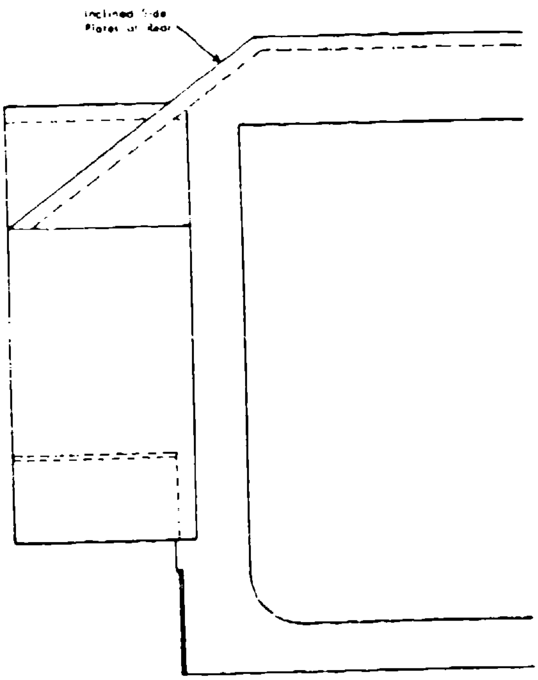
Inclined Side
Plates at Rear

AIFV, FMC DWG 4175730

Figure 4.2 Comparison of AIFV/M113A1 Hull Details - Rear View

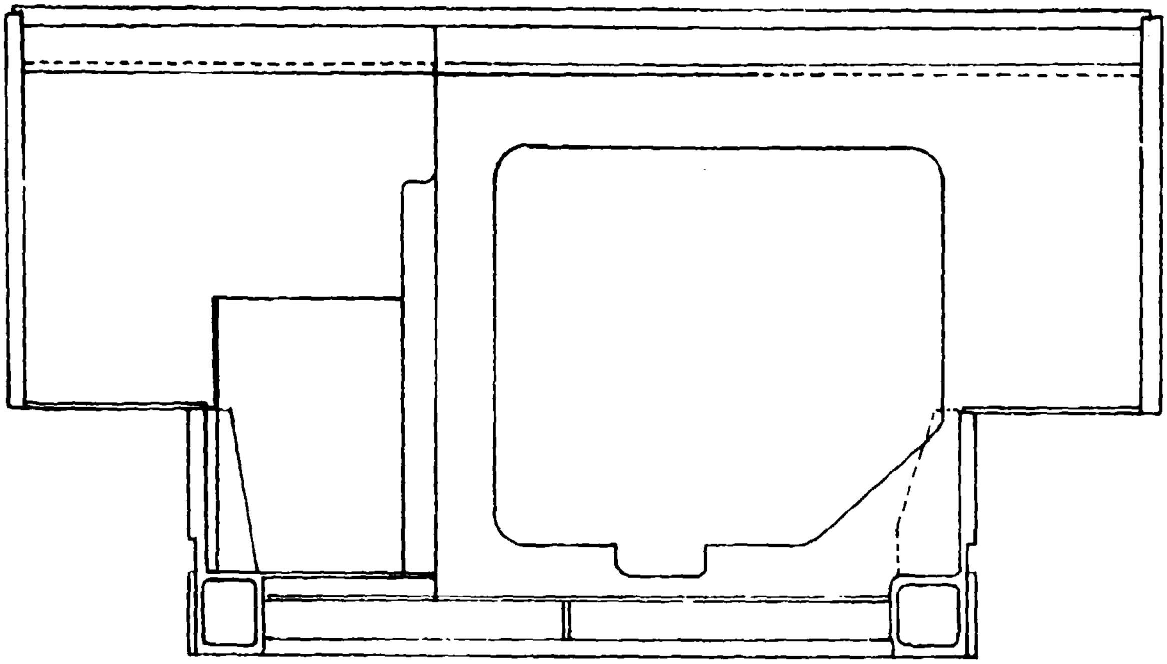

M113A1, FMC DWG 10932750

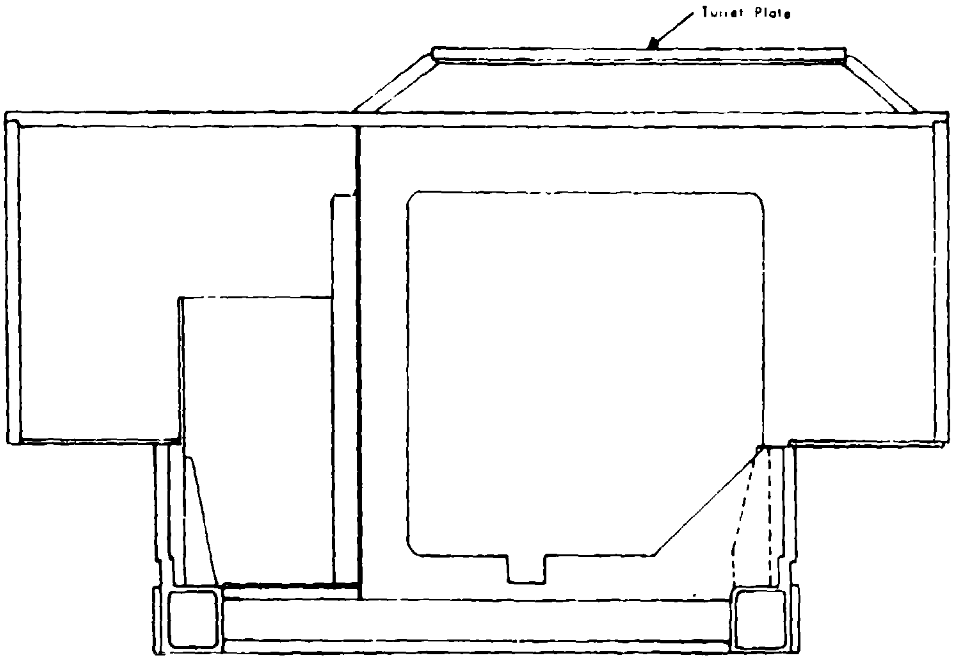
Turret Plate

AIFV, FMC DWG 4175730

Figure 4.3 Hull Section Views, Looking Forward

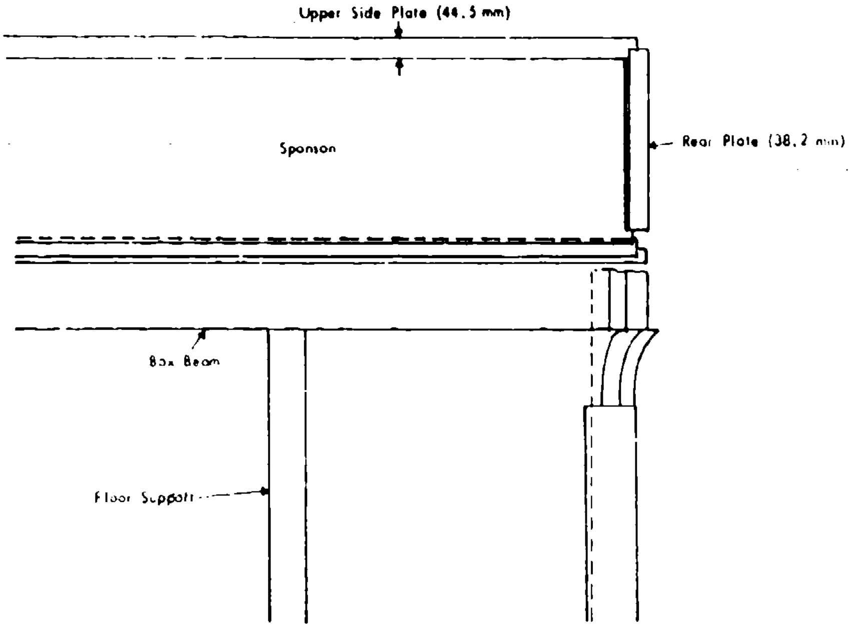
Upper Side Plate (44.5 mm)
Sponson
Rear Plate (38.2 mm)
Box Beam
Floor Support

M113A1, FMC DWG 10932750

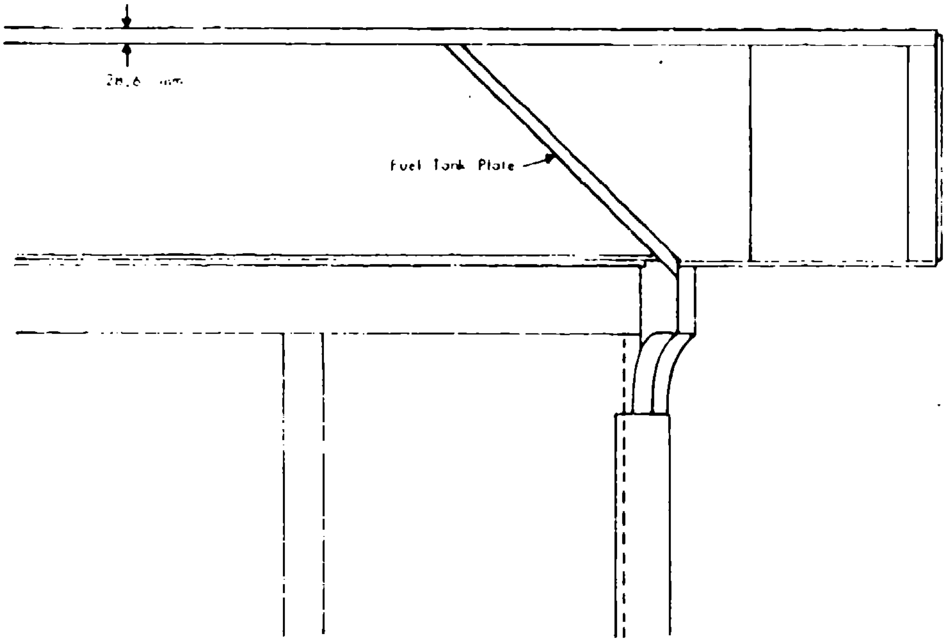
28.6 mm
Fuel Tank Plate

AIFV, FMC DWG 4175730

Figure 4.4 Comparison of Horizontal Sections of Vehicles, Above Sponson

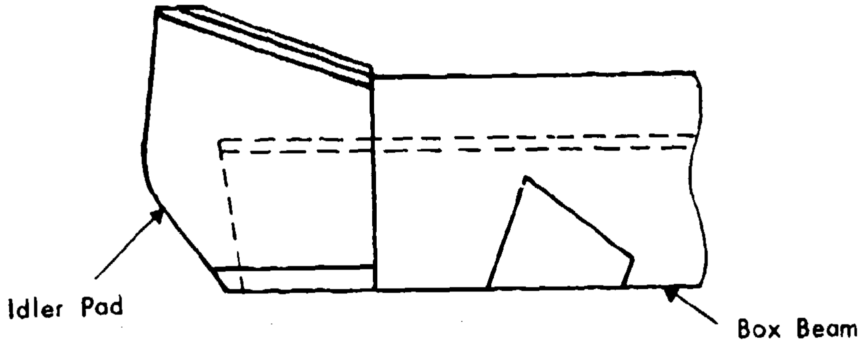
Idler Pad
Box Beam

Left Idler Pad (Viewed from Right FMC DWG 4169492)

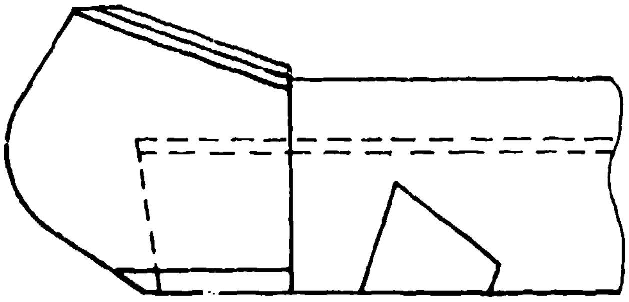

Right Idler Pad (FMC DWG 4169490)

Figure 4.5 Comparison of Left and Right Idler Pads for AIFV

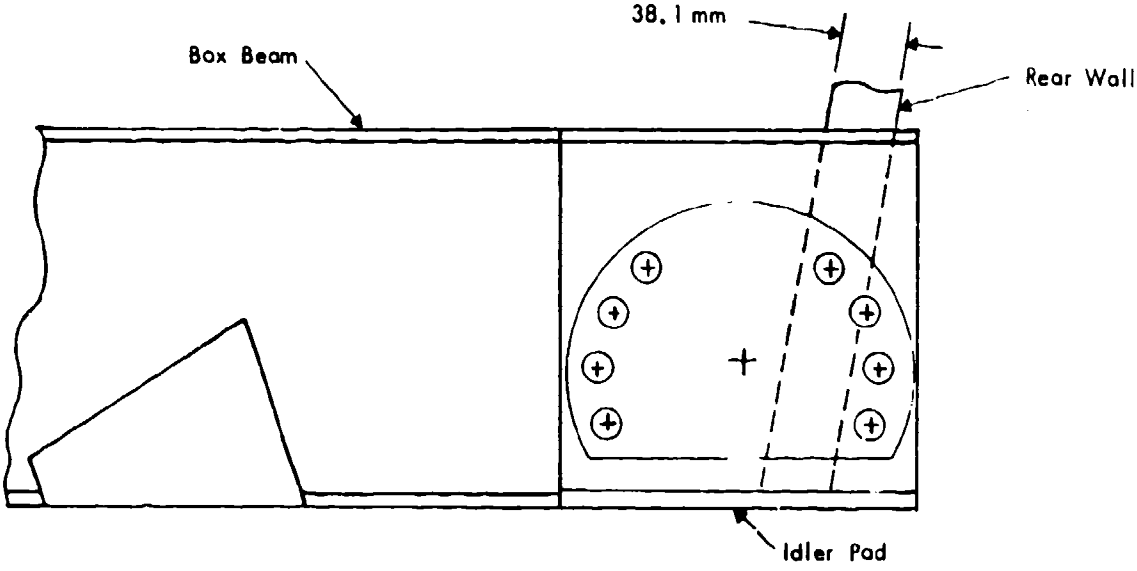
38.1 mm
Box Beam
Rear Wall
Idler Pad

M113A1, FMC DWG 10932751

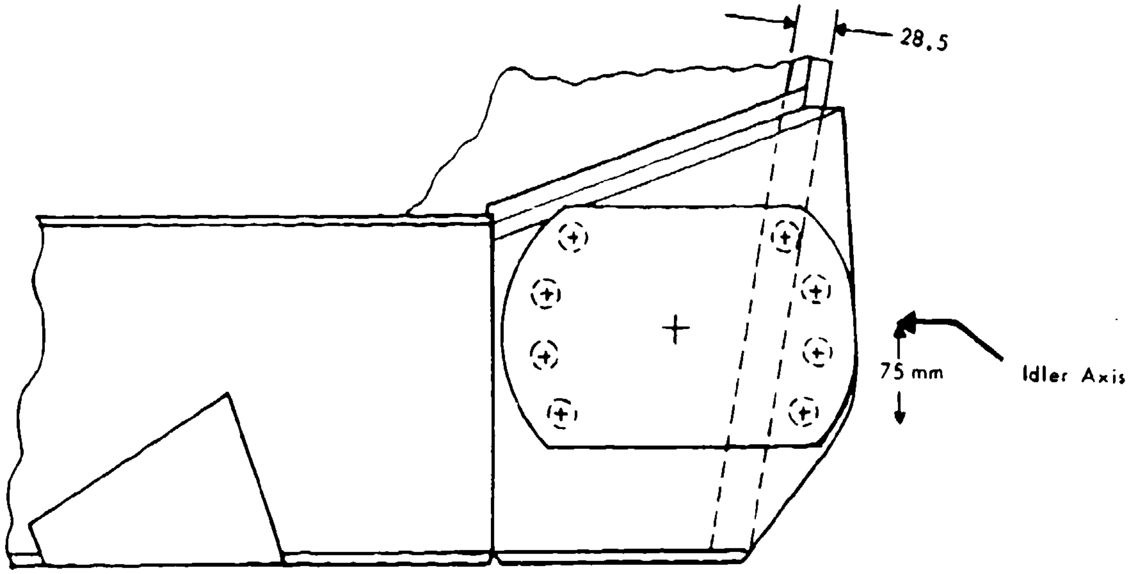
28.5
75 mm
Idler Axis

AIFV, FMC DWG 4179145

Figure 4.6 Comparison of Left Idler Pads for AIFV and M113

AIFV; the differences suggest the likelihood of asymmetries in the noise transmission characteristics of the idler attachments. Similar differences in longitudinal position of left and right idlers occur on the M113A1 and are to allow for fitting of the torsion bars from left and right sides; the left track has one more shoe than the right track. Figure 4.6 shows the differences in idler attachment pad location, with regard to vertical positioning of the idler spindle relative to the box-beam: the idler spindle on the AIFV is located some 64mm higher than on the M113A1 (on each side of the vehicle).

Certain directions for the comparison of the two classes of vehicles become clear from this brief comparison. Experimentally, it would be of interest to explore, in addition to absolute differences between the two vehicles, the potential asymmetries in hull dynamic response and attachment point inertance which may occur between left and right sides of each vehicle, and whether, for the AIFV, these are influenced by the turret mass. On the other hand, the influences of alternative idler locations, of fuel tank/rear plate configuration, and of the details of changes in hull cross section are more practically studied analytically with the finite-element model of the hull structure. This work is described later in the report. The work reported below describes the experiments carried out and the results of the various comparisons made of the two vehicles.

4.3 Power Flow Analysis

4.3.1 Review of Concepts

Statistical energy analysis (SEA) provides a convenient means of describing the flow of vibrational and acoustic power between connected systems, in terms of gross parameters such as the energy levels, modal densities, and overall physical properties of the connected structures and/or acoustic spaces involved. A review of the concepts involved can be found in references [16] and [17]; a summary of relevant equations, using metric units, is presented below.

The vibratory power dissipated in a panel structure W_d (in watts) is given by

$$W_d = \omega\eta\langle v^2\rangle m, \qquad (1)$$

where

ω $(=2\pi f)$ is the circular frequency (radians/s),
η is the total structural loss factor (that is, the sum of the acoustic radiation and structural dissipation components),
$\langle v^2\rangle$ is the space-average mean-square velocity $(m/s)^2$,
$\langle a^2\rangle$ is the space-average mean-square acceleration $(m/s^2)^2$ and
m is the panel mass (kg).

Expressed in engineering units and in terms of space-average mean-square accelerations, this equation becomes

$$L_{wd}\ (\text{dB re } 10^{-12}\ \text{watts}) = AL\ (\text{dB re 1 g}) + 10 \log \frac{\eta m}{f} + 131.8 \quad (2)$$

where

1 g = 9.8 m/s^2 and
AL is the acceleration level, calculated as $AL = 10 \log [\langle a^2 \rangle / (1\ g)^2]$

The power radiated from a plate W_r (in watts) is calculated from measured plate acceleration levels according to

$$W_r = S \rho c \sigma \langle a^2 \rangle / \omega^2 \quad (3)$$

where
S is the panel surface area (m^2),

ρc is the characteristic impedance of the acoustic medium (for air, ρc is about 415 mks rayls, where mks rayls = kg/m^2/s), and
σ is the (nondimensional) radiation efficiency of the plate.

σ is a function of the plate critical frequency f_c, the plate area, and the length of attached stiffeners. f_c is calculated as 12600/h, where h is the plate thickness in mm. In engineering form, equation (3) becomes

$$L_{wr}\ (\text{dB re 1 pW}) = AL\ (\text{dB re 1 g}) + 10 \log \sigma + 10 \log (S/f^2) + 150.0 \quad (4)$$

The net acoustic power flow into the vehicle interior is balanced by that absorbed on the vehicle bounding surfaces and by its occupants, W_{abs} (in watts). For a reverberant acoustic space, with air as the acoustic medium this balance is given as

$$L_{wr} = W_{abs} = \langle p_i^2 \rangle V \omega \eta_i / \rho c^2 \quad (5)$$

where

$\langle p_i^2 \rangle$ is the space-averaged mean-square interior acoustic pressure (Pa^2),
V is the interior volume (m^3), and
η_i is the interior acoustic loss factor

Equation (5) may be expressed in engineering terms by

$$L_{wa}\ (\text{dB re 1 pW}) = L_p\ (\text{dB re } 20 \mu\text{Pa}) + 10 \log (V f \eta_i) - 17.5 \quad (6)$$

where the interior speed of sound is taken as 343 m/s. It is noted that the interior acoustic loss factor relates directly to the interior reverberation time T_{60} as $\eta_i = 2.2/(T_{60} f)$. Equations (2), (4), and (6) describe the balance of structural and acoustic energy levels within the vehicles: these may be calculated from measurements of acceleration levels and structural loss factors, measurements of the interior noise levels and acoustic loss factors, and from the system geometry.

In the following sections, these quantities measured on the AIFV vehicle are contrasted with existing data for the M113A1 vehicle presented in Reference [17]. M113A1 data were recorded on vehicle number SJ136, at 32 km/hr (20 mph) during normal underway paved track operation. AIFV numbers NSJ0005 and NSJ0002 were used for tests; underway data at a range of track speeds were recorded and analyzed for both. Emphasis here is placed on the NSJ0005 vehicle, as this vehicle is the quieter of the two, although limited NSJ0002 data is presented to allow comparisons between these two vehicles to be made. Comparisons between vehicles are made at 32 km/hr (20 mph).

4.3.2 Measured Results

4.3.2.1 Hull Vibration Levels

Vibration levels were measured at about 40 locations on those interior radiating surfaces of the AIFV expected to determine the interior acoustic power flow. Table 4.1 presents space-averaged mean-square acceleration levels for the major radiating interior panels. The analysis was carried out in one-third octave bands, but data is presented in octave bands, and in general, three measurement locations were used to calculate the average for each panel. The standard deviation in acceleration level between different locations on the same panel was, in general, less than 1 dB at 250 Hz and less than 0.5 dB at 1000 Hz.

The AIFV vibration levels on the left-hand hull panels are generally 3 to 5 dB greater than those on the corresponding right-hand panels, as shown in Figure 4.7(a) for the sponsons and upper side plates. This is in contrast to M113A1 data which shows the right-hand panel vibration levels to be marginally greater than those on the left-hand side (Figure 4.7 (b)). Similar but weaker trends were observed on the NSJ0002 vehicle as for the NSJ0005 vehicle.

Figures 4.8(a) and 4.8(b) compare the underway acceleration levels on similar hull surfaces of the AIFV and M113A1 tracked vehicles: almost universally, the AIFV levels are 7 to 10 dB lower than those on the M113A1 hull.

It is clear from these data that the suspension attachment point response and the force-to-noise transfer functions should be examined for asymmetries between left and right sides of the vehicle.

4.3.2.2 Interior Noise Levels

The dependence on forward speed of the A-weighted interior sound levels for the AIFV vehicles tested is presented in Figure 4.9. The mean sound levels and the associated 1σ limits are shown for the NSJ0005 vehicle and found to plateau to a maximum level of 110 dB(A) as forward speed increases above 40 km/hr (25 mph). This is in contrast to data measured for two other vehicles, NSJ0002 and NSJ143, in which the sound level increases with increasing speed above 30 km/hr.

TABLE 4.1

SPACE-AVERAGED MEAN SQUARE ACCELERATION LEVEL, DB RE 1 G FOR THE AIFV NSJ0005 AT 32 KM/HR (20 MPH).

PANEL	AREA (m2)	THICKNESS (mm)	Octave Band Center Frequency - Hz							
			63	125	250	500	1k	2k	4k	8k
Bottom Plate	4.1	28.1	-1.6	-1.4	-2.2	-5.0	-5.8	-5.3	-7.2	-16.1
Floor Plates	4.1	5.0	-0.8	3.4	0.4	0.2	2.2	-4.3	-5.6	-13.8
Upper Side Plate:										
Left	3.4	28.1	-8.8	-6.2	-4.1	-6.9	-6.9	-7.1	-5.7	-14.2
Right	2.4		-11.7	-13.3	-6.9	-5.6	-6.8	-9.4	-8.7	-17.8
Inclined Side Plate:										
Left	1.4	38.1	-2.6	-6.5	-5.2	-8.8	-7.3	-9.7	-9.8	-17.1
Right			-9.1	-9.2	-7.4	-10.2	-10.2	-13.7	-14.7	-22.0
Sponson:										
Left	2.0	12.5	-6.5	-8.3	-6.4	3.8	2.8	1.9	5.3	-3.9
Right	1.3		-7.8	-10.4	-7.4	0.9	-2.6	-1.1	1.0	-9.6
Lower Side Plate:										
Left	1.1	31.8	-2.1	-5.0	-5.4	-6.1	-3.8	-6.2	-5.7	-12.2
Right	0.8		-3.3	-10.8	-7.2	-8.3	-4.9	-4.5	-4.9	-13.6
Engine Access Panel	1.0	6.0	-1.9	-2.3	-0.6	-2.5	-1.4	-1.2	-4.1	-13.4
Ramp	2.3	38.1	-9.9	-8.8	-11.9	-11.5	-12.2	-20.2	-20.6	-30.5
Top Plate	9.6	38.1	-5.5	-2.1	-7.1	-7.9	-7.5	-14.9	-14.3	-23.8
Cargo Hatch	1.0	38.1	2.3	-5.5	-6.4	-7.7	-8.5	-8.2	-9.1	-11.6

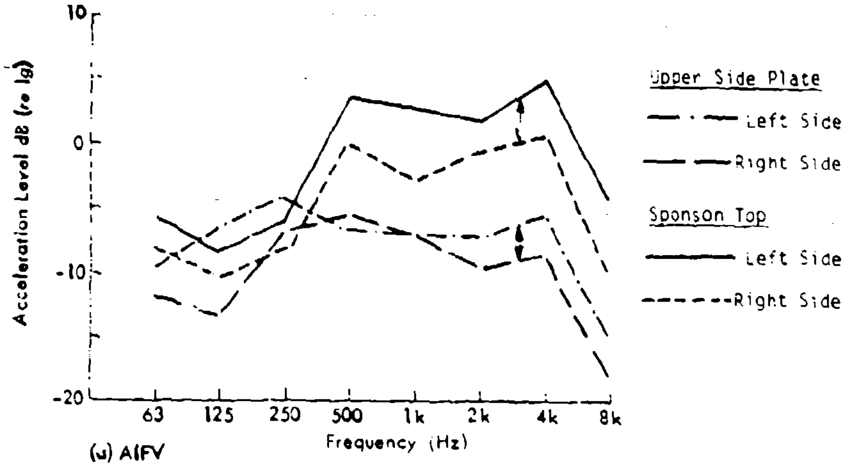

(a) AIFV

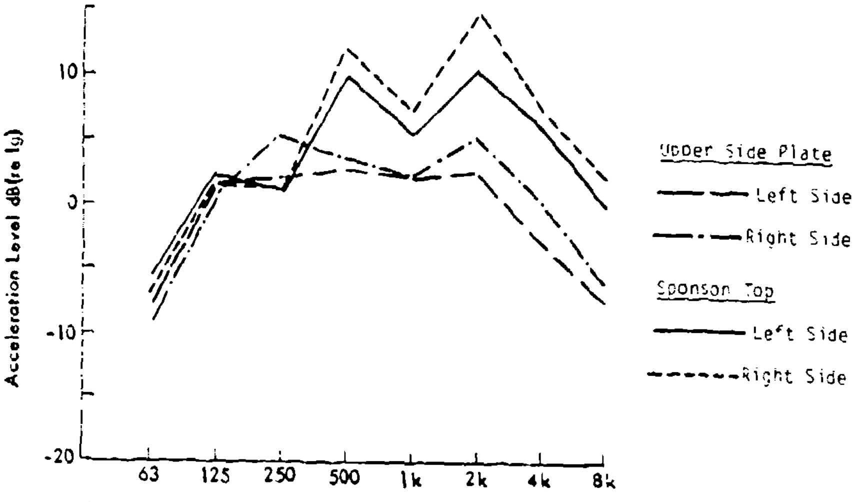

(b) M113A1

Figure 4.7 Comparison of Hull Acceleration Levels on Left and Right Hand Sides of Tracked Vehicles at 32 km/h (20 mph) (a) AIFV #SJ0005, (b) M113A1 (on blocks (16)).

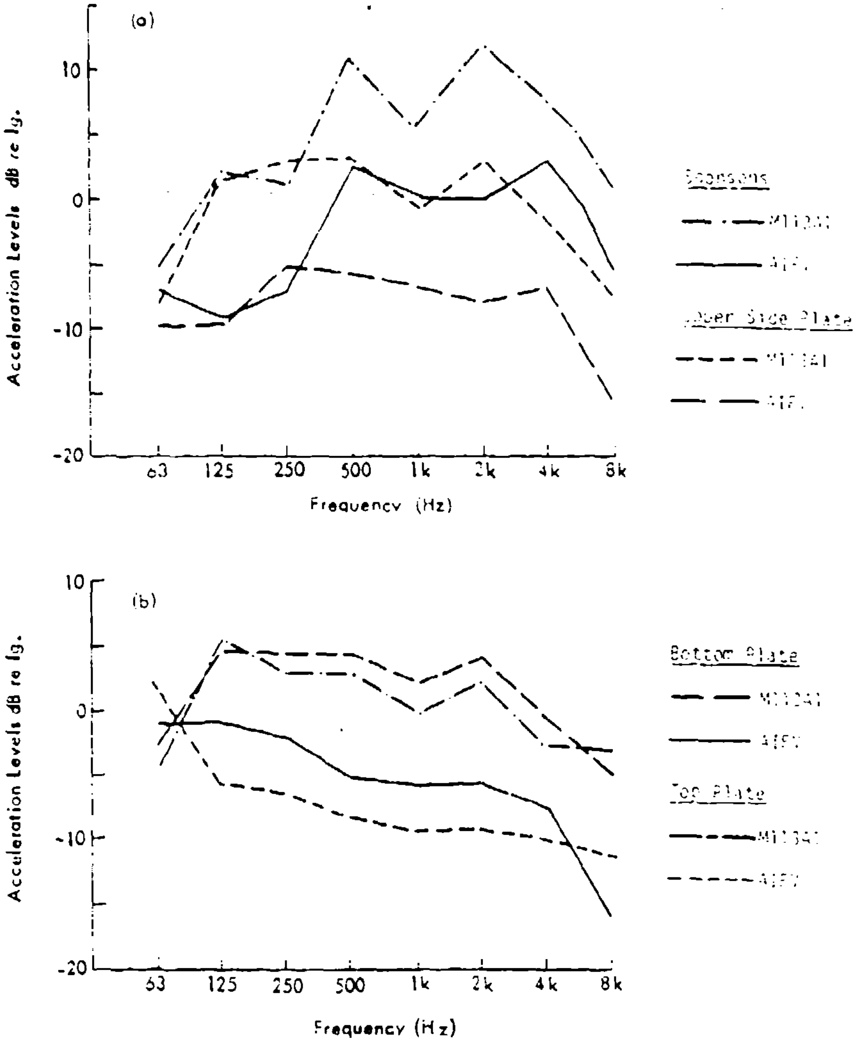

Figure 4.8 Comparison of Acceleration Levels on Similar Hull Surfaces on AIFV and M113A1 Tracked Vehicles Underway at 32 km/h (20 mph).

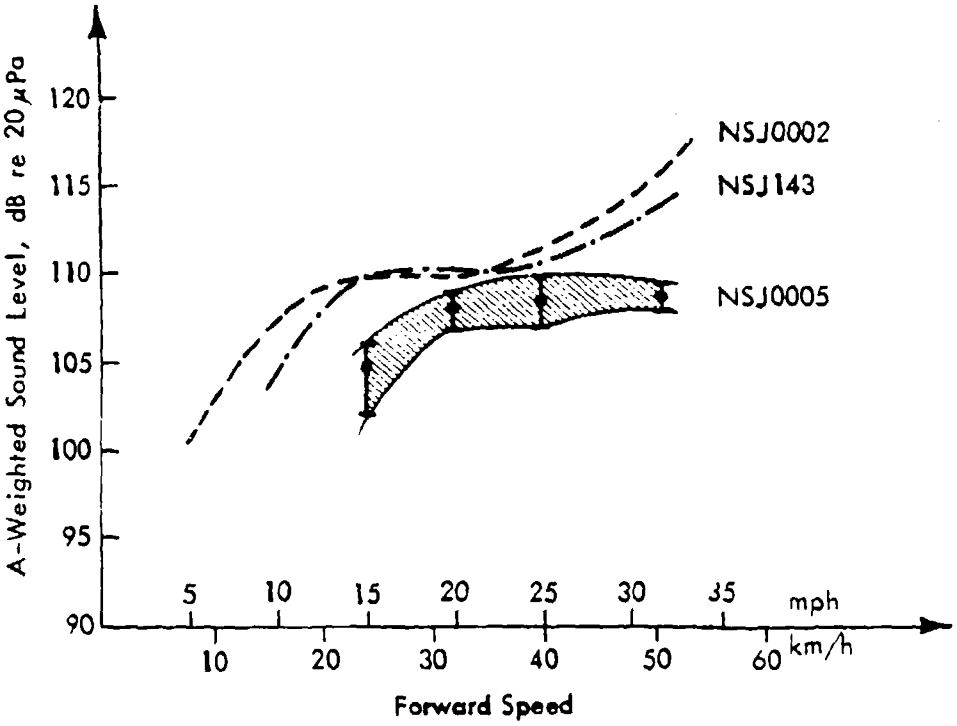

Figure 4.9 Dependence of A-Weighted Interior Sound Level on Vehicle Speed for the Vehicles Tested.

Figure 4.10 shows interior sound level spectra for the under way AIFV vehicles tested at a forward speed of 32 km/h (20 mph). Also shown is the spectrum of the M113A1 sound level, taken from Figure 6 of [16]. The interior spectrum levels for the AIFV are generally 5 dB lower than those in M113A1 vehicle, the differences for AIFV NSJ0005 being only marginally less than the differences in hull panel acceleration levels presented in Figure 4.8. Measured octave band spectra of the AIFV interior sound levels, showing the dependence on vehicle forward speed, are given in Figures 4.11 and 4.12 for vehicles NSJ0005 and NSJ0002, respectively; the speed characteristics of the two vehicles are quite different, reflecting slight differences in construction detail, tolerances, or track condition. The differences in interior sound levels between the two AIFV vehicles compare closely with the differences in hull panel acceleration levels. For example, at those forward speeds where NSJ0002 sound levels exceed the NSJ0005 levels, NSJ0002 acceleration levels exceed the NSJ0005 acceleration levels by similar amounts.

4.3.2.3 Hull Radiation Efficiencies

While the structural characteristics of the lower section of the AIFV and M113A1 vehicles are essentially the same in terms of their radiation properties, the upper portions of the AIFV are smaller in area and thinner than for the M113A1, with resulting differences in radiation efficiencies. Figure 4.13 compares the calculated radiation efficiencies for various AIFV hull elements with those for the M113A1 hull taken from Reference [17]. The AIFV appears to have slightly greater radiation efficiencies, but the differences are generally less than 3 dB. This 3 dB, when subtracted from the 7 to 10 dB difference in acceleration levels between AIFV and M113A1 vehicles, matches closely the differences in interior sound level shown in Figure 4.10 to exist between the two vehicles.

4.3.2.4 Structural and Acoustic Loss Factor Data

Loss factor information for the hull and interior space is used to determine the energy dissipation occurring in the two systems. Structural decay measurements were made using an impulse technique, while acoustic decays involved interrupting a steady-state interior acoustic signal and observing the decay rate.

Structural loss factors for AIFV and M113A1 vehicles are presented in Figures 4.14 and 4.15. Data were measured on the larger hull surfaces, but there appears little significant difference between the different locations. Further there are no significant differences between the loss factors of the two vehicles, being typical of welded built-up aluminum or steel structures. The bolt-on armor plating does not appear to provide any significant hull damping because the foam core is not sufficiently stiff to resist deformation. The calculated radiation loss factor for the AIFV roof is shown in Figure 4.14, ($\eta_{rad}=2\rho c S \sigma / \omega m$): this curve, which is representative of all the

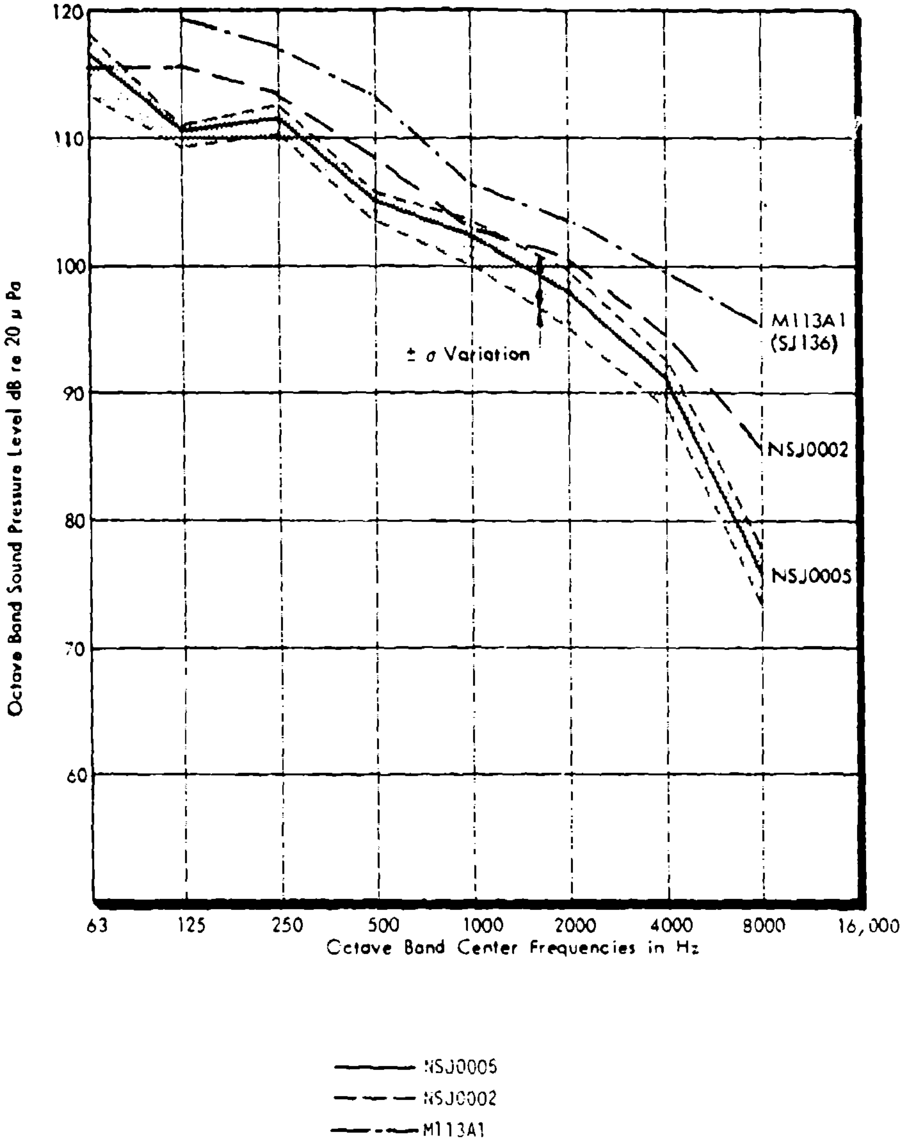

Figure 4.10 Crew Position Interior Sound Level Spectra for Underway AIFV Vehicles at 32 km/h (20 mph).

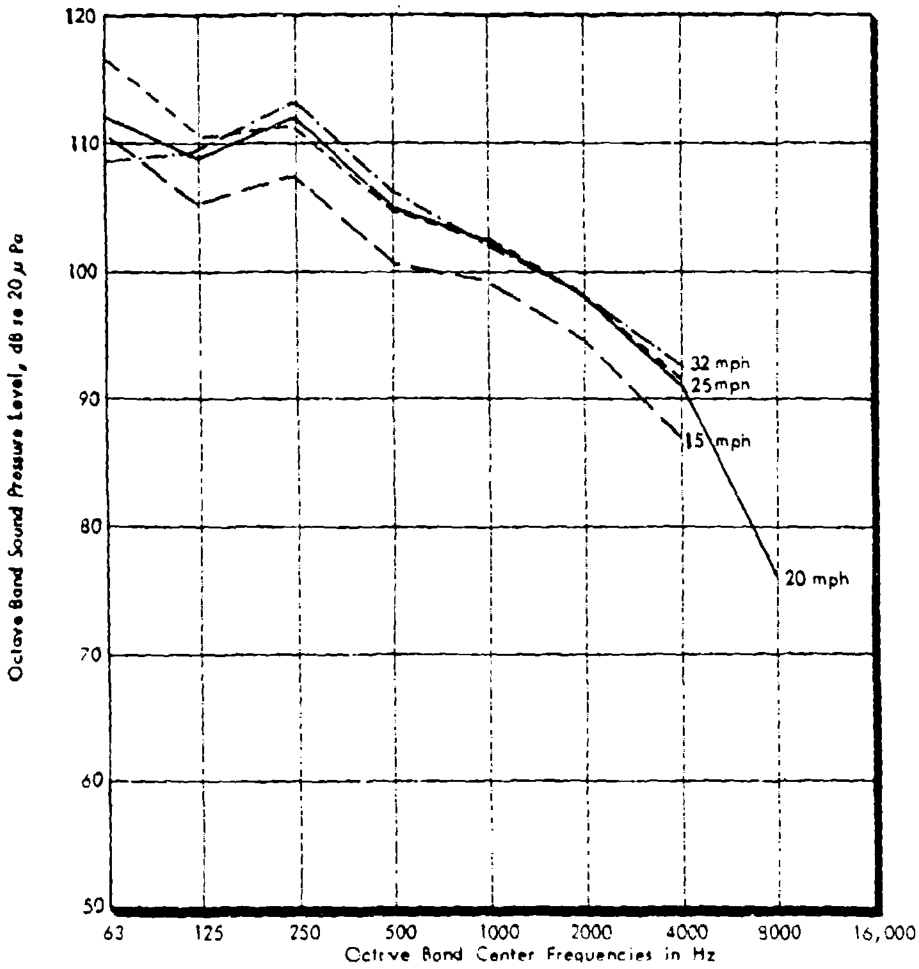

Figure 4.11 Interior Sound Level Spectra, AIFV NSF0005, Showing the Effect of Forward Speed.

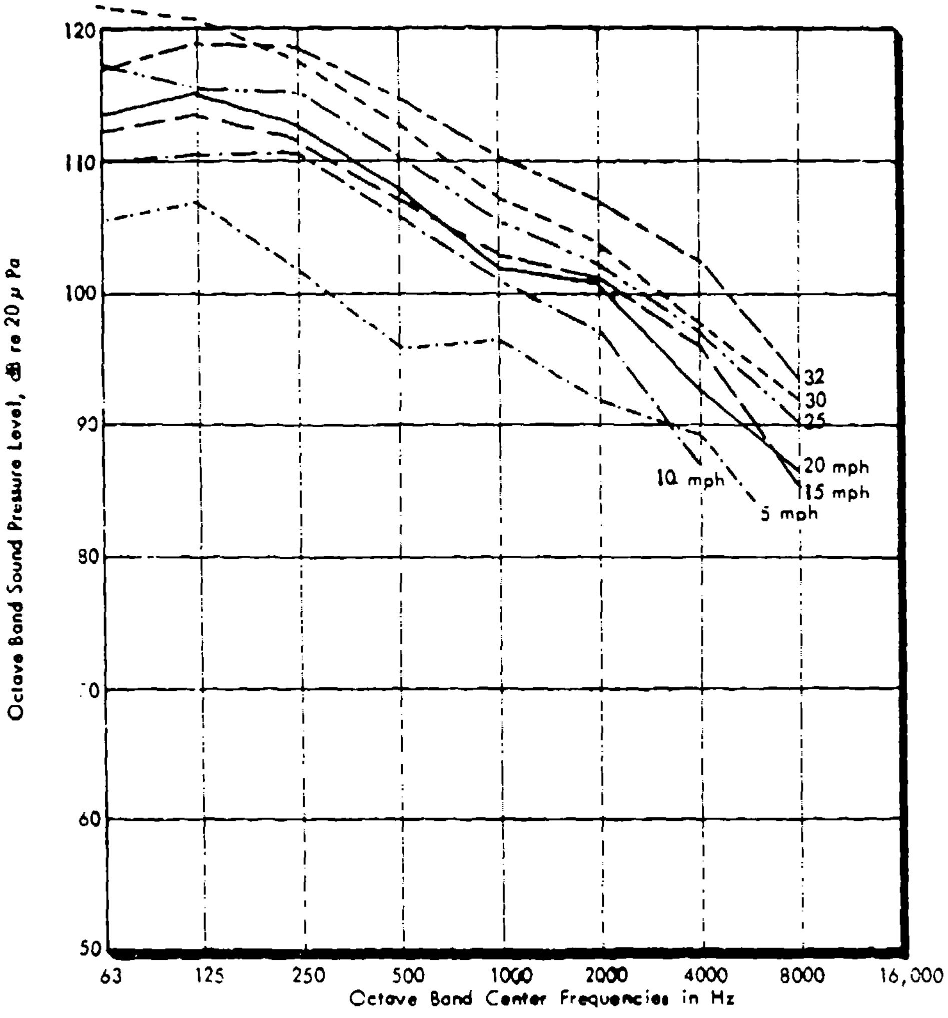

Figure 4.12 Effect of Forward Speed on Interior Sound Level Spectra for AIFV NSJ0002.

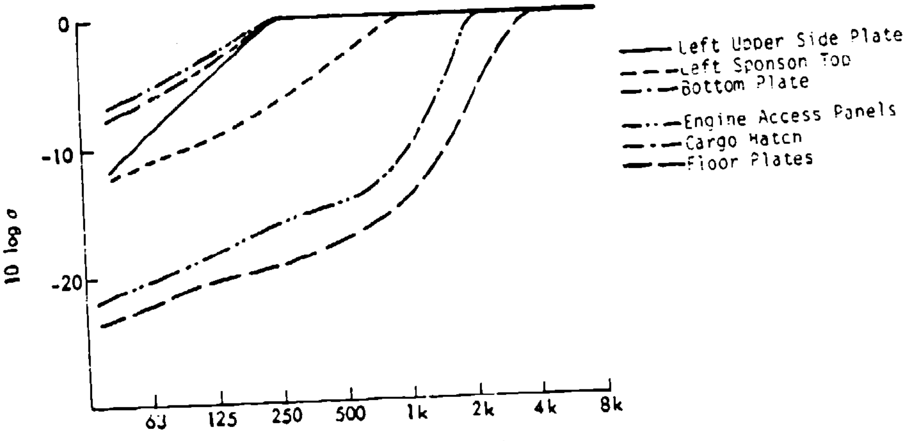

(a) AIFV (NSJ0005)

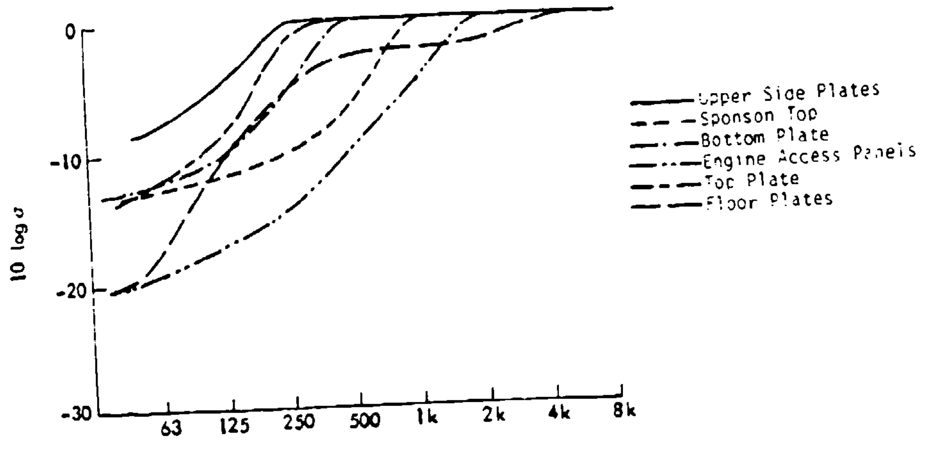

(b) M113A1 (SJ136)

Figure 4.13 Calcualted Radiation Efficiencies for Typical Hull Panels.

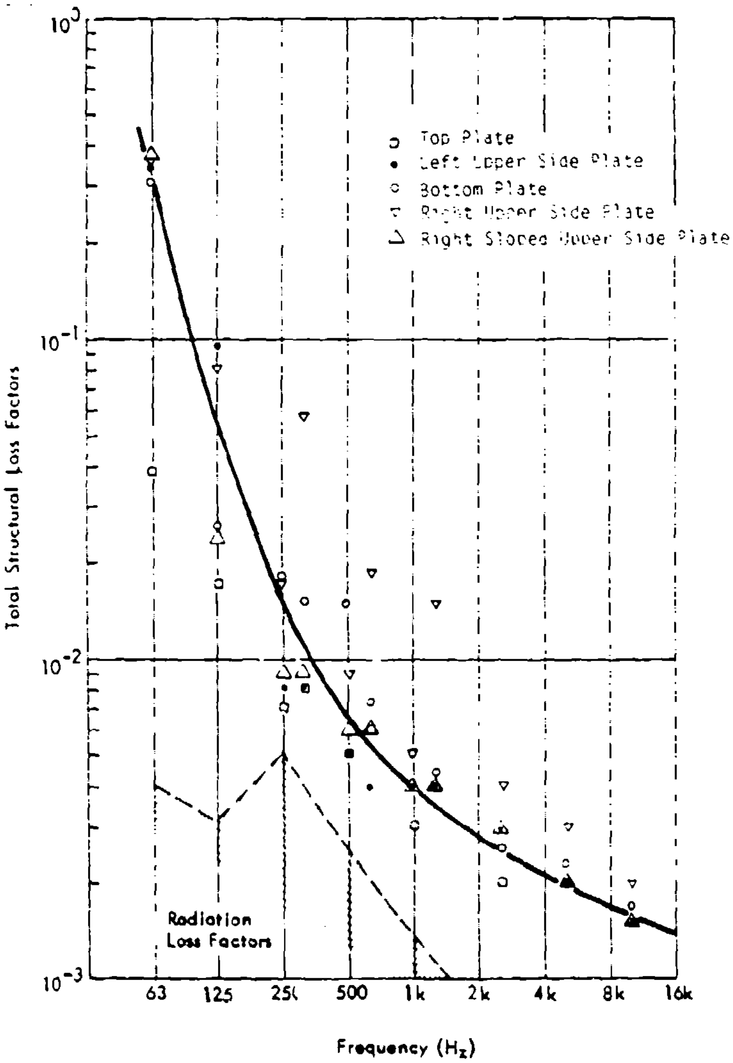

Figure 4.14 Structural Loss Factor Data AIFV (NSJ0005).

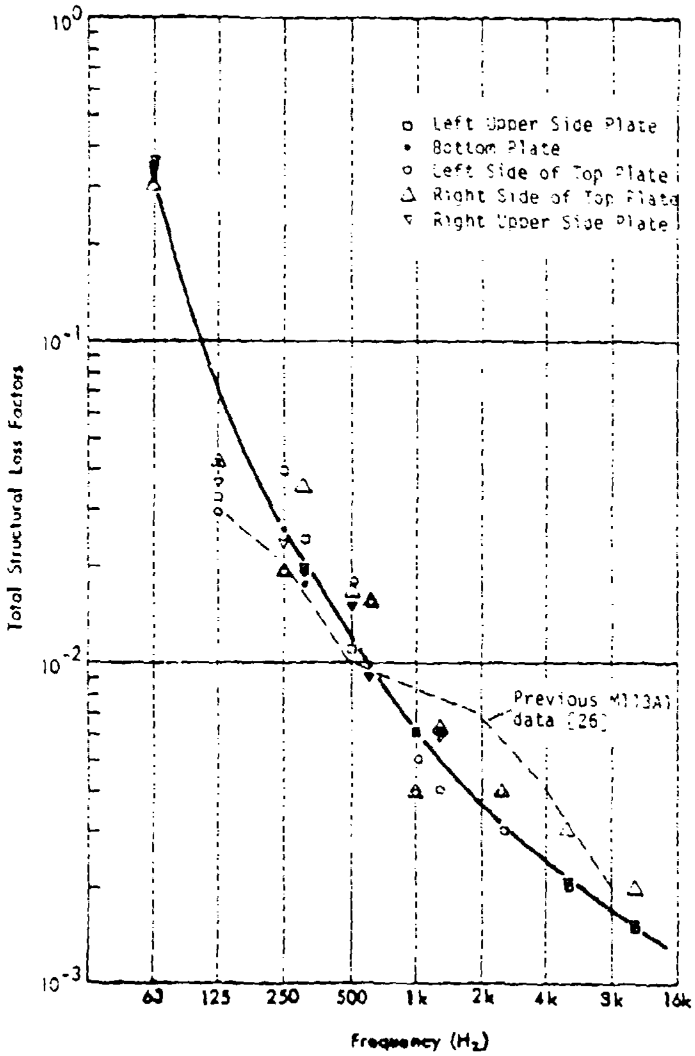

Figure 4.15 Structural Loss Factor Data M113A1 (S[illegible]36).

radiating surfaces, lies well below the hull total loss factor curves suggesting that internal losses dominate the energy dissipation process. As noted previously [26] there appears considerable scope for increasing the hull total loss factors, particularly at frequencies above 125 Hz. Whether this is practical below 500 Hz in view of the influence of long wavelength vibration modes [1], remains to be seen.

Acoustic loss factors of the interior space are presented in Table 4.2, together with the averaged hull loss factors. Good similarity between previous acoustic reverberation times and present data was found.

4.3.2.5 Power Flow Calculations

Calculations for the underway AIFV (NSJ0005) of the power dissipated in the hull structure and the power dissipated by radiation from hull panels into the hull interior, and calculations of the interior acoustic power level absorbed in the hull, were made following equations (1) through (6). The interior acoustic dissipated power levels were calculated from the measured octave-band noise levels (Figure 4.10) and the loss factor data in Table 4.2. Hull dissipated and radiated power levels for individual panels were calculated from averaged panel octave-band acceleration measurements (Table 1.1), hull loss factors (Figure 4.14) and calculated radiation efficiencies (Figure 4.13(a)).

TABLE 4.2

LOSS FACTOR DATA FOR HULL STRUCTURE AND INTERIOR ACOUSTIC VOLUME FOR THE AIFV VEHICLE

Octave Band Center Frequency (Hz)	Hull Loss Factor	Interior Volume Loss Factor
63	0.30	0.065
125	0.055	0.037
250	0.015	0.021
500	0.0065	0.012
1k	0.0040	0.0074
2k	0.0028	0.0037
4k	0.0022	0.0025
8k	0.0016	0.0014

The power balance results are presented in Figure 4.16 for 32 km/hr (20 mph) forward speed. Also shown are the baseline interior acoustic power levels for the M113A1 vehicle [26]. The acoustic power radiated from the hull surfaces (Figure 4.16, curve 3) closely matches the acoustic power level dissipated (i.e., absorbed) within the hull interior space (curve 2), as was found for the M113A1 vehicle [17]. The hull dissipated power due to structural damping mechanisms (Figure 4.16, curve 1)

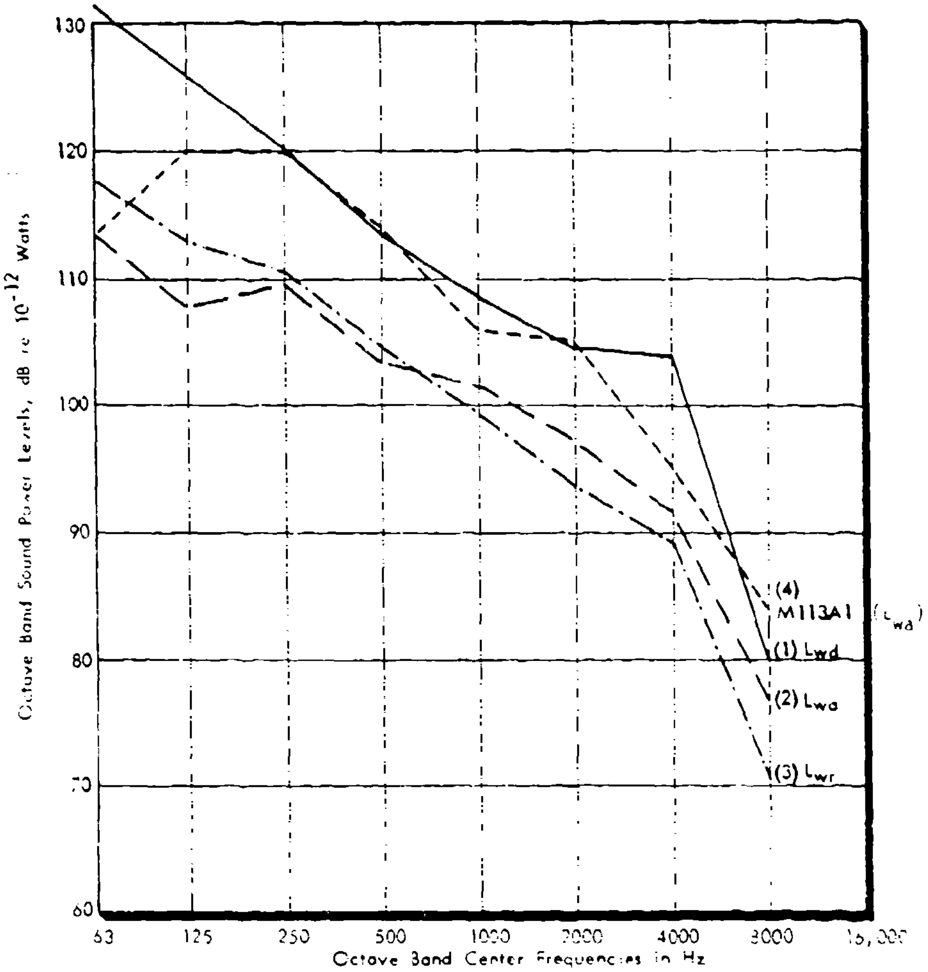

Figure 4.16 Comparison of Hull Dissipated (L_{wd}), Hull Radiated (L_{wr}), and Acoustic Dissipated (L_{wa}) Power Levels; AIFV (NSJ0005) at 32 km/hr (20 mph), Test Track Data.

exceeds by up to 10 dB the power dissipated by radiation from the hull surfaces, even allowing for radiation from the vehicle exterior. The acoustic disipated power levels for the M113A1 (Figure 4.16, curve 4) taken from [17], are up to 10 dB greater than those presently measured on the AIFV NS00005 under similar test conditions (curve 2), consistent with the differences in interior noise level spectra.

Figure 4.17 shows the calculated major contributors to the hull radiated power levels for the AIFV at 32 km/hr (20 mph). The bottom plate is clearly the dominant source at frequencies less than 500 Hz, and the panel elements on the left side of the vehicle contribute significantly greater power than those on the right side. Figure 4.17b shows the calculated major contributors to the hull radiated power levels for the M113A1 at 32 km/hr (20 mph) for comparison with the AIFV. The contributions from the top panel, upper side panels and lower side panels (both left and right combined) are similar and to avoid confusion are represented by a single curve. The data used for the curves are from reference [17], where data for the left and right sides have been combined and only the totals presented. Thus, no distinction is made as to which side radiates more power. For the M113A1 vehicle, Figure 4.17b shows that the sides and top are the most important contributors. The AIFV top plate is a relatively weak contributor, in contrast to the situation for the M113A1. The smaller-element, stiffer cross-section of the AIFV hull appears to block the flow of vibrational energy from attachment point to the vehicle top surface.

As for the M113A1, however, barriers would not be a practical form of noise control due to the relatively large radiating areas.

4.3.3 Discussion

The major observations to be made from these measurements and calculations are:

1. The AIFV hull vibration levels, particularly in the top plate, are significantly lower than in the M113A1 vehicle during underway track operation. These differences are similiar to the differences in interior sound levels.

2. The major radiating hull elements are the bottom plate and the upper side plates at low frequencies, with the sponsons becoming dominant at frequencies above their fundamental spanwise resonance. This is in contrast with the M113A1 where the top plate controlled the interior sound levels.

3. Statistical Energy Analysis provides a useful framework for understanding the power flow between structure and interior space even at frequencies as low as 250 Hz.

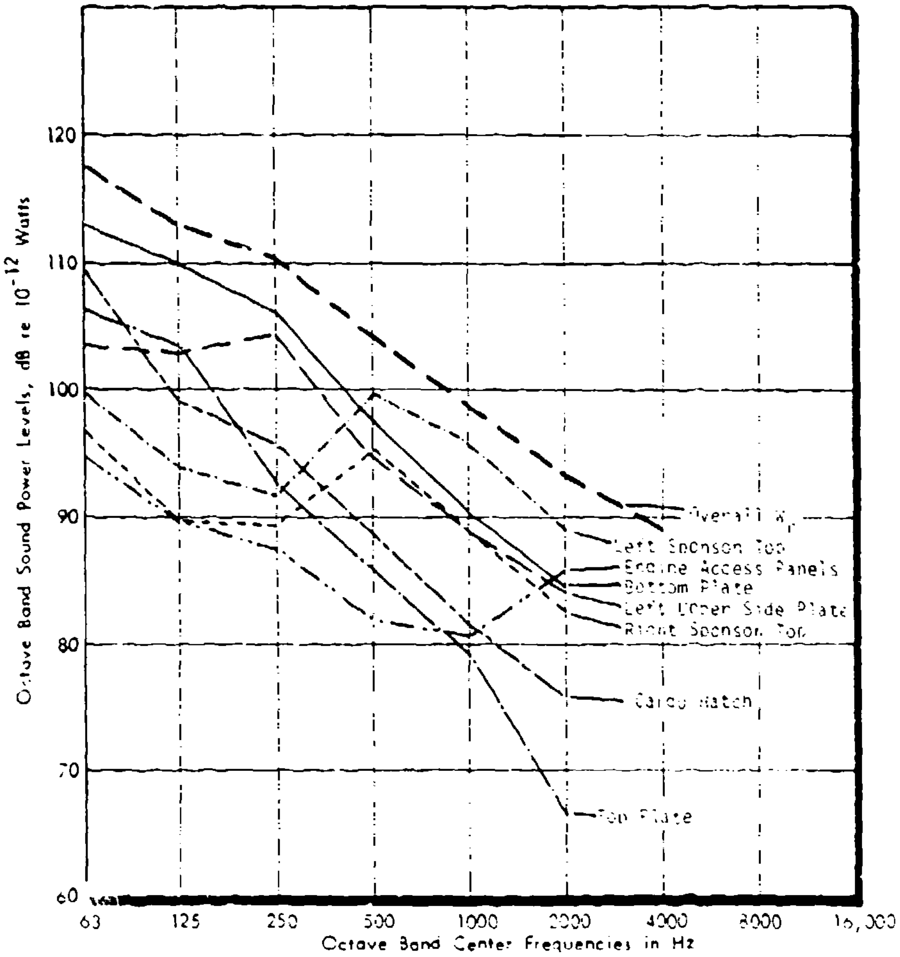

Major Contributors Within 10 dB of Total Radiated Power

Figure 4.17a Major Contributors to the Hull Radiated Power Levels, AIFV (NSJ0005) at 32 km/H (20 mph) Test Track Data.

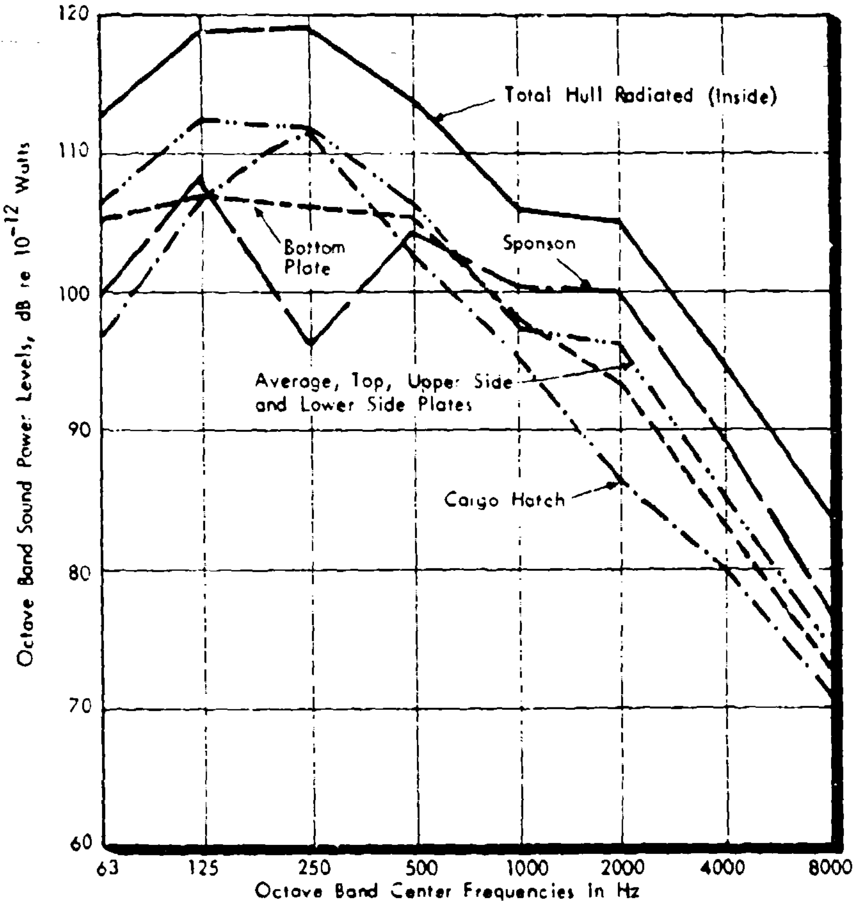

Figure 4.17b Major Contributors to the Hull Radiated Power Levels, M113A1 Vehicle at 32 km/h (20 mph) Supported on Jackstands

Previous experiments showed that surface damping treatments are unlikely to significantly reduce interior sound levels, even though the response of the hull is primarily resonant. This is mainly due to the difficulty in damping modes with a long structural wavelength, which are important contributors to the overall structural response and acoustic radiation.

Composite structures of the same mass and bending stiffness (for strength purposes), and consequently having the same resonance frequency distribution, will be no more amenable to damping than the existing plate configuration: this is because the wavelength of the structural modes will be unchanged as a function of frequency. Composite structures of the same mass but lower stiffness (ignoring strength considerations) will have a higher modal density, but will be more amenable to structural damping techniques. It is believed that these two factors will offset each other, since the vehicle's resonant response is proportional to the modal density (which will increase) and inversely proportional to the structural loss factor (which will increase). In fact, preliminary analysis indicates that the vehicle response will increase, rather than decrease as required. While composite structures involving laminated damping layers may provide an advantage, an analysis of the potential benefits as a function of structural stiffness, mass, and loss factor (which itself depends on these two parameters) should be developed to guide any empirical study. It is recommended that such studies be undertaken before any experimental work is considered.

4.4 Hull Attachment Point Transfer Function Analysis

4.4.1 General

Attachment point noise-to-force transfer functions (T.F.'s) and inertances were measured on AIFV and M113A1 vehicles for various configurations in an attempt to determine the influence of the differences in hull construction on the power accepting capability of the two hulls. The measured data are presented and discussed below. The instrumentation system used is shown in Figure 4.18. Inertance is defined as the transfer function between acceleration output and force input, where the acceleration is measured at the point of application of the force,

$$H(j\omega) = \frac{a(j\omega)}{F(j\omega)} = \frac{|a|e^{j\alpha}}{|F|e^{j\beta}} = \frac{|a|}{|F|}e^{j(\alpha-\beta)}$$

so that $|H(j\omega)| = \frac{|a|}{|F|}$ is the inertance magnitude and

$\phi(j\omega) = (\alpha-\beta)$ is the inertance phase angle.

4.4.2 Noise-to-Force Transfer Functions

Differences between left- and right-side noise-to-force T.F.'s at the idler spindle in both vertical and horizontal directions were measured on the AIFV NSJ0005 and M113A1 SJ136 vehicles: the reduced data are

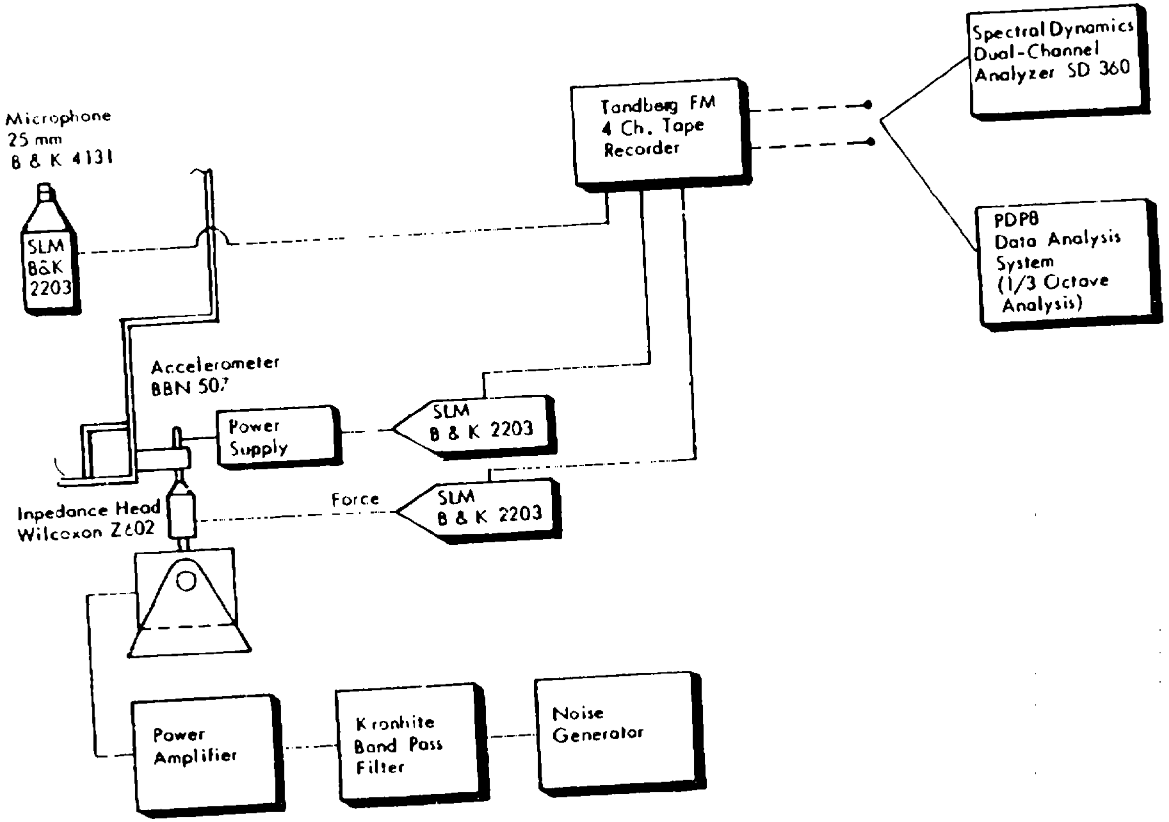
Microphone
25 mm
B & K 4131
SLM
B&K
2203
Accelerometer
BBN 507
Power
Supply
SLM
B & K 2203
Force
SLM
B & K 2203
Inpedance Head
Wilcoxon Z602
Tandberg FM
4 Ch. Tape
Recorder
Spectral Dynamics
Dual-Channel
Analyzer SD 360
PDP8
Data Analysis
System
(1/3 Octave
Analysis)
Power
Amplifier
Kronhite
Band Pass
Filter
Noise
Generator

Figure 4.18 Instrumentation for Hull Inertance and Transfer Function Measurements.

shown in Figures 4.19 to 4.21. Figure 4.19 (a) shows left- and right-side noise-to-force T.F.'s for horizontal excitation of the idler spindle. The right-side T.F. is marginally higher than the left-side in the mid-frequency range, in comparison to the situation for the M113A1 hull (Figure 4.19 (b)), where differences of up to 6 dB in T.F. occur between 400 Hz and 1 kHz. Comparison of the average of left- and right-side horizontal data for the two hulls, as in Figure 4.21, shows that the noise-to-force T.F. for M113A1 hull exceeds that for the AIFV by 3 dB over most of the frequency range from 100 Hz to 1 kHz. (These trends are also reflected in the left/right AIFV/M113A1 horizontal inertance measurements as seen in Figures 4.22 and 4.23 in Section 4.4.3).

Data for vertical excitation of the idler spindles are presented in Figures 4.20 and 4.21. The right-side T.F. for the AIFV exceeds that for the left side by a value of about 3 dB over the whole frequency range (Figure 4.20(a)) in contrast to the case for the M113A1 hull (Figure 4.20(b)) where the left and right T.F.'s are similar. These are in contrast to the acceleration level differences between left and right sides of the AIFV vehicle shown in Figure 4.7(a). Left/right averaged data for the two hulls are compared in Figure 4.21(a), where the absolute differences in T.F. magnitude are seen to be about 10 dB at about 125 Hz decreasing to 1 to 2 dB at 1 kHz. (Again, these differences are in general agreement with those found in inertance measurement to be presented in Section 4.4.3).

We note that the present T.F.'s for the M113A1 hull are in good agreement with those previously presented in [16], Figure 35, which involved a similar measurement configuration.

4.4.3 Hull Inertance Transfer Functions

4.4.3.1 Left/Right Asymmetries - AIFV

Left- and right-side idler inertance measurements, both magnitude ($|H_2|$) and phase (ϕ), for horizontal and vertical excitation of the AIFV hull, with turret mounted on vehicle, are presented in Figures 4.22 and 4.23. In both directions, considerable asymmetry between left and right sides of the AIFV hull idler inertances exist, although this is strongest in the vertical direction and in the region of 1 kHz. At low frequencies, the horizontal hull inertances increase smoothly at about 12 dB per doubling of frequency, and the phase angle between acceleration and force is 180°, characteristic of a stiffness-controlled system. As frequency increases, hull resonances produce fluctuations in inertance magnitude and decreases in phase angle. In the vertical direction, the inertance magnitude fluctuates strongly at low frequency about the smooth horizontal inertance function; correspondingly strong variations in phase angle occur. Hull resonances are apparently more easily driven by a vertical idler force than by one in the horizontal direction. This is more clearly seen in Figure 4.24 where horizontal and vertical inertances are compared over the frequency range up to 200 Hz.

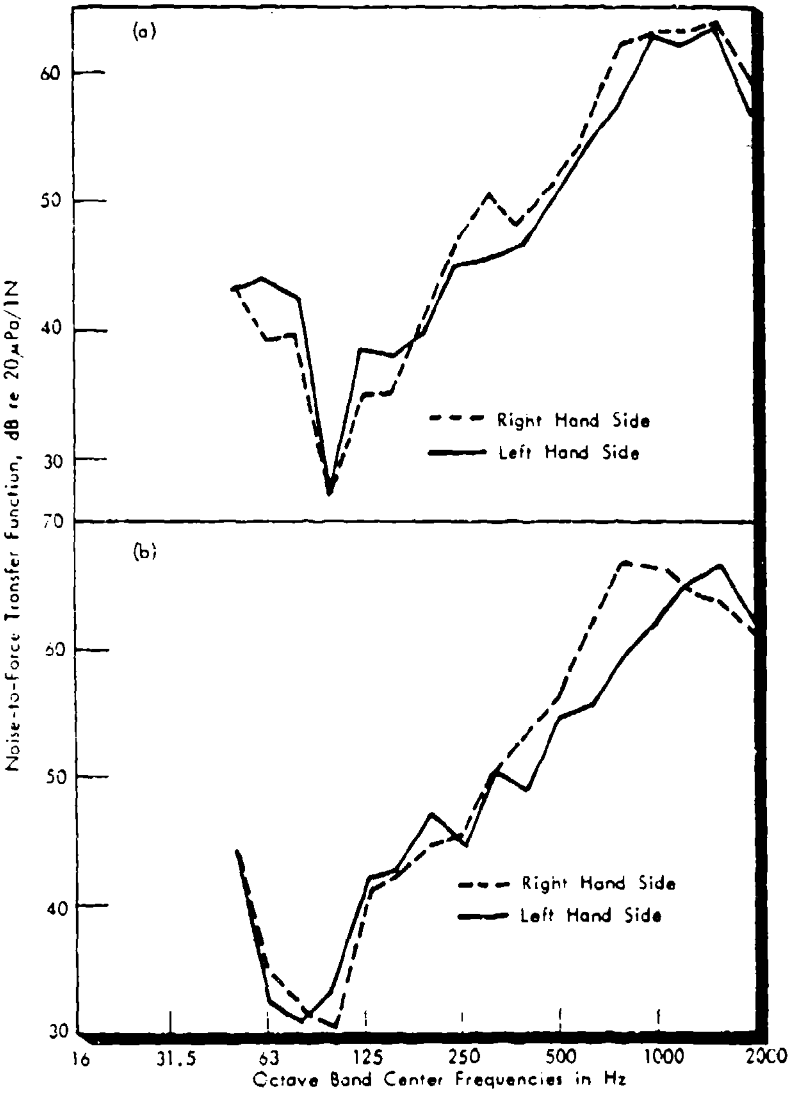

Figure 4.19 Noise-to-Force Transfer Functions for Horizontal Excitation of Idler Spindle (a) AIFV (b) M113A1.

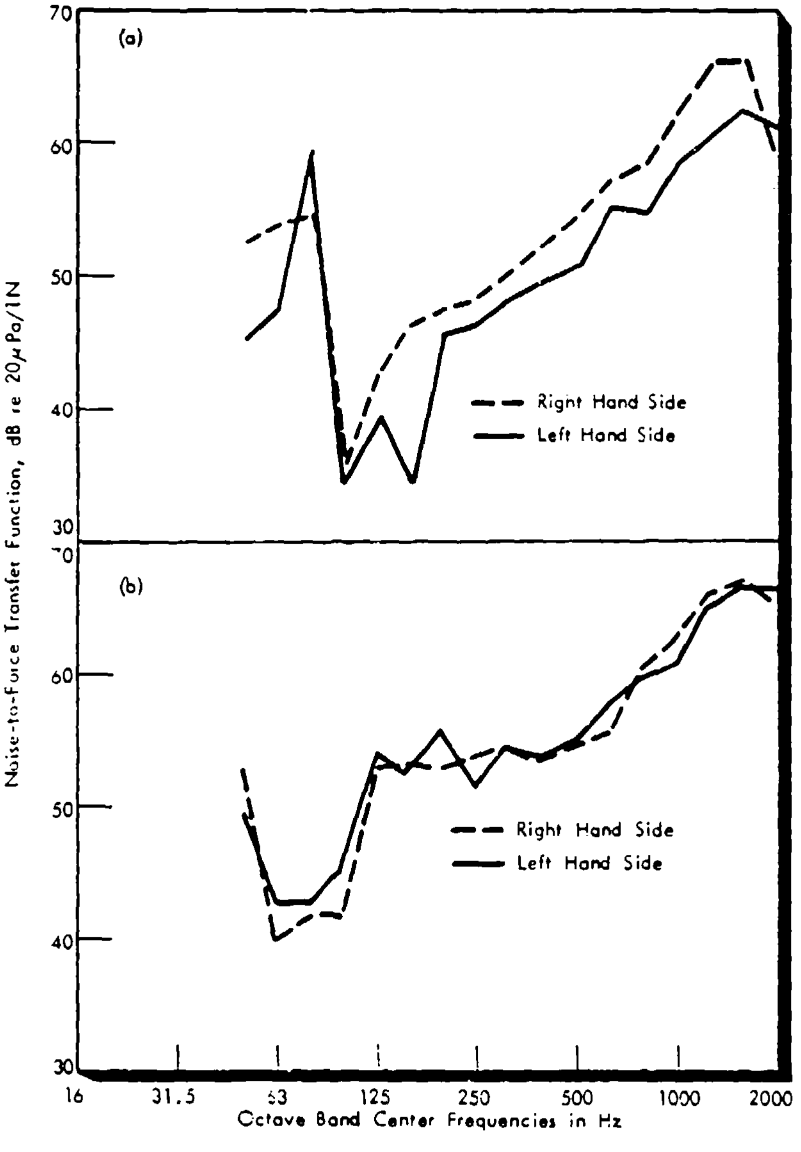

Figure 4.20 Noise-to-Force Transfer Function for Vertical Excitation of Idler Spindle (a) AIFV (b) M113A1.

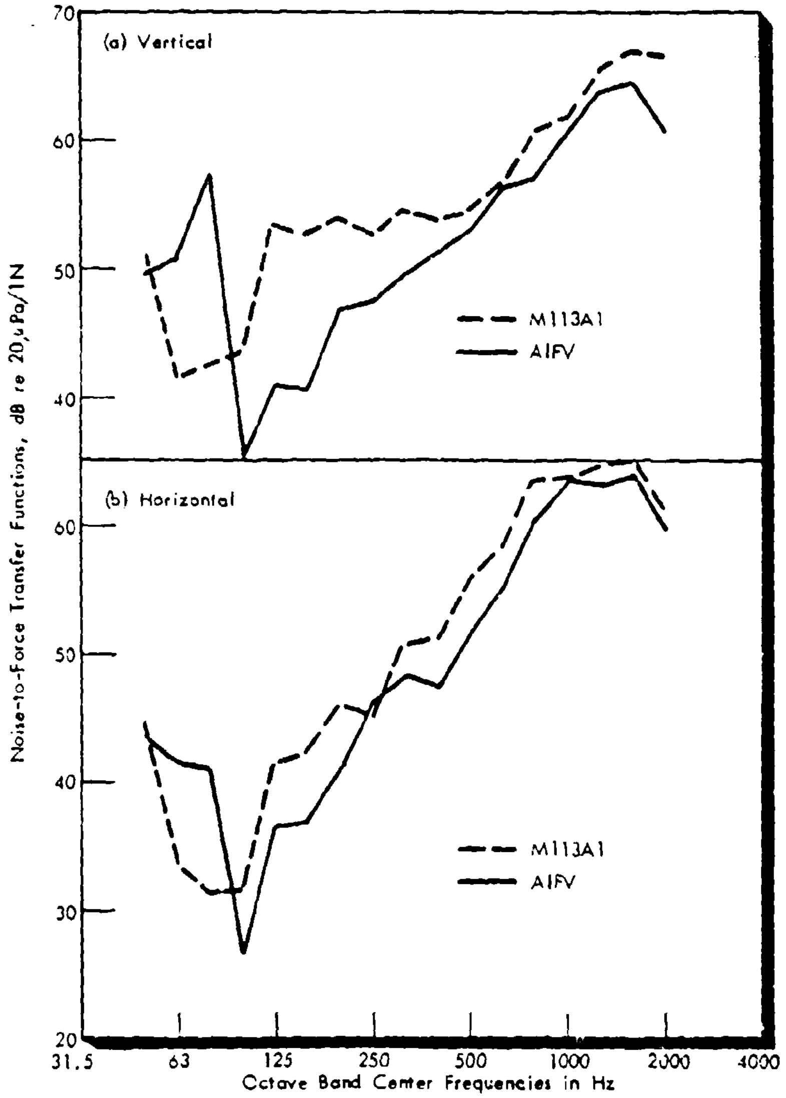

Figure 4.21 Noise-to-Force Transfer Functions for (a) Vertical and (b) Horizontal Excitation of Idler Spindles. (Average of Left and Right Idlers Presented: 50N Pink Noise Force Input).

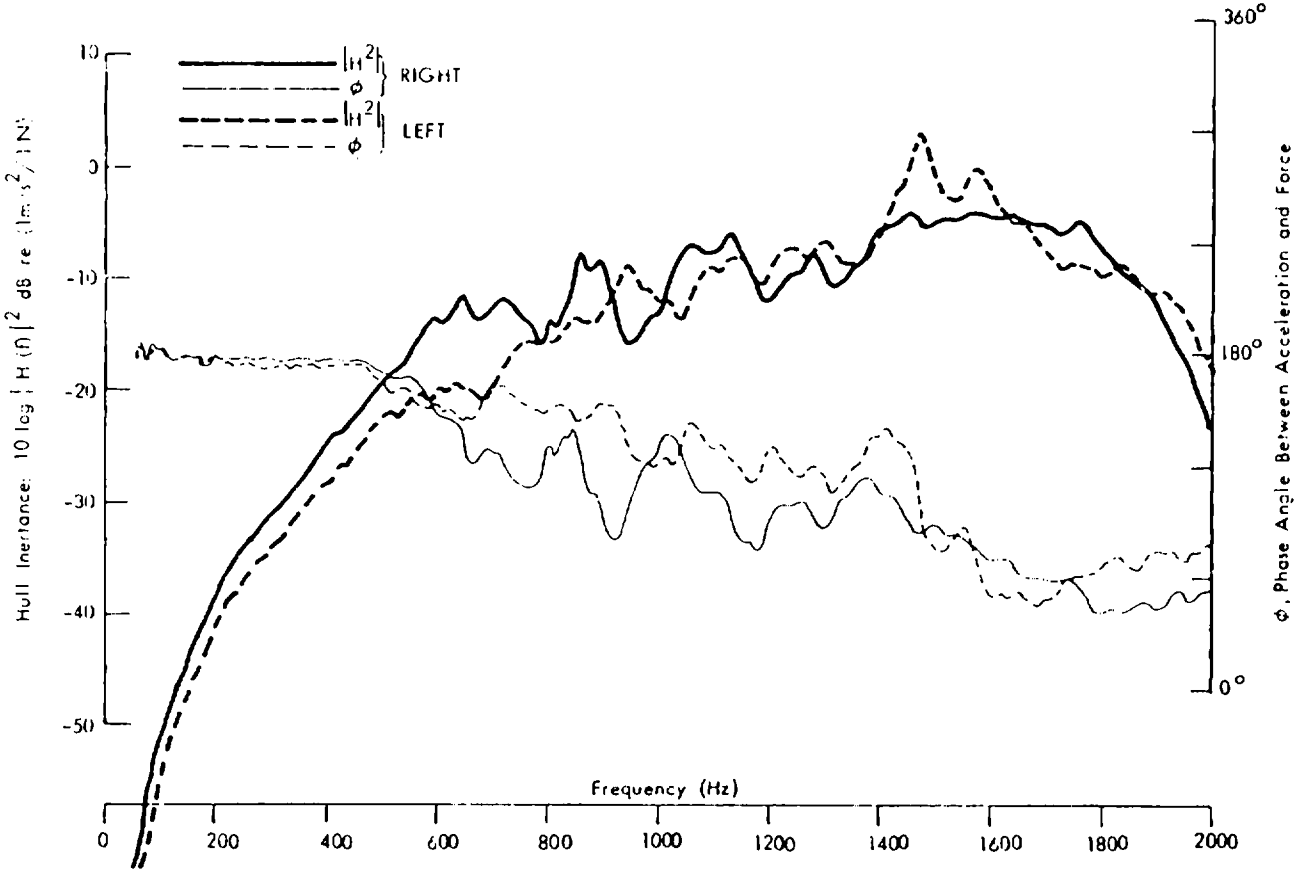

Figure 4.22 Comparison of Left and Right Side Horizontal Inertances on AIFV Idler Spindles (Turret on Vehicle).

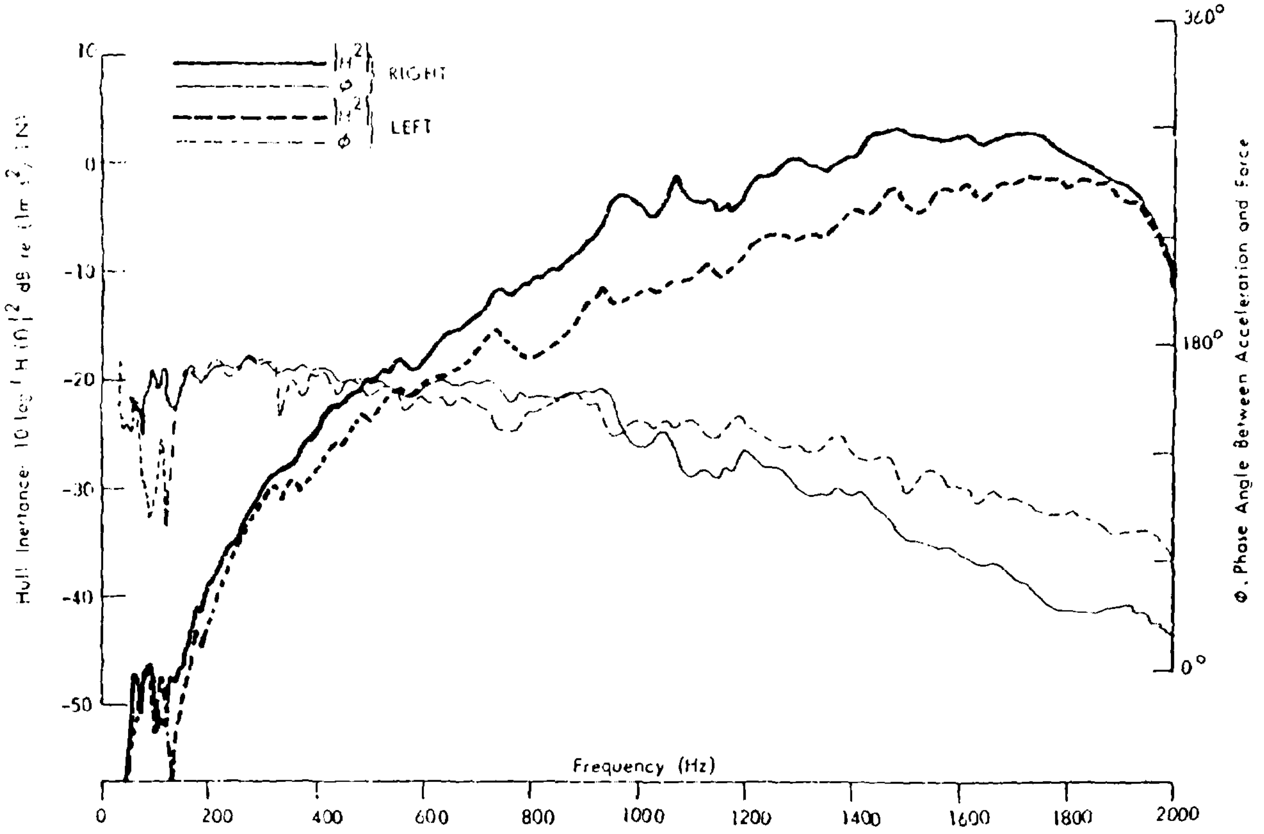

Figure 4.23 Comparison of Left and Right Side Vertical Inertances on AIFV Idler Spindles (Turret on Vehicle).

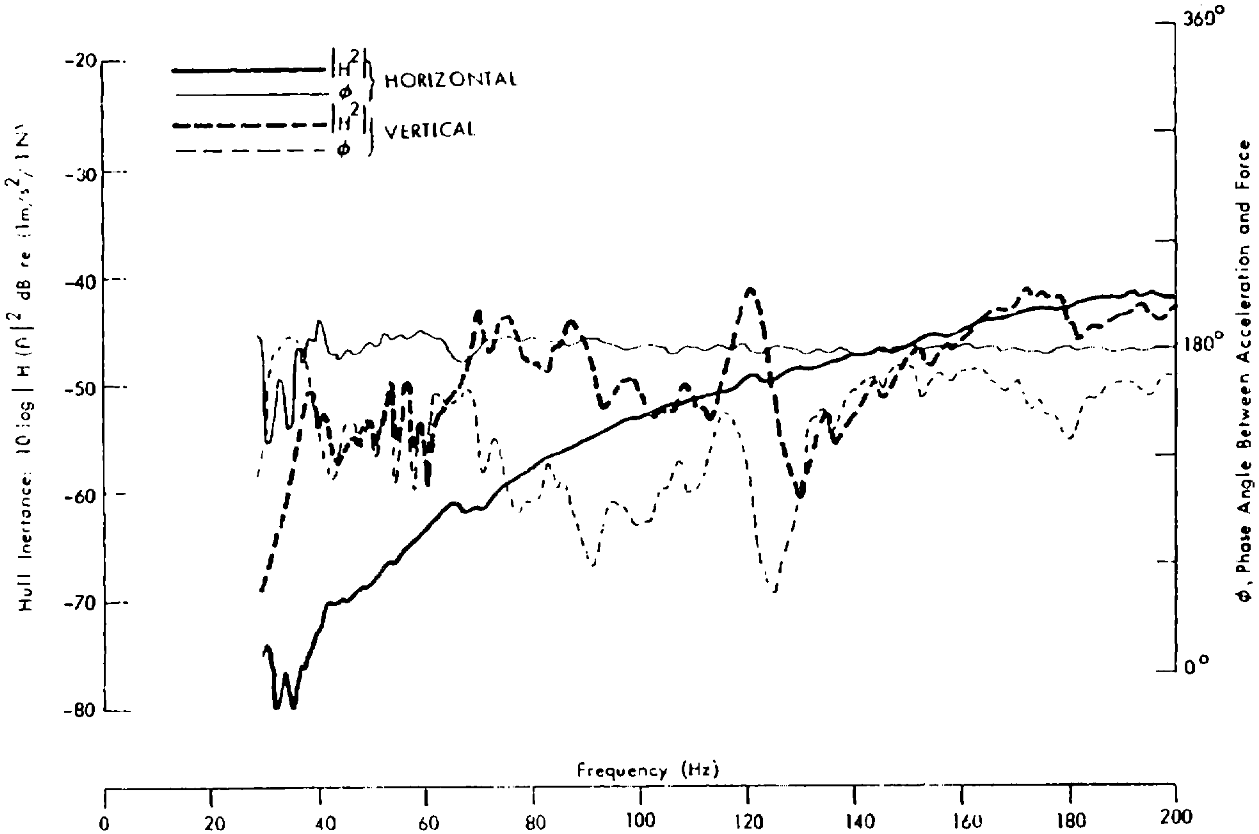

Figure 4.24 Comparison of Horizontal and Vertical Left Idler Spindle Inertances on AIFV Vehicle (Turret and Vehicle).

Similar results are observed at the final drive attachment points. Figures 4.25 and 4.26 show the horizontal and vertical inertances respectively. Only small inertance differences between left and right sides exist in the horizontal direction, but in the vertical direction stronger asymmetries (up to 8 dB) occur. Of greater importance is the 5 to 8 dB difference between vertical and horizontal inertance over the low frequency range up to 250 Hz. As for the idler spindle, stronger coupling occurs between the hull and final drive attachment point for vertical excitation than for the horizontal direction. We also note that the magnitudes of the idler inertances are greater than those for the final drive, in both excitation directions.

4.4.3.2 Left/Right Asymmetries - M113A1

Left- and right-side inertance asymmetries in the horizontal and vertical directions on the M113A1 idler spindles are shown in Figures 4.27 and 4.28. The right side idler attachment is 3 to 5 dB stiffer in the horizontal direction over much of the frequency range to 2 kHz. There is close correspondence in vertical inertance over most of the frequency range except below 200 Hz, where stronger coupling to resonant modes occurs for the right idler. These asymmetries are reflected in the noise-to-force transfer functions presented in Section 4.4.1.

The vertical and horizontal idler inertance functions for the M113A1 are compared at low frequencies in Figure 4.29. A 10 dB difference in inertance function magnitude reflects the great differences in hull stiffness in the horizontal and vertical directions. Further, the mean phase angle difference (about 90°) between vertical and horizontal directions reflects the differences in the nature of the hull dynamic response and power acceptance characteristics: the hull response is influenced at some frequencies by structural resonances for vertical excitation, but dominated by hull stiffness (mainly in the horizontal direction) for horizontal excitation. These trends were also evident in the AIFV results, in particular Figure 4.24.

4.4.3.3 Effect of the AIFV Turret

Inertances at idler and final drive attachment points were measured with the turret mass both mounted on and removed from the AIFV hull. Since the turret mass represents only 10% of the total vehicle mass, the turret was not expected to have a significant effect on the attachment point inertances at high frequency where the turret effect will be localized to the turret area. In contrast, at low frequencies where structural wavelengths are of the order of the vehicle length, differences were expected since the turret effect is no longer localized.

Figure 4.30 shows the left-side, horizontal idler inertance functions with and without the turret mass in position: no significant differences in inertance magnitude or phase exist. Similar results are found for the vertical inertance function, although at frequencies below 200 Hz, some minor changes in magnitude and frequency response occurred, as

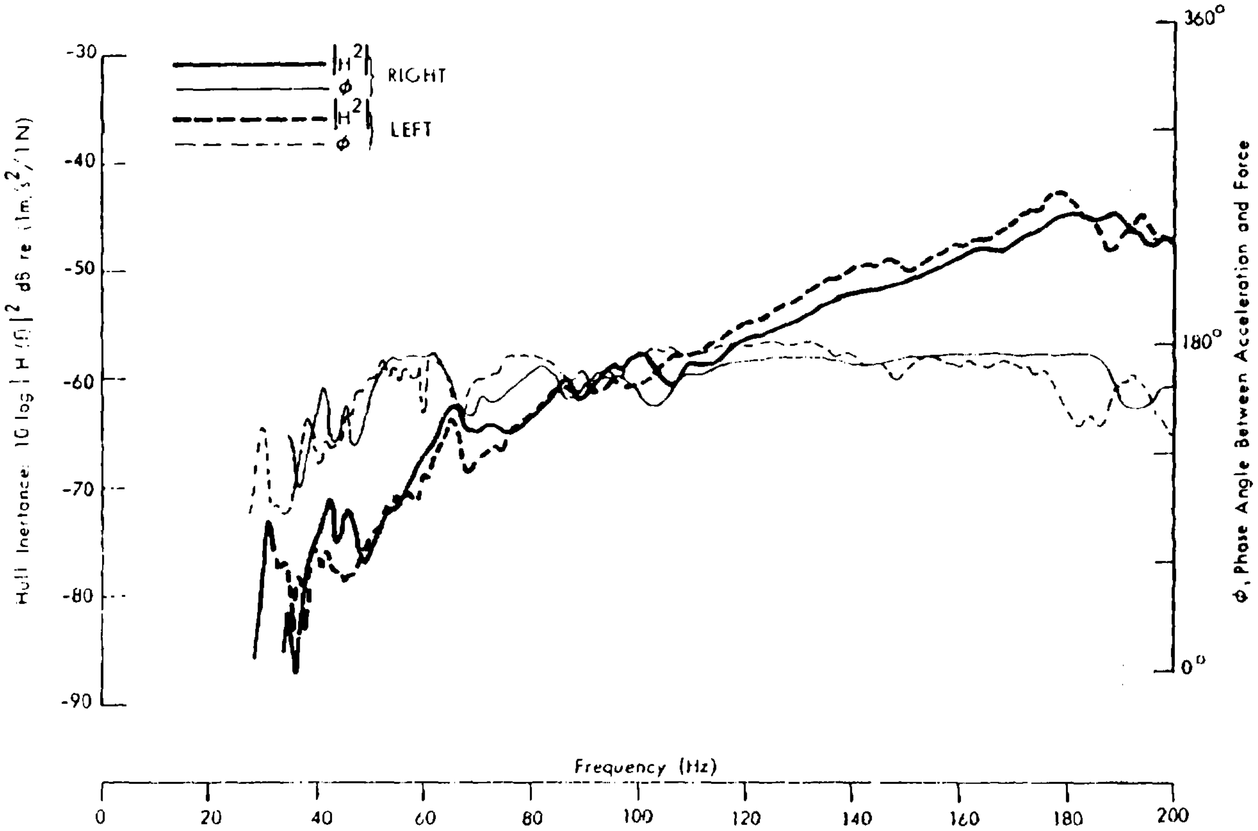

Figure 4.25 Comparison of Left and Right Side Horizontal Final Drive Inertances on AIFV Vehicles (Turret on Vehicle).

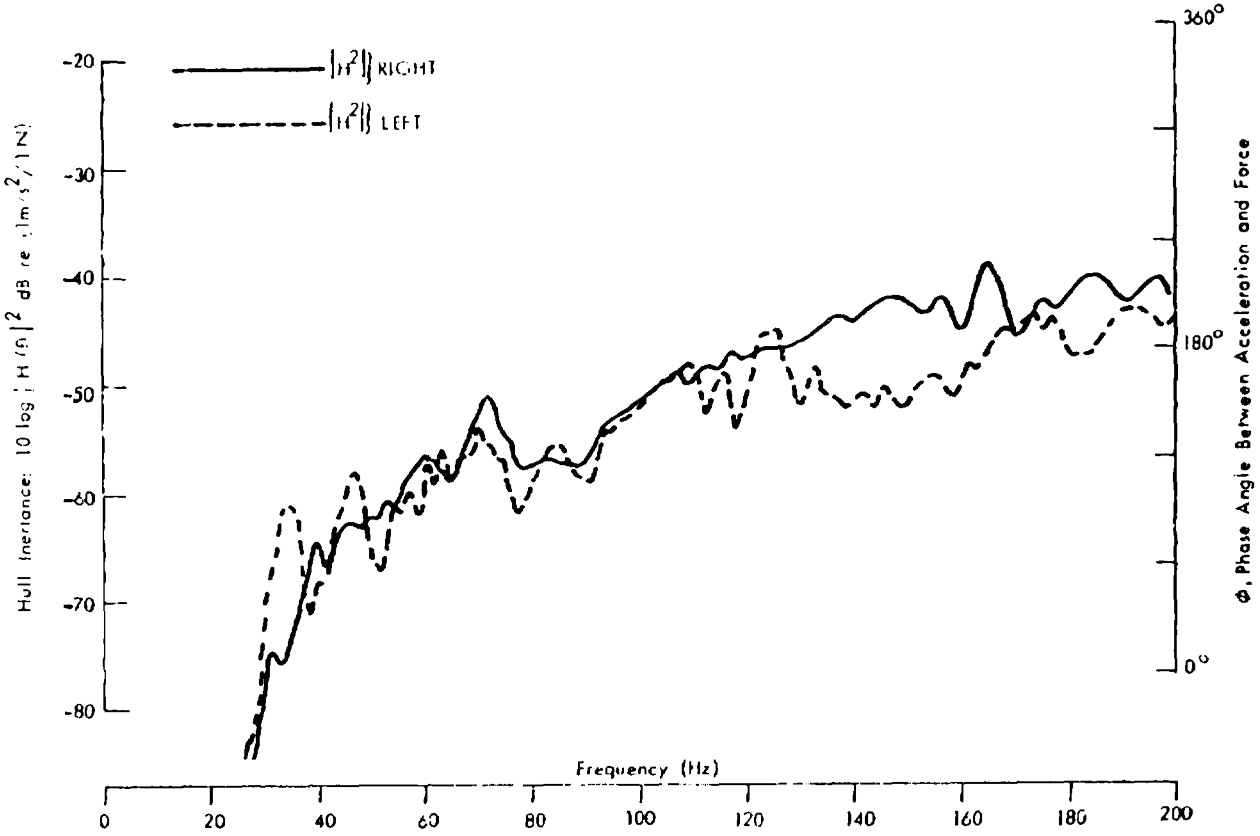

Figure 4.26 Comparison of Left and Right Side Vertical Final Drive Inertances on AIFV Vehicle (Turret on Vehicle).

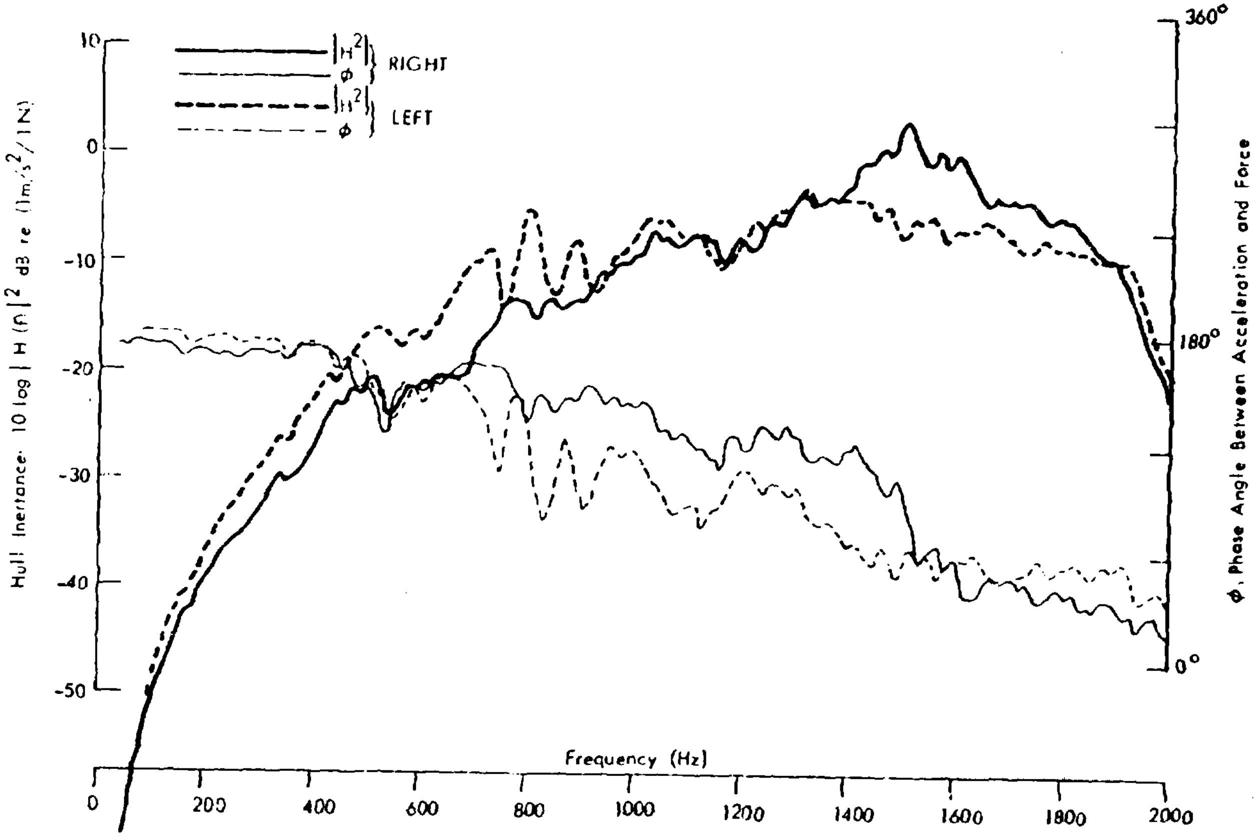

Figure 4.27 Comparison of Left and Right Side Horizontal Inertances on M113A1 Idler Spindles.

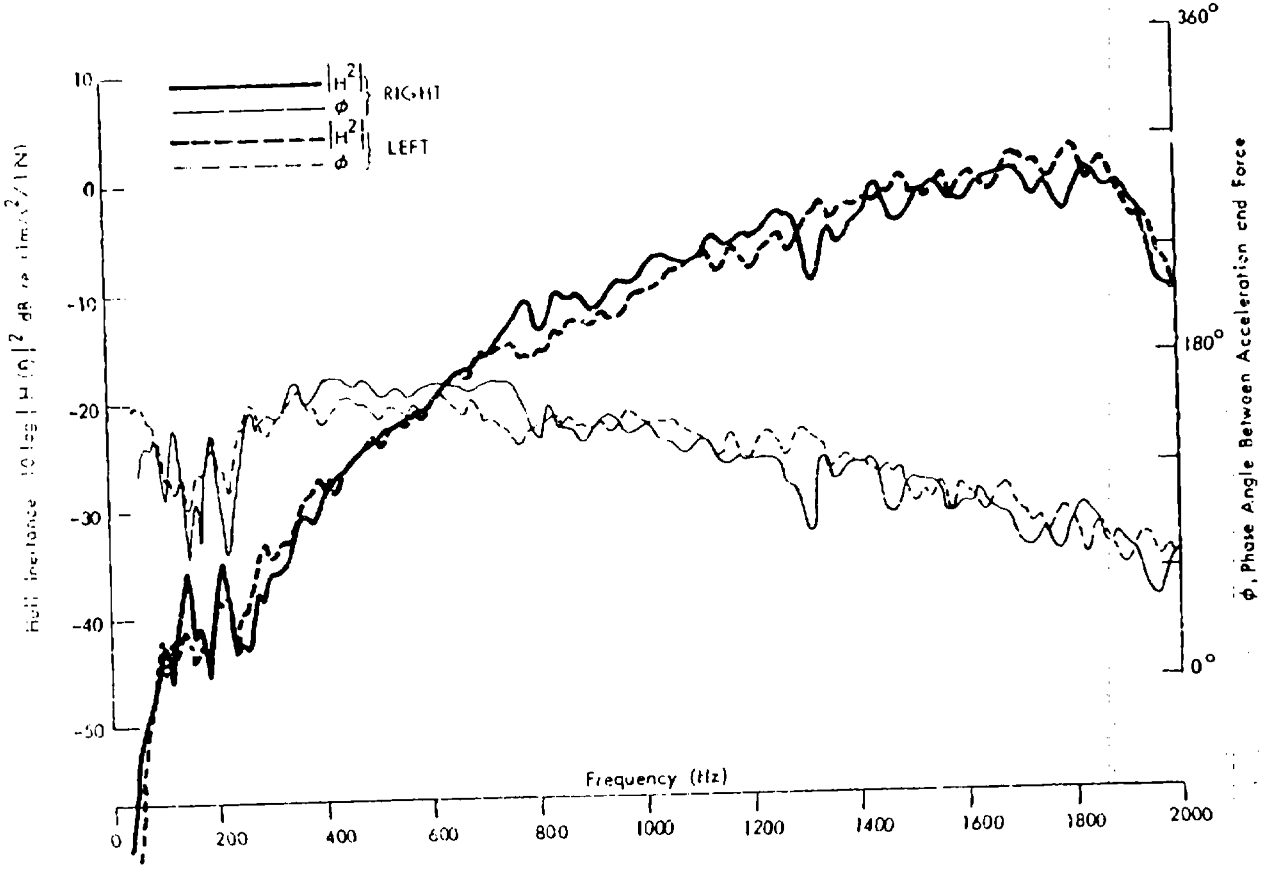

Figure 4.20 Comparison of Left and Right Side Vertical Inertances on M113A1 Idler Spindles.

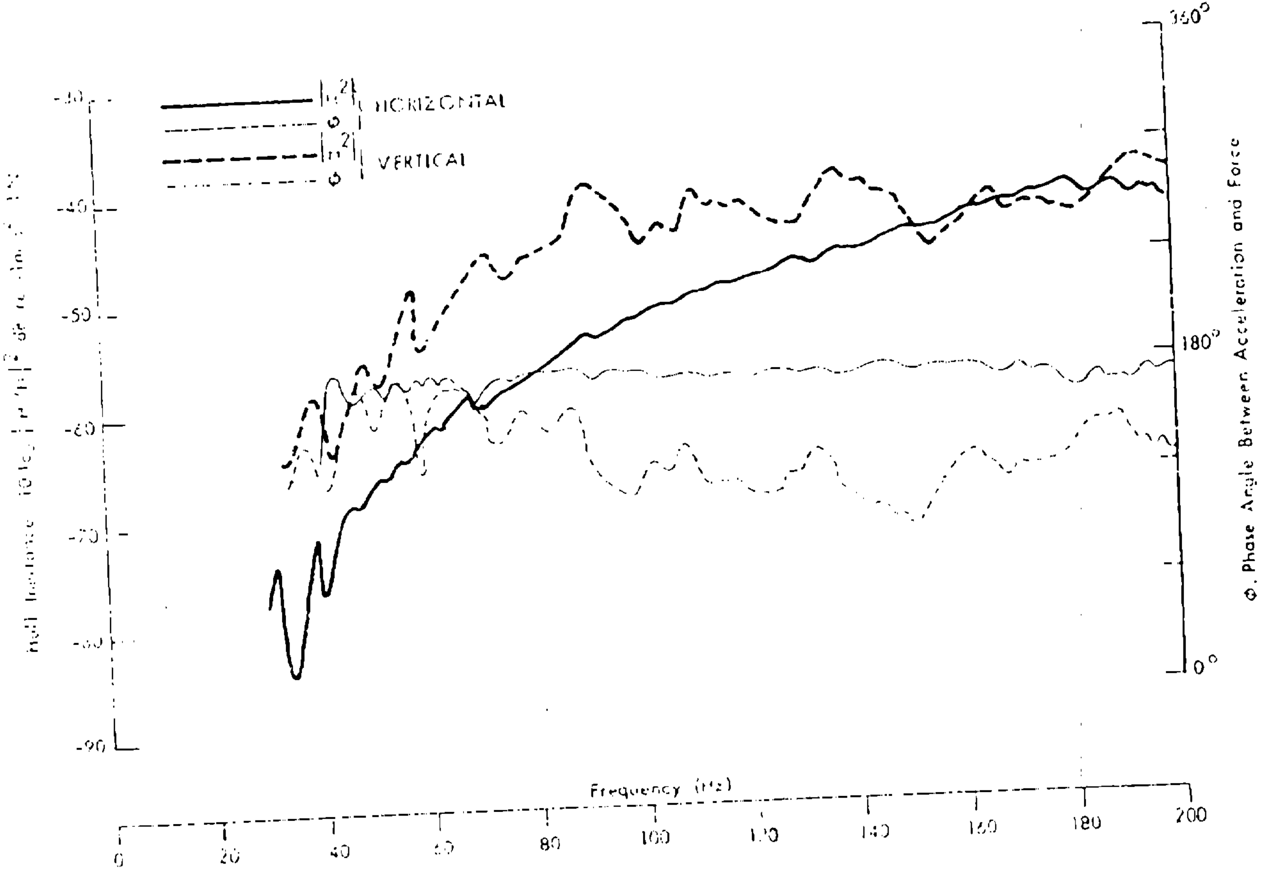

Figure 4.29 Comparison of Horizontal and Vertical Left Idler Spindle Inertances of M113A1 Vehicle.

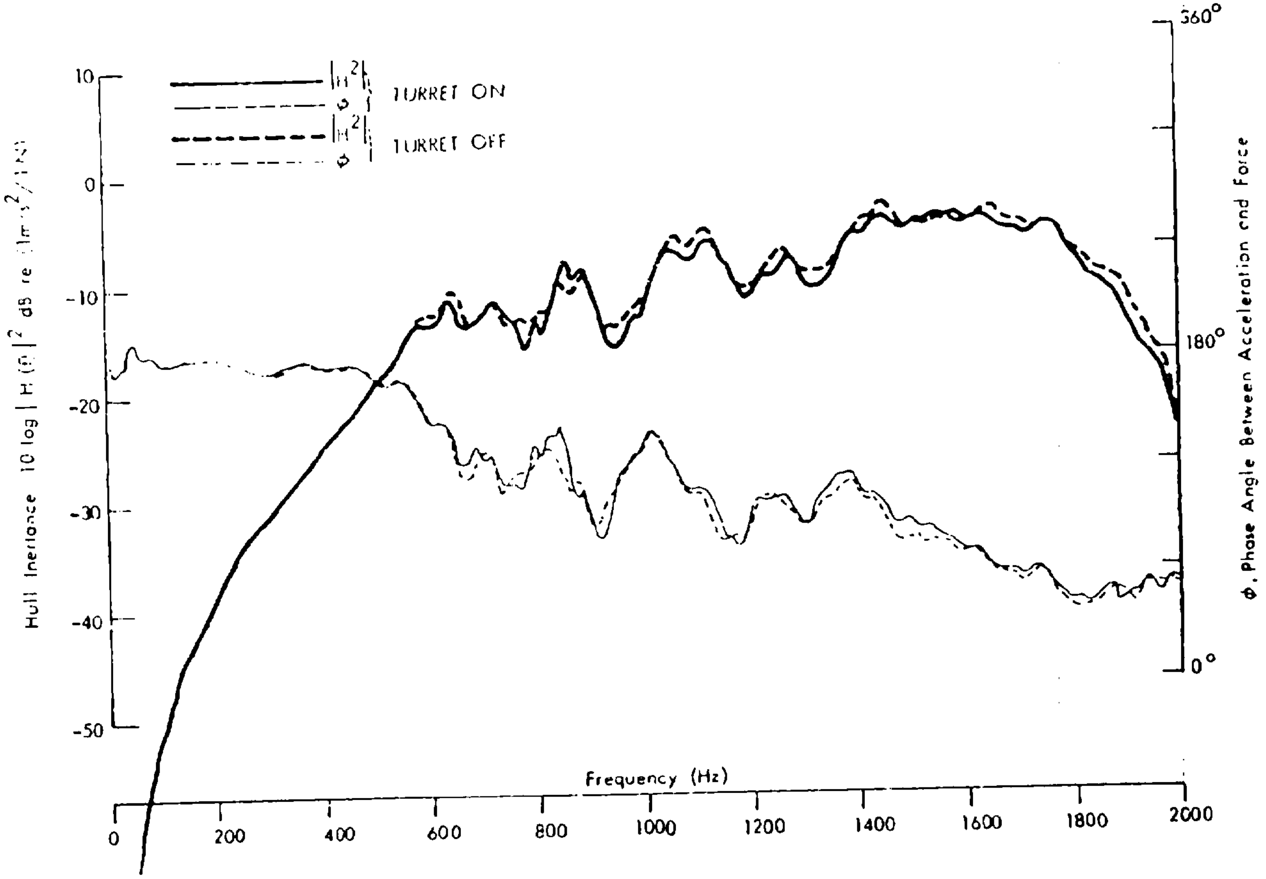

Figure 4.30 Effect of Turret Mass on Horizontal Idler Inertance Function of AIFV (Right Side).

shown in Figure 4.31. Results for the right side of the AIFV were generally the same as for the vehicle left side. Likewise, the turret mass had no significant effect on final drive inertance functions. An example is shown in Figure 4.32.

4.4.3.4 AIFV/M113A1 Comparisons

Figure 4.33 presents direct comparison of the left-side, idler spindle inertance functions measured for vertical excitation. While there are general similarities in the results, certain differences are clear. At frequencies below 250 Hz both vehicles exhibit a resonant response. This is characterized by phase variations from 0° and strong fluctuations in inertance magnitude with frequency. The frequency range over which this occurs is wider for the M113A1 than for the AIFV. At the same time the inertance magnitude of the M113A1 is up to 10 dB greater than that for the AIFV. It appears that the M113A1 structure will more easily accept low frequency power for vertical idler forces than will the AIFV structure. The same trend exists for measurements on the right side of the vehicles. At higher frequencies, the M113A1 inertance exceeds that of the AIFV by about 3 dB, while the phase variations are essentially the same. The power accepting character of the right idler at high frequencies is similar.

The horizontal inertance functions of the idlers of the two vehicles are similar as shown in Figure 4.34.

Figure 4.35 compares final-drive vertical and horizontal inertance functions for AIFV and M113A1: the instrumentation system involved was similar to that in Figure 4.18 and is described in [17]. The M113A1 vertical inertance is much the same as that of the AIFV, but the mid-frequency horizontal inertance of the M113A1 final-drive is about 2 dB greater than that of the AIFV.

Figure 4.36 shows the inertance measured at the bottom of the roadarm attachment (on the bearing housing) for the AIFV and M113A1 vehicles: the transfer functions are similar, and both indicated a primarily stiffness-controlled response at the roadarm/hull attachment points.

It appears that the major differences between the two vehicles lie in the power accepting characteristics of the idler in the vertical and, to a minor extent, horizontal directions at low frequencies.

4.4.4 Discussion

The following major observations can be made from these measurements:

1. At frequencies below 250 Hz, the vertical inertance of each hull is greater than that in the horizontal direction.

2. The vertical idler inertance of the M113A1 hull is greater than that of the AIFV hull, particularly between 100 and 300 Hz.

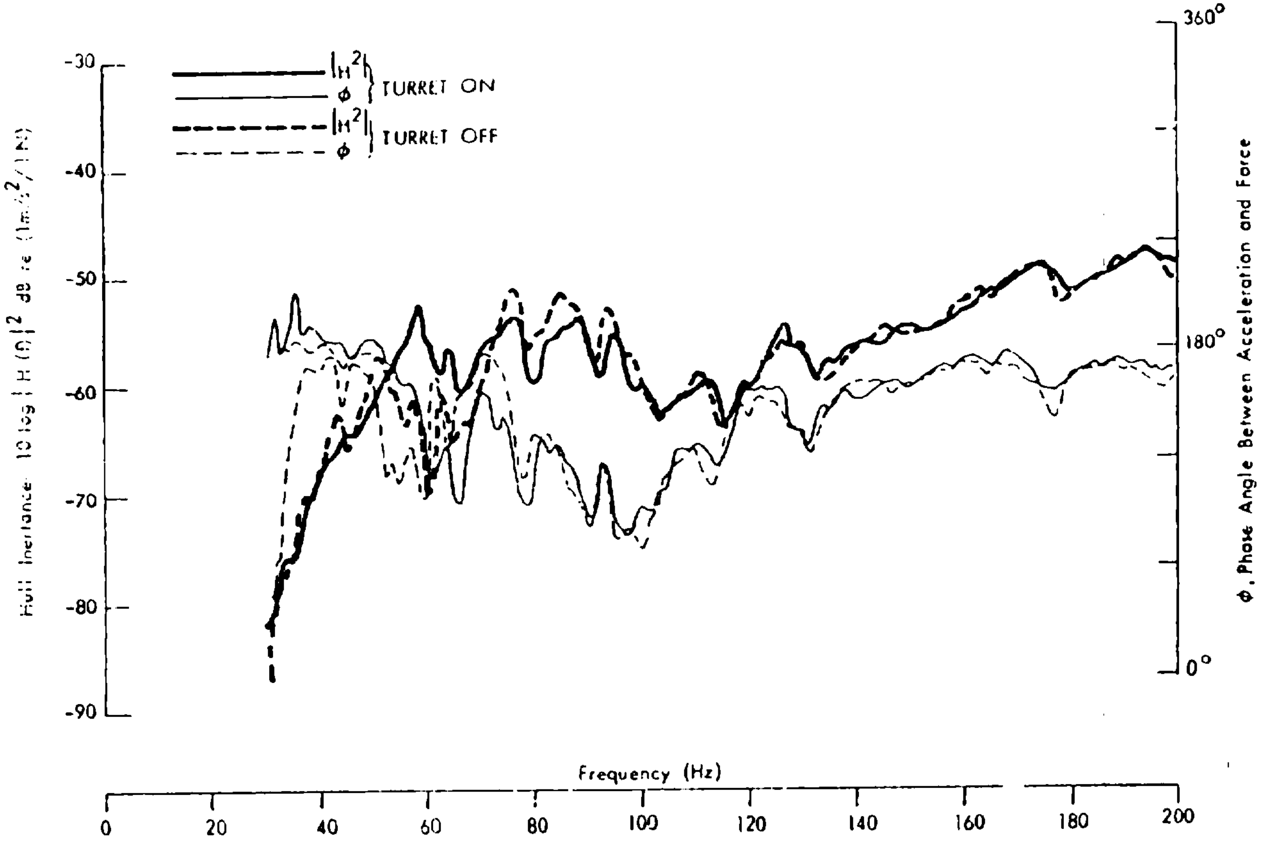

Figure 4.31 Effect of Turret Mass on Vertical Idler Inertance Function on AIFV (Right Side).

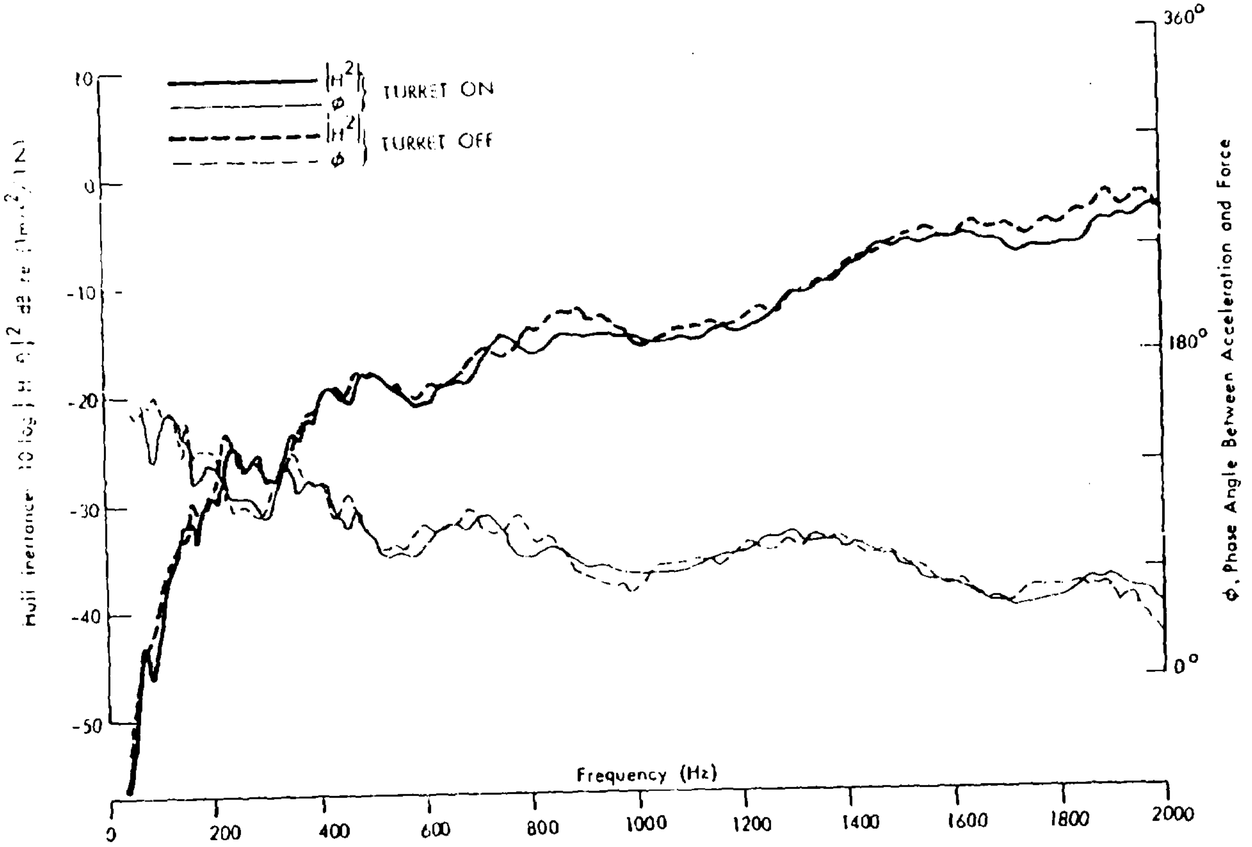

Figure 4.32 Effect of Turret Mass on Vertical Final Drive Inertance Function of AIFV (Right Side).

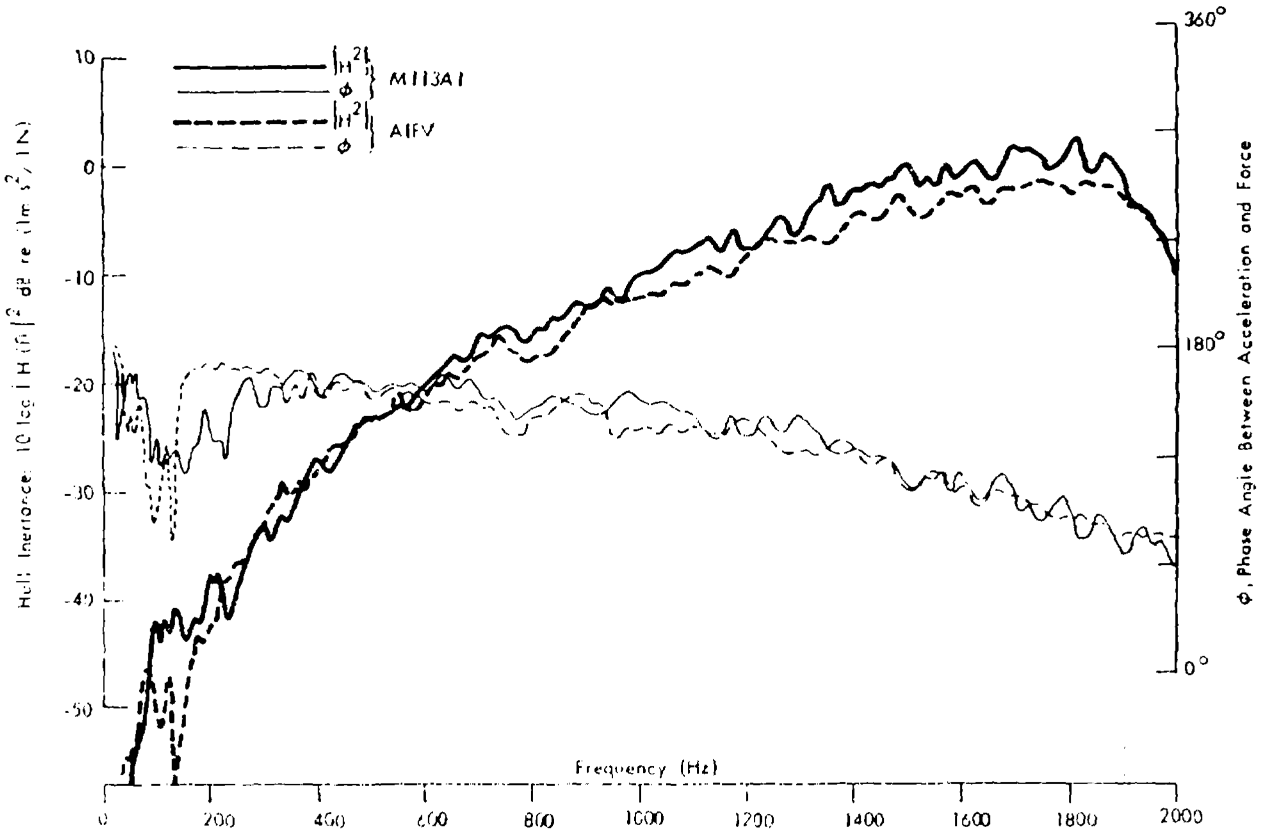

Figure 4.33 Comparison of Vertical Inertance Functions for M113A1 and AIFV Vehicles (Left Side).

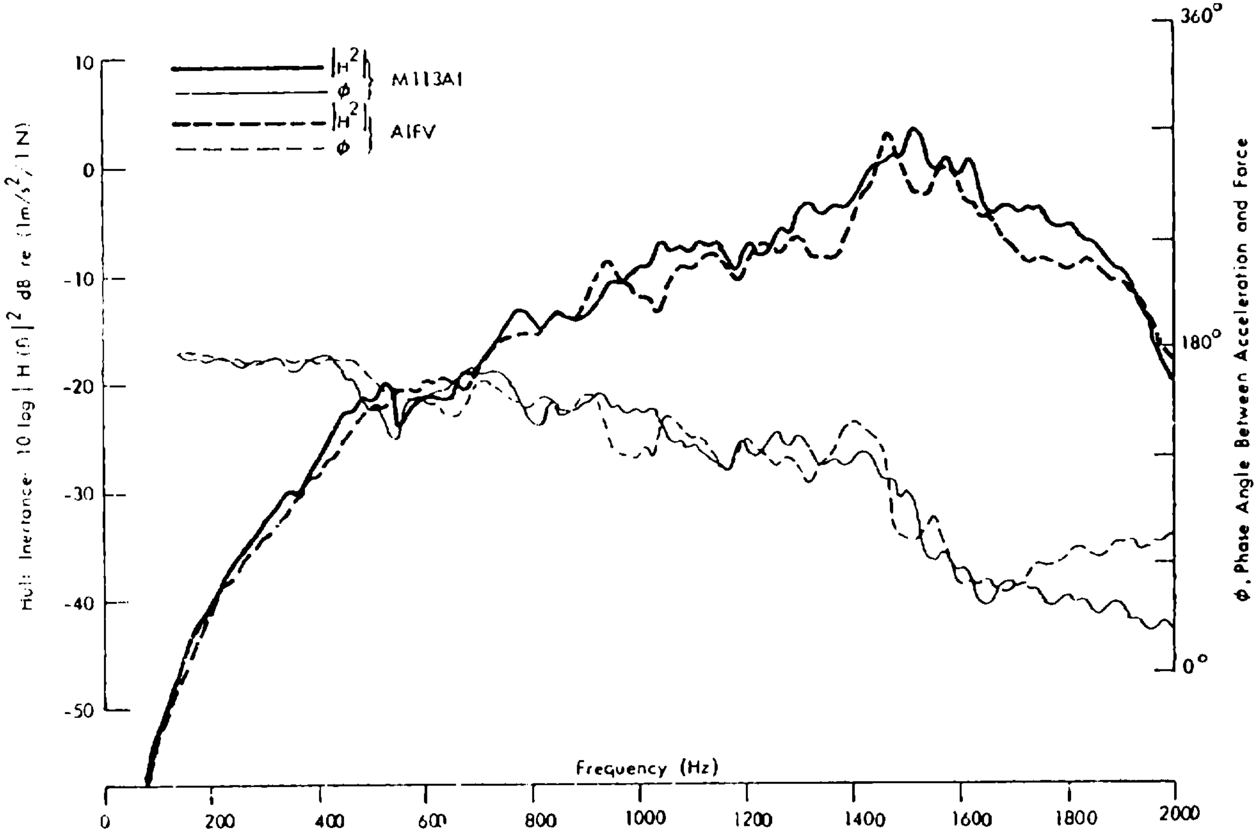

Figure 4.34 Comparison of Horizontal Inertance Functions for M113A1 and AIFV Vehicles (Left Side).

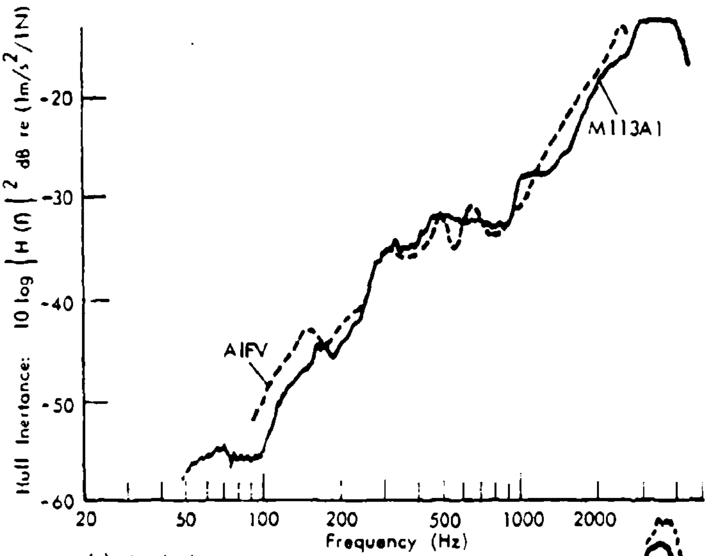

(a) Vertical

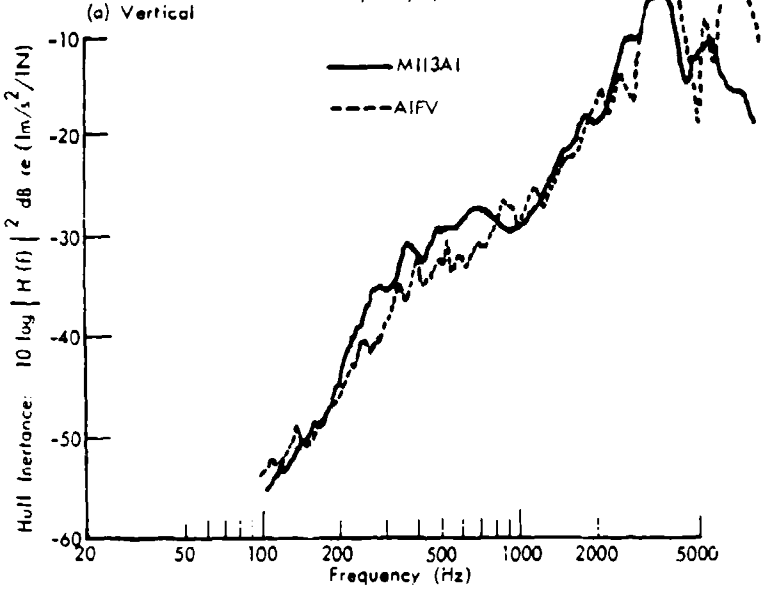

(b) Horizontal

Figure 4.35 Comparison of AIFV and M113A1 Inertance Functions: Final Drive Attach.

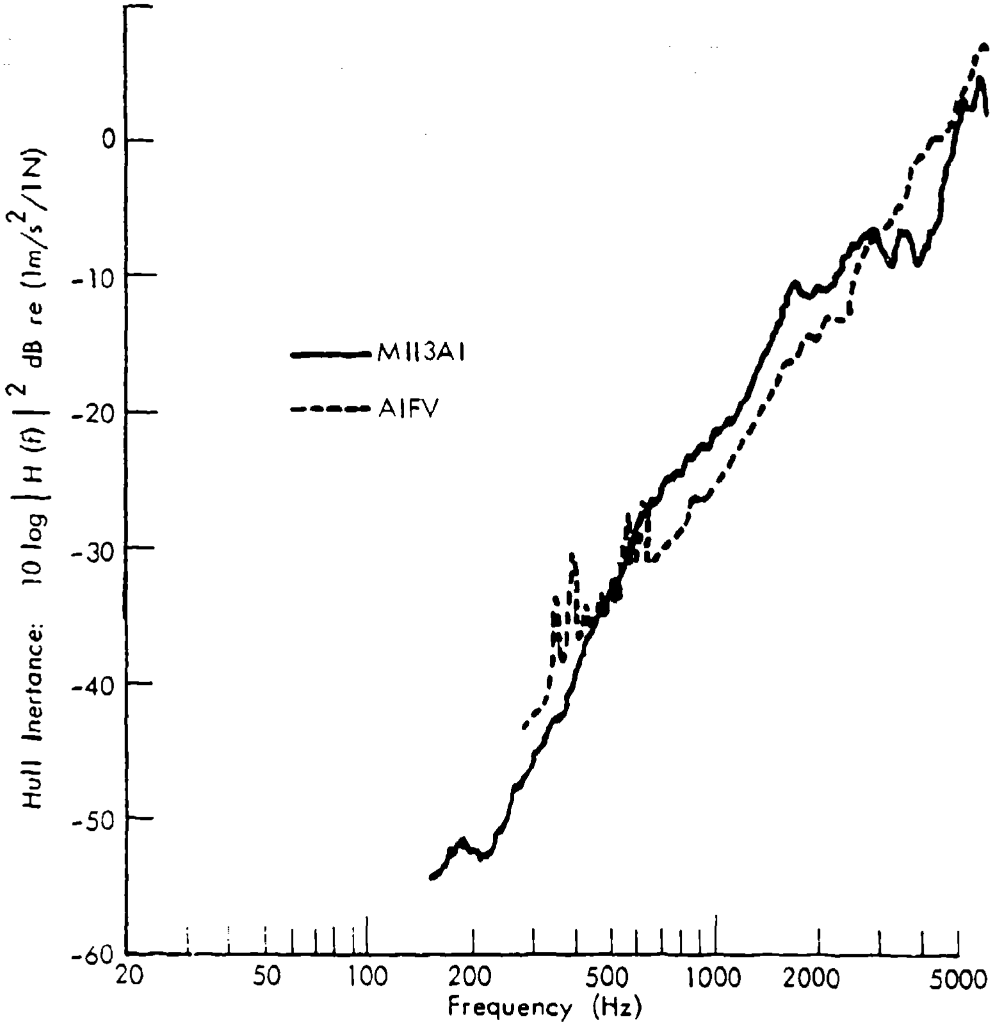

Figure 4.36 Roadwheel Attach Inertance, Measured at Bottom of Attach.

3. Assuming equal force input to the attachment points in both horizontal and vertical directions, the vertical idler forces will control the interior noise levels in each hull. However, from [16] it can be deduced that the horizontal idler forces can exceed by up to 10 dB those developed in the vertical direction.

4. The turret mass does not significantly impact the vehicle inertance functions.

5. Strong asymmetries between left- and right-side inertances and noise-to-force T.F.'s exist for the AIFV, but these are less evident in the M113A1 data. These may result from longitudinal idler mounting differences.

In Section 4.4.2, the noise/force T.F.'s for the M113A1 were found to be between 3 and 10 dB greater than the corresponding T.F.'s for the AIFV vehicle and these differences are similar to the inertance differences reported in Section 4.4.3. This is not necessarily expected since the inertance function is an integrated measurement of the power accepting and structural dissipation characteristics of the hull structure, while the noise/force T.F. also incorporates the hull radiation characteristics. A more direct relation between response/force and noise/force T.F.'s would be found if response measurements were made on the major radiating areas such as the top and bottom plates. However, in general it is believed that reductions in the attachment point inertances will lead to similar reductions in the hull vibration response and in turn in the interior noise levels.

Appropriate structural modifications are not immediately obvious from the reported measurements and so an analytical model was to be developed to provide guidance in the hull redesign process which aims to produce a 5 to 10 dBA noise reduction through practical hull modifications. The analytical modeling study on the baseline M113A1 vehicle is presented in the next section.

5. FINITE ELEMENT MODAL ANALYSIS OF AN M113A1 VEHICLE

5.1 General

The vibratory power acceptance characteristics of the M113A1 hull over the critical frequency range up to 500 Hz is influenced strongly by whole vehicle vibration modes, that is by modes whose wavelengths are comparable to typical hull dimensions. Finite-element (F-E) analysis was proposed as a feasible, economic modeling technique which would allow accurate calculation of hull resonance frequencies and mode shapes and, in turn, hull inertance and force-to-acceleration transfer functions and facilitate an understanding of the hull power flow for noise control purposes. This chapter reports the results of the F-E modeling study conducted: included are discussions of the basic modeling concepts and assumptions, a theoretical discussion for the prediction of vibration and noise levels, study results for initial and final F-E hull models, and study conclusions and recommendations for model use.

5.2 Summary of Equations for Generalized Structural Vibration Response and Interior Acoustic Power Radiation

The vibrational response of a bounding structure and the associated interior acoustic radiation into the bounded cavity can be derived from classical theory. A brief derivation of these results is presented in Appendix A and the major results are summarized below.

The vibrational response of the structure $w(\bar{x},\omega)$ due to a point harmonic force of amplitude $F(\omega)$ located at x_F at circular frequency ω is given by

$$w(\bar{x},\omega) = F(\omega)\sum_r \frac{\psi_r(\bar{x})\psi_r(\bar{x}_F)}{M_r Y_r}$$

Here, the structure is represented by its set of normal modes, where ψ_r, M_r, and Y_r are the mode shape, generalized mass, and modal receptance of the rth normal mode. In particular,

$$Y_r = \omega_r^2\left[1 - \left(\frac{\omega}{\omega_r}\right)^2 - i\eta_r\right]$$

where ω_r and η_r are the resonance frequency and loss factor of the rth mode, and

$$M_r = \int_{\bar{x}} m(\bar{x})\psi_r^2(\bar{x})d\bar{x}$$

where $m(\bar{x})$ is the surface mass density of the structure at x.

When several modes are resonant in a narrow frequency band of width $\Delta\omega$ and the amplitude of the excitation force $F(\omega)$ at $\bar{x}_F$ is constant over the analysis band, the vibrational response of the structure will be determined by the resonant peaks of those modes resonant in the analysis band ($r\varepsilon\Delta\omega$). In assessing the effects of structural modifications, estimates of space-averaged, mean-square displacements averaged over the narrow band of frequencies $\Delta\omega$ are more useful than point-to-point transfer functions, due to the spatial variation in surface displacement. An expression for these displacements is derived in Appendix A as equation (A.12). The band-averaged displacement spectrum is

$$\overline{w^2_{\Delta,A}} = \frac{\pi}{2\omega^3}\cdot\frac{\overline{F^2_\Delta}}{\Delta\omega}\cdot\sum_{r\varepsilon\Delta\omega}\frac{\left[\frac{1}{A}\int_A \psi_r^2(\bar{x})d\bar{x}\right]\psi_r^2(\bar{x}_F)}{M_r^2\eta_r} \qquad (12$$

where $F^2_\Delta = \frac{F^2(\omega)}{2} \Delta\omega.$ is the band-limited force spectrum level.

Here $\overline{w^2{}_{\Delta,A}}$ is the space-averaged mean-square displacement, averaged over $\Delta\omega$, developed on the structural element A in response to the band-limited force $F^2\Delta$ acting at $\bar{x}_F$. Such an element could be the roof or floor or sidewall, and each contribution to the total energy of vibration is indicated by the expression

$$\int_A m\psi_r^2(\bar{x})\,d\bar{x}$$

The term in square brackets describes the restraint provided by the structure on the region A of interest.

The quantities M_r, $\psi_r(\bar{x})$, and $\psi_r(\bar{x}_F)$ are calculated in the F-E computing procedure so that equation (A.12) can be evaluated by manipulation of the output file data.

The band-limited acoustic power $W'_{\Delta,A}$ in watts radiated to the cavity interior from the structural element A is derived as (Equation (A.19))

$$W_{\Delta,A} = \omega^2 \overline{w^2_{\Delta,A}} \bullet \overline{R_{rad,A}} \qquad (13)$$

$$W_{\Delta,A} = \frac{\pi}{2} \frac{F^2_\Delta}{\omega\Delta\omega} \bullet \sum_{r\in\Delta\omega} \frac{\left[\frac{1}{A}\int_A \psi_r^2(\bar{x})\,d\bar{x}\right] \psi_r^2(\bar{x}_F)}{M_r^2 n_r} \bullet \overline{R_{rad,A}}$$

where $\overline{R_{rad,A}}$ is the band-averaged radiation resistance for the structural element A, calculated from Statistical Energy Analysis. Such an approach will be valid within reasonable limits for frequencies of about 200 Hz and above. For example, using Equation (9.5.16) from [15] for the modal density of a rectangular parallelopiped, the M113A1 of interest will have 5 acoustic modes in the 200 Hz one-third octave band. Alternative approaches, while theoretically practical, will be excessively expensive, yet cannot be guaranteed to be more accurate due to imprecision in input data.

Equation (13) shows that the results for structural response of the various hull elements can be used to directly calculate the interior radiation. Likewise, noise reductions associated with different hull configurations can be assessed by changes in $w^2{}_{\Delta,A}$ and $R_{rad,A}$.

5.3 Modeling Procedure

The basic concept of the finite element method is that every structure may be considered to be an assemblage of individual structural components or elements. The structure must consist of a finite number of such elements, interconnected at a finite number of joints or nodal points. This finite character of the structural representation makes possible the analysis by means of matrix equations, as distinct from the continuum mechanics approach which becomes impractical for complex structures. Thus, and on account of the general simplicity of the M113 hull, F-E analysis was selected as the modeling procedure.

To make the validation of the finite-element model more direct, the bare hull was modeled in the configuration corresponding to the inertance and noise/force transfer function measurements described earlier. Extension of results to underway operation will require some additional modeling of the idler linkages. The hull model presently includes the idler spindle only. The bilateral symmetry of the hull suggested that only half of the structure needed to be modeled, and this was done with a combination of plate and beam elements using only about 150 nodes. In the modal extraction process symmetric and antisymmetric modes were generated in two computer runs where the hull centerline boundary conditions are maintained to have, respectively, zero vertical displacement but may rotate, or zero rotation but may deflect vertically: computer costs are thus significantly reduced. Very stiff members, such as the longitudinal box beams, the bottom plate stiffeners, the narrow sill plates bounding the ramp door and the cupola support frames, were modeled with equivalent beam elements. Massive elements such as the batteries, fuel tanks, hatches, and the ramp door were represented as lumped masses located at boundary nodes. The vehicle engine, roadwheels, track, and suspension elements were considered isolated from the hull and therefore omitted, as were the forward engine hatch cover plates.

Large plate elements such as the top plate, bottom plate, and upper side plates were represented by plate elements connecting a grid of node points distributed approximately uniformly over the hull surfaces. The local stiffness characteristics of the idler spindle and mounting pad were represented by a beam of equivalent stiffness, determined from a static analysis of the idler pad area using a finite element modeling technique, EASE2, which is supported by Engineering Analysis Corporation, Los Angeles. The local stiffness characteristics were added into the hull model.

Mode shapes, resonance frequencies, and modal masses were computed using the STAR program of the MRI/STARDYNE Static and Dynamic Structural Analysis System, developed by Mechanics Research Inc., Los Angeles.

Transfer functions, both drive point inertance and hull acceleration-to-idler force T.F.'s, were calculated using DYNRE2 program of the MRI/STARDYNE System. In this, loss factor data from previous measurements were used. T.F.'s were computed for both symmetric and antisymmetric modes and combined as vectors.

Validation was to be carried out by comparison of measured and computed idler inertance and hull acceleration-to-force T.F.'s. Limited noise-to-force T.F.'s were to be computed for comparison with measurement.

5.4 Results

5.4.1 Initial Model Configuration

The initial modeling array of nodes and plate elements is shown in Figures 5.1 (a), (b) and (c) in isometric view, and Figure 5.1 (d) in a single projection where all the elements and nodes are connected as modeled.

The top plate consisted of a rectangular array, 9 elements along the top plate length and 4 elements across half the top plate width. Rectangular cutouts represent the cargo hatch and the commander's cupola. The inclined front was represented as 9 rectangular plate elements, the asymmetry of the engine access opening being ignored due to its remoteness from the drive point. The hatch plates were omitted for simplicity.

The upper side plate was represented by rectangular and triangular plate elements, with two interior nodes from the sponson to the top plate, and about 10 interior nodes longitudinally. The sponson was represented by a single longitudinal line of plates, i.e. no interior nodes were used across the sponson width following the argument that the lowest sponson mode was measured to be above 500 Hz. Likewise the lower side plate contained no interior nodes across its vertical dimension, being represented by a line of rectangular plates.

The bottom plate was represented by a set of rectangular and triangular plates with a series of beams located approximately where the floor plate supports exist in the actual vehicle. To include the effects of the engine bulkhead, bottom and top plates are tied together with plate elements at node locations 400, 412, and 310. Only one interior node was used between the center of the bottom plate and the lower side plate.

The box beam was represented by a line of beam elements located at the junction of the lower side plate and the bottom plate, with appropriate torsional and bending stiffnesses. The rear hull above the sponson was represented by a set of three plate elements bounded on the ramp side by a stiffening beam element. The sill which extends around the ramp was represented by beam elements, although the sill at the bottom plate line was omitted. The mass of the ramp was represented by a series of point masses located at the base of the ramp-nodes 1200 and 1201, the ramp being considered to provide no significant stiffening to the bounding sill of the hull rear panel.

The equivalent beam representing the local stiffness characteristics of the idler pad was attached to the hull at node 1202 and extending essentially as on the real vehicle: thus a node at 1250 occurs 125 mm (5 in) from 1202, which is the corner of the vehicle. Two additional nodes, 1251 and 1252, oriented vertically and horizontally, are located very close to node 1250, and this allows the response to be calculated at the point of application of the force (1250).

An isometric view of the nodal arrangement is shown in Figure 5.2. The support system for all nodes corresponds to the hull supported to allow

(a) Side Plate

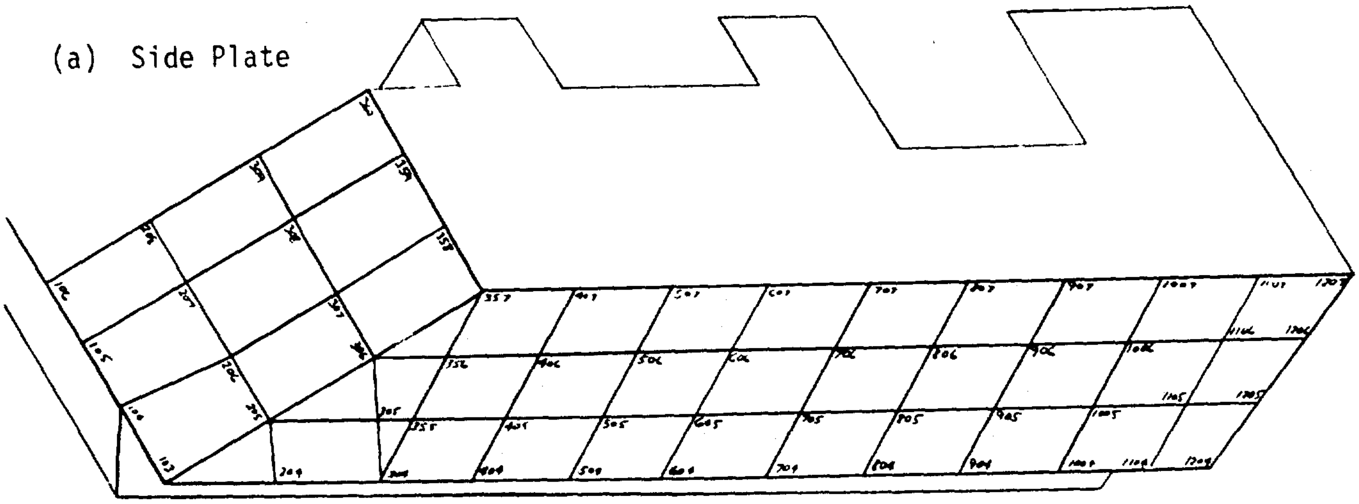
357
407
507
607
707
807
907
1007
1107
1207
356
406
506
606
706
806
906
1006
1106
1206
355
405
505
605
705
805
905
1005
1105
1205
209
304
404
504
604
704
804
904
1004
1104
1204
106
105
104
103
205
206
207
305
306
307
358
359
360

(b) Bottom Plate

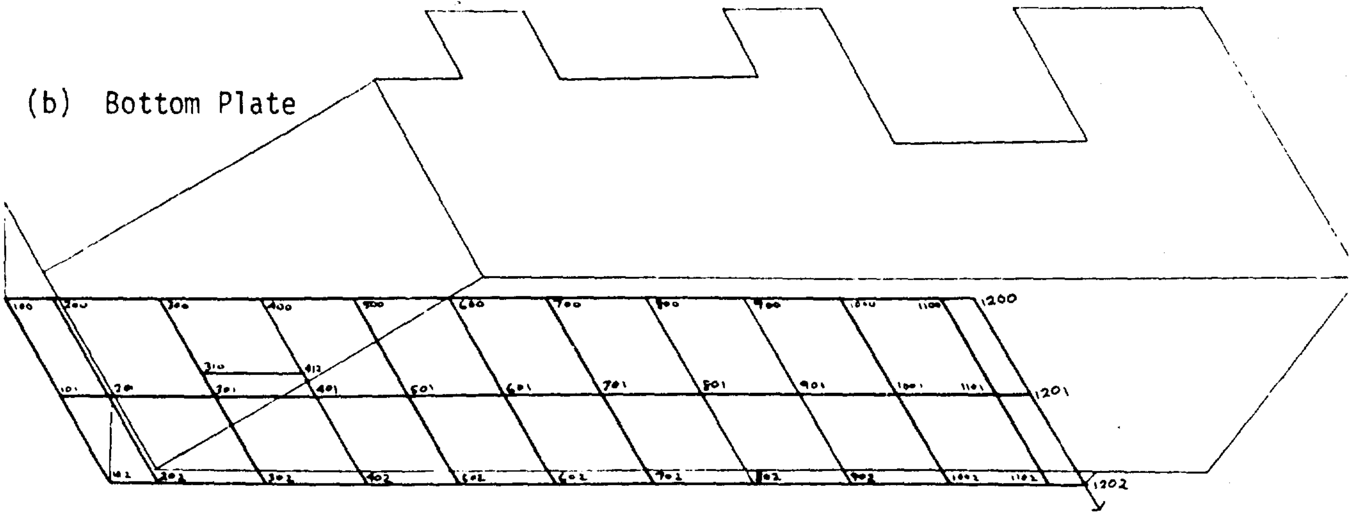
100
200
300
400
500
600
700
800
900
1000
1100
1200
310
412
101
201
301
401
501
601
701
801
901
1001
1101
1201
102
202
302
402
502
602
702
802
902
1002
1102
1202

(c) Top Plate

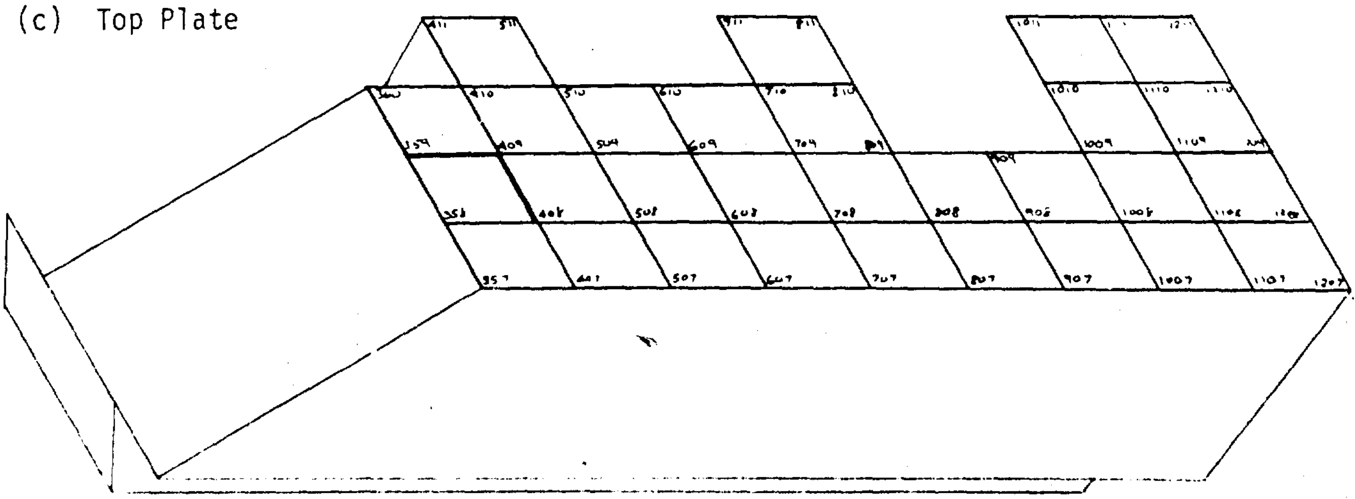
411
511
911
1011
1211
360
410
510
610
710
810
1010
1110
1210
359
409
509
609
709
809
909
1009
1109
1209
358
408
508
608
708
808
908
1008
1108
1208
357
407
507
607
707
807
907
1007
1107
1207

Figure 5.1(a) to (c). Isometric View of Node Locations - Initial Hull Model.

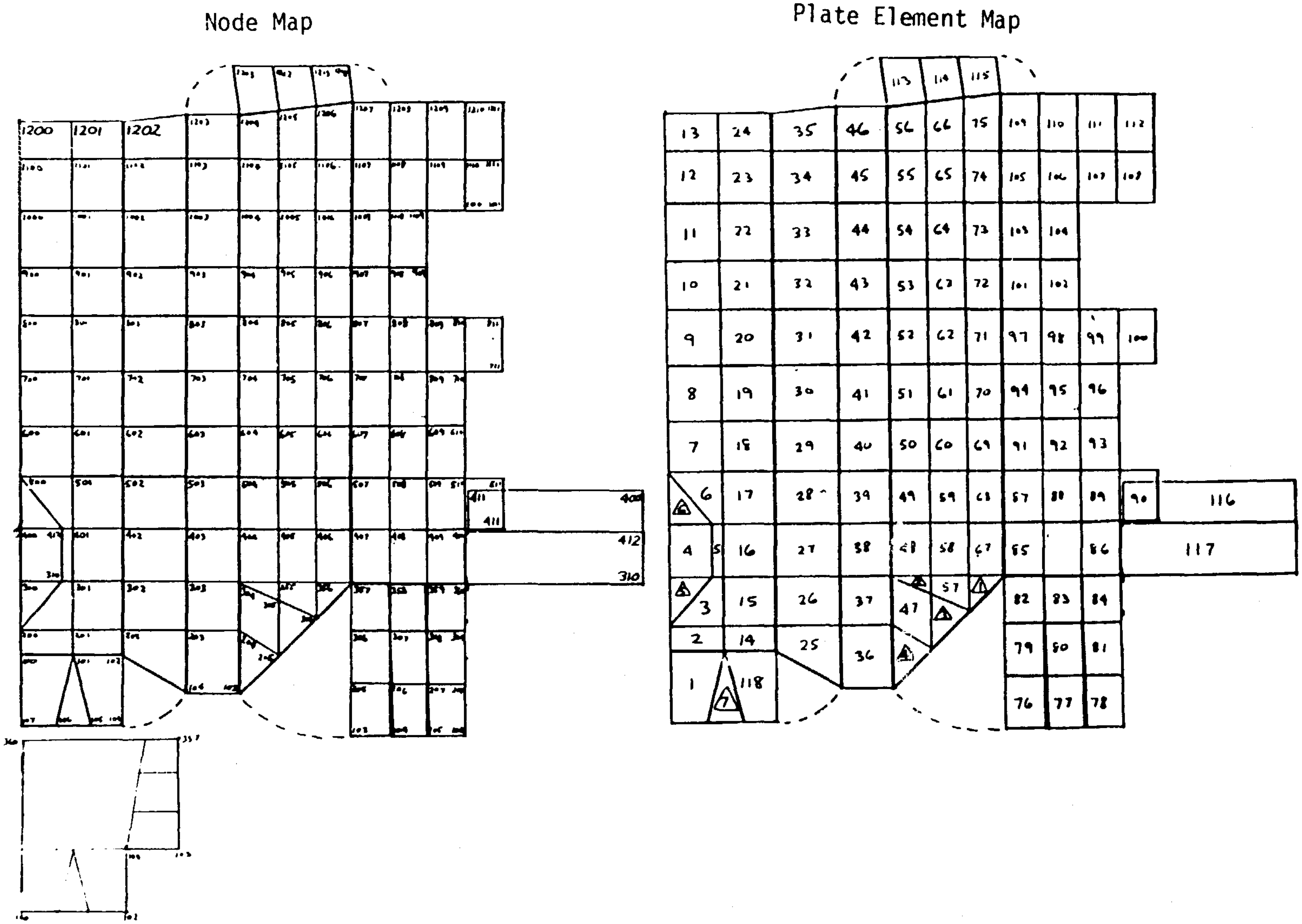
Node Map
Plate Element Map
1200
1201
1202
400
412
310
411
116
117
118

Figure 5.1(d). Element Projections.

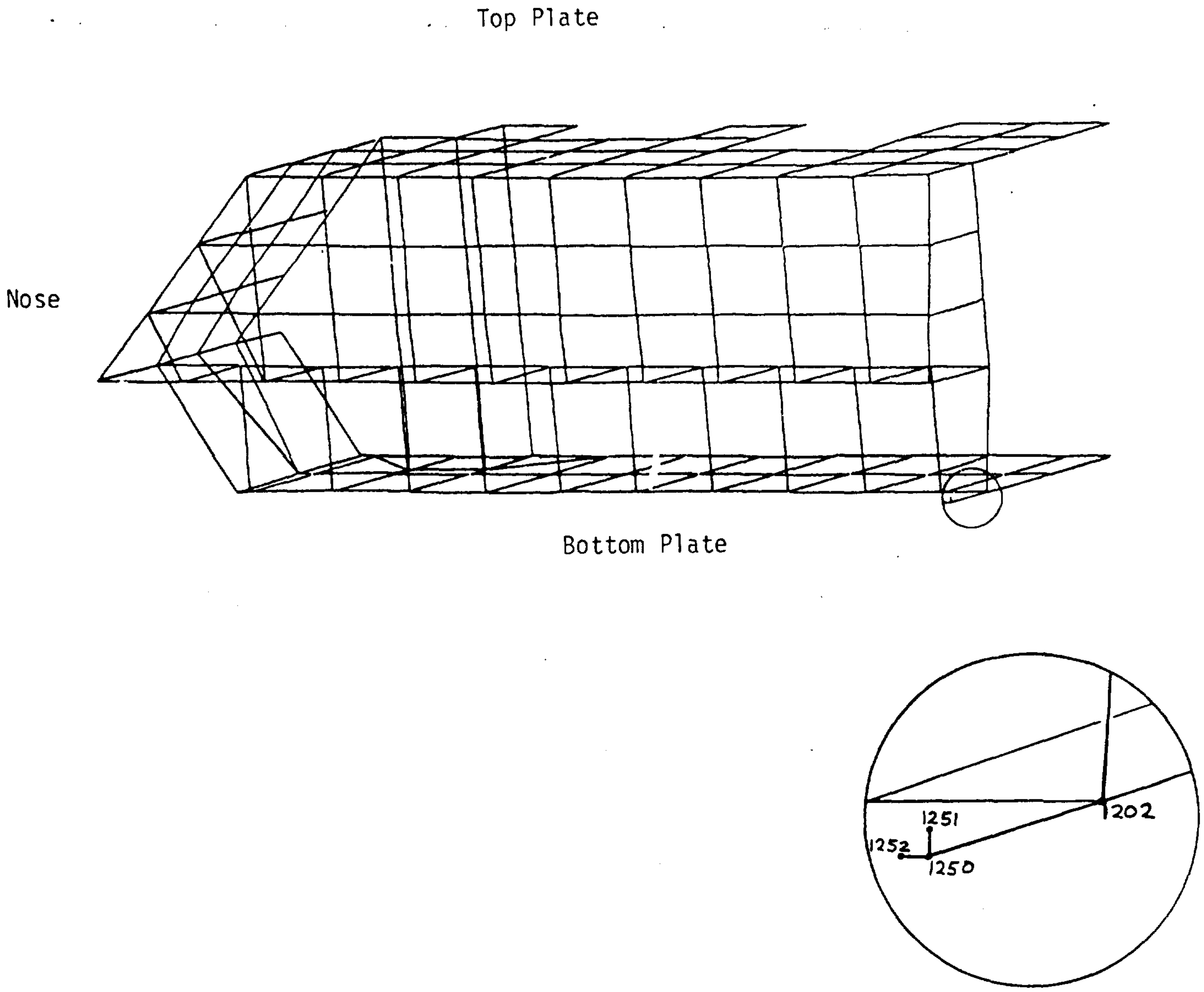
Top Plate
Nose
Bottom Plate
1251
1252
1250
202

Figure 5.2. Isometric View of Hull Elements - Initial Hull Model

unrestrained vibration. Thus, the actual grounding occurring during measurements (i.e., wooden cribbing arbitrarily placed in from each corner of the hull under the rear sill) was not modeled directly -- rather the free-force supports were thought most representative of the actual support conditions, although at high frequencies the supports should not affect the results to any great degree.

The degree of detail employed in the hull model adequately represents the elastic behavior of the vehicle in all but one respect; the local deflections near the point of application of force. Providing sufficient detail in the vicinity of the idler attach pad in the hull model would be prohibitively expensive and would decrease overall accuracy. Instead the local flexibility is simulated in another finite element model, a detailed representation of the rear lower corner region using the local geometry model shown in Figure 5.3 (a), which shows the nodal arrangement of the left-hand idler pad viewed from the centerline of the vehicle. In this analysis the idler was considered as a rigid body attached to the hull at the eight bolt locations. Loads developed in the idler in response to a horizontal or vertical force at the idler free-end were transmitted to the idler pad and surrounding structure through the bolt locations common to both idler and pad. The results constitute the stiffness matrix of only those local elastic details which are not represented in the hull elements. This local stiffness matrix is incorporated into the hull model as an equivalent beam. (The equivalent beam method is used because it is more convenient than applying an actual stiffness matrix; the solution is exact.)

Figures 5.3 (b) and (c) show the idler pad distortions produced by vertical and horizontal idler forces. Considerable out-of-plane deflections are produced by an in-plane force, as indicated in the idler pad flexibility matrices presented in Table 5.1. In this the deflections of the idler free-end to vertical and horizontal forces are presented in Table

TABLE 5.1 IDLER ATTACH PAD FLEXIBILITY

M113A1 - Left Side Pad

$$\begin{vmatrix} \frac{\delta_x}{F_x} & \frac{\delta_z}{F_x} \\ \frac{\delta_x}{F_z} & \frac{\delta_x}{F_z} \end{vmatrix} = \begin{vmatrix} .2633 & .0440 \\ .0440 & .2959 \end{vmatrix} 10^{-6} \frac{\text{in}}{\text{lb}}$$

M113A1 - Right Side Pad

$$\frac{\delta}{F} = \begin{vmatrix} .5983 & .1227 \\ .1227 & .4201 \end{vmatrix} 10^{-6} \frac{\text{in}}{\text{lb}}$$

(x - direction is horizontal (longitudinal) and z - direction is vertical)

Equivalent Beam: Length = 5 in.

$I_{x'} = 22.52 \text{ in}^4$

$I_{z'} = 31.60 \text{ in}^4$

$\theta = 34.84°$

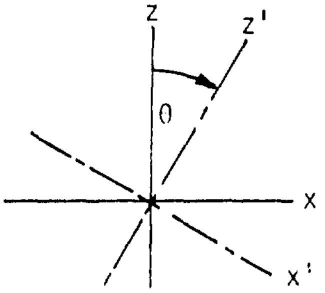

$I_{x'} = 20.58 \text{ in}^4$

$I_{z'} = 11.12 \text{ in}^4$

$\theta = 27.01°$

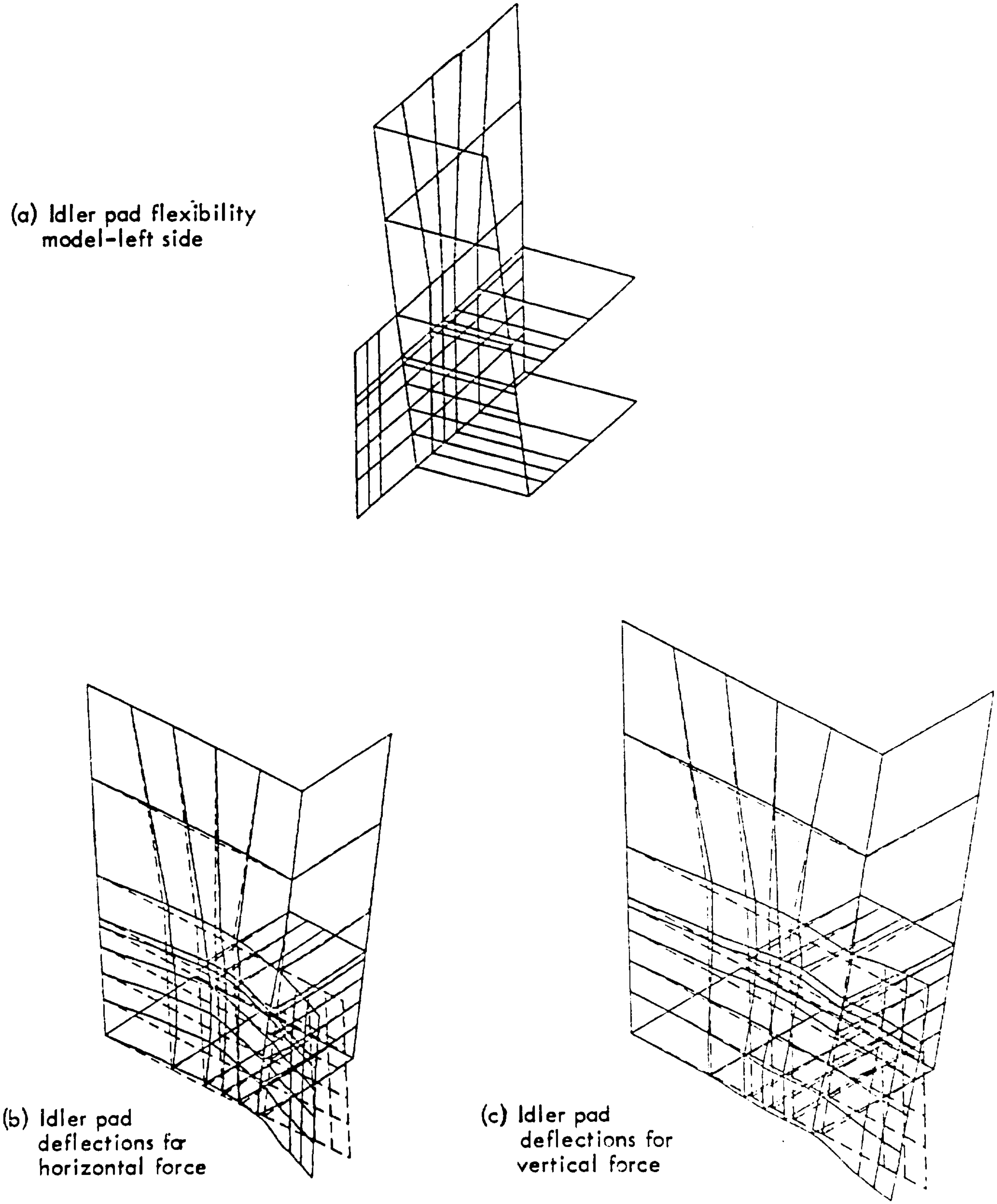

(a) Idler pad flexibility model-left side

(b) Idler pad deflections for horizontal force

(c) Idler pad deflections for vertical force

Figure 5.3. Idler Pad Static Flexibilities.

5.1. In this table, the deflections of the idler free-end to vertical and horizontal forces are presented for both left and right sides of the M113A1 idler attach. The left side horizontal and vertical flexibilities are approximately equal, but are less than the corresponding right side flexibilities by about a factor of 2: the mounting location of the left idler spindle is more forward of the plane of hull rear plate than that of the right side idler, and this forward location appears somewhat stiffer to idler forces. Table 5.1 also includes the characteristics of the equivalent beams used to represent the local deflection characteristics of the idler attach area. The equivalent beam has different vertical and horizontal stiffnesses and is inclined at angle θ (the angle of the principal axes of displacement relative to vertical) to produce the cross-coupling shown in Figures 5.3 (b) and (c). These characteristics are added to the F-E model in the modal extraction process in the program STAR.

The STARDYNE procedure consists of stiffness matrix formulation, eigenvalue/eigenvector determination, and dynamic response analysis, the first two steps being carried out in the program STAR and the latter in DYNRE2. In formulation of the stiffness matrix [K], the stiffness matrices for the individual finite elements are first computed and transformed, as required, in a form relating to a global coordinate system. Finally, the individual element stiffnesses contributing to each nodal point are superimposed to obtain the total assemblage stiffness matrix [K]. The eigenvalues (natural frequencies) ω^2 and eigenvectors (normal modes) q of the structural system are found by solving the equation

$$\omega^2 [m] \{q\} - [K]\{q\} = 0$$

where [m] is the (diagonal) mass matrix: the LANCZOS Modal Extraction Method was used. DYNRE2 uses these results to calculate the dynamic response (T.F.) of the structure for a set of unit sinusoid excitations applied to a specific node (idler) on the structure. References [5] and [6] contain theoretical and user information.

Appendix B contains sample input and output data for the initial hull F-E model for both the STAR and DYNRE2 programs. Sections B and C of Reference [6] will demonstrate the formats used for the various input and output data. In summary, Tables B.1 and B.2 contain, respectively, input and output data for program STAR and Tables B.3 and B.4 contain, respectively, input and output data for program DYNRE2: information in these tables should be self-explanatory. More general results for the initial model are described in the following paragraphs.

Table 5.2 presents abbreviated modal extraction data for both antisymmetric and symmetric centerline boundary conditions with comments concerning the nature of the resonant modes. Mode numbers 1 to 3 are translational modes of the undistorted vehicle, while higher modes involve distortion of the vehicle shape in bending and twisting. Figures 5.4 (a) to (o) show isometric views of typical vehicle mode shapes: both symmetric and antisymmetric examples are included. The annotation in Table 5.2 under the ** columns seeks to suggest the regions of the hull structure possessing the maximum kinetic energy. At low frequencies the

Table 5.2 -- MODAL EXTRACTION DATA: INITIAL HULL MODEL

MODE NO	SYMMETRIC MODES NATURAL FREQUENCY f_r	GENERALIZED WEIGHT M_r	MAX TRANSLATION NODE-DOF	**	ANTISYMMETRIC MODES NATURAL FREQUENCY f_r	GENERALIZED WEIGHT M_r	MAX TRANSLATION NODE-DOF	**
1	-.0	5398.7	100-1		-.0	3394.1	1208-2	
2	-.0	1572.4	107-3	T	-.0	3683.3	1207-3	T
3	.0	5318.5	1211-3		.0	1976.1	103-2	
4	22.2	304.44	1200-3	C	19.9	1820.4	1201-3	C
5	30.2	155.44	811-3	C,R	41.3	327.89	1201-3	C
6	38.5	104.95	1011-3	C,R	53.1	1333.5	704-2	C
7	45.5	488.57	1011-3	C	62.6	237.28	610-3	R
8	56.5	338.63	1200-3	F	74.3	235.45	909-3	R
9	62.8	100.53	311-3	R	85.8	628.94	909-3	C
10	66.6	164.47	800-3	F	98.7	742.06	610-3	C
11	79.9	76.618	1211-3	R	111.5	285.22	309-3	R
12	93.7	578.54	909-3	C	115.8	185.91	309-3	R
13	99.0	166.17	511-3	R,F	129.4	185.30	208-1	R
14	101.7	130.99	1211-3	R,F	150.5	133.62	909-3	R
15	107.6	136.03	600-3	F	156.2	854.75	505-2	C
16	114.5	119.46	811-3	R	167.4	418.60	610-3	C
17	118.6	122.14	309-1	F,R	179.6	929.51	509-3	C
18	136.6	209.21	711-3	R,F	190.2	336.35	805-2	C
19	145.6	110.26	511-3	R,F	198.6	116.08	901-3	F
20	162.2	217.30	1011-3	R	207.8	241.44	810-3	R
21	169.9	379.75	800-3	F	209.5	304.88	901-3	F,R
22	176.7	271.46	1000-3	F	219.2	212.09	701-3	F,R
23	177.4	230.66	909-3	R	222.0	444.19	510-3	R,S,F
24	193.4	372.63	509-3	R,F,S	230.5	460.20	810-3	R,S,F
25	200.8	401.06	709-3	R	236.9	701.31	309-3	R,S,F
26	219.5	361.43	605-2	R,F,S	245.9	165.46	810-3	R,S
27	225.5	116.17	1111-3	R	250.2	158.84	208-1	R
28	230.6	233.80	1111-3	R,S,F	252.5	188.72	1212-1	R,S
29	241.5	180.46	701-3	F,R	258.3	116.93	501-3	R,F
30	246.5	65.230	107-1	F	261.2	149.51	501-3	

** T = Translational Modes
F = Bottom plate well defined
R = Top plate well defined
C = Combined element, whole body motion
S = Side motion well defined

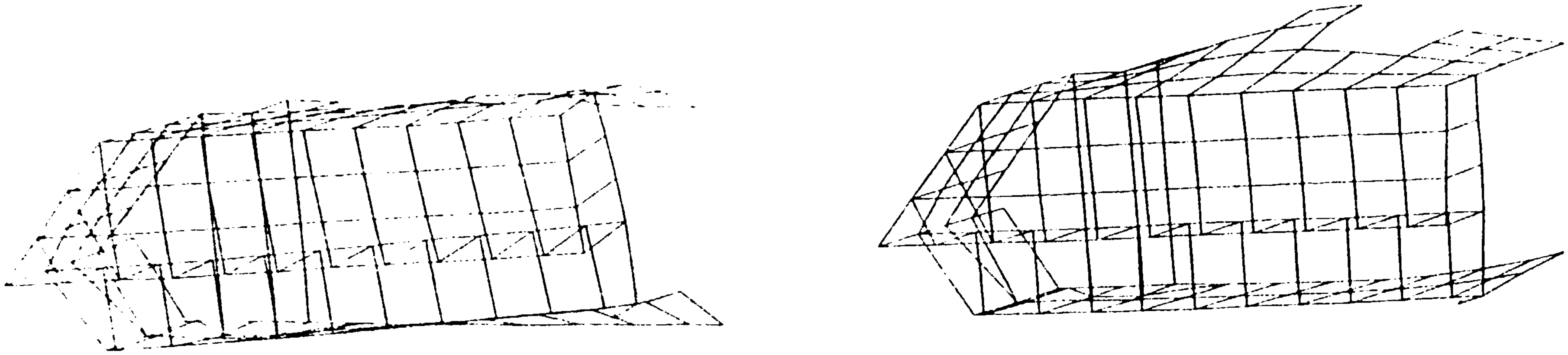

(a) 19.6 Hz Antisymmetric

(b) 30.3 Hz Symmetric

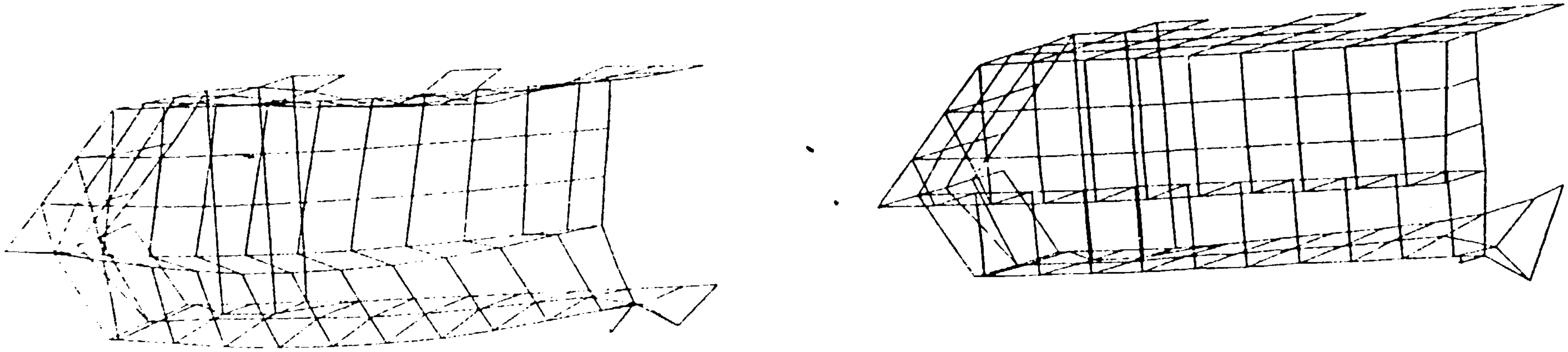

(c) 53.2 Hz Antisymmetric

(d) 56.4 Hz Symmetric

Figure 5.4. Typical Vibration Mode Shapes for Initial Model of M113 Hull

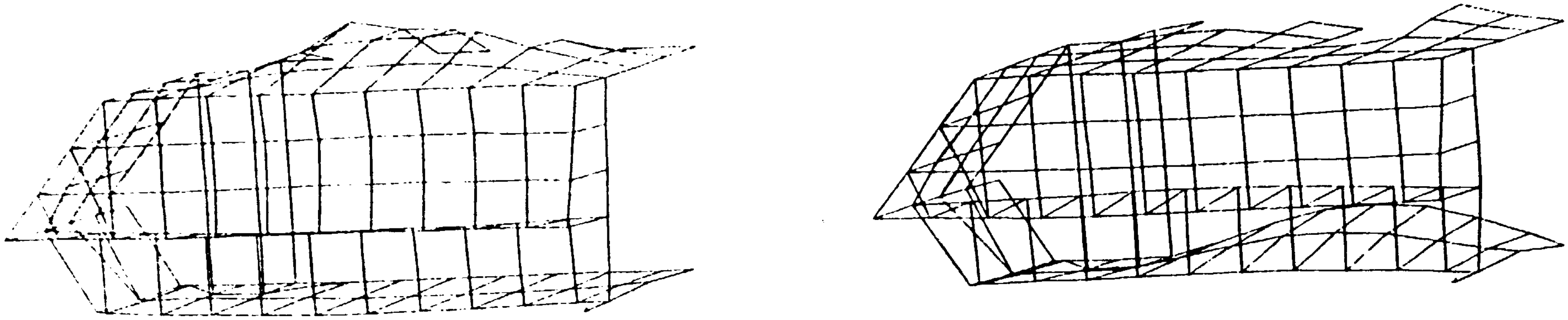

(e) 62.7 Hz Antisymmetric

(f) 66.8 Hz Symmetric

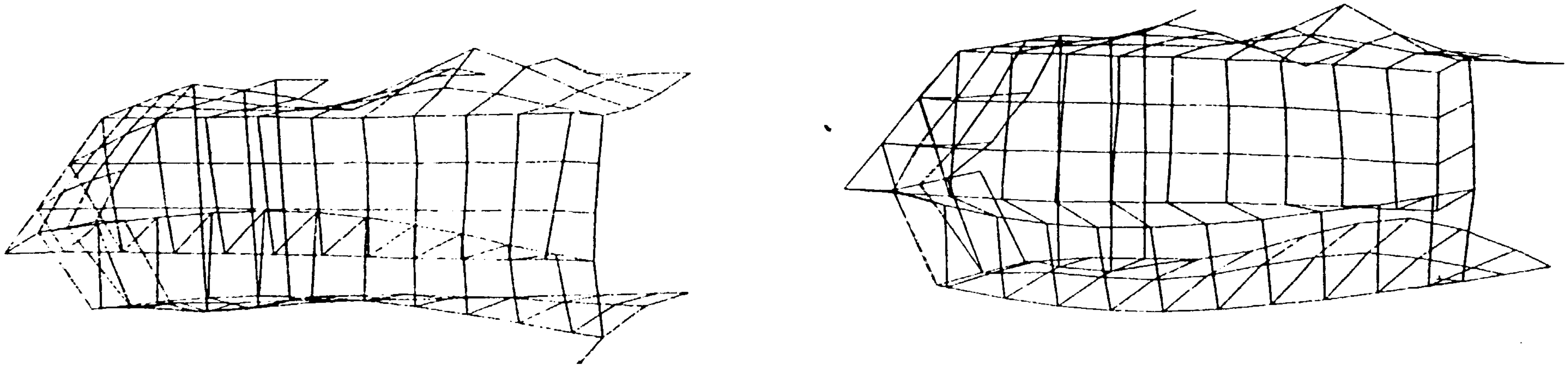

(g) 85.9 Hz Antisymmetric

(h) 93.7 Hz Symmetric

Figure 5.4. Typical Vibration Mode Shapes for Initial Model of M113 Hull

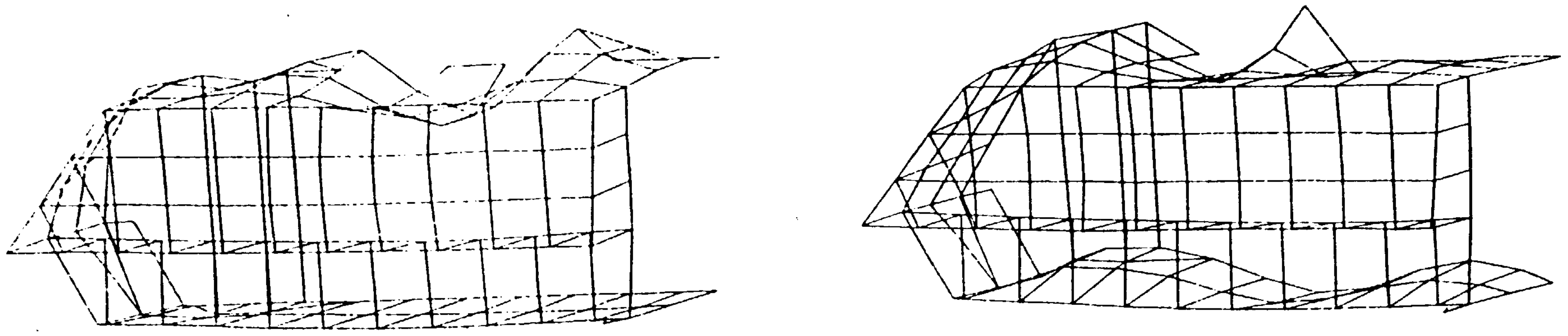

(i) 111.6 Hz Antisymmetric

(j) 136.6 Hz Symmetric

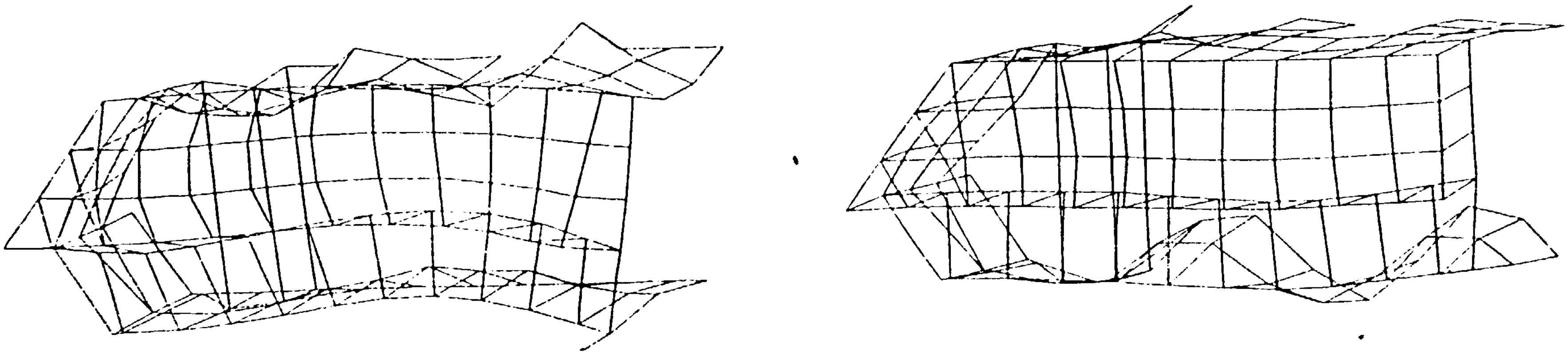

(k) 156 Hz Antisymmetric

(l) 176 Hz Symmetric

Figure 5.4. Typical Vibration Mode Shapes for Initial Model of M113 Hull

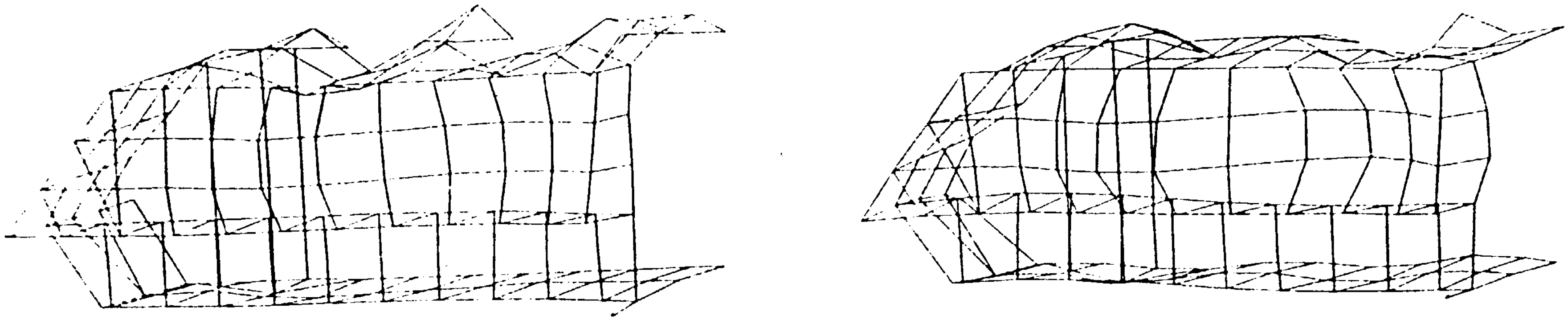

(m) 207 Hz Antisymmetric

(n) 219.7 Hz Symmetric

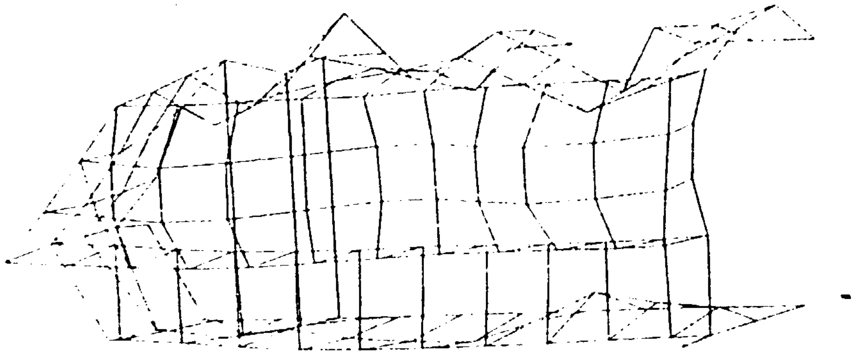

(o) 222 Hz Antisymmetric

Figure 5.4. Typical Vibration Mode Shapes for Initial Model of M113 Hull

vibration modes involve twisting, dilatation, and bending of the whole vehicle; as frequency increases, the structural wavelength decreases and the modal kinetic energy becomes confined to elements of the structure, in particular the bottom and top plates. This behavior is reflected in the generalized weight parameter M_r which decreases as mode order increases. The density of hull vibration modes generally tends to increase with increasing frequency, approaching at 250 Hz the modal density of a flat plate of area and mass equal to the total area and mass of the bare hull, viz., about 0.35 modes/Hz, as shown in Figure 5.5. The modal overlap, i.e., the ratio of modal bandwidth ($=f_r\eta_r$) to separation betweenresonant modes, is greater than unity so that a relatively smooth resonant idler inertance would be expected.

Examination of these mode shapes suggests certain potential modeling deficiencies. For example, in Figures 5.4 (c) and 5.4 (d) the deflection of the lower rear plate sill is large and out of, character with the nearby deflection pattern suggesting incorrect stiffness representation in the sill. In Figure 5.4 (g) substantial bottom plate, lower side plate, and sponson bending and twisting occurs, and one expects that inaccuracies in deflection adjacent to the idler may be generated due to there being no interior nodes in the sponson and lower sideplate. In Figure 5.4 (j) locally high deflections of the cupola boundary suggest a lack of boundary stiffness. In Figures 5.4 (l) and 5.4 (o) the node spacing is barely one-half the structural wavelength: more interior nodes are probably required for good representation of the bottom plate and top plate dynamics above 160Hz.

Root-mean-square inertance functions for the vehicle left-side idler for horizontal and vertical excitations are shown in Figures 5.6 (a) and (b), where the acceleration is measured in the direction of the applied force. In this calculation, modes of order greater that 13 were given a loss factor of 0.040, while lower order modes had a loss factor of 0.1. As both symmetric and antisymmetric modes have the same phase angle spectrum, the sum is found by arithmetic addition. In general, the antisymmetric modes are computed to make a stronger contribution than the symmetric.

We note that the vertical idler response to horizontal excitation (Figure 5.6 (c)) is much stronger at low frequencies than the horizontal due to cross coupling induced by the inclined rear plate of the hull. The vertical response to vertical excitation (Figure 5.6 (b)) is much stronger than for horizontal, reflecting the more direct coupling of vertical idler forces to resonant and nonresonant hull modes.

Comparisons between measured data and computed inertances are shown in Figure 5.7. In general, the measured and computed data have quite similar characteristics for both vertical and horizontal excitations. For the horizontal direction, fair agreement occurs at low (less than 40 Hz) and high (greater than 140 Hz) frequencies, but the computed curve is about 10 dB less than the measured results at about 80 Hz: it appears that significant errors in the horizontal hull stiffness have been made. In the vertical direction, however, the computed inertance generally exceeds the measured data, but has the same fluctuating (modal) characteristics.

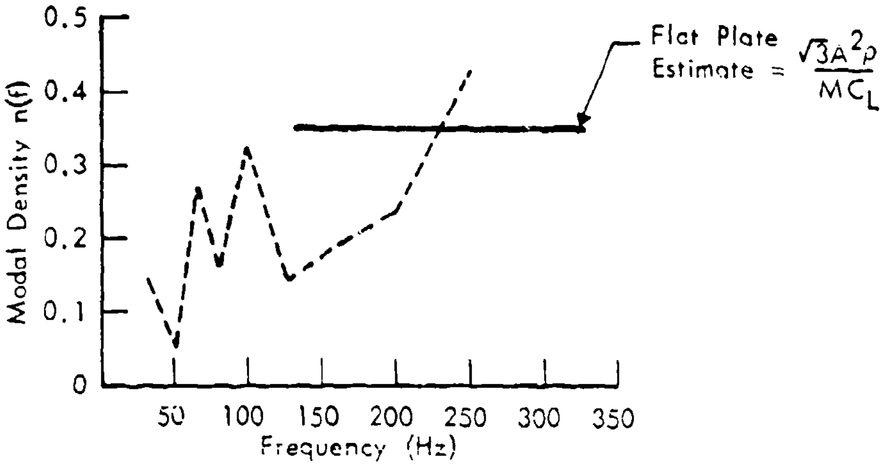

Figure 5.5. Hull Modal Density.

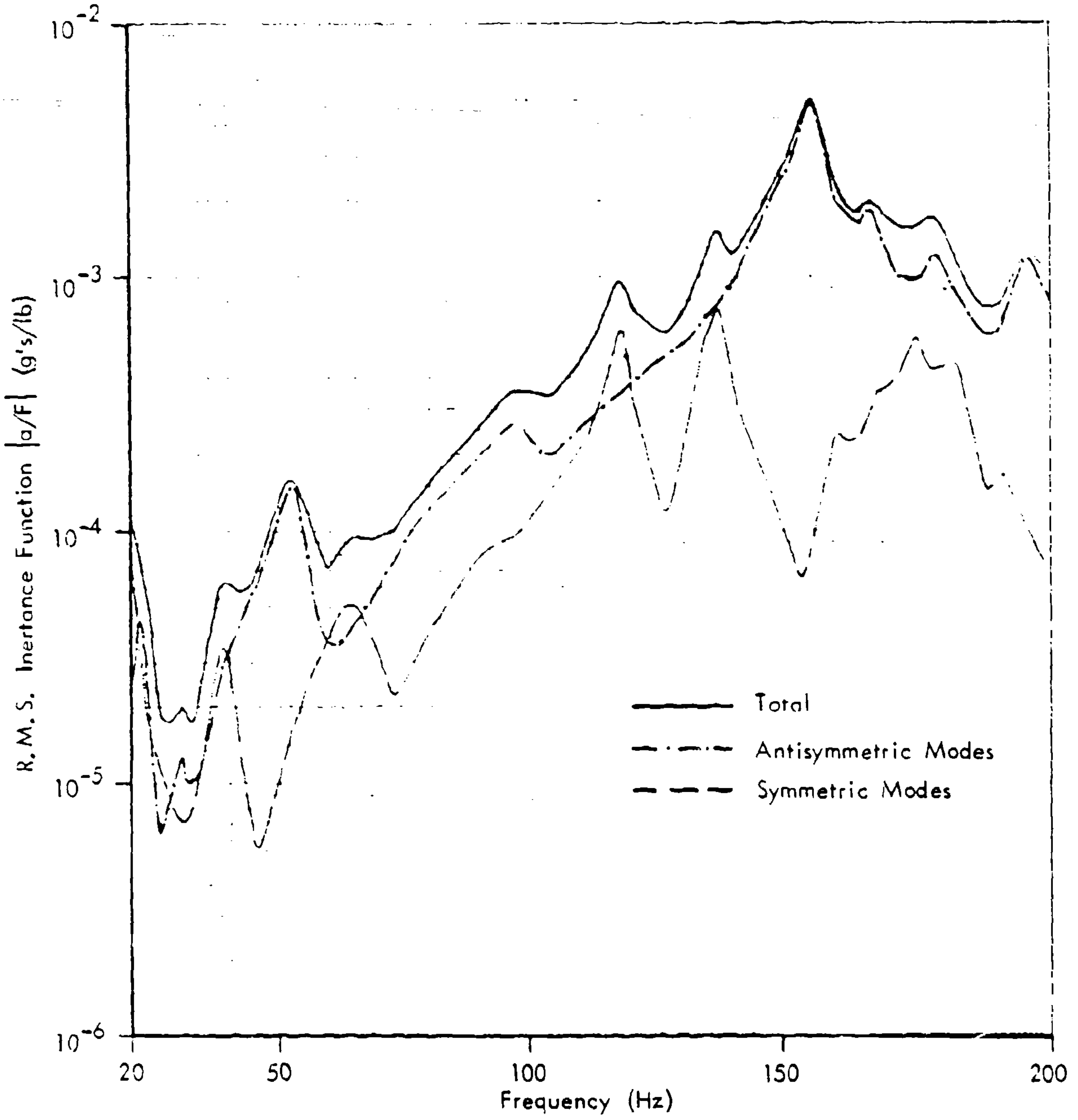

Figure 5.6(a). Horizontal Idler Response to Horizontal Idler Excitation.

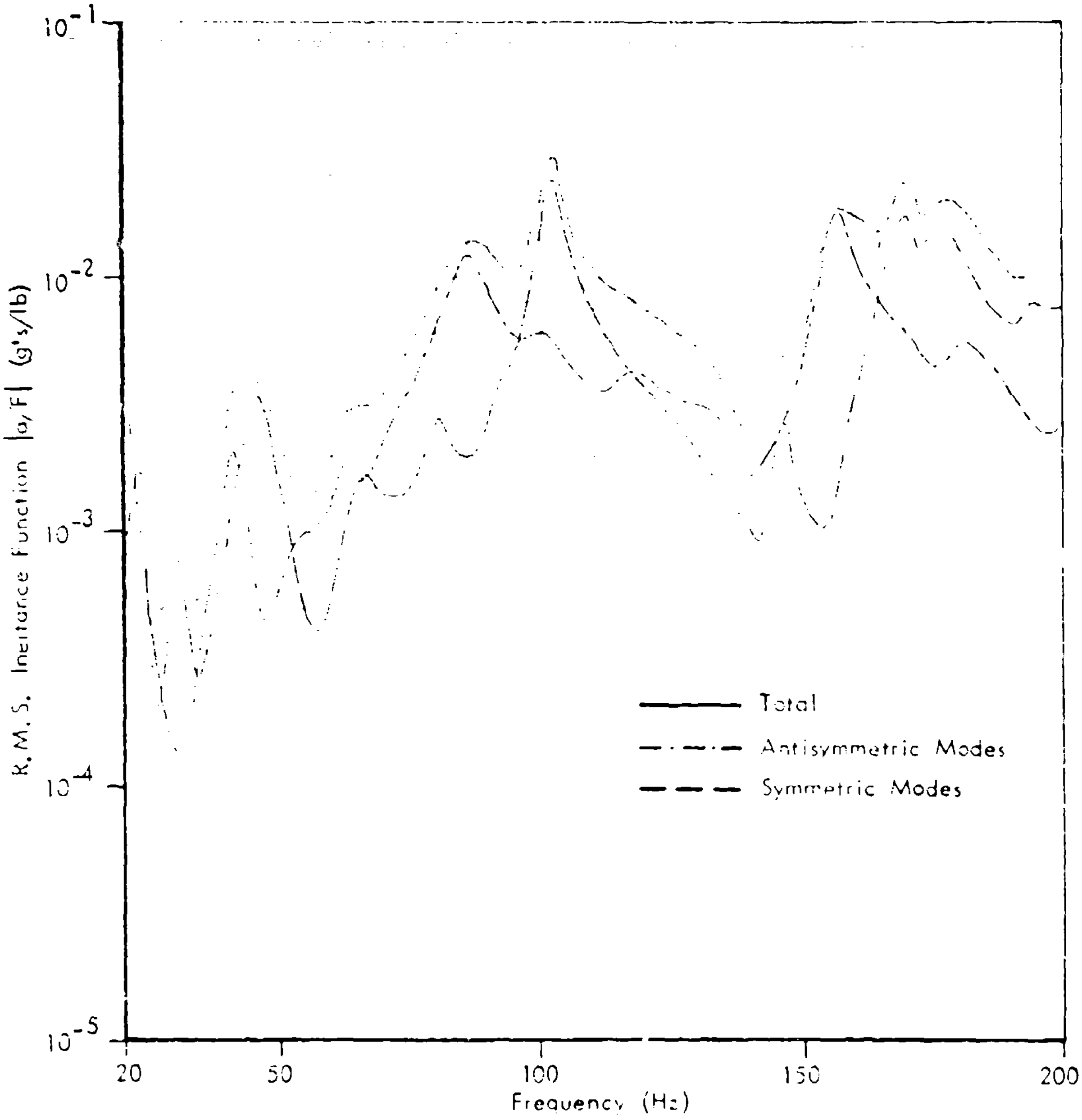

Figure 5.6(b). Vertical Idler Response to Vertical Idler Excitation.

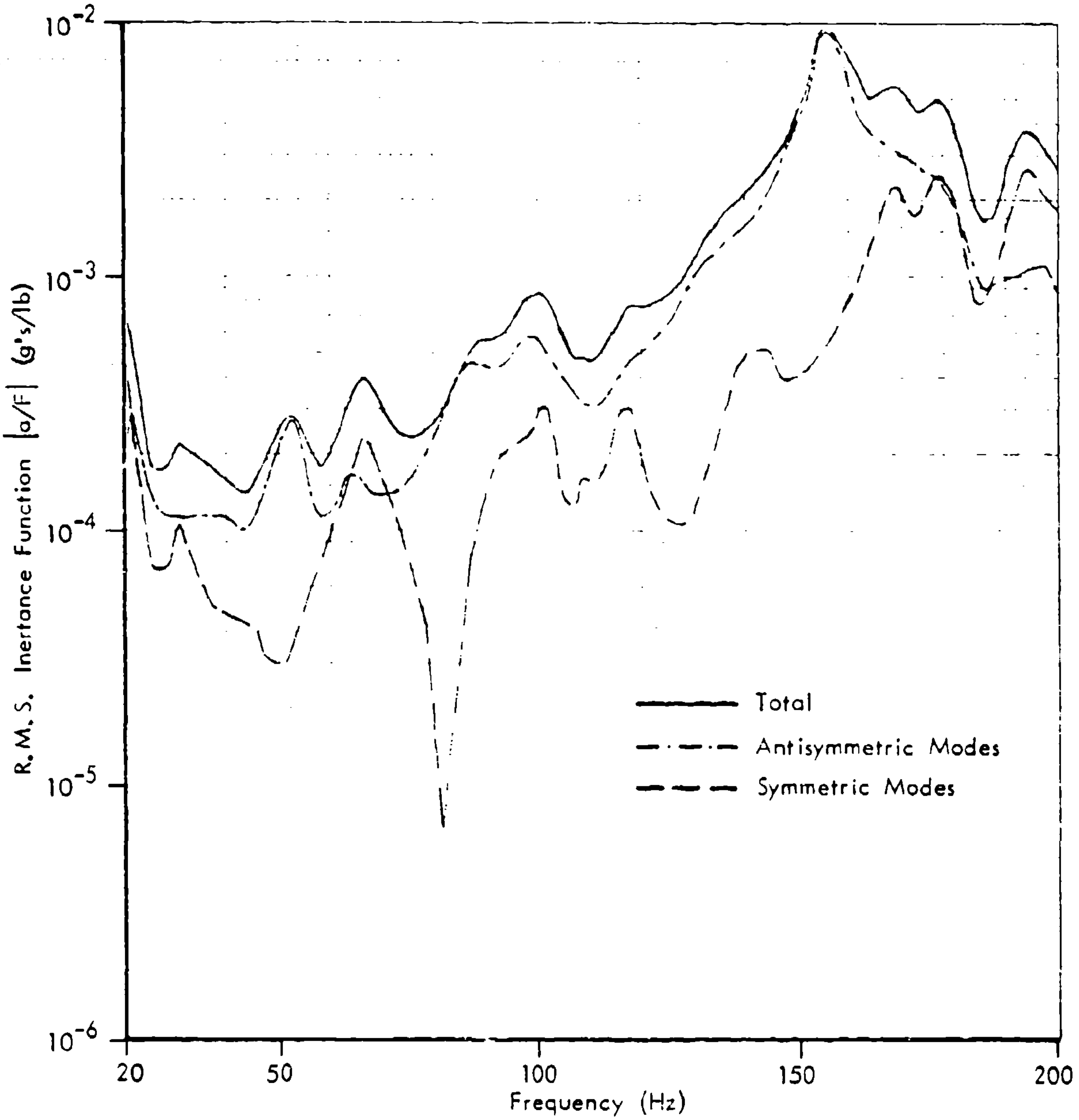

Figure 5.6(c). Vertical Idler Response to Horizontal Idler Excitation.

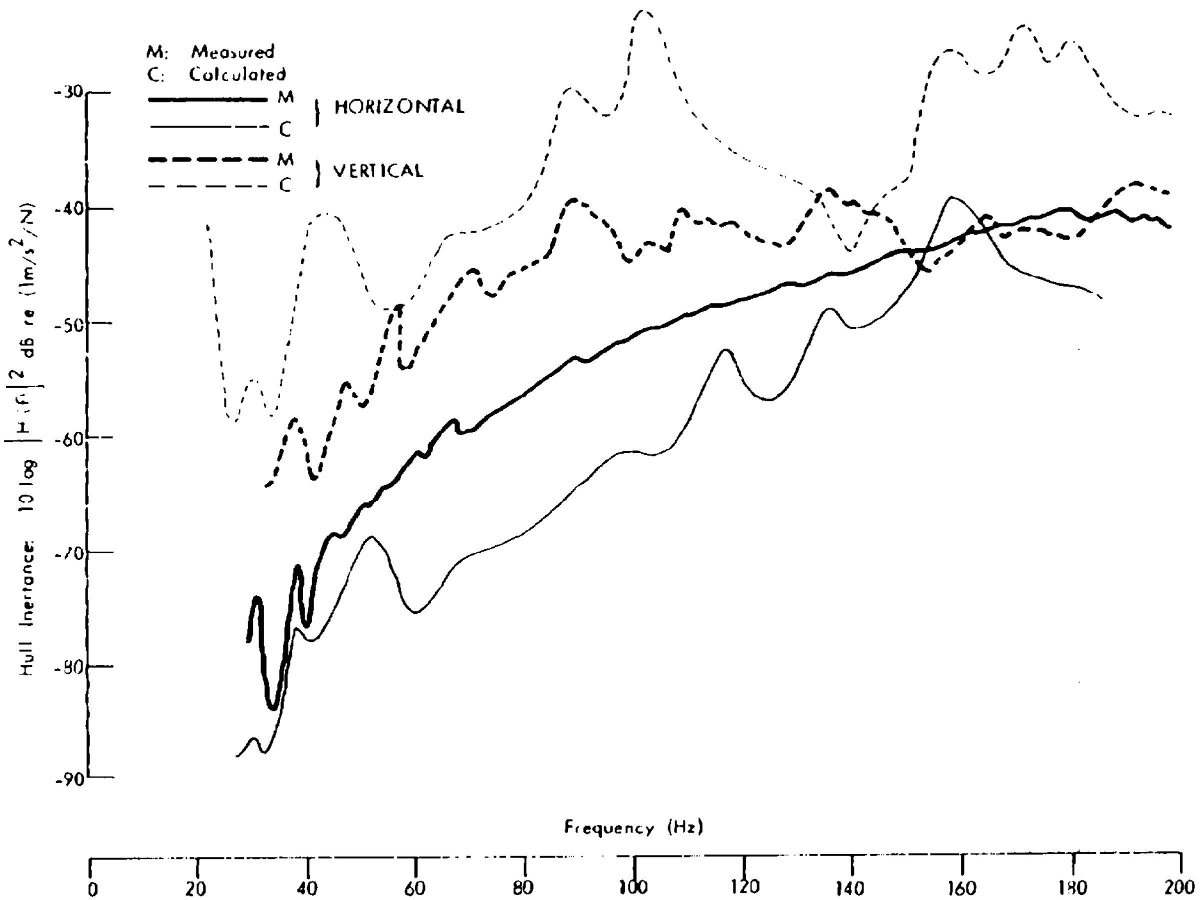

Figure 5.7. Comparison of Measured and Calculated Horizontal and Vertical Left Idler Spindle Inertances on M113A1 Vehicle.

Upgrading the loss factor to conform with measurements will improve the agreement only slightly for vertical excitation, but not effect the horizontal results.

Figures 5.8 (a) and (b) present measured and computed acceleration-to-force transfer functions for a single point on, respectively, the hull top and bottom plates for both vertical and horizontal excitations at the idler. For horizontal excitation, the computed top plate response lies about 10 dB above the measured data over most of the frequency range, but tends to agree reasonably with the measurements above 160 Hz. Similarly, for vertical excitation the computed top plate response matches the measurements fairly well above 100 Hz. In Figure 5.8 (b), fair agreement exists between measured and computed bottom plate response over most of the frequency range, except for horizontal excitation at frequencies above 100 Hz, where the computed response lies 10 to 15 dB above the measured data. While single point comparisons tend to be poor due to the spatial variability normally encountered, it appears that the bottom plate and, to a lesser extent, the top plate, are perhaps insufficiently stiff so that larger deflections are being produced than occur in practice. The simple model for the structural loss factor used in these initialcalculations was a stepped function of frequency, i.e., $\eta = 0.10$ for modes of order less than and equal to 12, and $\eta = 0.04$ for higher order modes.

To refine the damping representation, the solid loss factor curve from Figure 4.15, representing the mean of the M113A1 experimental data, was then input to DYNRE2 and the various transfer functions recalculated. In this way, for frequencies below about 100 Hz and above 160 Hz, the loss factors were increased, but otherwise were marginally decreased. Figure 5.9 provides a comparison of the calculated inertances for the initial stepped and the measured loss factor formulations. At most frequencies the strong oscillating behavior of the inertance curves has been smoothed so that the general similarity between measured and computed results for both directions has been improved. The effect is weaker for horizontal excitation than for vertical excitation. However, the general 10 dB differences between measured and computed inertances remain.

Figure 5.10 compares the bottom plate transfer functions for the initial stepped and measured loss factor data with the measured data: a general improvement in the agreement between measured and calculated results has been achieved, although the strong calculated response peaks at 100 Hz and 160 Hz are unaffected. The bottom plate appears to be insufficiently stiff. The transfer functions for the top plate at two different nodes (708 and 1008), using the measured loss factor data, are compared with the top plate transfer function for node 1009 in Figure 5.11, where the effect of loss factor changes on the T.F. result for node 1009 was expected to be small. Of interest here are (i) the closer agreement which exists at most frequencies below 200 Hz, between measured and computed results, and (ii) the considerable variation between the calculated data at different nodes in the top plate. Node 1009 is located at the free edge of the cargo hatch, where the predicted mode shapes have somewhat unrealistic deflections, whereas the nodes 708 and 1008 are located away from model and hatch boundaries where relative node displacements are more accurate. Space-averaging of results, both measured and calculated, is necessary for reliable evaluation of data!

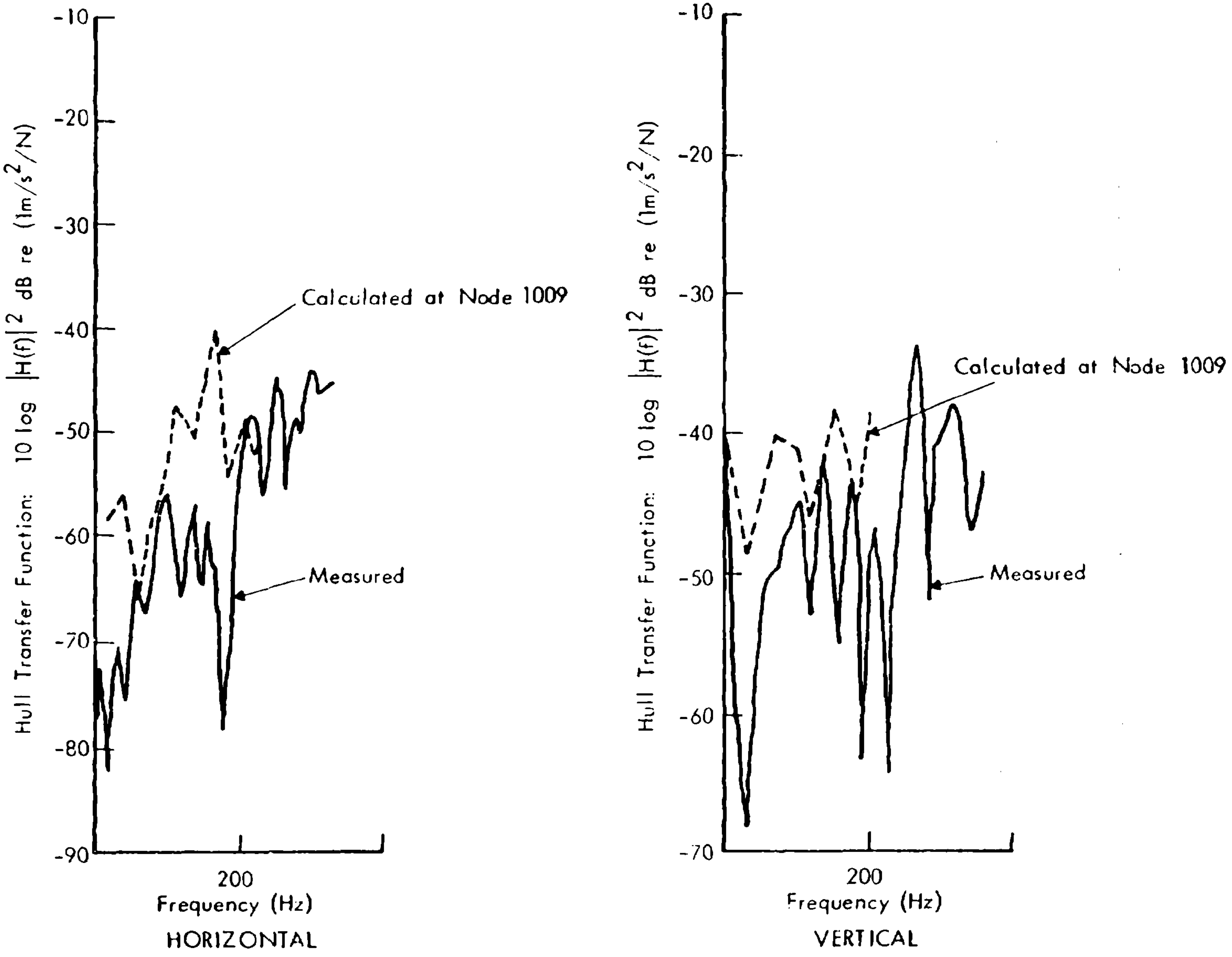

Figure 5.8(a). Top Plate Response to Idler Force.

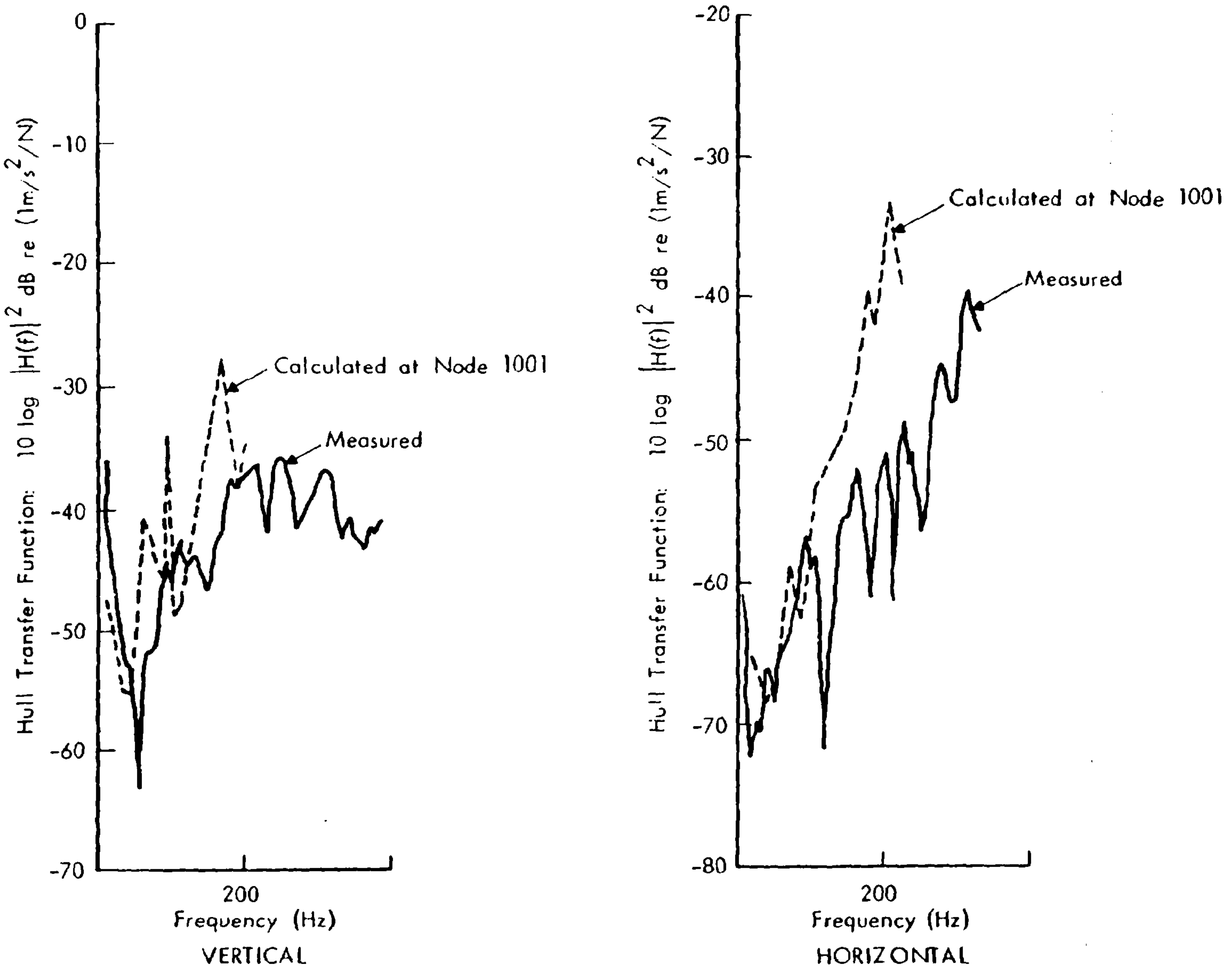

Figure 5.8(b). Bottom Plate Response to Idler Force.

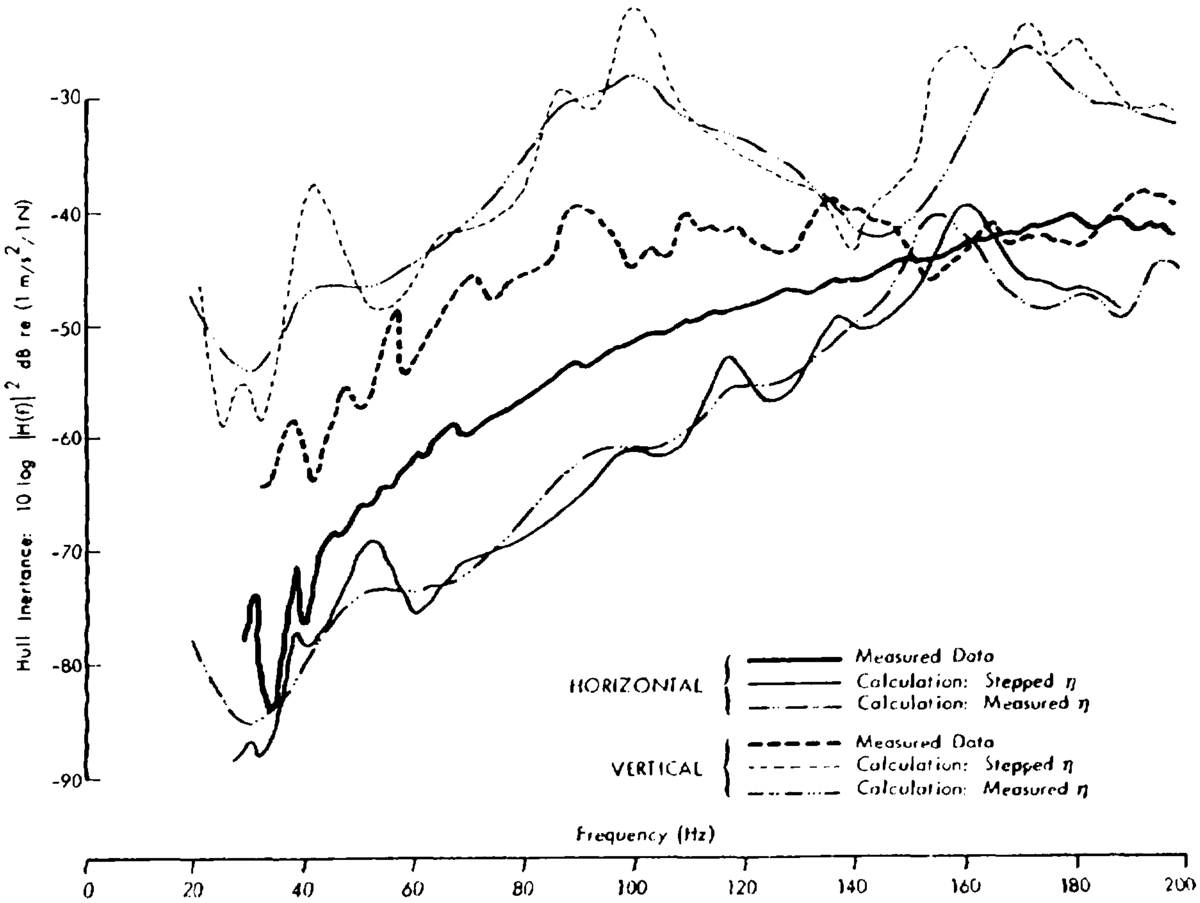

Figure 5.9. Effect of Variation in Loss Factor on Calculated Horizontal and Vertical Left Idler Spindle Inertances on M113A1 Vehicle.

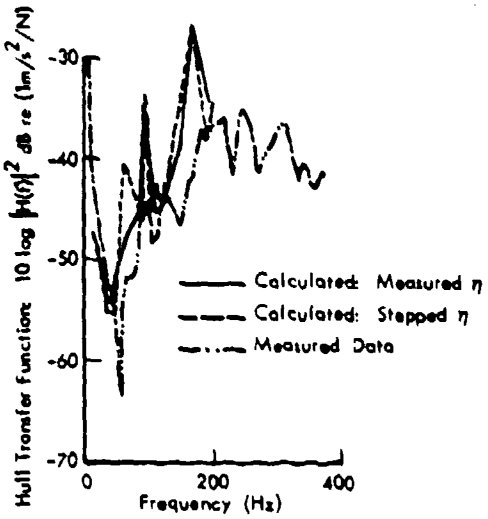

Figure 5.10. Effect of Loss Factor Changes on Calculated Bottom Plate Transfer Function (Node 1001) for Vertical Idler Force.

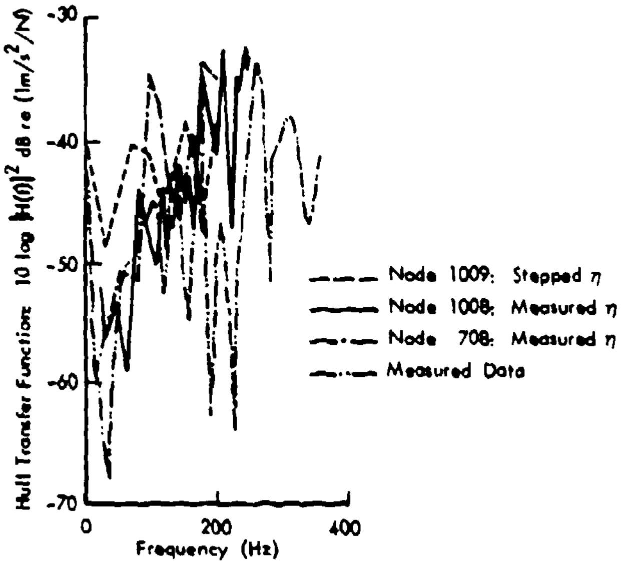

Figure 5.11. Top Plate Transfer Functions for Vertical Idler Force.

Modal extractions and transfer functions for the right-side idler were computed using the beam equivalent to the right-side idler deflection characteristics from Table 5.1. Results, identical to those already computed for the left-side idler (five significant figures), were calculated. In evaluation of the data it became apparent that the structural members controlling the overall stiffness characteristics of the idler inertance were located adjacent to the idler attach area, rather than the idler and the local structure themselves. For example, the flexibility of the box beam is much greater than that of both the idler beam itself and the combined idler and local attachment area, so that, to first approximation, the idler and attachment area rotate and deflect as a solid body against the restraint provided by the attached hull members, comprised of torsion box beam, bottom, side, and rear plates. Examination of the mode shapes reveals that little relative distortion of the box beam is predicted to occur between nodes 1002 and 1202, as shown in Figures 5.12(a) and (b) for two antisymmetric modes (85 Hz and 199 Hz). For example, the slope of the vertical displacement curve (X3) and the rotation of the box beam about its axis (θ) adjacent to the idler location (node 1202) are essentially constant between nodes 1002 and 1202. Since the idler and attachment area are more stiff than the connected structure by a factor of at least 100, changes in local stiffness by factors of two, as occur between left and right idler, will produce no significant changes in overall stiffness, mode shapes, or hull transfer functions, in accordance with the calculated results. Using this initial model, it appears that the hull stiffness, rather than the stiffness of the idler attach area, controls the hull power flow so that even large stiffness changes local to the (already very stiff) idler will have little impact on the hull vibration response.

Comparison of resonance frequency predictions with the limited experimental data available suggested that the geometry of hull had been represented sufficiently well. Errors in inertance magnitude were therefore proposed to result from inadequacies in modeling the stiffness characteristics of hull, including the area local to the idler attach. These tend to control the local mode shapes, i.e., the parameter $\psi_r(\tilde{x}_F)$. Therefore, detailed revision of the modeling processes was conducted for the stiffness contributions of the idler spindle and pad, box beam, and rear plate ramp sill. A minor error in the torsion constant of the box beam and the omission of the horizontal beam representing the lower rear plate were discovered. It was also considered that the support on wooden cribbing during inertance experiments may have strongly influenced the local mode shapes, but futher computations (modal extraction and transfer function for antisymmetric modes) showed that the hull support condition was of second order importance, resulting in only minor changes in low-frequency resonance frequencies, mode shapes $\psi_r(\tilde{x}_F)$, and transfer functions.

5.4.2 Revised Hull Dynamic Model

While the initial finite-element model of the M113 hull produced values of natural frequency which were in good agreement with experimental values, the vibration response levels were noticeably different. Response to vertical excitation was in excess of measured values, both at

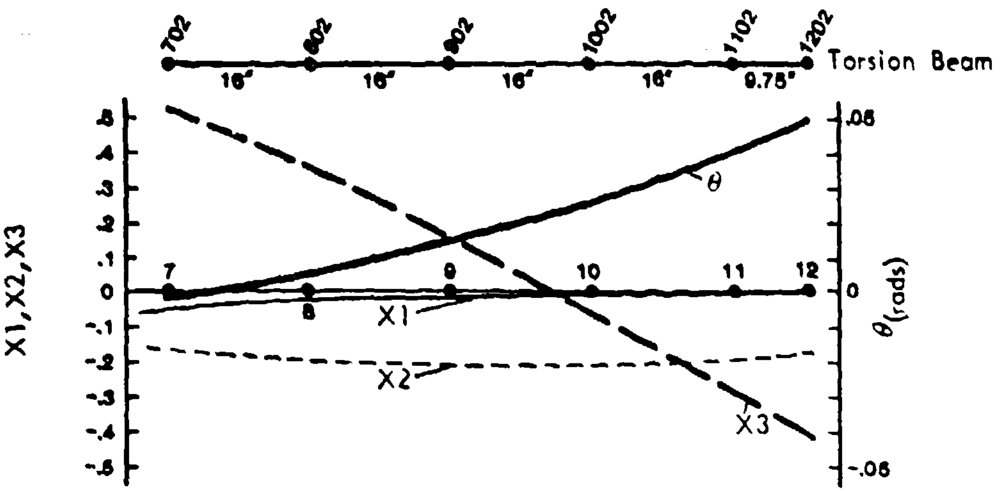

(a) Antisymmetric Mode Shape at 85.9 Hz

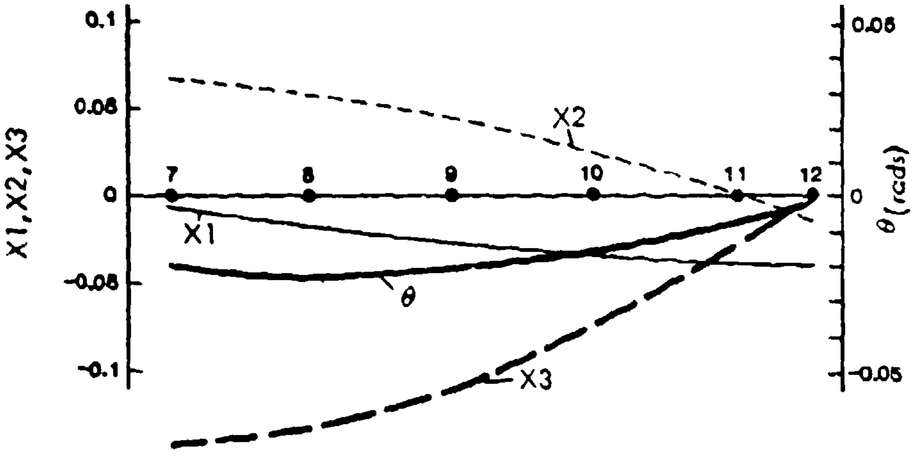

(b) Antisymmetric Mode Shape at 198.6 Hz

Figure 5.12. Representative Modes Shapes of Torsion Box Beam.

the driving point and in the major panels. Response at the driving point (the idler spindle) to horizontal excitation was less than that measured. Investigation of the problem included revision of the values of loss factor used and modification of the method of support. The results have suggested that second-order details in structural modeling were the most likely cause.

The model has therefore been made somewhat more detailed to represent those structural effects which provide local stiffness, introduce boundary effects, or provide interpanel coupling. As an example, the geometry of the driver's hatch and cupola was refined, and the flexural stiffness of the hatch rims were added. Also, the element detail was refined in the region of the idler to better accomodate the load paths resulting from idler excitation. An additional measure of the effects of changing idler location can be performed with this model, and better panel-averaged deflections can be computed. The effect of the lower side plate is now better represented, and possibly significant geometric details in the location of floor supports and in rear panel size have been revised. The model revision has required additional nodes, which with extension of the frequency range of interest, has caused the solution cost to roughly double.

The revised modeling array of nodes and plate elements is shown in Figure 5.13(a), in isometric view, and in Figure 5.13(b) in a single projection where all the elements and nodes are connected as modeled. As already noted, more detailed representations for the top and bottom plates have been made, including adding in the driver's hatch, refining the cupola, and upgrading the interpanel coupling characteristics of the stiffening members at the top of the rear plate and at the ramp sill. Plate elements have been used more extensively in the rear panel. Idler "equivalent beams" have been located at four positions (nodes 103 and 203, and 104 and 204) representing the geometric location of the left and right idlers on the M113A1 and AIFV vehicles, respectively. The stiffness of the floor plate supports has been increased from the initial incorrect and low values, and the longitudinal centerline floor plate support has now been included. The geometric location of these supports is now more accurate. More definition in the lower side plate has been included.

The local flexibility characteristics of the idler attach area was the same as used in the initial model, but the different idler characteristics are now located at different nodes to correspond to different idler configurations.

Modal extractions and dynamic response (T.F.) calculations for the revised hull model were performed as before, except for two loading conditions corresponding to sets of unit sinusoidal excitations applied at nodes 1 and 4 (the most extreme idler positions). Appendix C contains sample input and output data for this revised model for both the STAR and DYNRE2 programs. In summary, Tables C.1 and C.2 contain, respectively, input and data for programs STAR, and Tables C.3 and C.4 contain, respectively, input and output data for program DYNRE2. General results are described below.

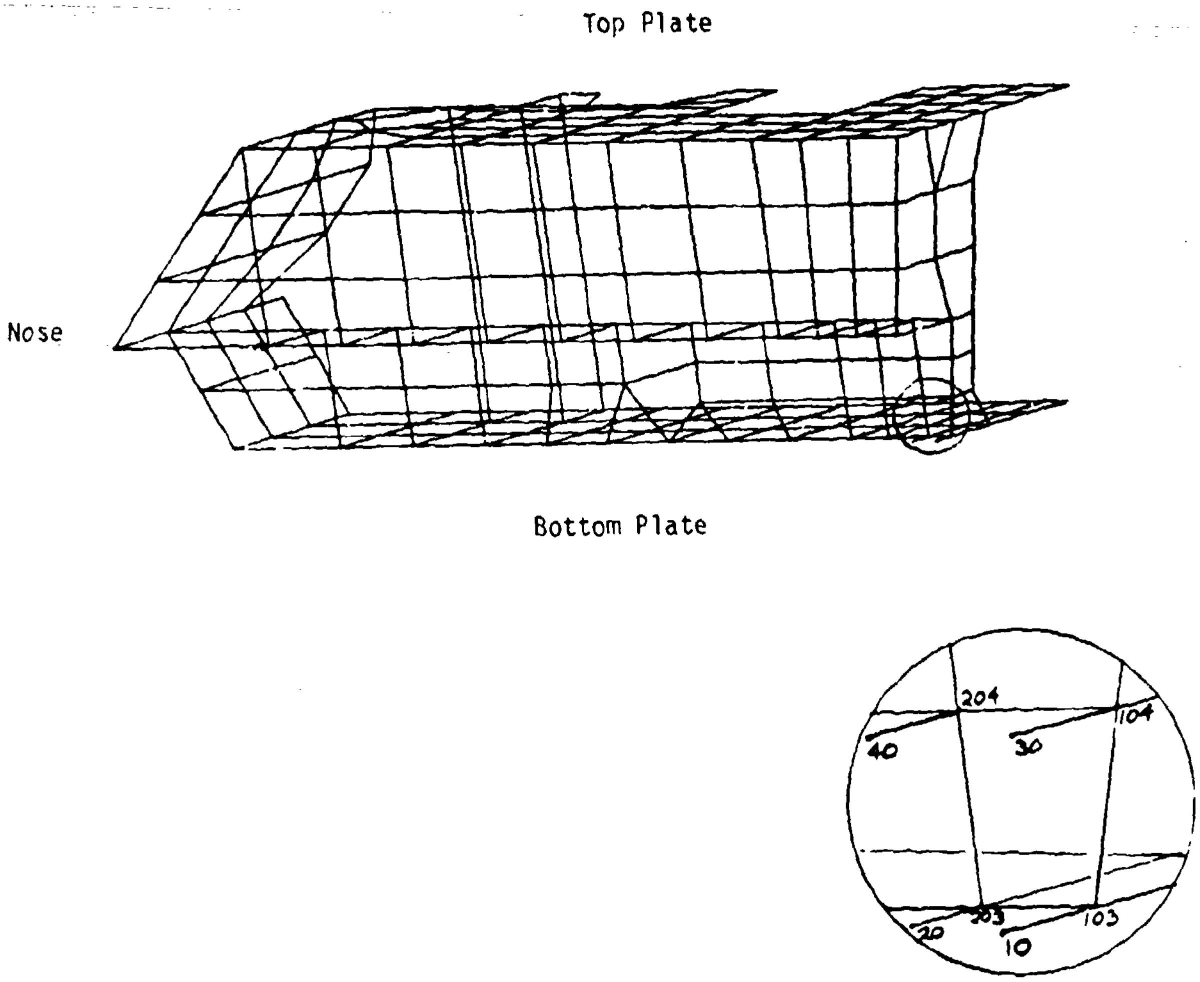
Top Plate
Nose
Bottom Plate
204
104
40
30
203
103
20
10

Figure 5.13(a). Isometric View of Hull Elements - Revised Hull Model.

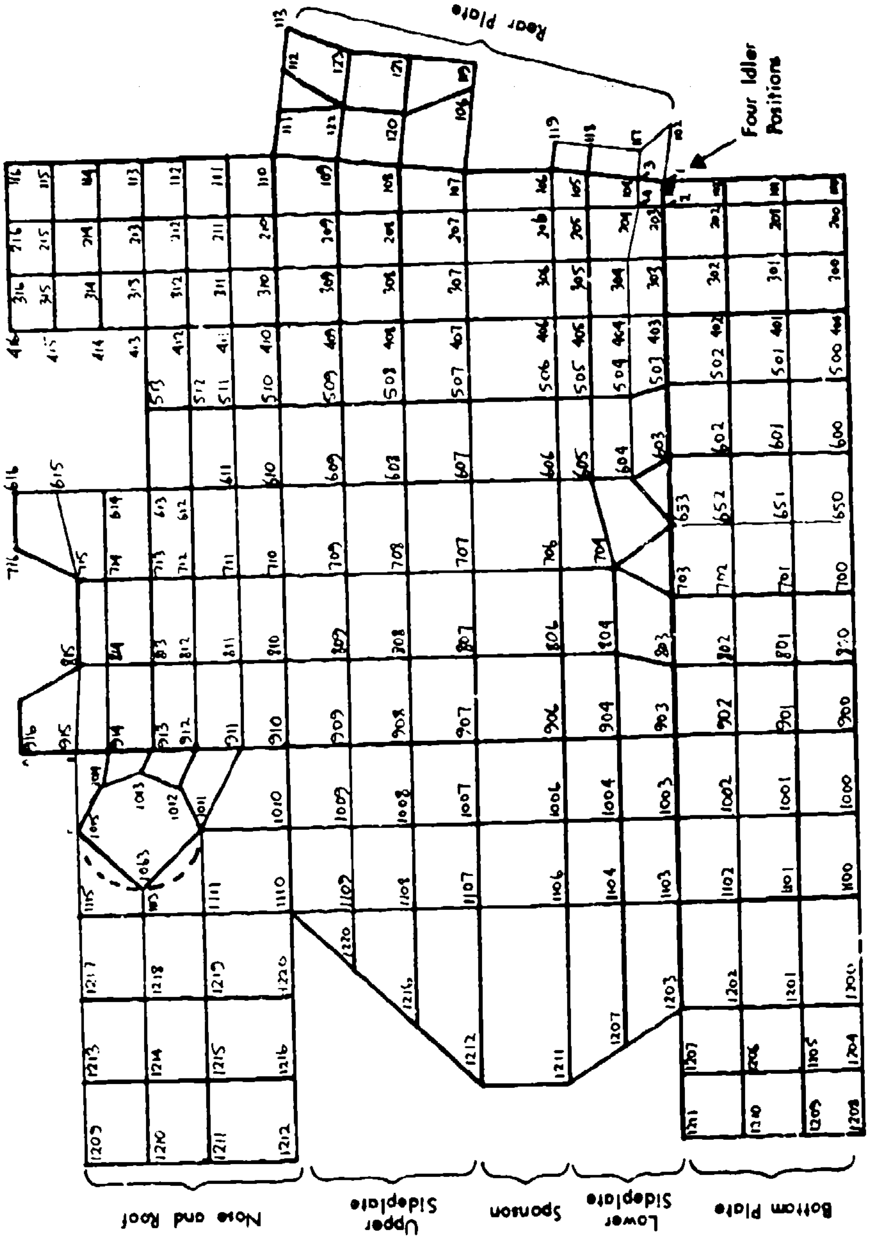
Rear Plate
Four Idler Positions
Nose and Roof
Upper Sideplate
Sponson
Lower Sideplate
Bottom Plate

Figure 5.13(b) Node Map of Revised Hull Model: Projection.

Table 5.3 presents abbreviated modal extraction data for both antisymmetric and symmetric centerline boundary conditions. Comparison of data in Table 5.3 with data from the initial hull model (Table 5.2) reveals that the distribution of resonance frequencies has remained much the same as for the initial model. However, the frequencies of the lowest order symmetric and antisymmetric modes have been increased by 50% and 100%, respectively, by correcting the bottom plate stiffness modeling; the modes associated with flexure of the rear sill have been eliminated by upgrading the representation for the rear hull plate. About 70 hull modes exist below 300 Hz.

Figures 5.14 (a) to (k) show isometric views of typical vehicle mode shapes, with symmetric and antisymmetric examples included. These shapes are, in general, very similar to those computed with the initial model, but are more precise and realistic due to the greater density of nodes in bottom, top, and lower side plates, and to the refined representation by plate elements of the rear hull plate. For example, Figures 5.14 (h) and (i) demonstrate the strong deformations occuring in the hull rear plate, which influence the power flow from idler to top plate. Figure 5.14 (k) shows how, even at frequencies as low as 300 Hz, the floor motion is restrained by the spanwise stiffeners, and subpanels tend to vibrate as individual elements.

Comparison of measured and computed inertances for the idler attach location on the left-side of the M113A1 is presented in Figure 5.15. The measured loss factor data from Figure 4.15 is used in the calculations. The agreement for vertical idler force is close, particularly at frequencies above 100 Hz, and much improved in comparison with the calculated results from the initial hull model. In general, the calculated inertance exceeds the measured data by about 3 dB. The calculated horizontal inertance is about 10 dB below the measured data over the whole frequency range. The horizontal stiffness of the hull has been overestimated even in the revised hull model with its improved hull definition in the idler attach area. However, since the vertical inertance is higher than the horizontal, and is closely predicted, further refinement of the representation for the idler attach area is not warranted at this stage. Further comparisons will be limited to vertical idler forces.

The calculated responses of the hull top plate at nodes 313 and 813 for vertical force input at the left-side idler is presented in Figure 5.16 together with the measured response near node 312. Considerable variability in response is predicted over the surface of the top plate; the computed variation between the two nodes at a particular frequency is generally about 7 dB. The measured data is quite similar to the calculated response of node 813. It is clear that space- and frequency-averaging of both measured and calculated transfer functions would make comparisons more valid. Similar comparisons with measured data for other hull surfaces have not been carried out on this basis but are left until suitable space-averaging software is available to automate the reduction of modal extraction data following the methods suggested in Section 5.2.

Table 5.3 -- MODAL EXTRACTION DATA: REVISED HULL MODEL

MODE NO	SYMMETRIC MODES NATURAL FREQUENCY f_r	SYMMETRIC MODES GENERALIZED WEIGHT M_r	SYMMETRIC MODES MAX TRANSLATION NODE-DOF	**	ANTISYMMETRIC MODES NATURAL FREQUENCY f_r	ANTISYMMETRIC MODES GENERALIZED WEIGHT M_r	ANTISYMMETRIC MODES MAX TRANSLATION NODE-DOF	**
1	-.0	5042.3	1203-1	T	-.0	3145.4	110-2	T
2	-.0	4740.1	116-3	T	-.0	3057.8	1203-2	T
3	.0	1621.1	1210-3	T	.0	2178.2	1211-2	T
4	29.5	134.55	616-3	R,C	42.4	1632.3	121-3	C
5	39.6	86.839	416-3	R	55.0	294.75	1217-3	R
6	55.0	1031.1	607-4	S	66.9	191.53	513-3	R
7	70.3	407.01	1217-3	F,R	72.3	716.65	1217-3	C,S
8	79.6	196.66	1217-3	R,C	86.0	90.934	1213-1	R
9	87.0	309.20	1217-3	R,F	89.3	130.29	414-3	R
10	90.8	764.48	907-2	C	103.0	1732.8	904-3	C
11	105.1	180.73	600-3	R,F	113.6	967.57	806-2	C,S
12	110.3	176.10	513-3	R,F	134.9	179.53	513-3	R
13	119.5	317.92	100-3	F,R,S	161.3	584.79	1213-1	C
14	121.5	226.43	513-3	R,S,F	165.3	703.50	1213-1	C,R
15	143.4	150.02	1213-1	R	171.3	305.41	513-3	C,R
16	152.1	133.02	700-3	F	174.2	318.10	513-3	C,R
17	157.8	120.93	416-3	R	186.4	175.15	513-3	C,R
18	168.6	401.30	216-3	R	199.6	275.64	1012-3	R,S
19	172.7	95.490	1100-3	F,R	208.8	156.50	1213-3	R
20	176.1	145.10	1100-3	R,F	213.3	485.47	408-2	R,S
21	189.2	373.63	513-3	S	216.6	101.90	121-1	R
22	197.3	232.60	216-3	S,R	230.9	221.37	121-1	R,S
23	206.3	113.65	1213-3	R	234.8	379.77	121-1	R,S,F
24	208.6	237.67	816-3	R	244.2	106.38	121-1	F,S
25	218.2	370.39	408-2	S,R	251.6	400.88	615-3	R,S
26	225.3	319.53	801-3	R,F	257.3	410.66	801-3	R,S,F
27	229.8	125.17	513-3	R,S	259.4	312.77	1008-2	S,R,F
28	239.4	47.134	121-1	F	265.4	142.25	121-1	R,S
29	245.1	72.512	121-1	F.R	273.0	115.84	501-3	F
30	254.9	430.86	121-1	R,S	282.7	171.30	501-3	R,F,S

** T = Translation Modes
F = Bottom plate well defined
F = Top plate well defined
C = Combined element, whole body motion
S = Side motion well defined

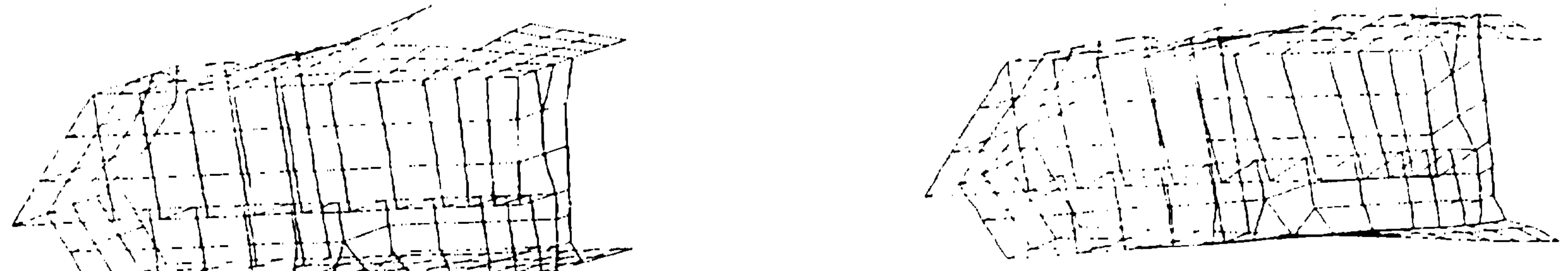

(c) 29.5 Hz Symmetric

(b) 41.3 Hz Antisymmetric

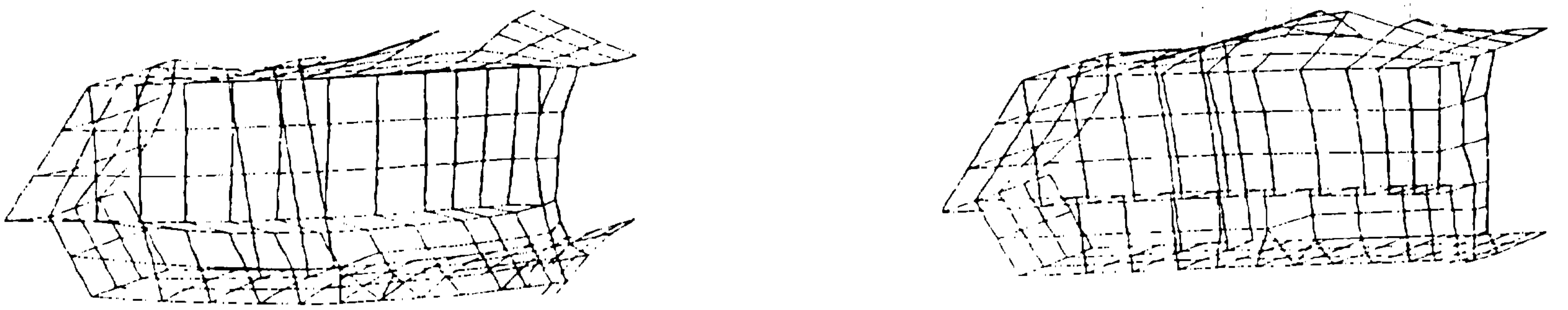

(c) 55.0 Hz Symmetric

(d) 62.6 Hz Antisymmetric

Figure 5.14 Typical Vibration Mode Shapes for Revised Model of M113 Hull.

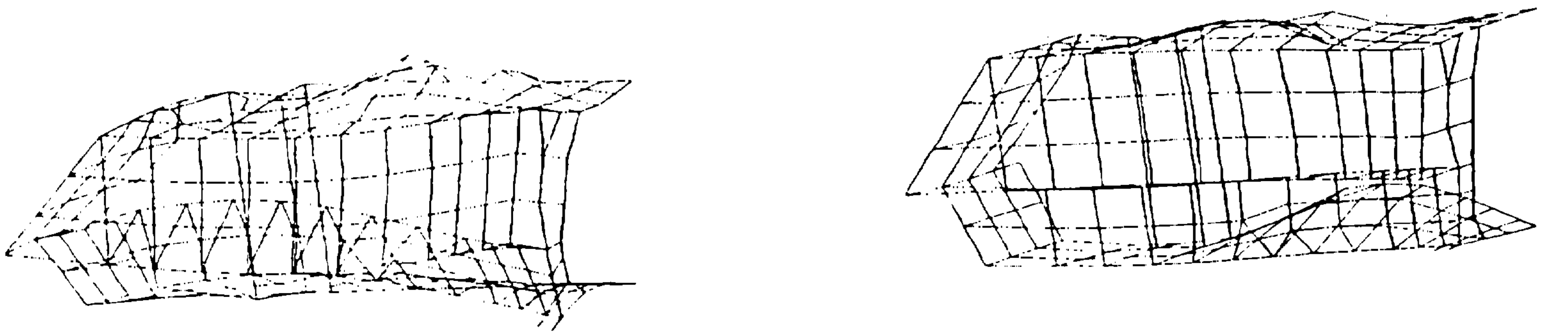

(e) 103.0 Hz Antisymmetric

(f) 105.0 Hz Symmetric

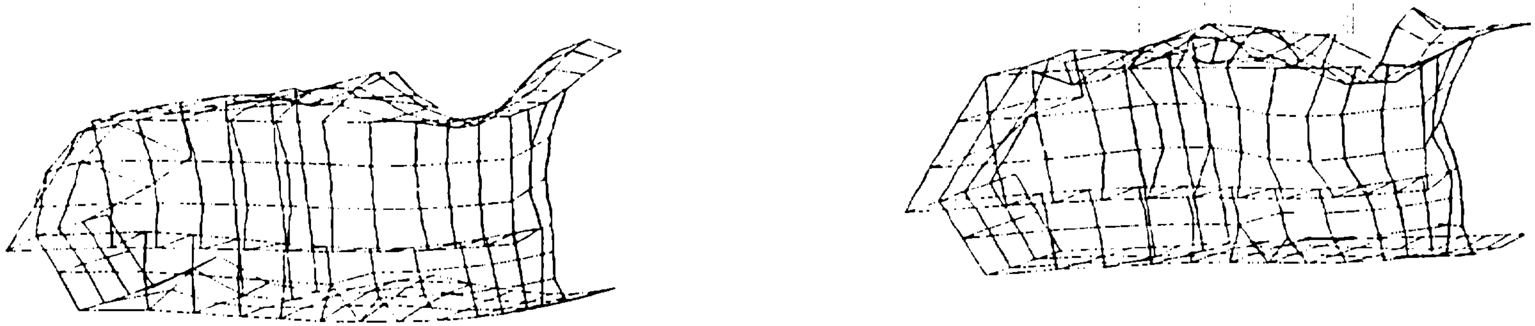

(g) 172.7 Hz Symmetric

(h) 213.3 Hz Antisymmetric

Figure 5.14 Typical Vibration Mode Shapes for Revised Model of M113 Hull.

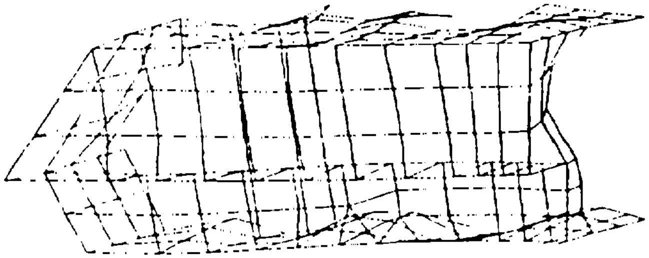

(i) 245.1 Hz Symmetric

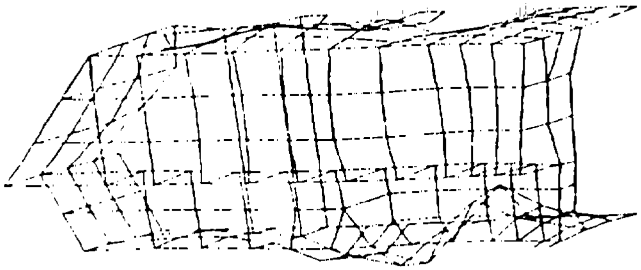

(j) 273.0 Hz Antisymmetric

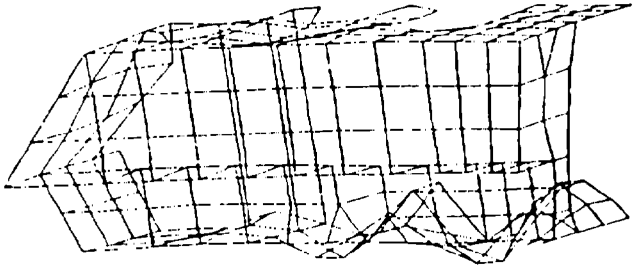

(k) 296.0 Hz Symmetric

Figure 5.14 Typical Vibration Mode Shapes for Revised Model of M113 Hull.

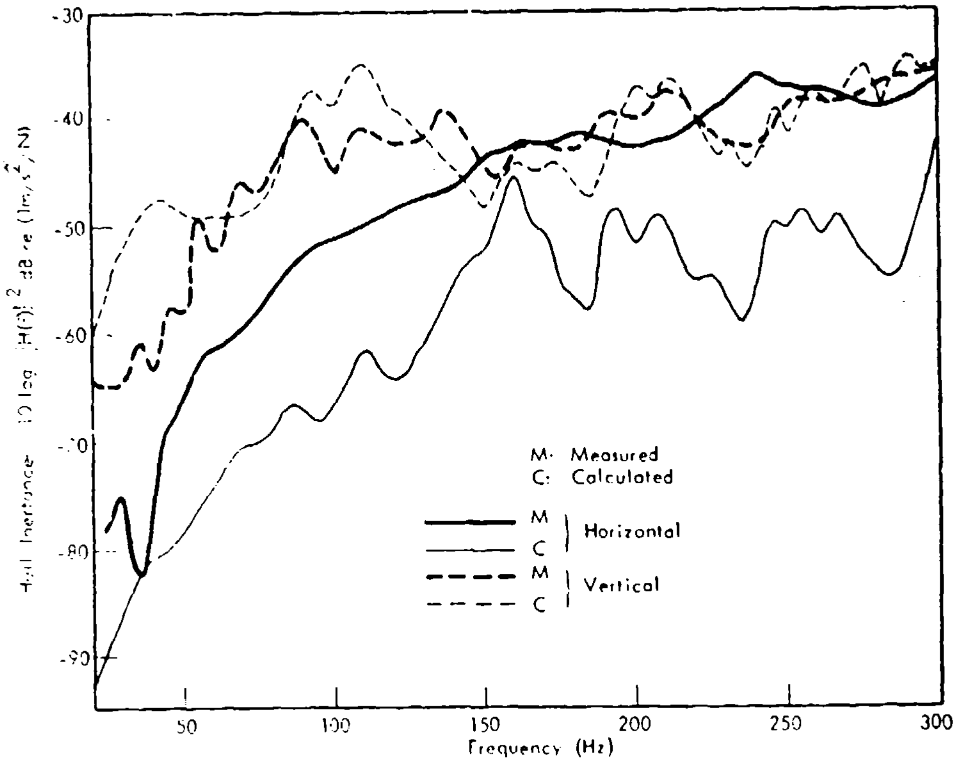

Figure 5.15 Comparison of Measured and Calculated Horizontal and Vertical Inertances for M113A1 Left Idler Spirdle: Revised Hull Model.

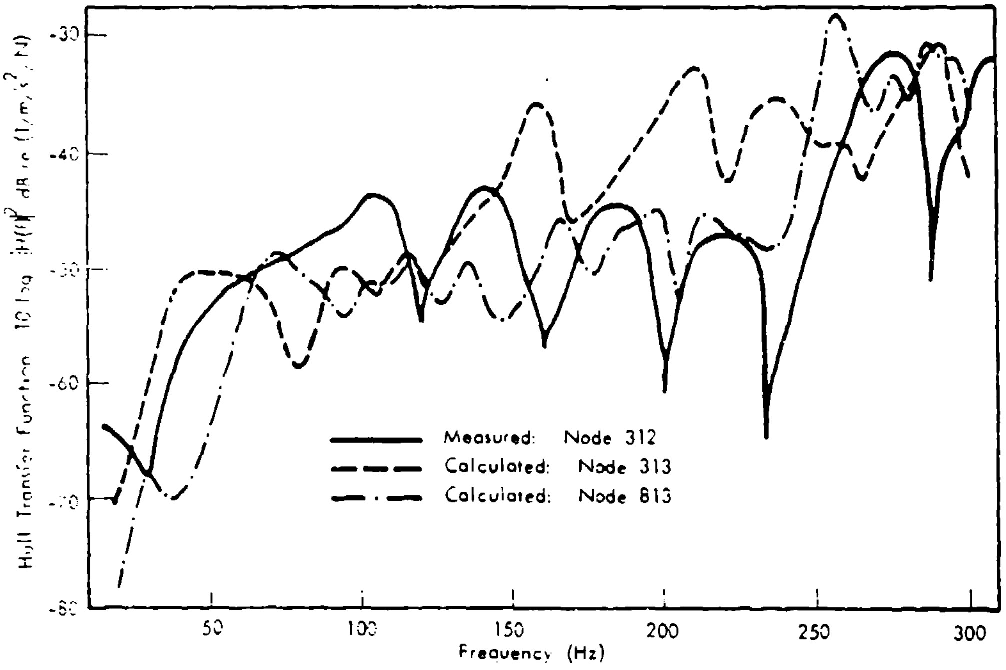

Figure 5.16 Acceleration-to-Force Transfer Function for Hull Top Plate: Comparison of Calculations and Measured Data.

The effect of different idlers and their location on idler inertances are shown in Figures 5.17(a) and (b) for horizontal and vertical force inputs, respectively. In these, different idler representations corresponding to left- and right-side idlers on both M113 and AIFV vehicles, as summarized in Table 5.4, have been incorporated into the hull model. Forces were applied to each idler in turn.

Table 5.4 EQUIVALENT BEAM PROPERTIES (5-inch idler spindle)

Idler	I_x' (in^4)	I_z' (in^4)	θ (degrees)	Equivalent Beam Node Location
M113A1-Left Side	22.52	31.6	34.84	103
M113A1-Right Side	20.58	11.12	27.01	203
AIFV-Left Side	21.11	35.77	27.46	104
AIFV-Right Side	23.42	13.14	32.04	204

The drive positions corresponding to the M113A1 idlers are 10 and 20 for left and right-sides respectively, while, for AIFV idlers, they are 30 and 40, respectively. R.M.S. inertance magnitudes (in g's/lb) are shown in Figures 5.17(a) and (b). In Figure 5.17(a) the horizontal location of the idler makes little difference to the horizontal inertance magnitude, but the upper location is calculated to have lower horizontal inertance; the difference being about 5 dB over the frequency range 125 to 250 Hz. These differences result from the locations of the idler equivalent beams at their 'correct' hull positions rather than from differences in idler properties (Table 5.4). In contrast to the horizontal inertance data, little significant difference in vertical inertances exists between the different idler locations, as seen in Figure 5.17(b). Figure 5.18 shows the calculated effect of idler characteristics, stiffness, and location on the top plate transfer function at node 313 for a vertical force input. No significant changes in transfer function are produced by varying the idler characteristics.

5.4.3 Frequency and Space-Averaged Calculations

The approach outlined in Section 5.2 may be used to calculate frequency- and space-averaged hull response-to-force and interior noise-to-force transfer functions. Several examples are now presented to demonstrate the nature of the predicted results.

Consider first the idler inertance. On frequency-averaging the inertance functions, (equation A.11a in Appendix A) and neglecting the cross-terms (i.e. $r \neq s$) in the equation following (A.11a), we find approximations to

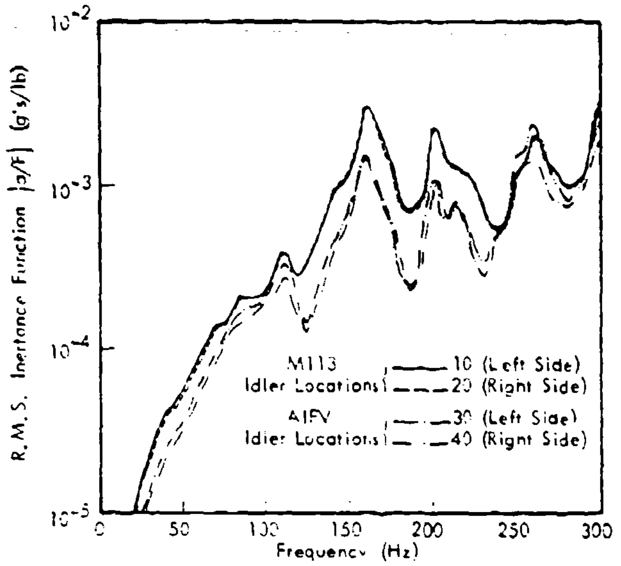

Figure 5.17(a) The Effect of Different Idlers and Their Locations on Horizontal Idler Inertance Functions.

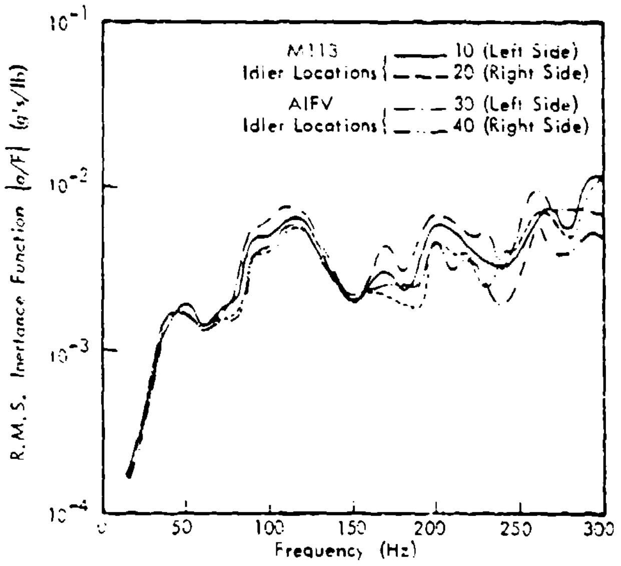

Figure 5.17(b) The Effect of Different Idlers and Their Locations on Vertical Idler Inertance Functions.

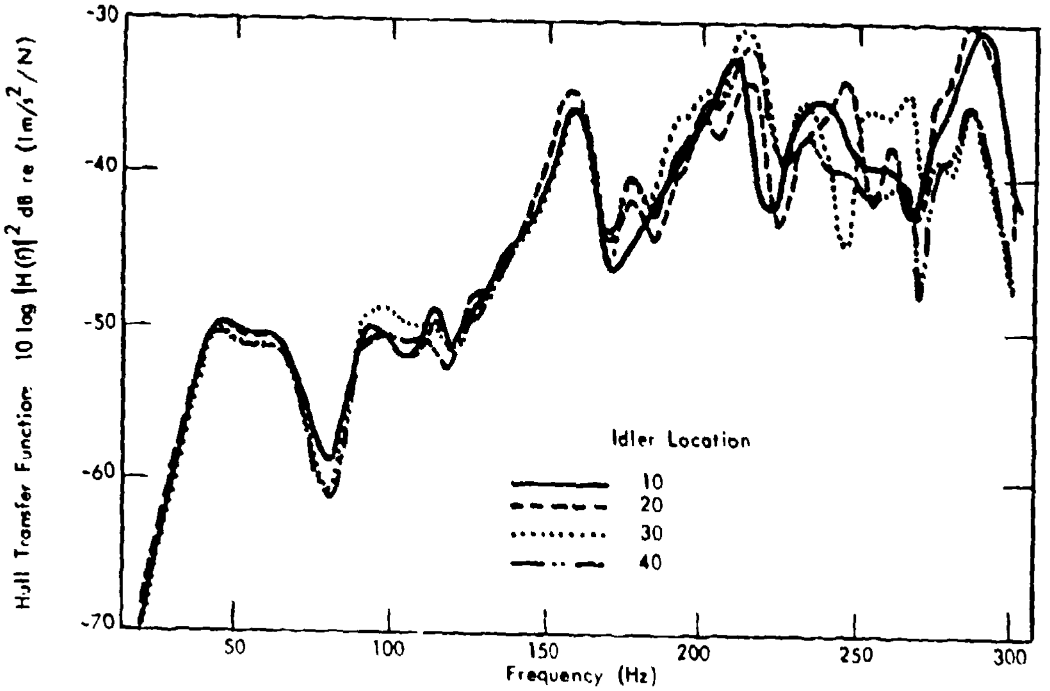

Figure 5.18 Effect of Idler Location on Top Plate Response: Vertical Excitation.

the idler inertance in terms of the vibration mode shapes at the idler, the modal masses and loss factors. The contributions due to nonresonant modes (i.e., modes with resonance frequencies outside the analyses bandwidth $\Delta\omega$, both stiffness-controlled ($\omega_r > \Delta\omega$) and mass-controlled ($\omega_r < \Delta\omega$)) can be distinguished from that due to resonant modes (whose resonance frequencies lie in the analysis band ($\omega_r \varepsilon \Delta\omega$)).

A typical set of results is shown in Figure 5.19, where the contributions of the nonresonant and resonant modes to the vertical idler inertance for idler 10 (left side M113A1) are compared with the total idler inertance, computed on a frequency-averaged basis. It is clear that, in general, resonant modes control the vertical idler inertance: only at 80 Hz and 160 Hz, and below 31.5 Hz, do nonresonant modes influence the idler inertance significantly. Comparison with the narrow-band vertical inertance function as in Figure 5.15, shows that close agreement exists between the two analytical results: the band-averaged data is more useful because the role of resonant modes is clearly identified.

The space- and frequency-averaged response transfer functions for the hull top plate, derived from equation (A.12) for resonant contributions, and from similar expressions for nonresonant modes, are presented in Figure 5.20. Again the vibration response in resonant modes controls the vibration level of the top plate. Comparison with the narrow-band calculated result from DYNRE 2 shown in Figure 5.16 shows agreement to be close.

Values of the parameter describing the contribution of panel elements to the hull vibrational energy (equation A.14) total modal masses M_r, are presented in Table 5.4 for several modes. As the normalized mass parameter approaches unity for any element, the energy of vibration becomes concentrated in that element. For example, for the antisymmetric mode resonant at 66.9 Hz, (see Figure 5.14(d)) the top plate contributes 83% of the modal generalized mass, while for the symmetric modes at 55.0 Hz (Figure 5.14(c)) and at 296.0 Hz (Figure 5.14(k)), the major contributions to the modal generalized mass are provided by the vehicle sides and sponson (82%) and the bottom (at least 77%), respectively. We note however, that for frequencies well above 100 Hz the normalized generalized masses of the top, bottom, and upper side plates tend to be about the same, suggesting the vibrational energy will be uniformly distributed over these similar structural surfaces.

The interior noise-to-idler force transfer function for each structural element can be derived as

$$\frac{\langle p_i^2 \rangle}{F^2} = \frac{A\rho^2 c^3}{V\eta_i} \cdot \frac{\sigma}{\omega^3} \cdot \frac{\langle a_{\Delta,A}^2 \rangle}{F^2} \qquad (m^{-4})$$

where, in frequency band $\Delta\omega$, $\langle p_i^2 \rangle$ is the space-average mean square interior acoustic pressure, F^2 is the mean-square idler force and $\langle a_{\Delta,A}^2 \rangle$ is the mean-square acceleration of elemental area A. V, ρc and η_i are the

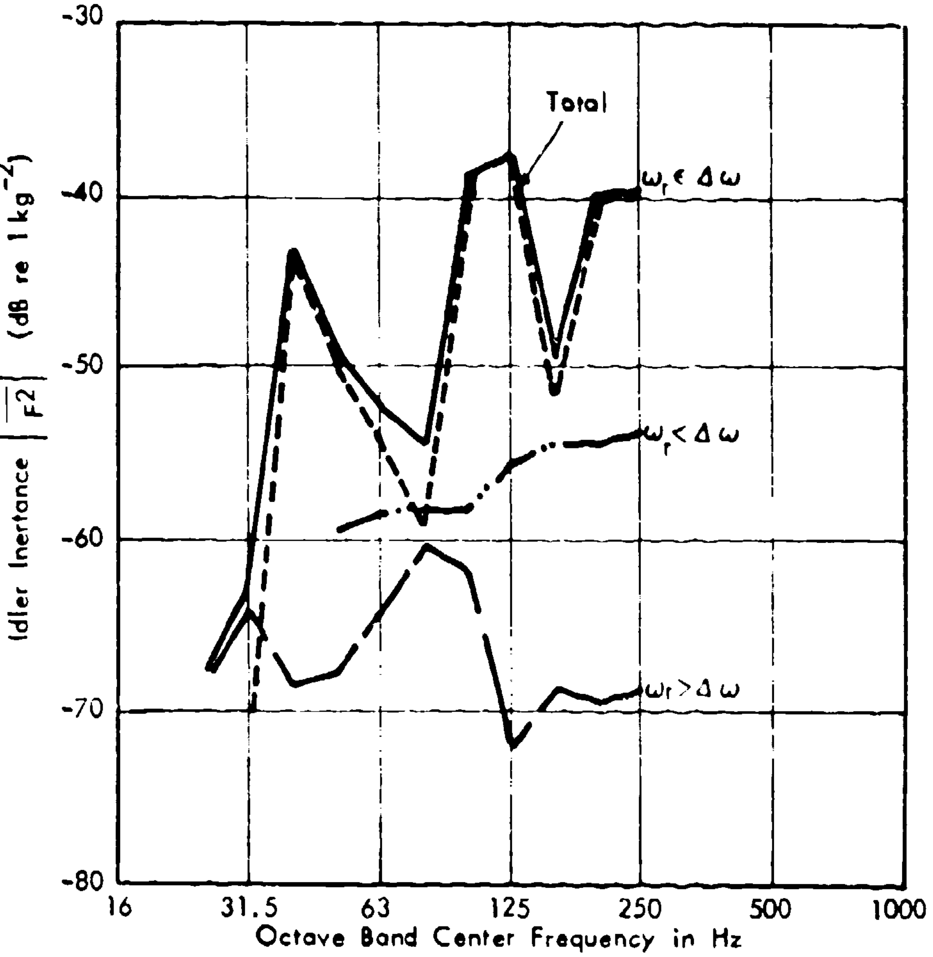

Fugure 5.19 Vertical Idler Inertance (10) of M113 Vehicle.

volume, characteristic impedance and acoustic loss factor of the hull interior space, and σ is the radiation ratio of area A. The transfer function between surface response and idler force $\langle u_i^2{}_{,A}\rangle/F$ is calculated with equation (A.12), for example, as shown in Figure 5.20. From tabulated values of σ, A and η_i, the noise-to-force transfer functions for each of the major radiating elements can be calculated, and then summed to give the overall measured noise-to-force transfer function. A typical example is presented in Figure 5.21 where predicted and measured noise-to-force transfer functions for vertical excitation of idler 10 (left-side M113) are compared. The agreement is quite satisfactory although a 3 dB overprediction has resulted.

TABLE 5.5

NORMALIZED GENERALIZED MASS OF STRUCTURAL ELEMENTS

Resonance Frequency (Hz)			Structural Element				
	Top	Upper Side	Lower Side	Sponson	Bottom	Rear Plate	Total*
29.5	.809	.030	.014	.014	.024	.013	.900
55.0	.051	.265	.252	.303	.069	.055	.995
66.9	.827	.046	.036	.022	.035	.023	.998
105.9	.309	.058	.069	.026	.401	.009	.872
134.9	.948	.039	.002	.005	.003	.003	1.000
176.1	.233	.105	.014	.009	.263	.011	.634
213.3	.388	.389	.053	.062	.024	.090	1.007
265.4	.507	.135	.044	.073	.031	.143	.983
296.6	.049	.022	.015	.010	.765	.009	.870

* In evaluating the vehicle generalized masses the inclined sections of the vehicle nose have been omitted from present calculations for simplicity. When the 'total' normalized generalized mass is less than 1.0, significant vibrational energy occurs in this area of the vehicle. Such hull vibrations are screened by the engine cover and do not radiate into the interior space.

While this presentation of band-averaged results is only preliminary, it appears that the approach is valid. The procedure gives results directly useful in the prediction of normally measured quantities of band- and space-averaged transfer function. The savings in data analysis manpower and computing costs using this approach are at least an order of magnitude.

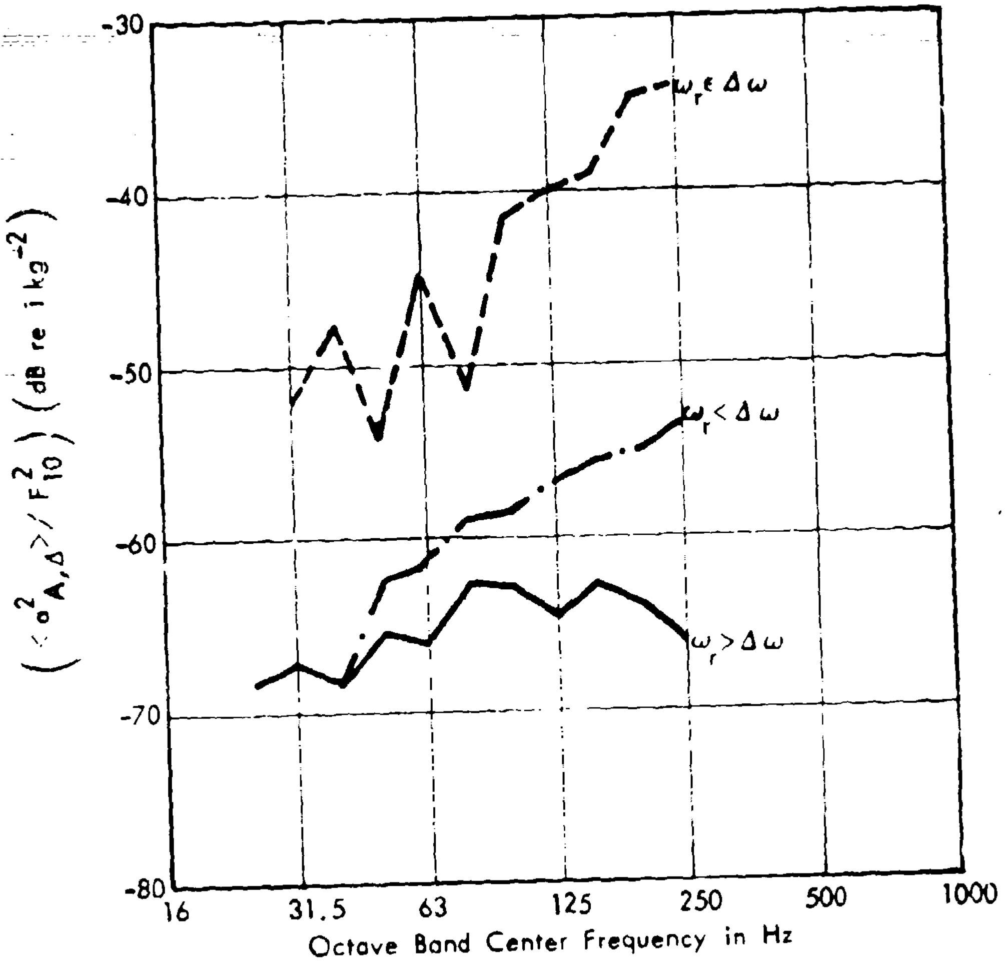

Figure 5.20 Contribution of Resonant and Nonresonant Modes to Top Plate Response for Vertical Excitation of Idler (10).

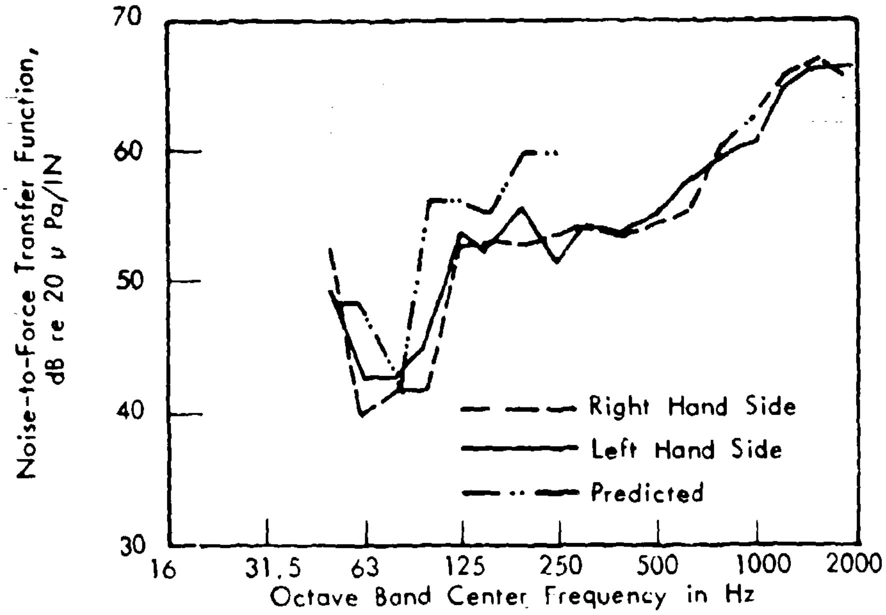

Figure 5.21 Comparison of Measured and Predicted Noise-to-Force Transfer Function for Vertical Excitation of Idler Spindle on M113A1.

5.5 Discussion and Recommendations

The main results of this development phase of the hull modeling study are summarized below.

1. An analytical model for the M113A1 armored personnel carrier has been constructed using the finite-element method. This model has been sufficiently detailed to allow reasonable predictions of mode shapes and resonance frequencies up to frequencies of about 300 Hz. Extension above 400 Hz using the current nodal arrangement is not recommended.

2. The idler has been represented by a beam of stiffness equivalent to the local hull stiffness at the idler attach position as determined from a separate static analysis. This approach seems to give consistent results and alternative modeling procedures would be extremely expensive.

3. Good predictions of the measured vertical idler inertance function have been made with the developed model, but the measured horizontal inertance function is underpredicted by about 10 dB. The reasons for this latter difference are unresolved, but it is felt that the differences do not result from the representations of the floor, box beam or idler. While some effort could be expended to resolve this, it is felt that the model should be used in its present form, since the required output from further stages of the model study will be changes in transfer function rather than the absolute value and it is felt that these changes will be accurately calculated.

4. The predicted effects of changes in the local stiffness of the idler, corresponding to left and right idlers on the M113 and AIFV vehicles, on the idler inertance suggest that changes in idler stiffness up to a factor of 10 will produce no significant changes in hull power flow or interior noise levels.

5. The frequency and space-averaging approach in interpreting the modal output from the finite element analysis is consistent with the conventional approach of using narrow band transfer function data. However, the averaging procedures developed are much more efficient and provide results directly useful and more related to the physics of the problem. While narrow-band information is useful, particularly measured modal data, in the present example only the frequency- and space-averaged results can be handled practically in the prediction process.

6. Using these averaging procedures, close prediction has been made of the measured noise-to-force transfer function for vertical excitation of the left-side idler of the M113 vehicle. The major contributors to the interior noise levels are predicted to be the top, upper side and bottom hull plates.

The following recommendations are made:

1. Further effort should be directed to finish the analysis of the noise-to-force transfer functions using the space- and frequency-averaging procedures developed. This should include complete automation of the space- and frequency-averaging procedures, for calculation of both hull response-to-force and noise-to-force transfer functions.

2. A model of the AIFV hull should be developed using similar principles to those followed for the M113A1. Calculations should then be made of the noise-to-force transfer function. Computed differences between AIFV and M113 results should be compared with measured differences as the final test of the modeling philosophies.

3. A limited experimental modal analysis of the M113 hull should be conducted as modeled to provide additional measured data with which to compare baseline predicted results.

6. PROTOTYPE COMPLIANT IDLER WHEEL DEVELOPMENT

6.1 Background

Earlier work has shown that an idler wheel would generate less interior noise if the wheel rim compliance were increased, that is, if the wheel had a "spring-like" rim, such as could be made with rubber or steel springs [2,18]. In a 1977 report of that work, an estimation was made of the noise reduction potential of compliant idler rims and hubs [16]. In subsequent work, an experimental idler wheel was designed and fabricated to validate the compliance concept and to optimize parameters. The description of this development is contained in Reference [17]; the acoustic testing was conducted in the current phase of work and is reported in Section 6.2.2 of this report.

Guided by the results of the experimental idler discussed above, a prototype idler was designed, fabricated, and tested. Compared to the experimental idler, the prototype was intended to be more practical and closer to a production design. The prototype demonstrated that the concepts previously developed could be utilized in a practical piece of hardware suitable for tracked vehicles. This prototype idler wheel is described in Section 6.3.

6.2 Experimental Idler Wheel

6.2.1 Conceptual Approach

The experimental idler served as a design tool to address specific areas of concern in the use of compliance for idler applications. These areas included the following considerations:

1. Magnitude of compliance needed for noise reduction (verification of estimates)

2. Importance of compliance in the tangential and axial directions, as compared with the radial direction

3. Selection of compliant material

4. Investigation of heat buildup problems due to hysteresis in the compliant material

5. Importance of the registration of track blocks with compliant elements

6. Assessment of the effect on exterior noise

7. Importance of "guide scrub" on interior noise

8. Estimate of durability

Items 3 and 4 are addressed extensively in Reference [17] and will not be disussed here.

A diagram of the experimental idler wheel appears in Figure 6.1, and photographs of the wheel mounted to the idler test stand are shown in Figures 6.2 and 6.3. This idler half consists of eleven spring-mounted "paddles" that support the track. During experimentation, the various spring rates and the shapes of the surfaces that bear against the track were varied. Noise, vibration, and temperature were then monitored.

This experimental idler is necessarily complex in design to permit changes to be made easily for experimental evaluation. This desirable feature necessitated the bolted-together design.

The experimental idler was designed to have a radial spring rate variable from approximately 1,000 to 20,000 lb/in (per paddle) through a choice of compliant element dimensions and materials. Initially, the radial spring rate was set at a calculated value of 4,000 lb/in for each paddle. The noise reduction was documented at this compliance, using the flat paddle ends rather than the raised paddle caps visible in Figure 6.3.

A more complete description of the experimental idler design rationale is contained in Reference [17].

6.2.2 Test Results

6.2.2.1 Compliance

Load-deflection tests were conducted to determine the actual values of radial and axial compliance in the experimental idler paddles. Values per paddle of 4,040 lb/in for radial spring rate and 6,568 lb/in for axial spring rate were obtained [4]. These are in close agreement with design predictions.

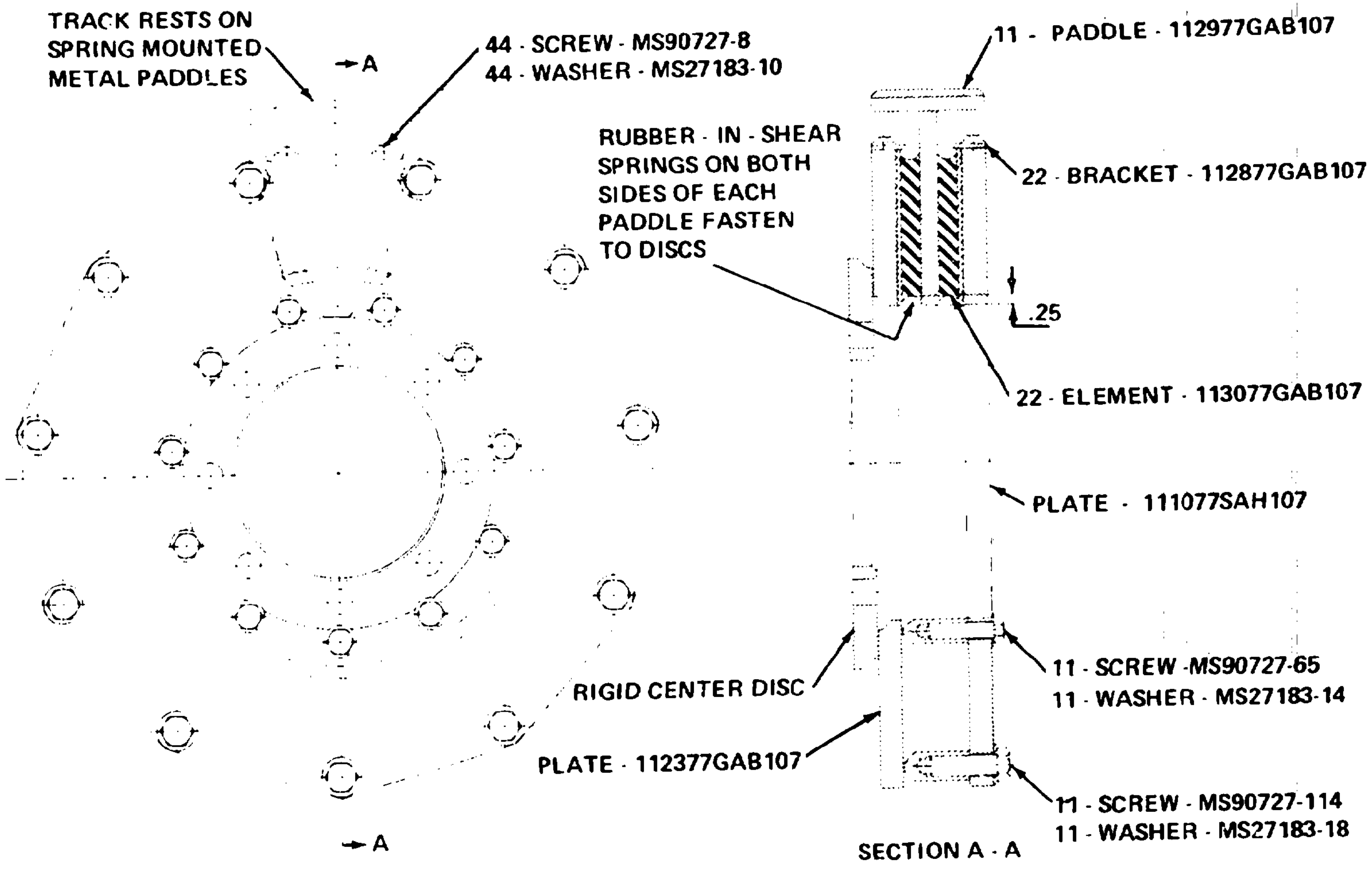
TRACK RESTS ON
SPRING MOUNTED
METAL PADDLES
A
44 - SCREW - MS90727-8
44 - WASHER - MS27183-10
11 - PADDLE - 112977GAB107
RUBBER - IN - SHEAR
SPRINGS ON BOTH
SIDES OF EACH
PADDLE FASTEN
TO DISCS
22 - BRACKET - 112877GAB107
.25
22 - ELEMENT - 113077GAB107
PLATE - 111077SAH107
11 - SCREW -MS90727-65
11 - WASHER - MS27183-14
RIGID CENTER DISC
PLATE - 112377GAB107
11 - SCREW - MS90727-114
11 - WASHER - MS27183-18
A
SECTION A - A

Figure 6.1 Schematic Diagram of the Experimental Compliant Idler Wheel.

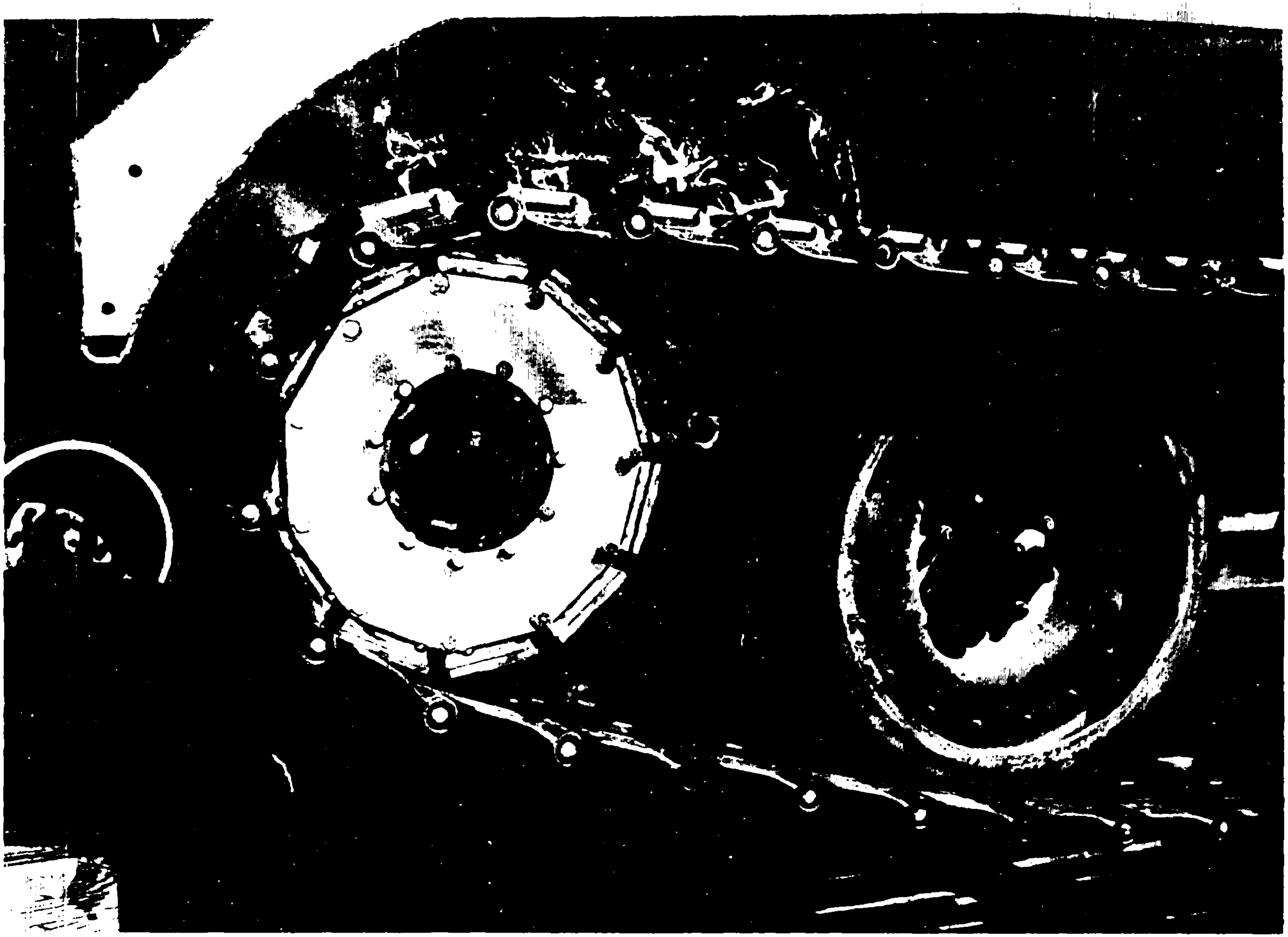

Figure 6.2 Experimental Idler Wheel Mounted on Test Stand.

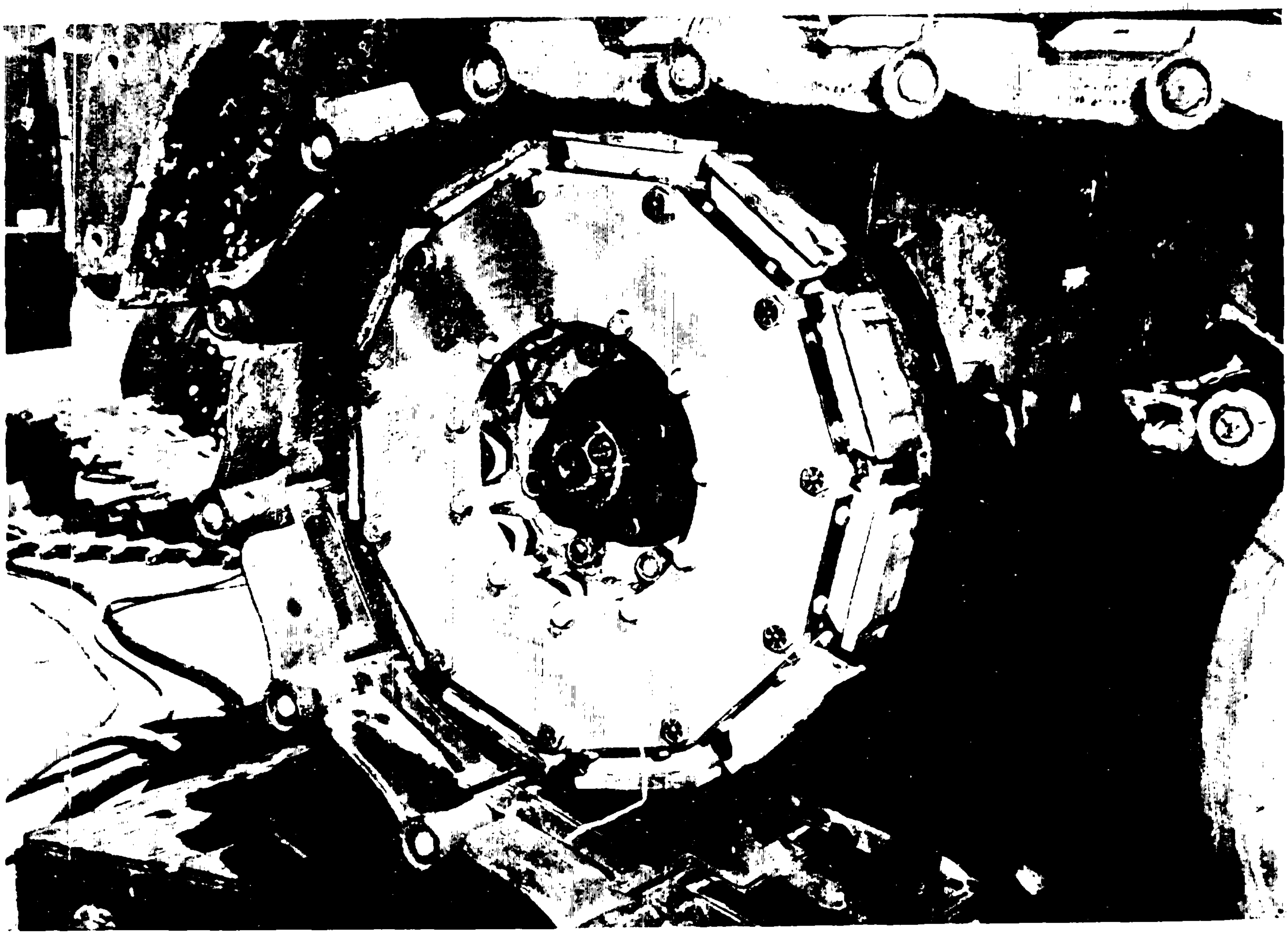

Figure 6.3 Experimental Idler Wheel Mounted on Test Stand (Close-up).

6.2.2.2 Interior Noise Reduction of the Experimental Idler Wheel

Figure 6.4 shows the crew area A-weighted noise levels of the standard and experimental compliant idlers as a function of speed. A-weighted noise reductions of between 7 and 12 dB were achieved. The tests were conducted on the FMC test stand so there was no noise input from the sprocket or roadwheels. This stand is described in Reference [17].

Octave band spectra of crew area noise are compared in Figure 6.5. In this figure, the upper curve is the standard idler tested at a track tension of 2,500 lb, which is typical of vehicles in operation. Compared to the standard idler, the octave band noise reductions are as much as 13 dB.

For the entire vehicle to comply with MIL-STD-1474 Category B, also shown in Figure 6.5, the experimental idler would require significant additional noise reduction. This assumes that the combined noise of the two sprockets, two idlers, and ten roadwheels has the same spectrum shape as the experimental idler wheel, but at a level 7dB higher. While this qualification probably will not be exactly met, it is a necessary assumption due to the unknown spectra of other prototype quieted suspension components that are not yet built. These additional reductions are as follows: For the crew area, 3 dB at 125 Hz; 8 dB at 250 Hz; and 1 dB at 500 Hz. For the driver's position, roughly 5 dB of additional noise reduction would be required, based on comparisons of idler noise spectra in the crew and driver locations [16].

In Reference [16], a simple estimation procedure, based on theory only, suggests "that interior noise will be reduced by about 4 dB(A) per halving of [idler wheel] rim stiffness." For the experimental idler, the stiffness has been halved almost four times, for a prediction of about 15 dB of A-weighted noise reduction. The observed noise reduction was 9 to 12 dB, with the most reduction coming at the highest speed tested (30 mph). Therefore, the reduction achieved is about 2.5 to 3 dB per halving of rim stiffness.

This estimate does not predict enough noise reduction to meet the goal for any reasonable rim stiffness. Therefore, to meet the Category B noise level in the crew area, the prototype idler must depend on a compliant hub, which is a more powerful noise reduction technique for a given total compliance.

6.2.2.3 Exterior Noise Reduction of the Experimental Idler Wheel

The exterior signature of the idler consists of two components: noise emitted due to hull vibration, and noise emitted directly from the idler and track. Noise due to hull vibration has a spectrum shape similar to interior noise, while the suspension-radiated idler noise may include squeaks, a clattering sound, or a rubbing sound caused by metal-to-metal contact.

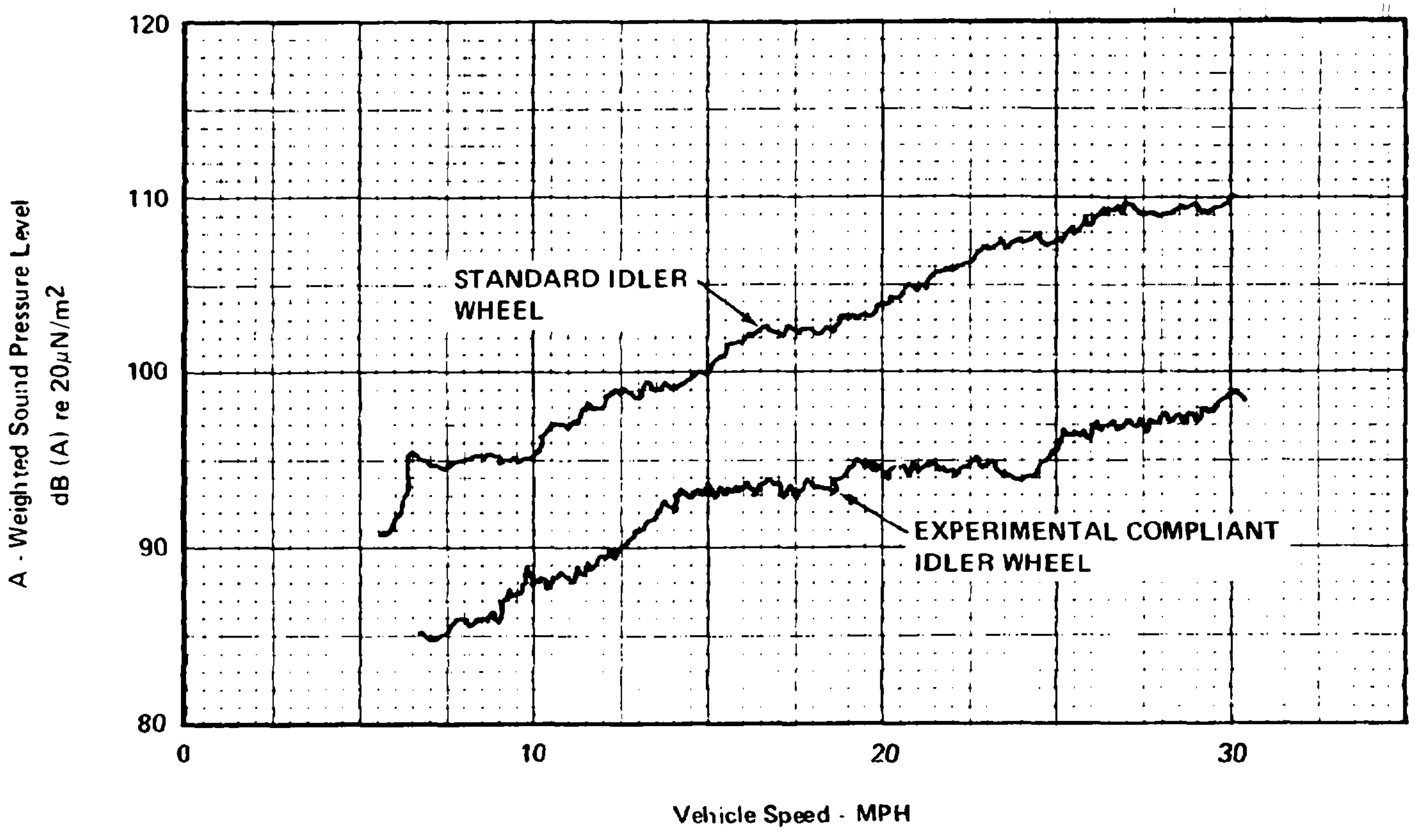

Figure 6.4 Interior Noise Reduction of the Experimental Compliant Idler.

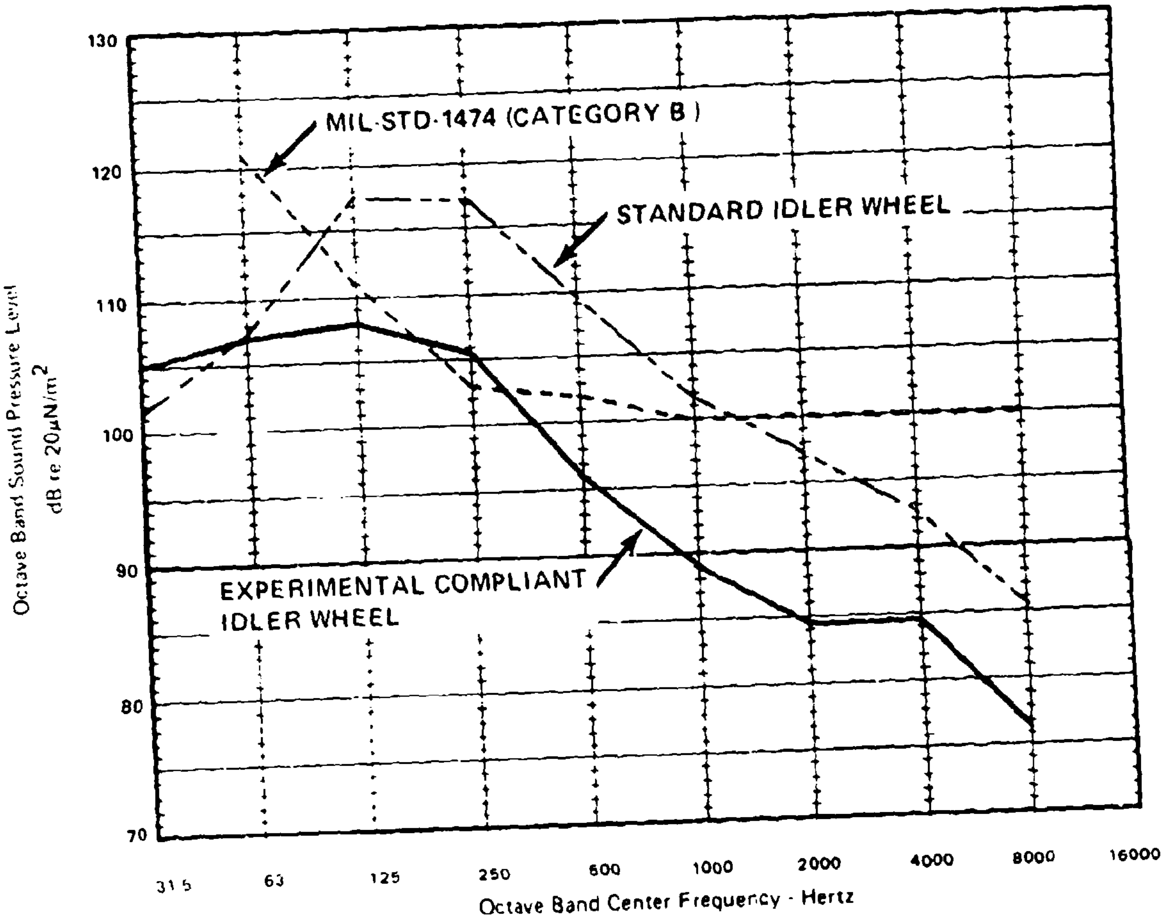

Figure 6.5 Interior Noise Spectra at 30 mph Due to Right Idler Wheel Only.

Exterior noise measurements were made on the standard (baseline) idler and on the experimental idler wheel. Because of test stand noise, the experimental idler data are inconclusive and are not presented here. Listening tests made while taking baseline data at 10, 20 and 30 mph revealed that the hull-radiated signature is most intense at and below 125 Hz and that sprocket clatter is audible at and above 1000 Hz. However, test stand suspension noise may be significant below 125 Hz and near 8 KHz. The data in Figure 6.6 show that the baseline idler signature level becomes roughly 5 dB more intense when the track speed is increased from 10 to 20 mph, and increases another 4 dB for a further speed increase to 30 mph.

Also plotted in Figure 6.6 are standard and specially quieted M113A1 exhaust noise spectra. Comparison of these spectra shows that, with the accelerator pedal fully depressed, the standard vehicle exhaust noise would probably be detected more easily than idler noise at 10 and 20 mph, but exhaust noise and track noise could be roughly equally detectable at 30 mph, depending on whether background noise and other conditions allowed the 125 Hz idler noise to be more audible than the higher frequency exhaust noise. For TARADCOM's low-signature M113A1 with a specially quieted exhaust, the standard idler noise would be more readily detectable at 20 and 30 mph even with the accelerator fully depressed. Thus, reducing idler noise would result in a reduction in the vehicle's distance to detection at the higher speeds, provided the exhaust noise is also reduced.

6.2.2.4 Durability of the Experimental Idler Wheel

Durability of the compliant elements, including heat buildup and fatigue testing, is discussed in References [9] and [16]. Durability on the test stand was very good, based upon approximately 220 miles of simulated operation and over two years of existence, most of that time mounted under tension to the test stand.

After about one year, the compliant elements were cut down in size and drilled to provide more axial and tangential compliance. During this operation, it was discovered that several of the bonds had begun to separate, with one separation occurring through about 25% of the bonded surface. The separations were a result of rubber extending beyond the edge of the mating steel surface to which it was bonded. This caused a large stress concentration. Most of the failures were entirely within the rubber material itself, although one failure involved actual separation of the adhesive from the steel surface. Failures were found only at points of major stress concentration.

For ease of manufacture, the main body of the idler was constructed of aluminum. Because the track strand on the test stand did not run "true" over the experimental idler, considerable wear occurred on the paddle surfaces, and where track guides contacted the inner idler disc. Part of the misalignment problem was due to the fact that a single wheel configuration was tested in a dual wheel application. Steel material would be used on production components and would greatly reduce these wear problems.

IDLER INDUCED NOISE

—A— 10 mph, 96 dB (C), 78 dB (A)

—B— 20 mph, 99 dB (C), 83 dB (A)

—C— 30 mph, 105 dB (C), 88 dB (A)

ENGINE EXHAUST NOISE

- - D - - Maximum noise levels in 2 - 3 gear, 600 to 2000 RPM, accelerator fully depressed, brakes "on", standard M113A1 production vehicle.

. . . . E . . . . Same, but for TARADCOM low signature demonstration M113A1 vehicle (Data taken at 50 feet, 6dB then added for distance compensation)

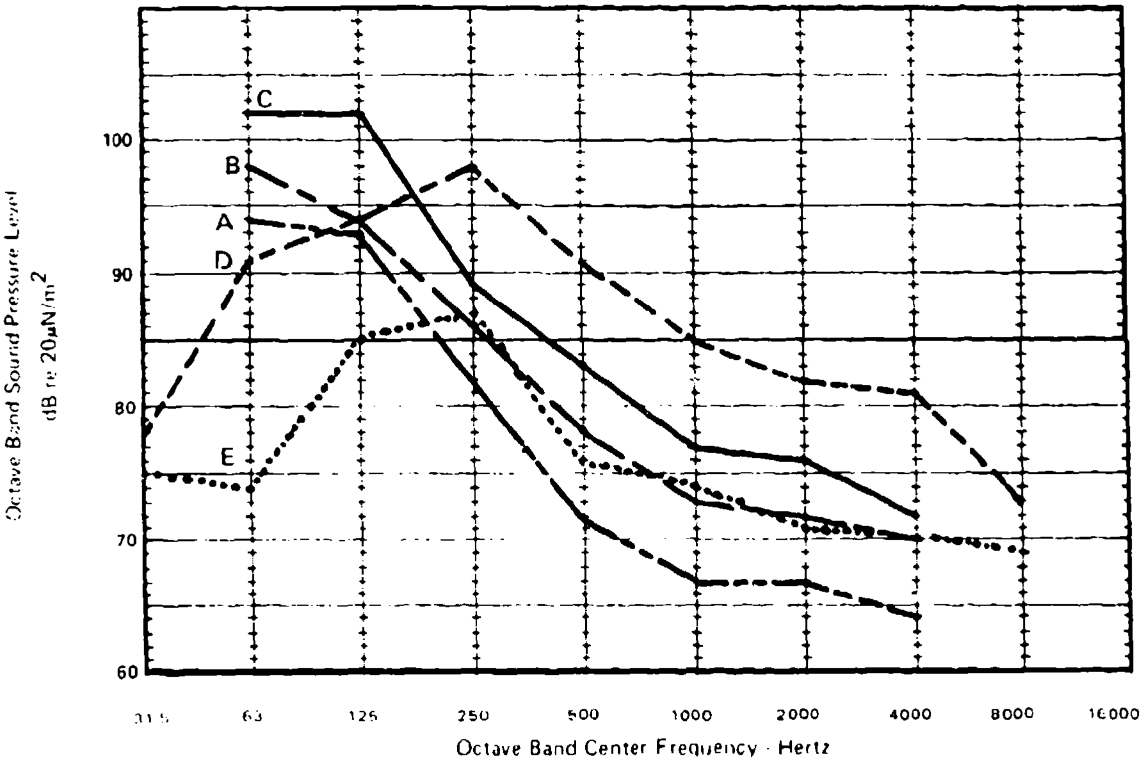

Figure 6.6 Exterior Noise of M113A1 Standard Idler Pair Compared to M113A1 Exhaust Noise at 25 Feet to the left.

6.2.3 Further Investigations with the Experimental Idler Wheel

6.2.3.1 Sources of Rapid Noise Level Variations

A test series was run on the experimental compliant idler wheel to determine any potential noise control benefits of indexing the track to the idler or sprocket, that is, by controlling the position of contact between the track shoe and a properly shaped noncircular wheel. These tests were inspired by the observation that track interior noise varies several decibels but with no obvious periodicity.

The purpose of the test was only to identify sources of noise level variations, but not to quantify each of them. A quantified analysis would have required the added expense of designing and constructing special electronic circuitry.

The data recording and analysis were done as follows. First, interior and exterior noise were simultaneously recorded. Then, two types of data analysis were conducted. In the first, the synchronized exterior and interior noise data were plotted, using a Bruel & Kjaer 2305 graphic level recorder (set to a paper speed of 10 mm/s and a writing speed of 100 mm/s). To synchronize the interior and exterior channels, hammer blows and a gain change were recorded simultaneously on both channels. The exterior noise channel recorded the relative positions of the track and idler paddles by a definite metal-on-metal clatter which occured only when the idler paddles contacted the bushing bosses of the tracks. The relative interior noise level changes were then identified by comparing the appropriate interior and exterior time histories. This comparison revealed the relative track-idler phasing which caused minimum and maximum interior noise levels.

The second type of analysis was to plot narrow band spectra of the D.C. level of octave-band-filtered interior noise, to reveal any cyclical nature in the normal fluctuations of interior noise. This was accomplished by setting a GenRad Model 1933 sound level meter to the appropriate octave band, and then taking the spectrum of the dc output using a Hewlett-Packard Model 5420 digital signal analyzer and plotter system. Because this dc signal is logarithmic, and the meter risetime may differ from the decay rate, the results are nonlinear and are not easily interpreted quantitatively.

All data discussed below were taken with the rounded idler caps shimmed to slightly increase their diameter. This caused the indexing between the track and idler to shift about every 1.5 seconds at 30 mph.

Looking at the sound level time histories, such as the samples shown in Figure 6.7 and 6.8, the following observations and conclusions were reached:

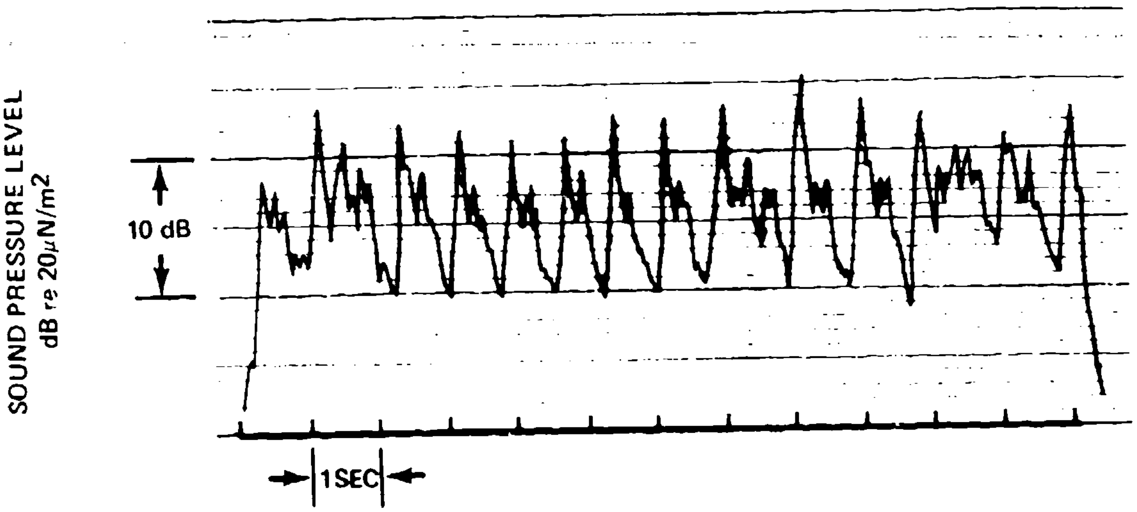

Figure 6.7 2,000 Hz Exterior Noise at 30 mph, 3 feet from Experimental Idler.

(Top tic marks denote instants of exterior noise peaks on Figure 6.7)

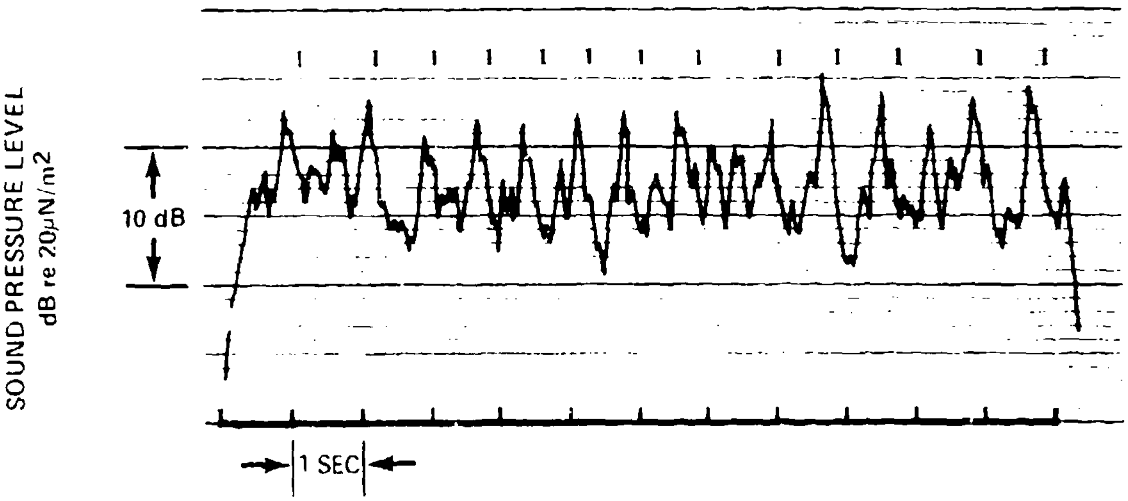

Figure 6.8 250 Hz Interior Noise at 30 mph, Due to Experimental Idler.

6.2.3.1.1 2000 Hz Octave Band Exterior Noise

The 2000 Hz octave-band exterior sound level time history plot Figure 6.7, shows a peak that corresponds to each shift of the track with respect to the idler wheel. These peaks are caused by periods of metal-on-metal impacts when the aluminum idler paddles strike the steel bushing bosses of the track shoes. During the moments of lower 2000 Hz noise, the idler paddle contact is against the rubber inner track pad.

The following paragraphs discuss the interior noise level variations in the most important octave bands:

6.2.3.1.2 1000 Hz Octave Band Interior Noise

At lower speeds, 10-20 mph, the exterior metal-on-metal impacts coincide with the interior noise peaks. However at 30 mph, the pattern is barely evident. Therefore, to minimize noise in this octave band, cushioning rather than indexing will be more reliable in reducing interior noise.

6.2.3.1.3 500 Hz Octave Band Interior Noise

At very low speeds, the sharp metal-on-metal impacts correspond to slight interior noise level peaks. No clear pattern is evident at higher speeds, and no definite conclusions are justified regarding the effectiveness of indexing for reducing interior noise.

6.2.3.1.4 250 Hz Octave Band Interior Noise

The sharp metallic impacts predominately correspond to interior noise peaks. However, a significant number of impacts correspond to minima of interior noise, especially at 30 mph, as shown on Figure 6.8. At 30 mph, the interior peaks occurred slightly more often than the exterior peaks. Again, no definite conclusions are justified.

6.2.3.1.5 63 Hz and 125 Hz Octave Interior Noise

At low speed, no clear pattern is evident, although a number of interior noise peaks correspond to the metallic impacts. At 30 mph, two interior noise peaks occur per 2000 Hz exterior peak, and every other one of these peaks corresponds to the metallic impacts. This observation suggests that the greatest amount of impact energy is converted to hull vibration when the track is contacted at the center of the shoes or at the pins. It follows that the least low frequency noise would be expected for contact at roughly the 1/4 and 3/4 locations between the pins. Clearly, indexing is a potentially useful means of reducing noise in these octave bands.

6.2.3.1.6 Summary of Interior Noise Level Variation

In the noise level time histories discussed, the A-weighted and octave band interior noise levels varied by the amounts tabulated below:

TABLE 6.1 VARIATIONS OF INTERIOR SOUND LEVELS

Frequency Band (Hz)	63	125	250	500	1000	2000	A-Weighted
Sound Level Variations (dB)	±5.5	±4	±4	±1.5	±4	±2	±2.5

Other than at 500 and 2000 Hz, indexing appears to have a marked effect on interior noise levels.

To summarize these observations:

1. At the higher frequencies, the interior noise peaks occur when the metallic noise peaks occur. This suggests that the high frequency vibration is simply transmitted into the hull.

2. At the lowest frequencies, there is no simple correlation between noise maxima and the amount of cushioning between the track and the idler paddles. Instead, the least noise occurs when the track impacts the idler at the 1/4 and 3/4 location on each shoe, which is an area of intermediate cushioning. Therefore, indexing is potentially more effective than cushioning for reducing low frequency noise.

3. At intermediate frequencies (250 and 500 Hz), both indexing and cushioning are probably moderately effective.

4. In the sprocket design, adjusting the position of the cushion relative to the sprocket teeth is a potentially useful technique for achieving up to 4 dB of A-weighted noise reduction. An estimate of 2 dB is more realistic.

6.2.3.1.7 Sources of Interior Noise Level Variations

Even casual observation reveals that the idler exterior and interior noise levels vary as the idler wheel goes in and out of phase with the track shoes. In addition to the indexing between the idler paddles and the track, there are apparently other sources of modulation. Because of the irregular pattern of indexing and interior noise, no one periodic phenomenon can account for all the previously discussed noise level variations. One might intuitively expect, therefore, that interior noise is also modulated by the revolution of the entire track, idler wheel rotation, and the low frequency oscillations bouncing) of the upper track strand, and possibly other drive motor-related cycles.

Because the interior noise is amplitude modulated, AM signal theory might apply, and the detected interior noise would therefore contain the mentioned fundamental rotational frequencies and their harmonics, as well as assorted sum and difference frequencies of each fundamental and its harmonics. This is indeed the case, as is discussed next.

The various frequencies of spectral peaks of the sound level meter dc output include those listed below, at 30 mph. An example of a corresponding spectrum appears in Figure 6.9.

TABLE 6.2 CALCULATED INTERIOR NOISE MODULATION FREQUENCIES

Modulation Source	Fundamental		1st Harmonic		2nd Harmonic	
Track Rotation (T)	1.371 Hz*		2.742 Hz*		4.1136 Hz	
Idler Wheel Rotation (I)	8.107	*	16.214	**	24.32	**
Unproven (U)	0.99	*	1.98	*	2.96	
T + U	2.36	*	4.72		7.08	
I - U	7.12	*	14.2	**	21.4	**
I - T	6.74	*	13.48	**	20.2	**
I - 2T	5.37	*	10.7		16.1	**
I - 3T	4.00	*	8.00		12.00	
I - 4T	2.63	*	5.26		7.89	
I - 5T	1.26	*	2.52		3.78	

Codes:	
*	Spectral peak observed
**	Not analyzed
No Mark	Not clearly observed

On most plots, the track and idler rotation (designated T and I, respectively, in Table 6.2) are evident. A peak at 0.99 Hz, possibly corresponding to a track strand resonance, is also apparent. A series of higher frequency period peaks begins at the idler rotation frequency and at each track multiple below this peak. Because of the approximately one percent uncertainty in spectral peak location, identification of the lower difference frequencies is uncertain in this brief analysis. Numerous minor peaks are also apparent; these may correspond to other sum, difference and multiple frequencies.

The qualitative data analysis suggests that nonuniformities in the track and idler wheel are the primary sources of altering the rate of

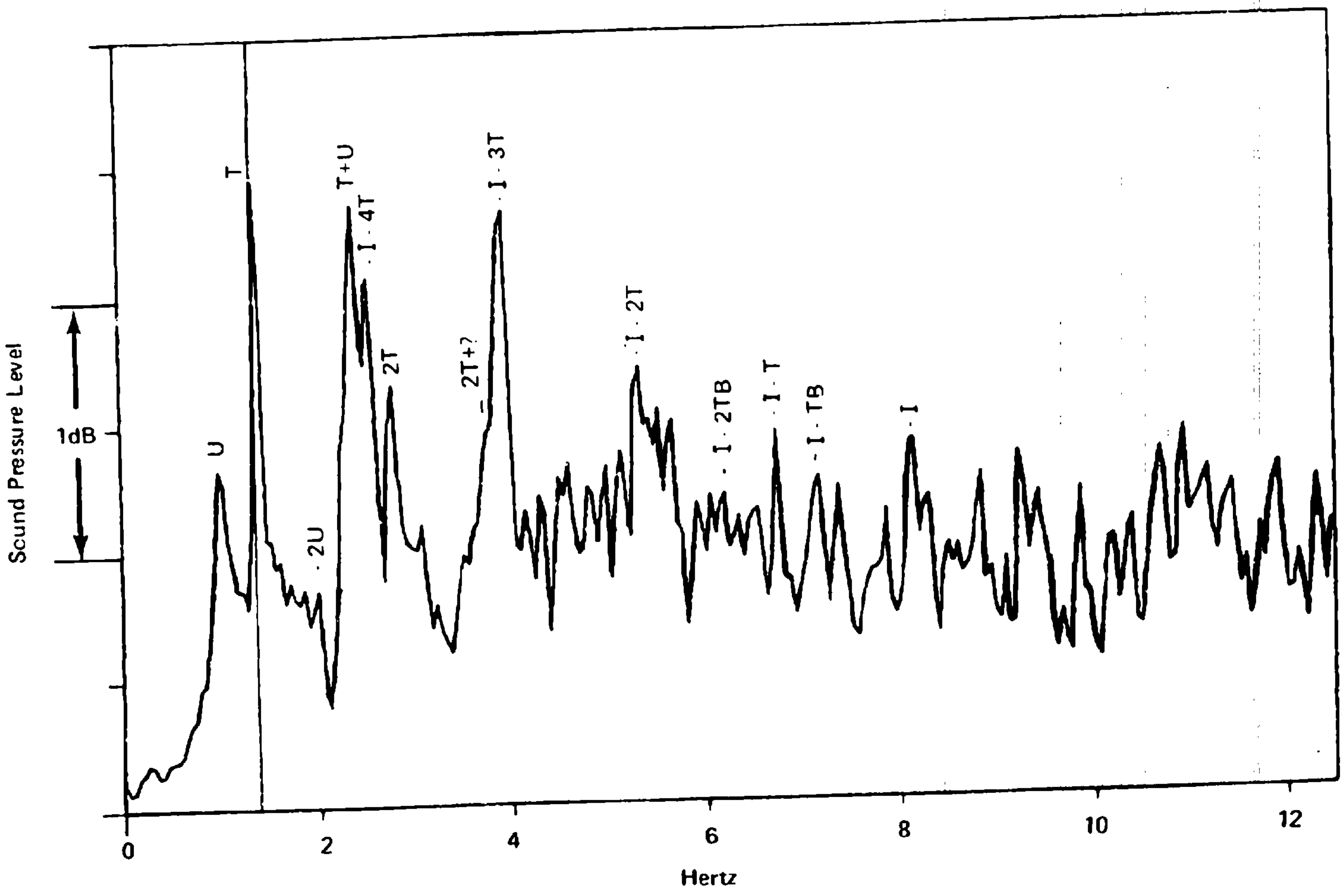

Figure 6.9 Spectrum of Sound Level Meter "DC" Output which Corresponds to Interior Noise Level Fluctuations.

indexing, which in turn affects interior noise level. It also demonstrates that the variation is not random, but instead is strongly linked to many regular periodic events -- perhaps even the impact of particular track shoes against particular idler paddles.

It was observed that the track wandered from side to side. At times, this motion appeared to correlate with the idler-track indexing changes, but no definite conclusions could be reached regarding this observation.

6.2.3.2 Shape of Experimental Idler Paddle Contact Surfaces

The experimental idler wheel was tested with both rounded and flat paddle surfaces contacting the track. The rounded paddle caps, similar to those visible in Figure 6.3, tended to contact the track at the pins. With the rounded caps removed, the exposed flat surfaces tended to contact the inner track pad rubber on the track shoes.

Figure 6.10 shows the increased noise level due to firm metallic impacts between the idler rounded paddles and track shoe steel forgings. While the metallic impacts caused no differences in the 250 Hz octave band, all higher octaves show a noise level increase, with the largest at 6 dB in the 8 kHz octave band. The A-weighted sound level was also slightly increased. For exterior noise, the metal-on-metal impacts are very objectionable and should be avoided in the prototype idler design.

6.2.3.3 Effects of Combined Axial and Radial Compliance Changes

As discussed in Section 6.2.2.4, the experimental idler was modified to increase axial and tangential compliance. Radial compliance reduced correspondingly. It was postulated that the axial idler vibration might be a major contributor to experimental idler interior noise. Consequently, tests were designed and executed with the reduced stiffness. The reduction was accomplished by drilling holes into and cutting away portions of the rubber springs. Radial and tangential compliance were calculated as being reduced by about 30 percent. The resulting axial stiffness was very low; axial hand pressure on the paddles caused an obvious deflection.

Vibration measurements taken near the edge of the disc on the experimental idler at 30 mph showed modest levels of radial vibration and much higher levels of axial and tangential vibration (Figure 6.11). The vibration spectra for the modified experimental idler are shown in Figure 6.12. The increased axial compliance resulted in raising and equalizing the vibration levels for the three directions. Greater vibration levels were due partially to the fact that the idler paddles occasionally "bottomed-out" on the disc support.

The resulting A-weighted interior noise level was 101 dB which is 2 dB higher than the original experimental idler. The interior octave band

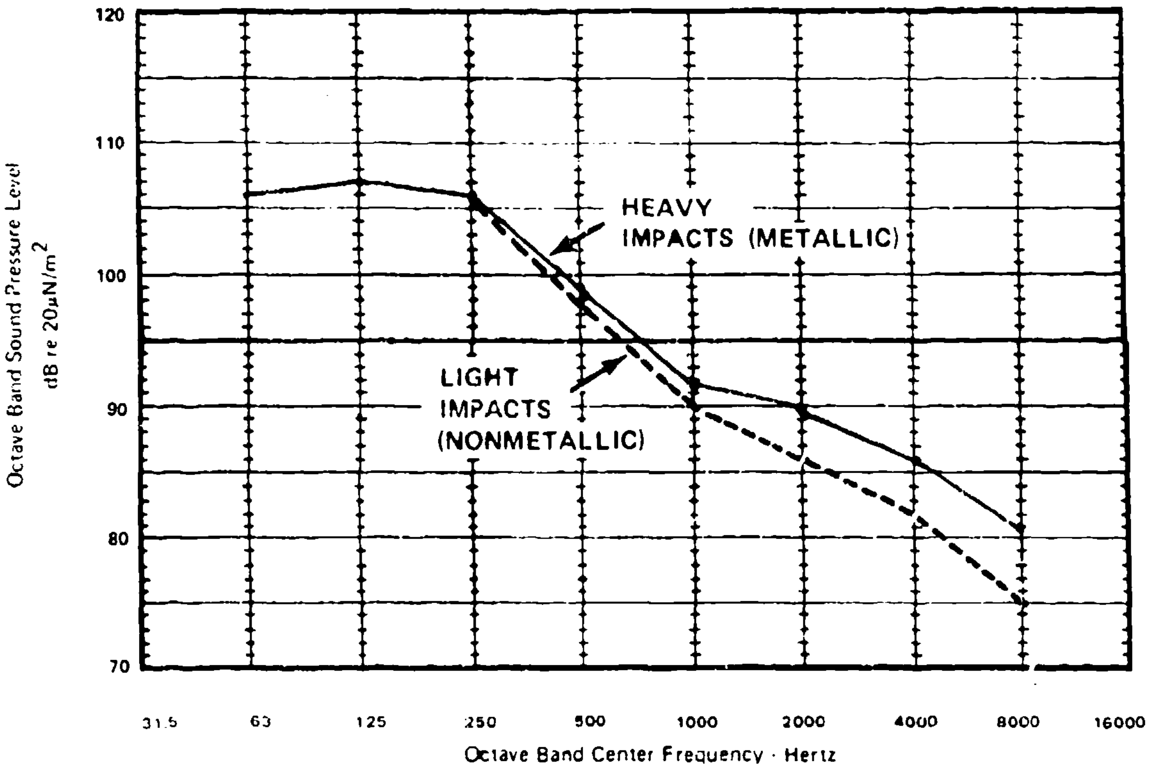

Figure 6.10 Effect of Metallic Track - Idler Impacts.
Compliant Idler, Rounded Paddle Tops versus Flat Tops.

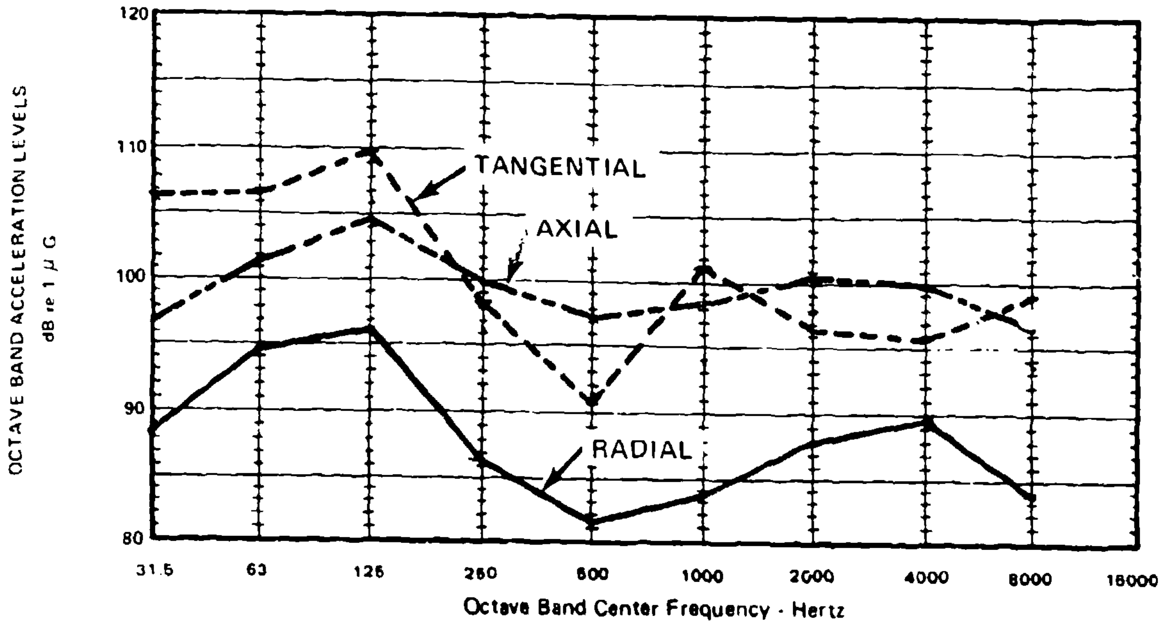

Figure 6.11 Triaxial Vibration Levels on the Experimental Idler Disc at 30 mph.

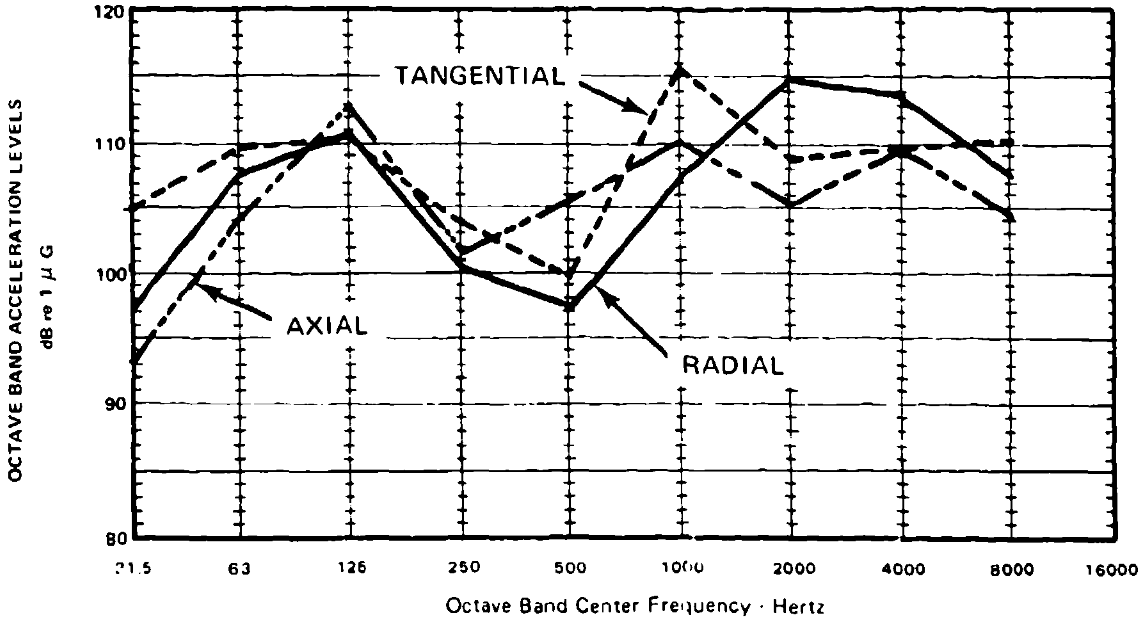

Figure 6.12 Triaxial Vibration Levels on the Increased Compliance Experimental Idler at 30 mph.

spectra are shown in Figure 6.13. Noise levels in the 63 and 125 Hz octave bands are the lowest ever measured for the experimental idler wheel. However, an apparent resonance appeared at 250 Hz, which nullified any potential acoustic advantage gained by the axial compliance. The noise levels of the 500 to 2000 Hz octave bands were essentially unchanged. The 4000 and 8000 Hz octave band sound levels are the lowest yet measured for an idler wheel. This high frequency reduction was not unexpected, based on experience with other rubber vibration-isolated systems. Unfortunately, it is of little value here, as the noise reduction is required at lower frequencies.

The apparent 250 Hz resonance is of concern because of its objectionable 110.8 dB level. It may be due to the soft axial compliance decoupling the idler wheel disk from the track. This decoupling would allow increased idler disk axial motion and also reduce any damping of idler resonances by the track. However, this seemingly plausible resonance is not supported by the acceleration spectra made on the idler wheel.

With regard to all future idler and sprocket designs, these experimental results strongly suggest that a low axial stiffness is not of great benefit and may allow resonances of the wheel to occur because of reduced damping.

6.2.3.4 Track Guide Scrub Noise

During some testing of the experimental compliant idler wheel, the track guides rubbed and scraped against the idler wheel. This scrubbing caused rapid wear of the aluminum idler disk and generated an audible scraping sound. This noise was barely audible inside the vehicle, and was more easily heard outside. To determine the significance of the scrubbing noise, the idler was tested with and without track-guide-to-wheel contact. The scrubbing was eliminated by canting the idler mount slightly so that the track shifted sideways and the guides did not touch the wheel.

Figure 6.14 shows the effect on interior noise of metal-on-metal rubbing between the track guides and the compliant idler wheel. The scrubbing produced a 2 dB increase in the 500, 1000 and 2000 Hz octave bands, and an overall A-weighted increase from 93 to 99 dB. These increases are consistent with earlier but inconclusive data. These data suggest that "hard" track guide scrub creates a 94 dB(A) noise level. Clearly, this number is approximate. Even so, the data suggest that scrub noise must be reduced in the prototype idler design.

6.2.3.5 Increased Diameter Idler

Since the experimental idler was larger in diameter than the standard M113A1 idler, a portion of the noise reduction was suspected to be due simply to the large size. The standard idler is 17.25 inches in diameter whereas the experimental idler diameter is 19.06 inches, a difference of 1.81 inches.

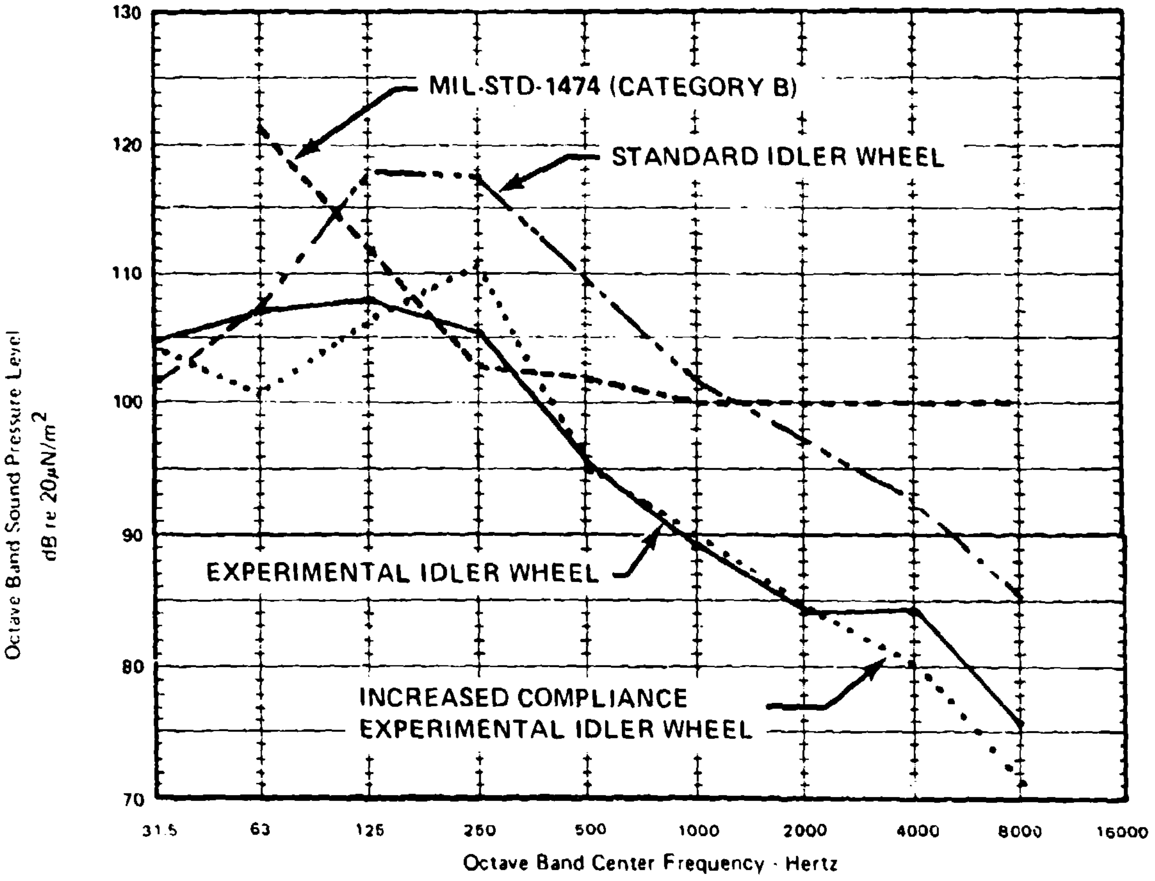

Figure 6.13 The Effect of Increased Compliance in the Experimental Idler at 30 mph, Interior Noise.

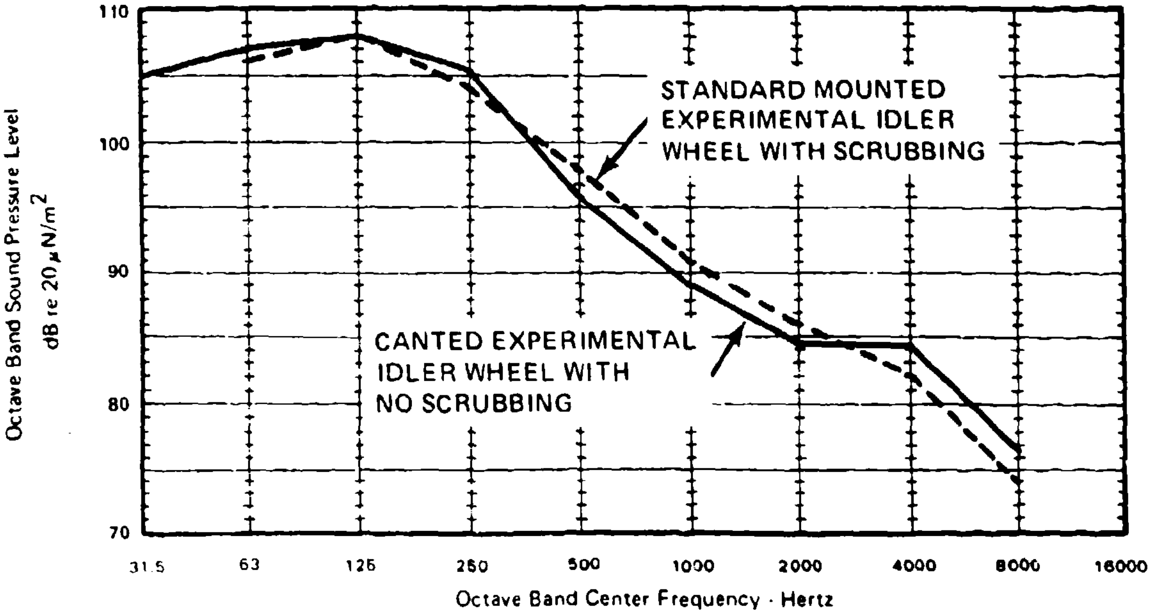

Figure 6.14 The effect of Track Guide Scrubbing on Interior Noise.

To investigate this concept, an increased diameter idler wheel, modified from a standard idler wheel, was tested. The increased diameter wheel measured 21 inches. Using the 2.75-inch larger wheels, it was found that at test stand speeds of 30 mph, A-weighted interior crew noise levels were reduced by 4 dB to a level of 106 dB. Consequently, up to 2 dB of the A-weighted noise reduction realized with the experimental idler may be due to the increased size. A comparison of standard and increased diameter idler noise is shown in Figure 6.15.

6.3 Prototype Idler Wheel

A prototype idler wheel was designed, fabricated, and tested. Figure 6.16 is a photograph of the prototype idler wheel mounted on an M113A1 vehicle. This prototype, compared to the previously described experimental idler wheel, is a simpler and more practical design which is more suitable for production. The A-weighted noise level goal for one idler wheel is 92 dB inside the crew area. Attaining 92 dB(A) for each idler, each sprocket, and for the roadwheels on each side would result in 100 dB(A) for the total vehicle noise level.

6.3.1 Design Goals

Considerations of production practicality and cost limitation required that the wheel be much simpler than the experimental wheel. A design consisting of three metal and two rubber pieces was selected, as shown in Figure 6.17. The goals in the design of the prototype compliant idler were as follows:

1. Noise level of 95 dB(A) or lower
2. Production feasibility
3. Service life of 2,000 miles or more
4. Simplicity
5. Relatively low cost
6. Fail-safe features to permit continued operation (at increased noise level) in the event of failure of the compliant members

6.3.2 Design Criteria

To achieve the above goals, the following criteria were used to guide design decisions:

1. Space limits: The idler shall be designed so that no changes to the hull are required on the M113A1 test vehicle.

2. Existing hardware: The idler must fit on to the existing M113A1 idler support assembly.

3. Diameter limits: The diameter of the idler shall not be too large to prevent the track from being accidentally "thrown" or to prevent common passage of debris drawn up by the track. If sufficient clearance is not allowed between the sponson and the wheel rim, the track or debris could become jammed between the idler and sponson. This could cause the idler, idler mount, or hull to fail.

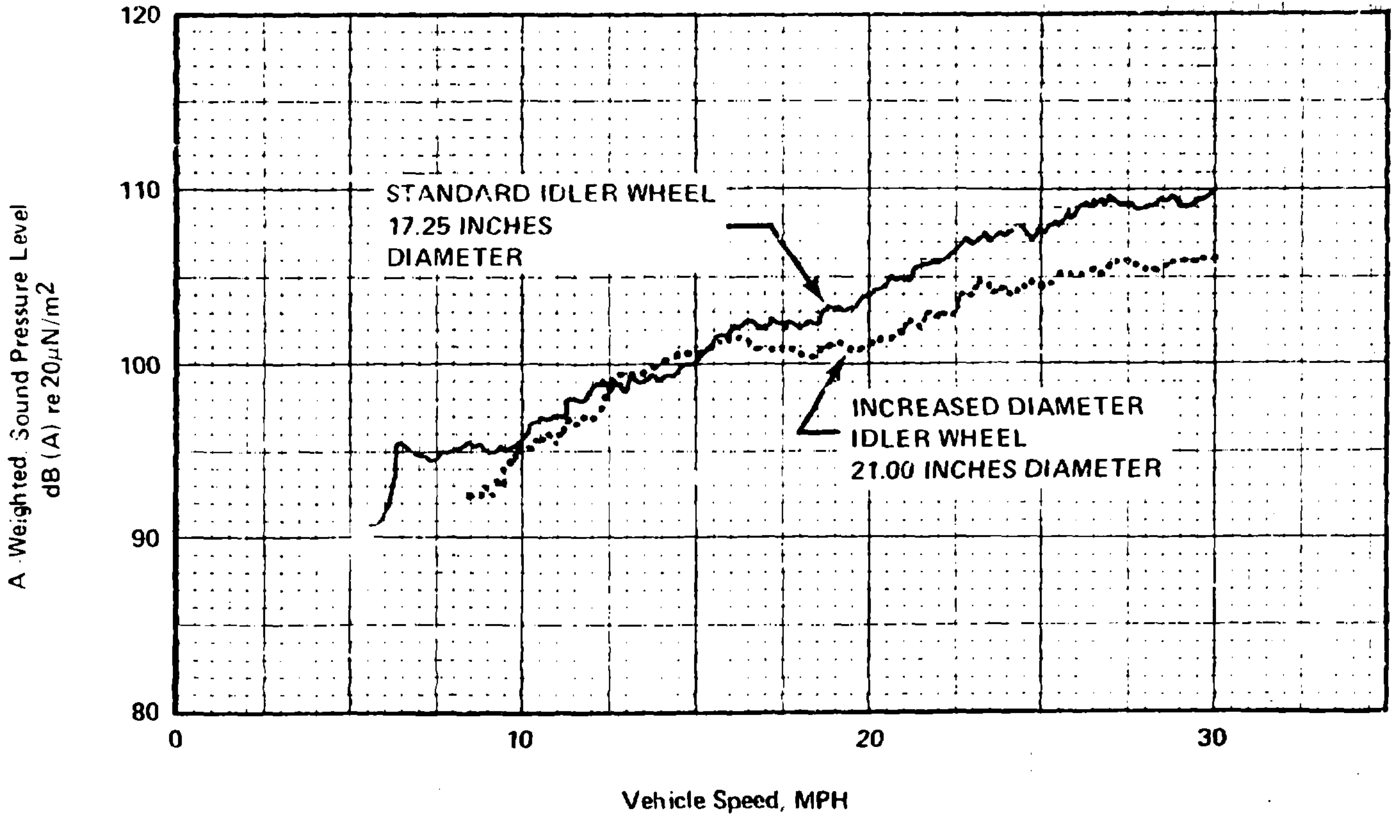

Figure 6.15 Interior Noise Reduction Due to a Large Diameter Idler Wheel.

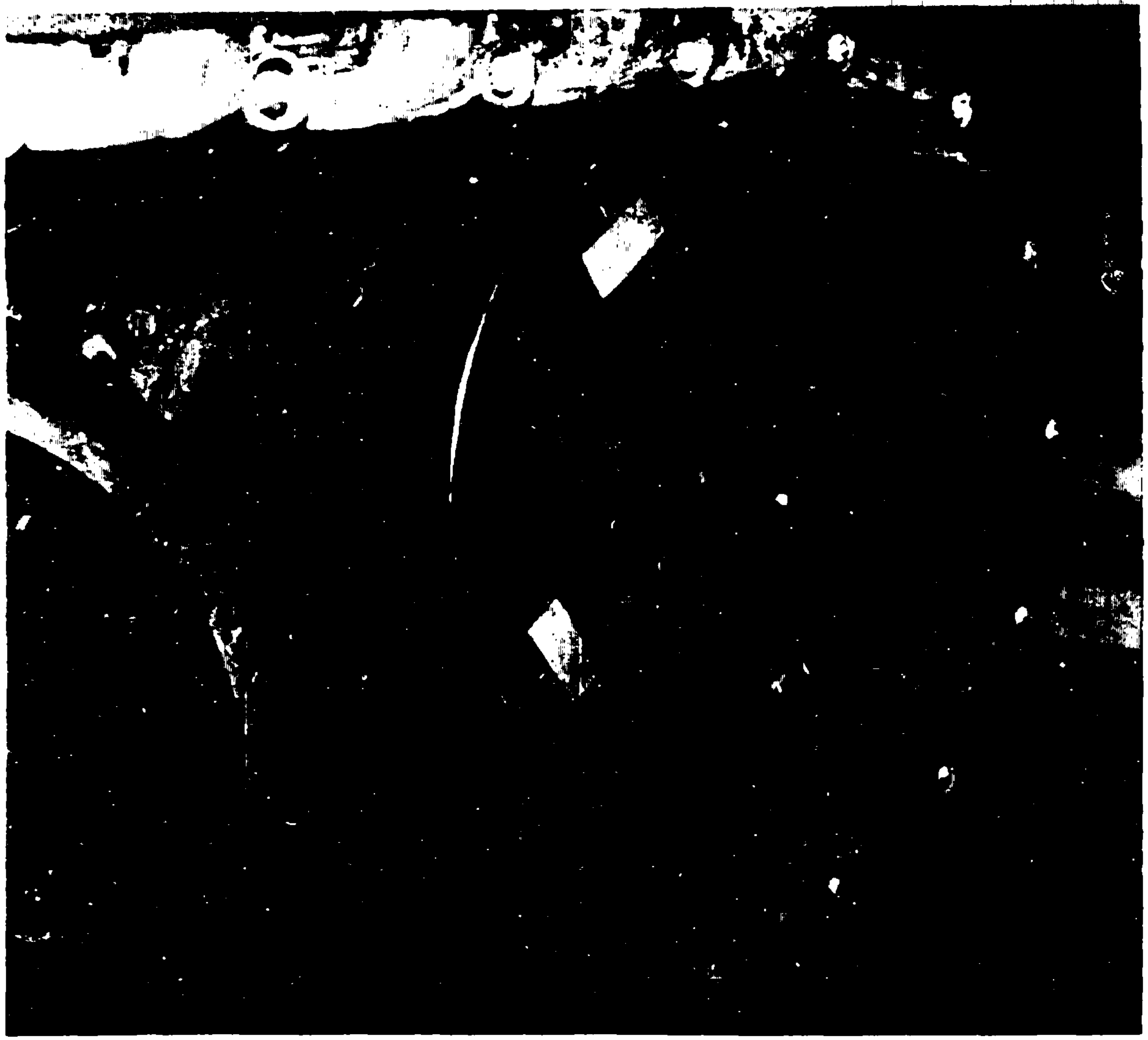

Figure 6.16 Prototype Idler Wheel Mounted on an M113A1 Vehicle.

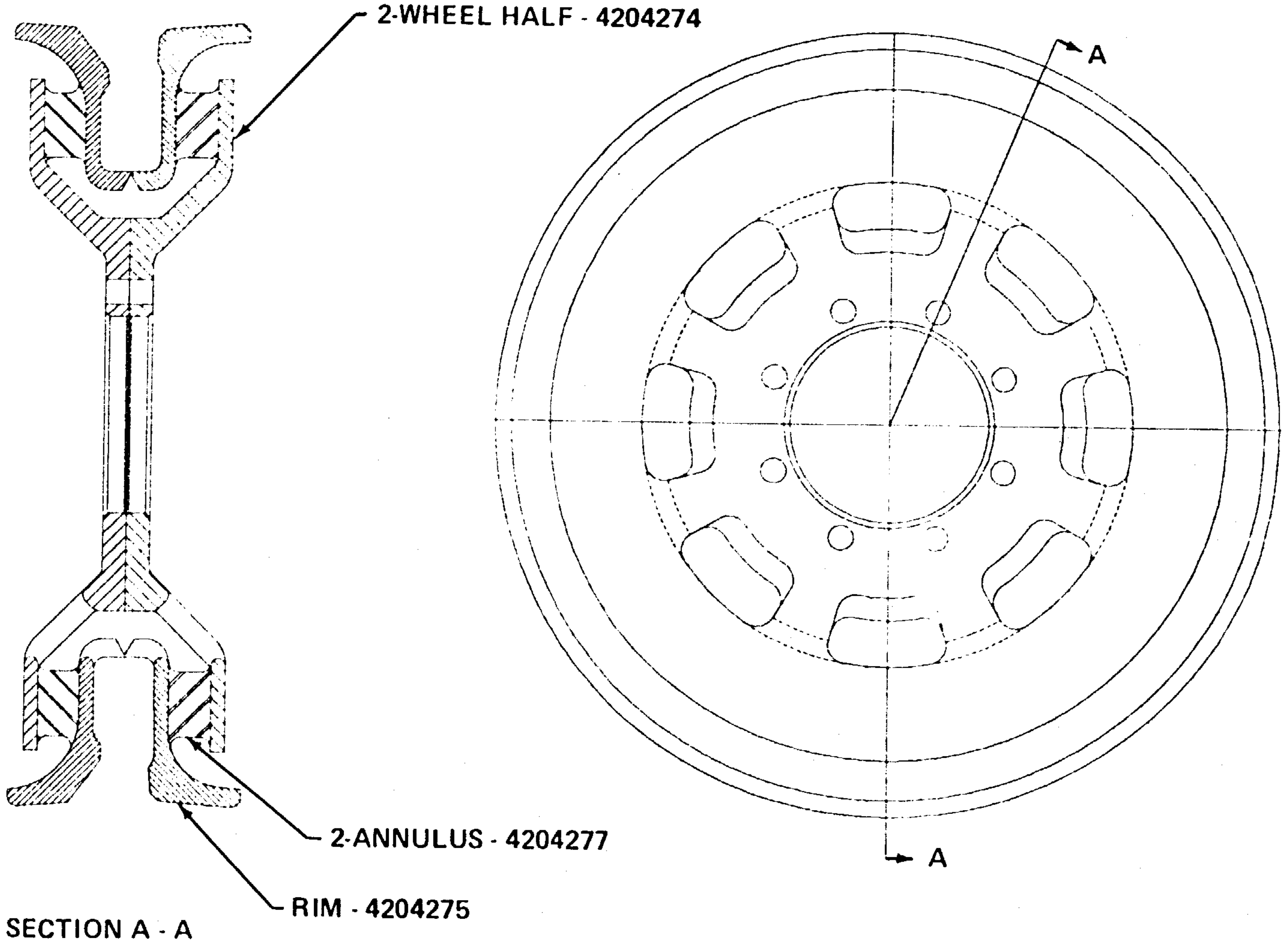
2-WHEEL HALF - 4204274
A
2-ANNULUS - 4204277
RIM - 4204275
A
SECTION A - A

Figure 6.17 Schematic Diagram of the Prototype Compliant Idler Wheel.

4. Rubber stresses: To ensure long life of the rubber compliances, shear stresses in the material shall not exceed recommended limits for rotative dynamic loading. For example, a limit of 75 psi is recommended for 30-durometer rubber when shear strain is 225 percent [8]. Much higher stress limits can be allowed for infrequent overloads.

5. Static load: The load that will be constantly imposed on the idler due to track tension may be as high as 10,000 lb under normal conditions. If an M113 is parked on a 60% slope, however, continuous track tension loads may reach 22,100 lb.

6. Dynamic loads: The fluctuating loads imposed on the idler during severe vehicle maneuvers may be as high as 15,000 lb. This load could occur if the vehicle "bottomed-out" on the idler wheel with a glancing blow.

7. Overload limit: An overload device shall be included to react to excessive loads and prevent excessive stress in the compliant elements. This device shall also act as a fail-safe feature.

6.3.3 Design Concepts

Several concepts were considered for the prototype compliant idler. The predominant reasons for accepting the rubber-in-shear design or, conversely, rejecting the other designs included: (1) the attainability of the desired radial compliance, (2) the degree of simplicity in the design and (3) the level of difficulty in manufacturing. The degree of simplicity greatly influenced the expectations of durability and practicality. The various concepts that were evaluated are discussed below.

6.3.3.1 Sectional Idler Rim

A concept similar to the experimental compliant idler, incorporating a number of radially symmetrical, independent compliant elements and a sectional idler rim was considered. The concept was rejected because of its complexity, difficult machining operations, and expensive assembly procedures.

6.3.3.2 Thin Flexible Rim/Rubber in Compression

This concept, shown in Figure 6.18, incorporates a flexible steel hoop "floated" on rubber in compression around a steel hub. The rubber compliance will be locally deformed at the point of track/rim contact, but will have less deformation on the side of the idler that is not in contact with the track.

The major two drawbacks are the risk of fatigue failure in the flexible rim and the low compliance in the rubber-in-compression element. Also, excessive point stresses in the rim could occur during track walk-off. Because the two main drawbacks appeared insurmountable, this concept was rejected.

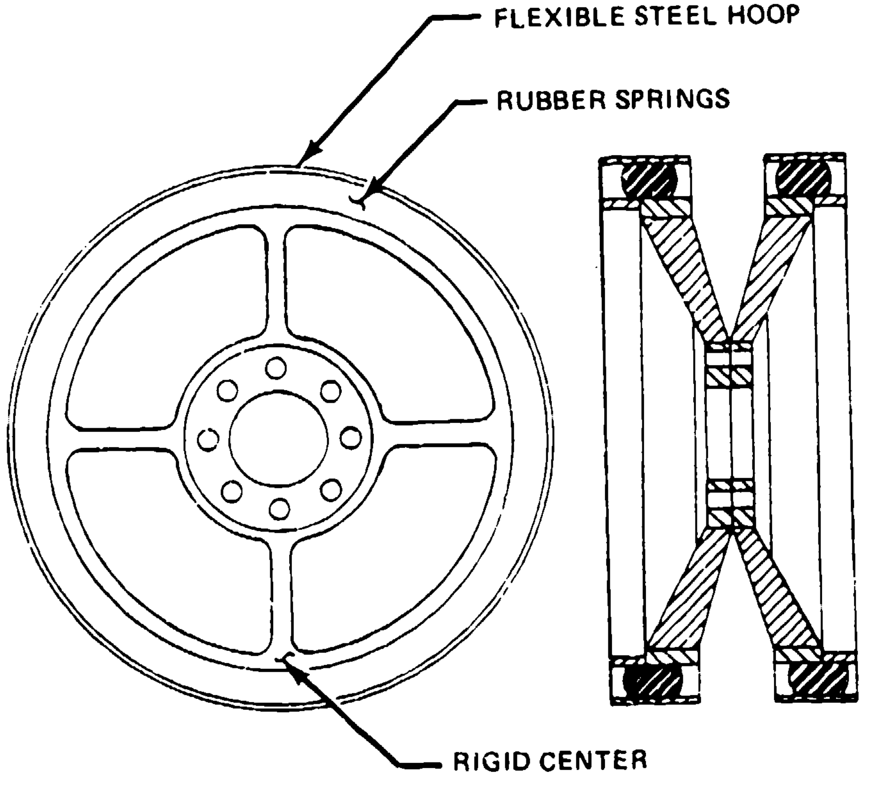
FLEXIBLE STEEL HOOP
RUBBER SPRINGS
RIGID CENTER

Figure 6.18 Idler Concept: Thin Flexible Rim; Rubber in Compression.

6.3.3.3 Thick Rigid Rim/Rubber in Compression

Figure 6.19 shows that this concept is similar to the above concept, except the floating rim is rigid. The isolators are fixed at their inner diameter to the wheel but not to the outer rim. Thus, the compliance is never placed in tension. Compressive loads are always distributed uniformly to the isolators because of the rigidity of the rim. However, the desired compliance was unattainable in this compression mode so the concept was rejected.

6.3.3.4 Rim of Rollers

Figure 6.20 shows a proposed idler wheel with compliant rollers acting as the wheel rim. The major advantage of this concept is that friction heating due to track shoe sliding is reduced. The disadvantages are limited compliance and complexity. Also, the roller concept might not be reliable in the required operating environments. Consequently, this design was not utilized.

6.3.3.5 Rigid Rim/Rubber-in-Shear

This concept was judged to be the most acceptable because it met or exceeded all of the design goals and criteria discussed in Sections 6.3.1 and 6.3.2. It was, therefore, chosen to be fully developed for prototype hardware. The assembly drawing of the design appeared earlier in Figure 6.17. Features of this design include:

1. Three steel parts and two rubber compliant rings. This relatively few number of parts will contribute to a low cost production unit.

2. Adaptability to production techniques. The steel parts are readily adaptable to casting or forging processes. The rubber will be fastened in place with a cyanoacrylate adhesive or vulcanization process.

3. Fail safe. The idler rim is held captive by the two wheels in the event of compliance failure. This would permit continued operation at increased noise levels.

4. Twenty-one inch diameter. This is 3.75 inches larger than the standard M113A1 idler, but will still permit the passage of debris or track throwing without jamming. Additional clearance is provided by the radial deflection allowed by the compliance.

5. Low rubber stresses. The maximum stress in the rubber compliances is limited to 45 psi. This is well within the recommended limit of 95 psi for 40 durometer rubber undergoing continuous rotative shear loading. Levels higher than 45 psi are not possible due to bottoming of the rim. The low levels of stress in the prototype design will contribute to long service life. (In the experimental idler, this type of rubber material was routinely stressed to 210 psi during an approximate test time of 220 miles).

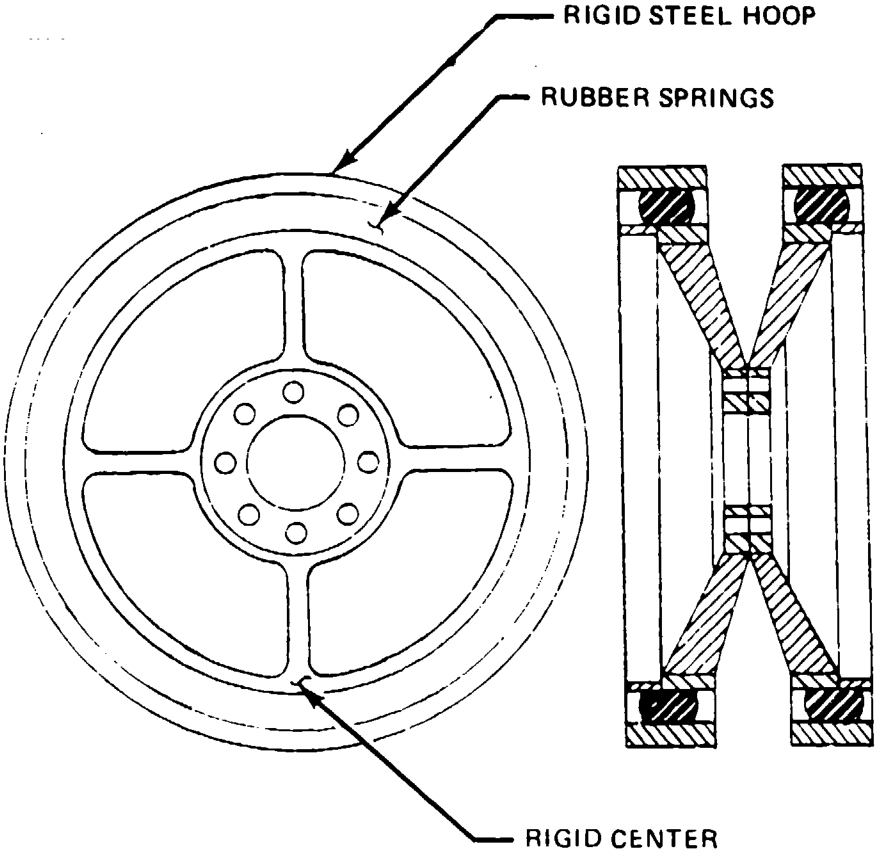
RIGID STEEL HOOP
RUBBER SPRINGS
RIGID CENTER

Figure 6.19 Idler Concept: Thick Rigid Rim; Rubber in Compression.

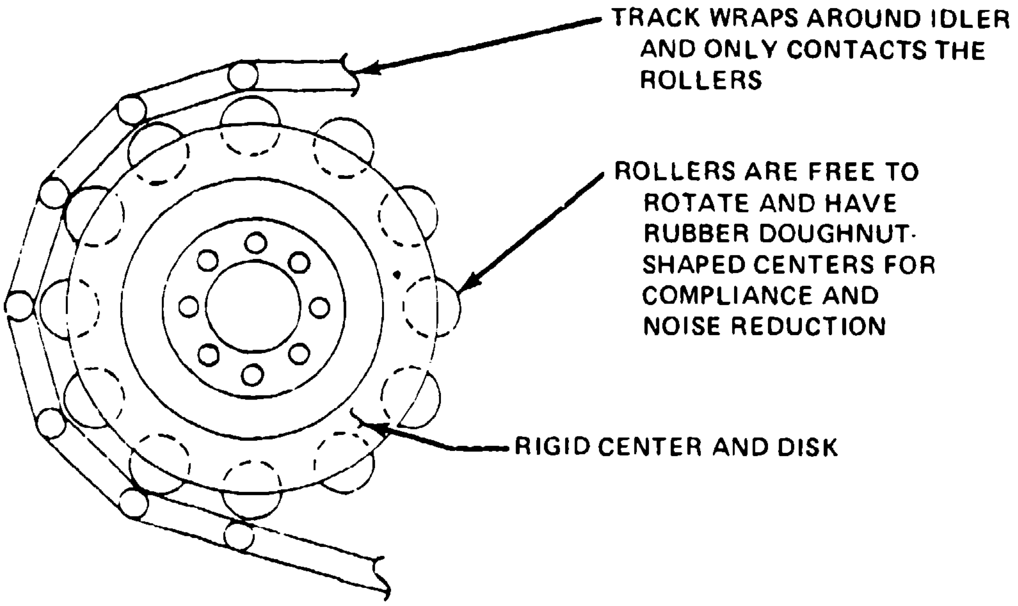
TRACK WRAPS AROUND IDLER AND ONLY CONTACTS THE ROLLERS
ROLLERS ARE FREE TO ROTATE AND HAVE RUBBER DOUGHNUT-SHAPED CENTERS FOR COMPLIANCE AND NOISE REDUCTION
RIGID CENTER AND DISK

Figure 6.20 Idler Concept: Rim Composed of Rollers.

6. A very simple working action. The rubber experiences rotative shear at limited levels of stress and strain. This type of limited movement is conducive to long service life.

7. Overload capability. The idler was designed to withstand dynamic loads of over 15,000 lbs.

8. A maximum deflection of .75 inch. This will allow for noise reduction at all but the most severe of vehicle maneuvers. Shock input to the vehicle from the idler bottoming during rough terrain operation will also be greatly reduced.

9. Internal cut-outs to allow passage of debris drawn into the wheel by the track guides. To avoid trapping objects between opposing spokes, the standard M113A1 idler wheels are mounted with spokes staggered. Larger cut-outs would be required if this staggered arrangement was desired on the prototype idler. In either case, the base of the spokes in the rim are the means of limiting the deflection during overload conditions.

10. Inclined rims. The rims are inclined inward to utilize the compliance of the inner track shoe pads. The outer edges are highest and contact the inner track pads first. The inner pad is deflected most at this point. As the pad deflects, more and more of the rim contacts the rubber pad. The effect is that of an increasing spring rate shock absorber.

    Another concept for the rim contour was to provide two circumferential bumps of different heights [10]. This would have produced a dual rate spring effect when contacting the inner track pad. However, the valley between the bumps could prevent a misaligned track guide from recovering. Therefore, the ramp concept was adapted.

11. Chamferred inner edges of each rim. It is known that the track is most frequently thrown inward toward the hull. The chamferred edges help the track guides to realign into the center of the idler. The exaggerated chamfer on the inboard half significantly reduces the occurrence of the track throwing problem [13].

6.3.4 Results

The actual prototype idler that was used for testing was fabricated from high strength steel plate and molded natural rubber. The wheel halves were machined individually but the rim was welded together from rough-machined halves, then final machined. The basic designs are compatible with forging or casting processes for high production rates. The rubber annuli were molded from a high grade, low loss, natural base rubber compound. They were attached at assembly with a cyanoacrylate adhesive. The rubber hardness that was achieved was somewhat softer than the nominal design specifications: 35A instead of 40A durometer. Noise reductions for the test prototype may consequently be slightly better than expected. Bottoming-out load capabilities will also be reduced.

6.3.4.1 Compliance

The calculated design spring rate for the prototype idler is 8247 lb/in. This value is for a rubber hardness of 40A durometer as required by the design. For a hardness of 35A durometer, as was achieved, the spring rate is 6927 lb/in. These values consider that the dynamic shear modulus exceeds the static modulus by 20 percent [8]. No tests were made to determine the actual level of compliance.

6.3.4.2 Interior Noise Reduction of the Prototype Idler

The noise of the prototype compliant idler was measured on the idler test stand and compared to tests of the standard idler on the same stand. Track tension was 2,500 lbs in both cases.

Figure 6.21 shows A-weighted crew area noise levels of the standard and prototype idler wheels as a function of speed. Noise reductions of from 10 to 15 dB(A) were achieved. At 30 mph, the noise level was 95 dB(A); therefore an additional 3 dB(A) of noise reduction would be required to meet the idler wheel goal of 92 dB(A).

Figure 6.22 shows crew area noise spectra of the standard and prototype idler wheels. The prototype idler octave band noise levels were reduced by 6 to 20 dB in the frequency range of 63 to 8000 Hz.

For the entire vehicle at 30 mph to comply with MIL-STD-1474, Category B, the prototype idler would require an additional noise reduction of 5 dB in the 250 Hz octave band. No further noise reduction would be required in any other octave band. This statement assumes that the combined noise of the two quieted sprockets, two quieted idlers, and ten quieted roadwheels has the same spectrum shape as the noise due to the prototype idler wheel. This assumption, though not exact, is presently necessary because the other low-noise components have not yet been developed.

6.3.4.3 Exterior Noise Reduction of Prototype Idler Wheel

Figure 6.23 shows the acoustic signatures in octave bands for 30 mph operation of the standard and prototype idler wheels, as measured on the FMC test stand.

A reduction of 3 to 6 dB was measured at frequencies between 250 and 2000 Hz. The actual signature reduction was probably greater and cannot be measured accurately on the present test stand. This is suspected because the measured interior noise reduction in these octave bands is 11 to 16 dB, which is far greater than the 3 to 6 dB exterior reduction. As the interior and exterior noise reduction of hull-radiated noise must be identical, the measured exterior prototype idler noise must contain noises from other sources; the likely candidates are the test stand assembly and direct radiated noise from the track, sprocket and idler. A listening test suggests that the test stand and its drive sprocket are the sources.

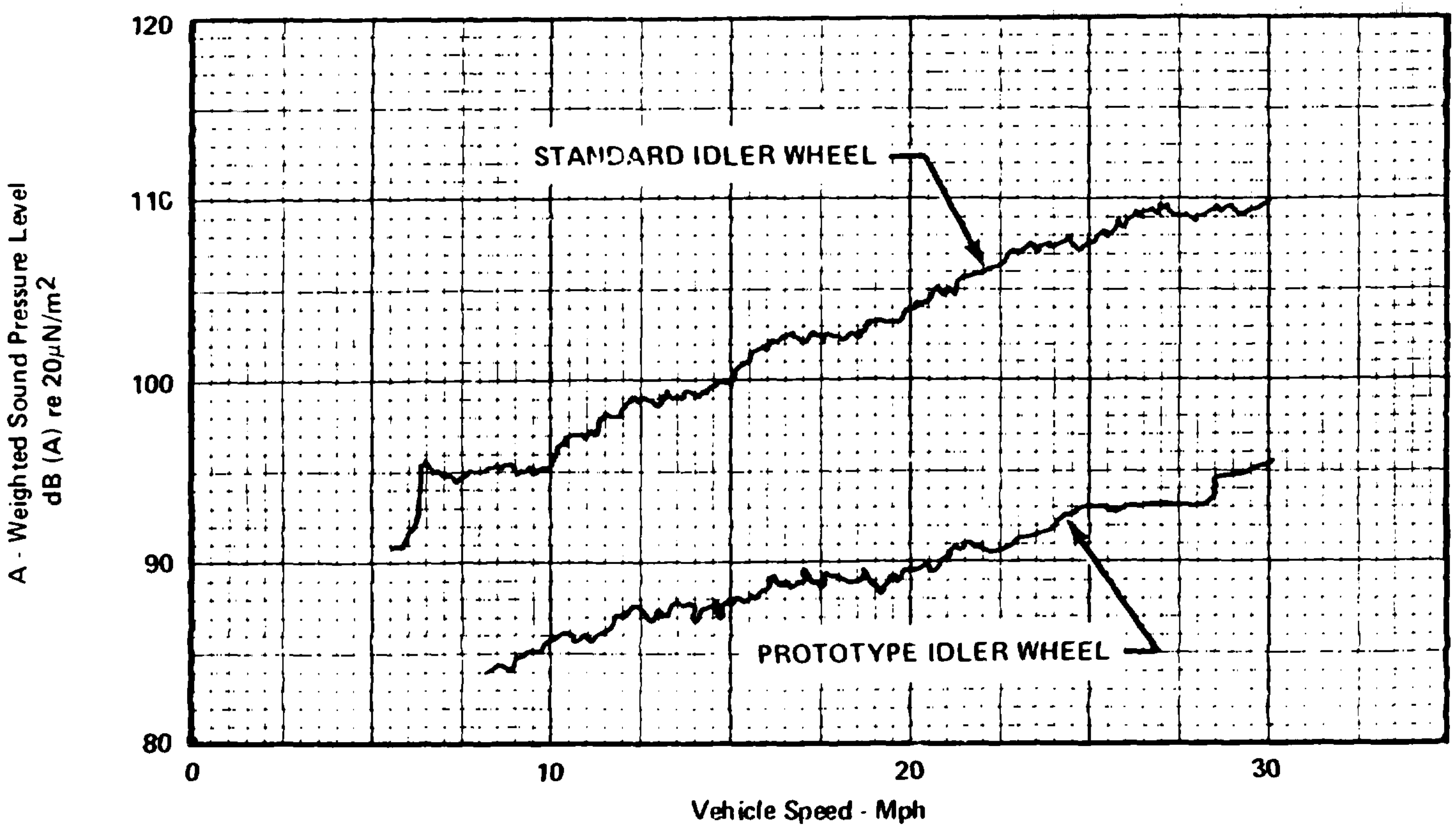

Figure 6.21 Interior Noise Reduction with the Prototype Compliant Idler Wheel.

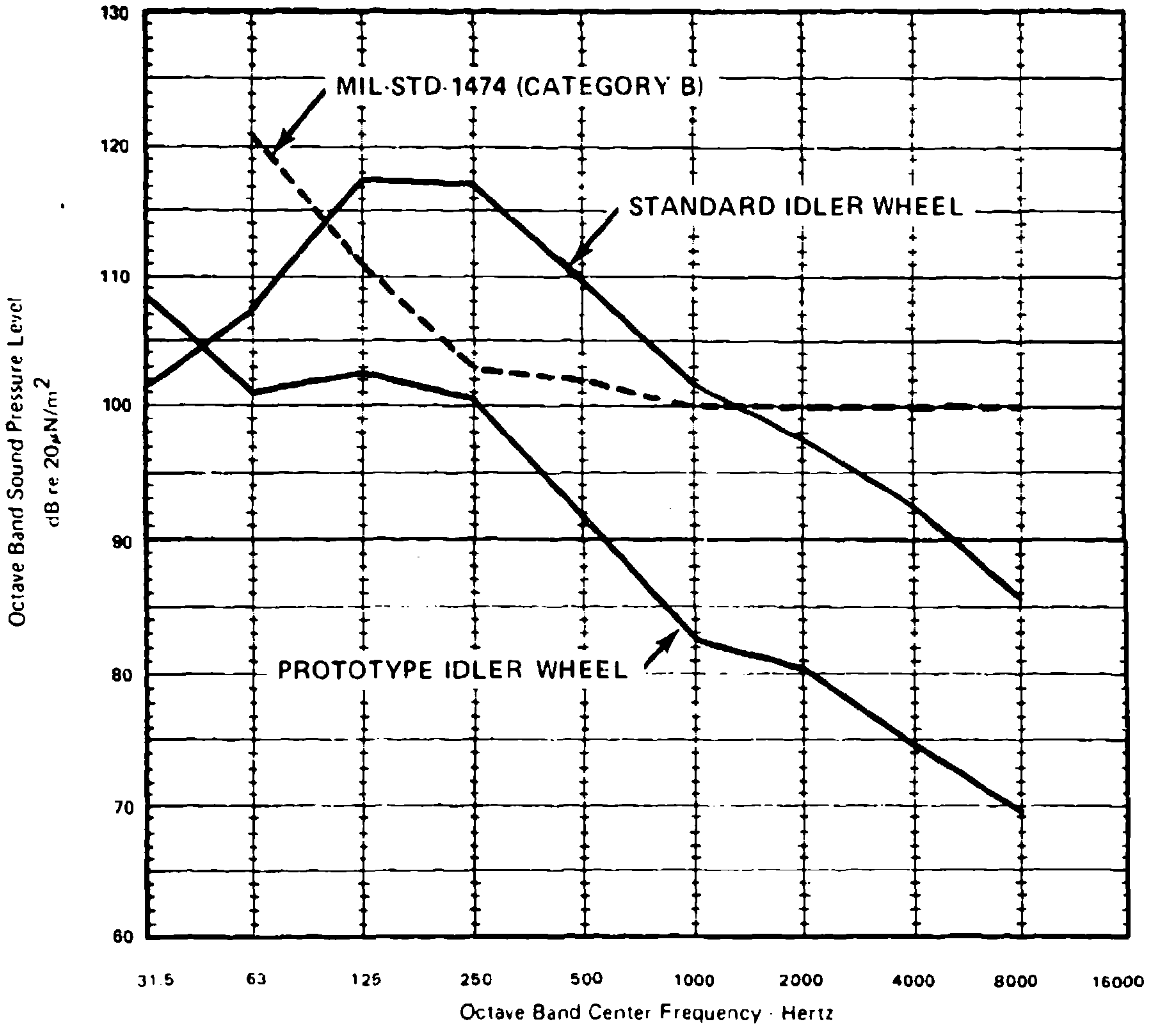

Figure 6.22 Interior Noise Spectra Comparison for the Standard and Prototype Idler Wheels.

IDLER INDUCED NOISE

A —— - - ——Standard idler,
30 mph, 105 dB(C), 88 dB(A)

B ——————Prototype idler,
30 mph, 97 dB(Flat), 85 dB(A)

ENGINE EXHAUST NOISE

C - - - - - - Maximum noise levels in 2-3 gear, 600 to 2000 RPM,
accelerator fully depressed, brakes "on",
standard M113A1 production vehicle.

D —— - - ——Same, but for TARADCOM low-signature demonstration
M113A1 vehicle. (Data taken at 50 feet, 6 dB then
added for distance compensation)

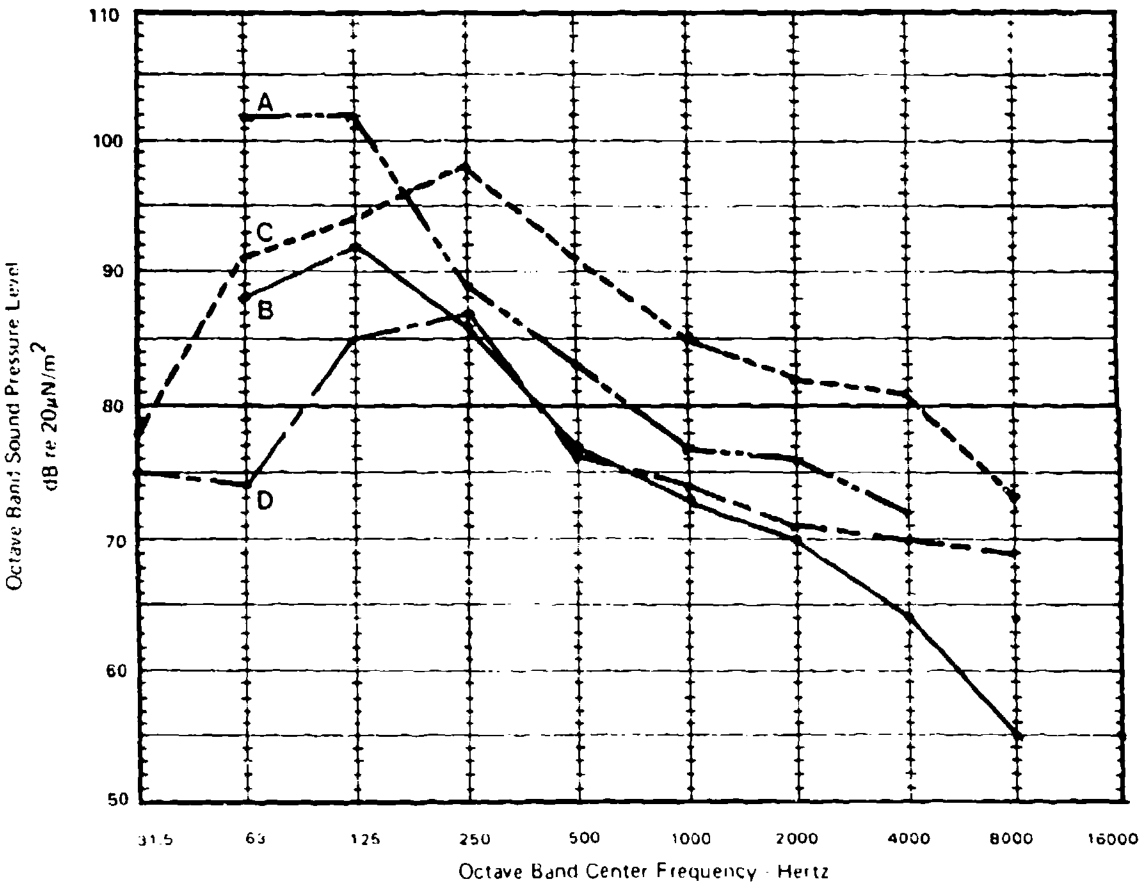

Figure 6.23 Exterior Noise Spectra of M113A1 Standard Idler Pair, Prototype Idler and M113A1 Exhaust at 25 Feet to the Left of the Hull.

Although the exact acoustic signature of the prototype idler is apparently too low to be measured on the test stand, it can still be concluded that the exterior idler signature has been reduced to well below the maximum exhaust noise of a standard M113A1, and thus would not lead to detection. The present data are not adequate to determine if the actual acoustic signature of the prototype idler wheel could lead to vehicle detection more readily than exhaust noise from TARADCOM's low-signature M113A1.

6.3.4.4 Durability of the Prototype Idler

A limited amount of test mileage was accumulated on the prototype idler during noise measurement tests. It is estimated that a total of about 31 miles were completed with the idler operated on the test stand at various track tensions up to 2,500 lb. Of the four bond surfaces that exist, three were in excellent condition but one was peeling away at the inner diameter and peeling slightly at the outer diameter. Apparently, poor assembly efforts were at fault because all bonds have endured the same operating conditions and environment. Rubber overlap at steel edges was not a factor in this failure. No appreciable wear was observed on any of the steel components mainly because of good track alignment and no occurrence of idler "bottoming-out".

Based upon earlier fatigue testing [4] and upon examination of the experimental idler paddle bonds, this prototype idler could easily provide over 2,000 miles of service life, excluding the possibility of a foreign object causing a catastrophic failure of a rubber element. The annuli are, of course, the weakest links in the assembly. The main hazard involving the rubber is the possibility of a hard or sharp object becoming jammed between the rubber and a solid moving steel component. Cut-outs near the inner diameter and the small clearances at the rim will minimize the threat of debris damage. Furthermore, considerable wear of the rubber material could be sustained before failure occurs. Actual vehicle durability tests would be the only means of determining accurate field service life expectations.

The second weakest link in the assembly is the rubber-to-steel bond. The experimental and prototype idler wheels employed a cyanoacrylate adhesive. This adhesive proved to be the most desirable in laboratory fatigue tests. Even though this adhesive loses up to fifty percent of its shear strength when exposed to water, the bond shear strength exceeds that of the rubber by a factor of up to sixty. A vulcanized bond has been proposed as an equally reliable means of attaching the rubber. However, the configuration of the prototype idler might prove to be too restrictive for the molds required by the vulcanizing process.

Durability of the steel wheel halves and rim is expected to exceed that of the standard M113 idler wheel. This is because of the reduced impacts that will be experienced. Excessive wear, of course, could result if catastrophic rubber failure occurs. Nevertheless, these parts could probably be reused several times with new rubber annuli. Rebuild cycles could be predicted with field testing.

6.3.4.5 Conclusions and Recommendations

The prototype compliant idler wheel demonstrated a substantial reduction in idler generated interior noise. Although the design goal of 92 dB(A) was not met (95 dB(A) was achieved), development of the prototype idler wheel was a very successful step in reducing the M113A1 vehicle interior noise. If the sprocket and roadwheel induced noise can be reduced by as much as was done with the prototype idler, subsequent hull modifications and/or improvements in the compliant suspension members should enable the interior noise goal of 100 dB(A) to be met. Although field testing of the prototype idler wheel has not been conducted, because of the rugged idler wheel construction and conservative rubber stress levels, service life is estimated to be at least 2000 miles.

Future compliant idler work should include the following areas:

1. Investigate design modifications necessary to make the compliant idler wheel completely compatible with standard manufacturing techniques to reduce unit manufacturing costs. This might include replacement of the glued rubber to steel bonds used in the prototype idler with vulcanized-in-place rubber parts.

2. Investigate design modifications to facilitate field replacement of failed compliant elements.

3. Conduct a field test program to determine the durability and service life of the compliant idler wheel.

7. EXPERIMENTAL SPROCKET CARRIER DEVELOPMENT

7.1 Conceptual Approach

Based upon the successful demonstration of noise reduction on the compliant idler, similar concepts were extended to the sprocket. The sprocket presents a greater challenge for noise reduction than the idler because of the necessity to transmit high torque loads through the compliances.

As with the experimental idler, the experimental sprocket is a tool which will aid in the design of the prototype sprocket. The design and testing of the experimental sprocket was intended to address the following areas:

1. Exploration of the constraints and limitations involved in compliant sprocket design.

2. Assessment of the practical amount of torsional deflection that should be allowed before lockout

3. Determination of the effects of both torsional and radial loading on the compliant elements, including heat buildup

4. Determination of the effects of axial deflections and axial tilting, especially with regard to the overload mechanism

5. Selection of the balance between torsional stiffness and radial compliance for required torque transmission and optimal noise reduction

6. Selection of a compliant material

7. Magnitude of expected interior noise reduction

8. Assessment of the effect on exterior noise

9. Estimate of durability

7.2 Design Goals

The goals in the design of the experimental compliant sprocket were:

1. A-weighted noise level of 95 dB or less

2. Ability to be tested on the test stand or on an operating vehicle

3. Service life of 100 miles or more

4. Fail-safe features to maintain an operational sprocket and prevent a thrown track, in the event of compliance failure

5. Ability to transmit the torques encountered in typical vehicle maneuvers

6. Ability to lock out the compliance during the transmission of very high torque loading

7.3 Design Criteria

To achieve the above goals, the following criteria were used to guide design decisions:

1. Space limits: The sprocket shall be designed so that no changes to the hull are required on the M113A1 test vehicle.

2. Existing hardware: The sprocket must fit on to the existing M113A1 final drive assembly.

3. Pitch: The pitch of the sprocket shall not be changed from that on the M113A1 vehicle. This dictates a 10 tooth sprocket of the same diameter as the M113A1 sprocket.

4. Rubber Stress: To ensure adequate life of the rubber compliances, stresses in the material shall not exceed recommended limits for rotative dynamic loading, e.g., 75 psi for 30 durometer rubber when shear strain is 225% [8].

5. Static load that will be constantly imposed on the sprocket due to common track tension may be as high as 9,000 lb. radially. If an M113A1 is parked on a 60% slope, track tension may impart loads up to 11,200 lb radially and 9,156 ft-lb. torsionally.

6. Dynamic loads: The fluctuating loads imposed on the sprocket during severe steering maneuvers may be as high as 5,600 lb. radially and 2,570 ft-lb torsionally [12]. This occurs during hilly cross-country maneuvers.

7. Torque: The maximum torque that the sprocket must transmit is 11,300 ft-lb at an acceleration of up to 1 g. This occurs during panic skid stops [14].

7.4 Design Concepts

Development of the experimental sprocket initially focused on the compliant mechanism. A complex rubber-in-shear system was finally chosen after other concepts proved impractical. Design of the overload torque device was then pursued. A ten-degree torsional deflection was used for a torque wind-up limit. This ten-degree angular deflection was considered appropriate for both long-life stress levels in the rubber compliances and workable clearances to allow isolation of the sprocket during usual operations. The extremely restrictive size envelope was the major obstacle throughout the whole design effort.

In the following subsections, the various compliance concepts that were evaluated are discussed. A description of the final design, including the overload torque mechanism, is presented in Section 7.4.4.2.

7.4.1 Rubber in Radial Compression and Torsional Shear

The phrase "rubber in compression" has been used in this report whenever a design concept employed rubber in radial compression. Almost all of the concepts provided torque transmission via the shear mode. Various concepts using rubber in compression were compared by evaluating predicted performance characteristics for similarily sized structures. Trends in performance changes were observed with certain modifications and their particular advantages were investigated. No effort was made to systematically identify or categorize these trends.

Procedures for predicting performances of the rubber-in-compression concepts were basically the same, so only the description of the first concept will go into any detail.

7.4.1.1 Solid Pair of Rubber Rings

The basic concept for rubber in compression involved a pair of solid rubber rings. The individual ring size was chosen to be compatible with standard M113A1 sprocket dimensions: 15.125" O.D. x 12.375" I.D. x 3.625" wide. The rings would be press-fit between the inner and outer hoops for a ten percent preset compression. Each ring was to be bonded to an inner hoop but not to an outer hoop. This avoided placing any rubber in tension. Torque would be transmitted at the outer mating-part line by friction. This concept is illustrated in Figure 7.1.

To evaluate this design, it was assumed that the compression loads were reacted by an equivalent flat block of rubber. This equivalent block was of the same thickness as the ring but with flat dimensions equal to the projected area of the ring inner diameter. The shape factor, rubber hardness and simulated dimensions were then used to approximate the total sprocket radial compliance. The torque capability was predicted from the ring dimensions.

This solid rubber ring concept proved unacceptable because excessively high radial compliances were predicted whenever acceptable torque capabilities were found. Conversely, acceptable radial compliances occured only with excessively low torque capability. This negative relationship between the two desired performance characteristics could not be reversed by any change in basic rubber material.

Other practical difficulties were anticipated with this concept. First, the task of press fitting these large flat rings between the two hoops would be difficult. Second, the probability was low that the total outer surface of the rubber would provide enough friction to actually transmit the predicted torque output.

7.4.1.2 Directionally Modified Compliance

The addition of circumferential holes or radial holes were two modifications intended to improve the performance of the rubber in compression concept. The objectives of these two approaches was to decrease radial compliance while maintaining a high torsional shear strength. Each modification employed a pair of rubber rings that were assembled from rectangular blocks with holes through them.

The individual blocks were as thick as the solid ring and as long as the width of the ring. Orientation of the holes determined whether they were circumferential or radial. The blocks were to be press-fit side-by-side between the inner and outer hoops.

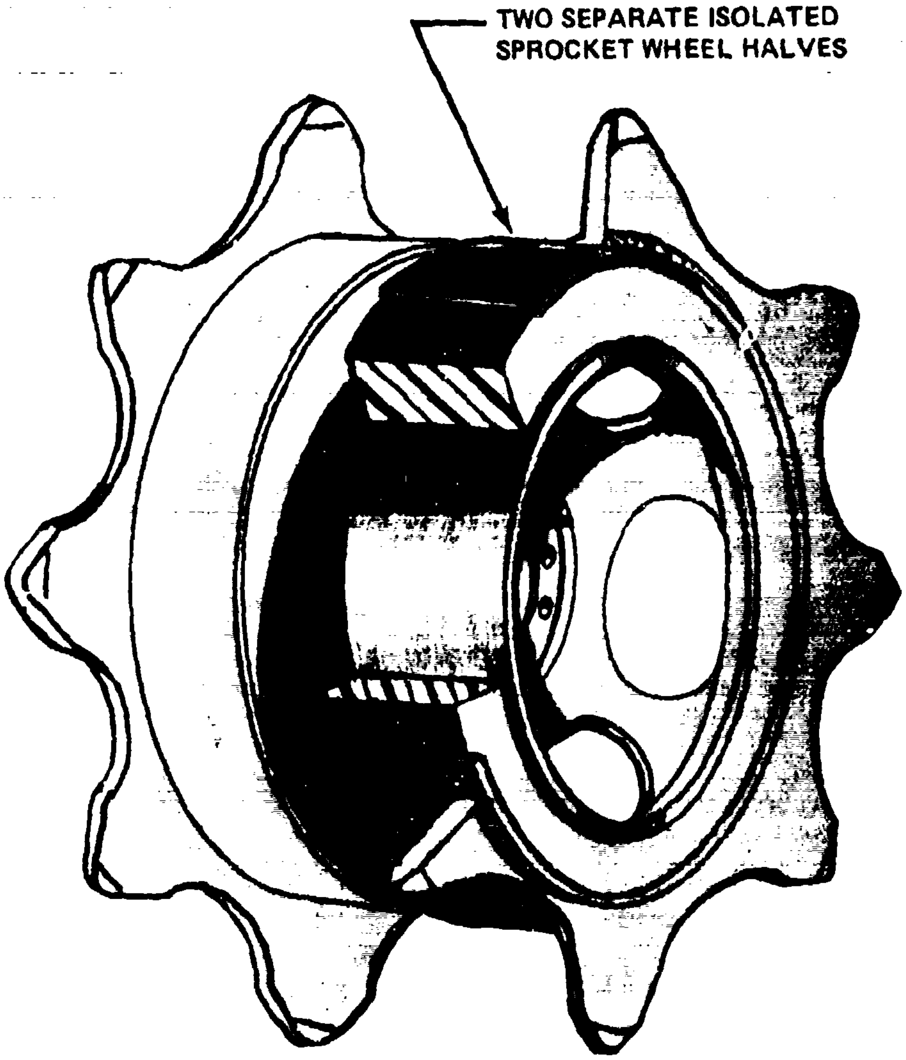
TWO SEPARATE ISOLATED SPROCKET WHEEL HALVES

Figure 7.1 Sprocket Concept: Solid Rubber Ring in Compression.

As with the solid rings, the radial compliance was assumed to be provided by an equivalent block of rubber, as thick as the ring and of an area equal to the projected inner diameter. All blocks contributed to torque. Figure 7.2 shows an assembled modified rubber ring with circumferential holes. The radial hole modification would have looked similar.

Various sizes and patterns of holes in both directions were investigated. However, no modification of either type resulted in sufficiently low radial compliance while maintaining a high torsional stiffness. Only round holes were considered but other shapes did not seem promising. Consequently, rubber in compression was considered impractical.

7.4.1.3 Three Concentric Ring Pairs

One of the original design concepts proposed for the experimental sprocket involved three pairs of rubber rings in compression. This design is illustrated in Figure 7.3. The large pair of rings provide most of the compliance and torque capability. The other two ring pairs provide additional compliance.

The fact that this concept could not achieve the desired spring rates proved to be the major drawback. Other difficulties included complexity and instability. The concept also depended upon an eleven tooth sprocket, larger than the M113A1 sprocket. This was considered undesirable since performance and load characteristics of the complete vehicle power train would be altered.

7.4.1.4 Rubber in Radial Compression and Radial Shear

Another original concept combined the ideas of using rubber in compression and rubber in shear. The proposed design was to have four pairs of rubber rings; a large and a small set in shear and a set of soft and hard pairs in compression. This configuration is shown in Figure 7.4. To accomodate the complex structure a larger than standard sprocket was again proposed.

The major drawbacks to this concept were the complexity, the large size and the inability to obtain both the desired compliance and torsional stiffness.

7.4.2 Compliant Fabric Isolator

An unconventional fabric isolator system was another proposed possibility. The fabric weave pattern was to have strong "threads" of various compliances, woven in three different directions. As assembled, one set of threads would extend in a radial direction, from the inner hoop to the outer hoop. The other two sets of threads would form opposing spiral arcs, stretching from the inner hoop, around and outward to the outer hoop. All of the threads would be secured at both ends.

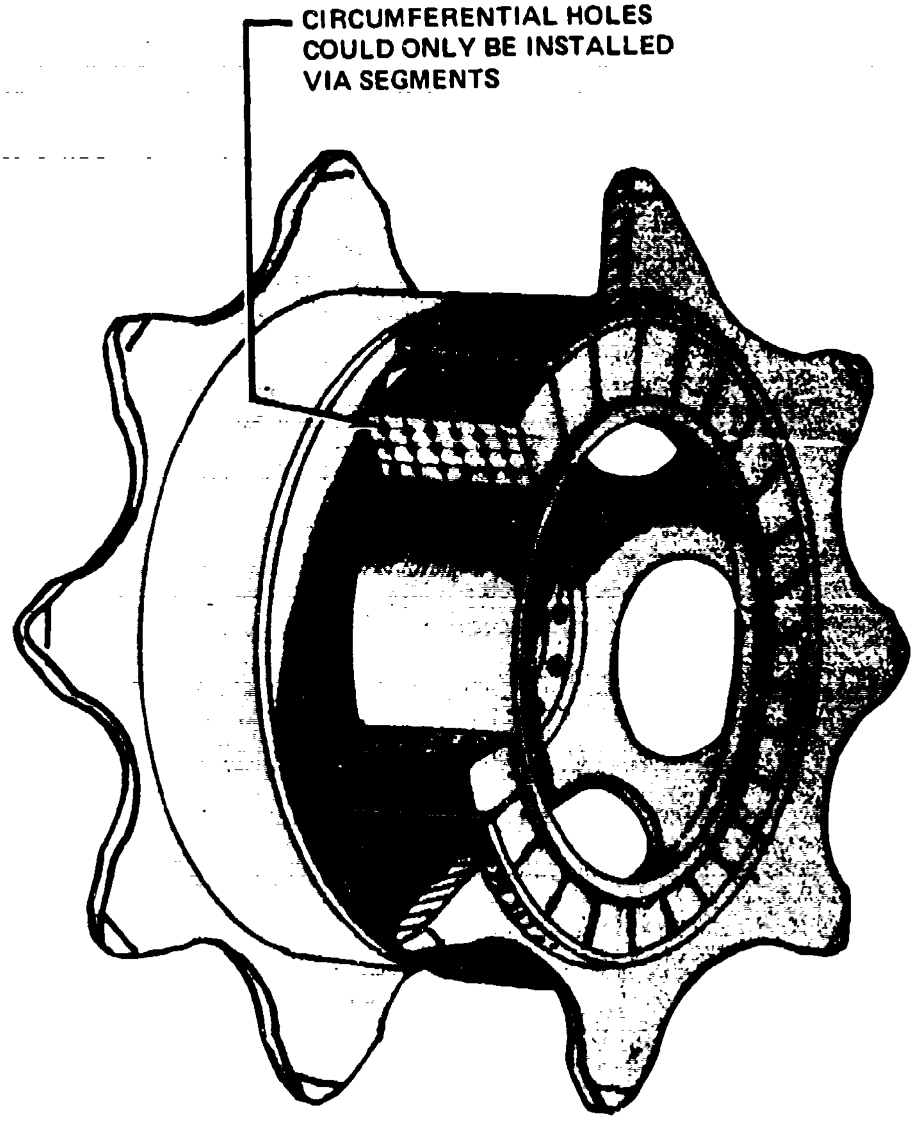
CIRCUMFERENTIAL HOLES COULD ONLY BE INSTALLED VIA SEGMENTS

Figure 7.2 Sprocket Concept: Segmented Rubber Ring in Compression with Circumferential Holes.

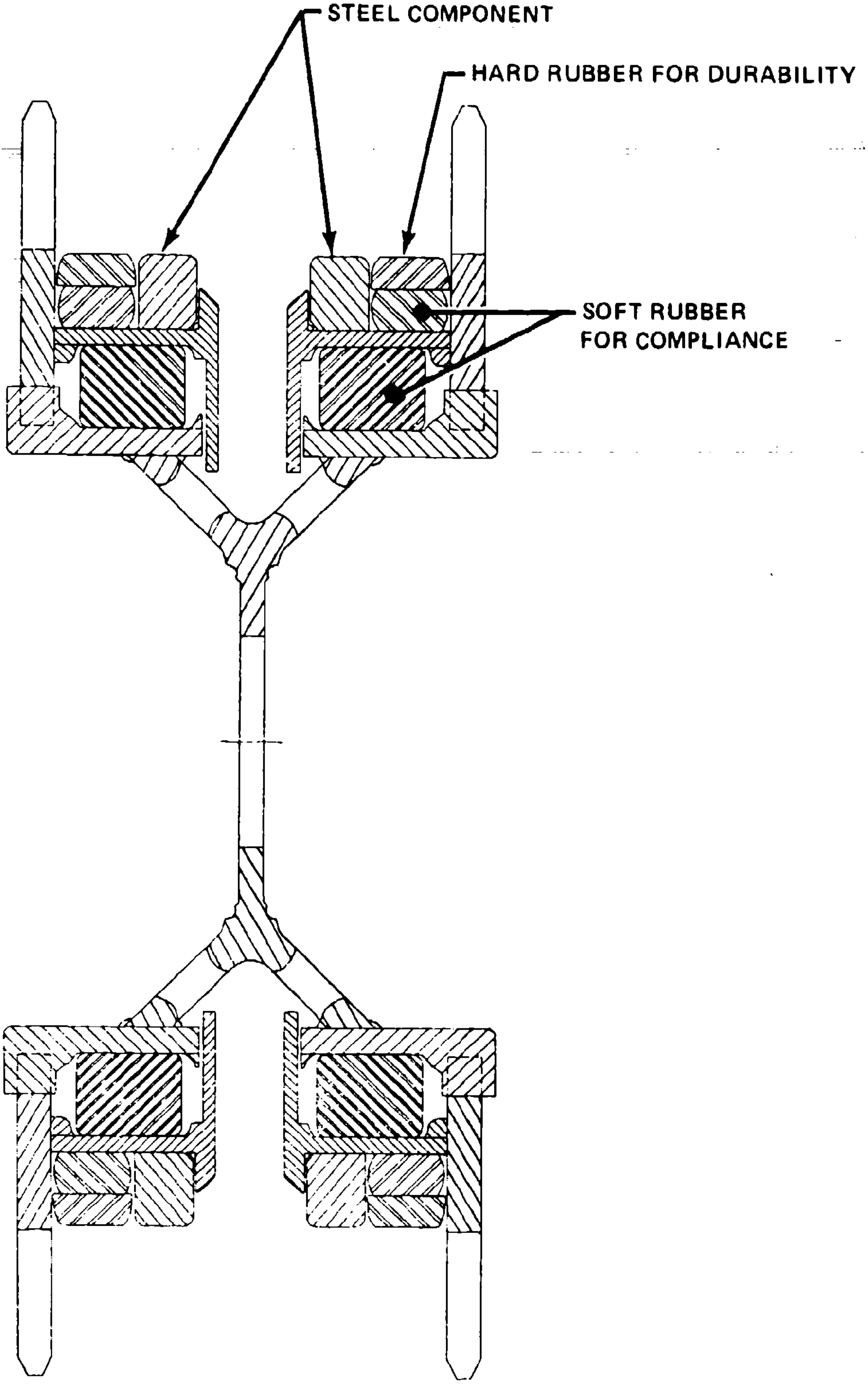
STEEL COMPONENT
HARD RUBBER FOR DURABILITY
SOFT RUBBER
FOR COMPLIANCE

Figure 7.3 Sprocket Concept: Three Rubber Ring Pairs in Compression.

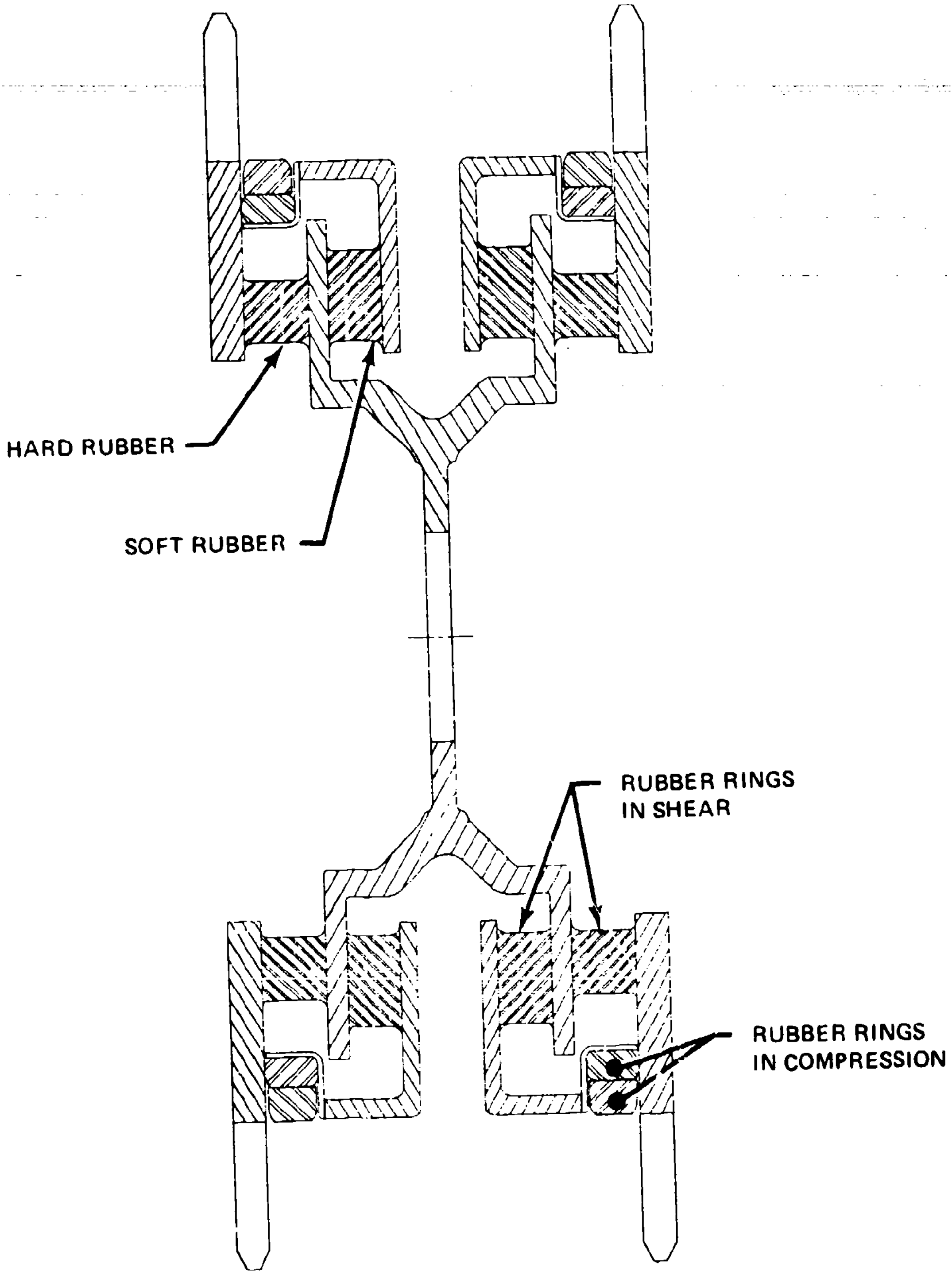
HARD RUBBER
SOFT RUBBER
RUBBER RINGS IN SHEAR
RUBBER RINGS IN COMPRESSION

Figure 7.4 Sprocket Concept: Rubber in Both Radial Compression and Radial Shear.

The sum of the tensile compliances for the radial threads, being stretched in one direction, would have provided the total sprocket radial compliance and strength. The spiral arc threads would have combined to provide torsional stiffness in either direction.

The configuration is shown in Figure 7.5. The cross section shows each type of thread as a different layer when, in fact, they would be interwoven.

This concept was not pursued becuase it would have required excessive research and experimentation, and therefore, was unpredictable at this stage.

7.4.3 Overload Gear with Rubber Separators in Compression

One sprocket concept proposed the use of rubber segments that were encased by steel on two sides to provide resistance to radial and torsional forces. The configuration is shown in Figure 7.6.

This concept was not seriously investigated because the operating deflections for desired compliances would have been excessive when related to the small size of the individual rubber elements. Design complexity, fatigue, instability, and wear were also considered to be major drawbacks.

7.4.4 Rubber in Shear

The rubber in shear concept involved pairs of flat rubber rings similar to those used in the prototype idler. In the sprocket application, they not only provided radial compliance but torsional stiffness as well. The contradictory relationship between minimizing radial compliance while maximizing torsional stiffness was again encountered. A smaller ring had the beneficial effect of reducing radial compliance to desired levels but it also had the negative effect of reducing the moment arm and, thereby, the torsional strength. Similar contradictory relationships were found when modifications were made in the areas of size, hardness, stress and strain.

7.4.4.1 Single and Double Pairs of Annuli

In the study of single and double pairs of rubber annuli, acceptable levels of performance and durability could only be obtained with oversized designs. At the larger sizes, desired workable deflections produced excessive stresses and strains. Considerable effort was expended to avoid more complex configurations. However, no variation of rubber strength, size, or shape was found to be practical. Low radial compliances could easily be designed but compatible torque capability only increased with size or number of annuli. The only recourse was to increase the number of compliant elements.

ONLY THOSE THREADS IN TENSION ARE ACTIVE

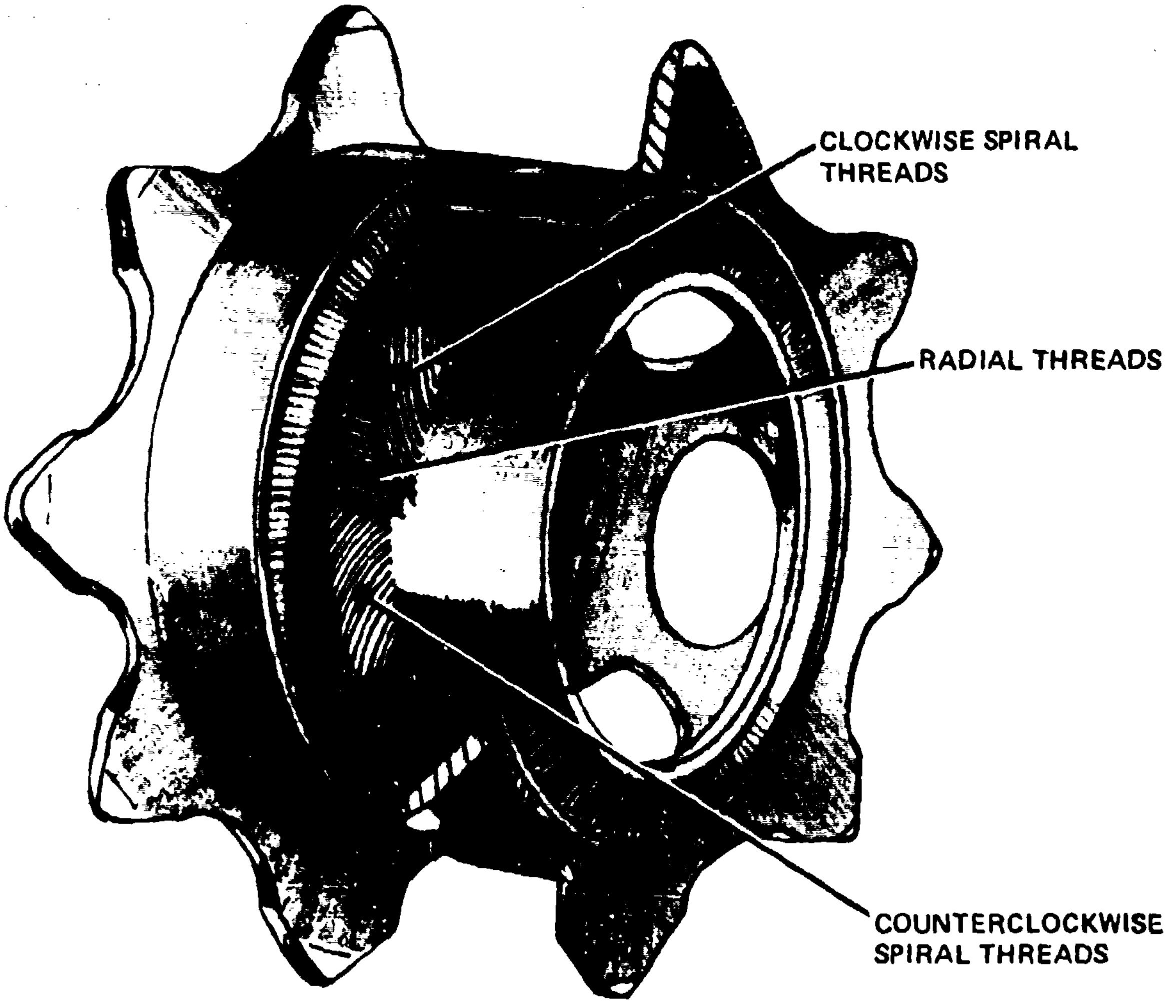
CLOCKWISE SPIRAL THREADS
RADIAL THREADS
COUNTERCLOCKWISE SPIRAL THREADS

Figure 7.5 Sprocket Concept: Fabric Isolator.

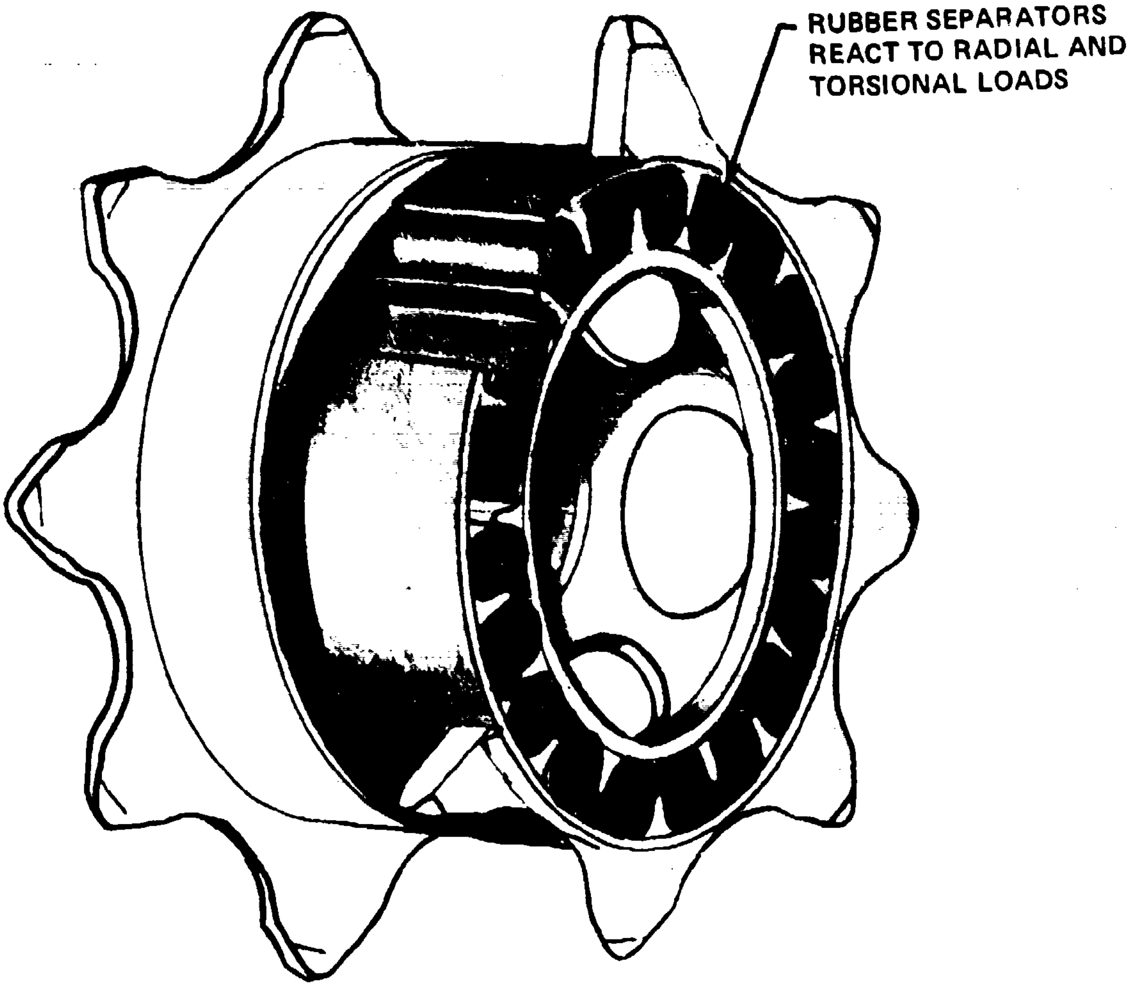
RUBBER SEPARATORS REACT TO RADIAL AND TORSIONAL LOADS

Figure 7.6 Sprocket Concept: Overload Gear with Rubber Separators in Compression.

7.4.4.2 Triple Annuli Pairs

A set of three pairs of rubber annuli was found to provide the best performance characteristics within the size and stress constraints. The final design is shown in Figure 7.7. The other assembly components and the torque overload device are also shown. A photograph of the experimental sprocket mounted on the test stand is shown in Figure 7.8. Each rubber annuli is attached, at one surface, to the inner steel hoop and, at the other surface, to the outer steel hoop. The attachment is made via the inner and outer steel supports which are welded to their respective hoops. A preset compression of ten percent is put into the inner and outer pairs of annuli. A preset compression of twenty percent is put into the middle pairs. The preset compression improves fatigue life. The original means of fastening the supports was by blind rivets, but since availability was a problem, welds were used.

The outer hoop supports a modified M113A1 sprocket wheel and an internal disk with large spline teeth for overload. The main support is bolted to the hub which provides mating spline teeth for the sprocket component. Each sprocket wheel is floating on the compliant structure during normal operation. There is no metal contact in the internal spline during normal conditions because the design provides enough backlash for up to ten degrees of angular deflection in either direction. Maximum radial deflections of one-half inch are also limited by the mechanical stops incorporated into the overload device.

The standard M113A1 sprocket cushions were mounted on the outer hoop before the halves were assembled to the hub. No fastening feature was included for the cushions. A proposed large hose clamp could have been installed adjacent to the cushions if necessary to stop lateral or rotational movement.

7.5 RESULTS

7.5.1 Compliance

The calculated radial spring rate for the experimental compliant sprocket is 17,538 lb/in. This value was calculated for a rubber hardness of 40A durometer with a dynamic shear modulus 20% greater than the static shear modulus. No tests were made to measure the actual compliance achieved in the experimental sprocket.

7.5.2 Interior Noise Reduction of the Experimental Sprocket

The experimental sprocket noise was measured on the FMC test stand as was done for the idler wheels, however, additional measurements were taken at the driver's position. The sprocket was driven by the track and was freewheeling [16]. No torque loading was involved.

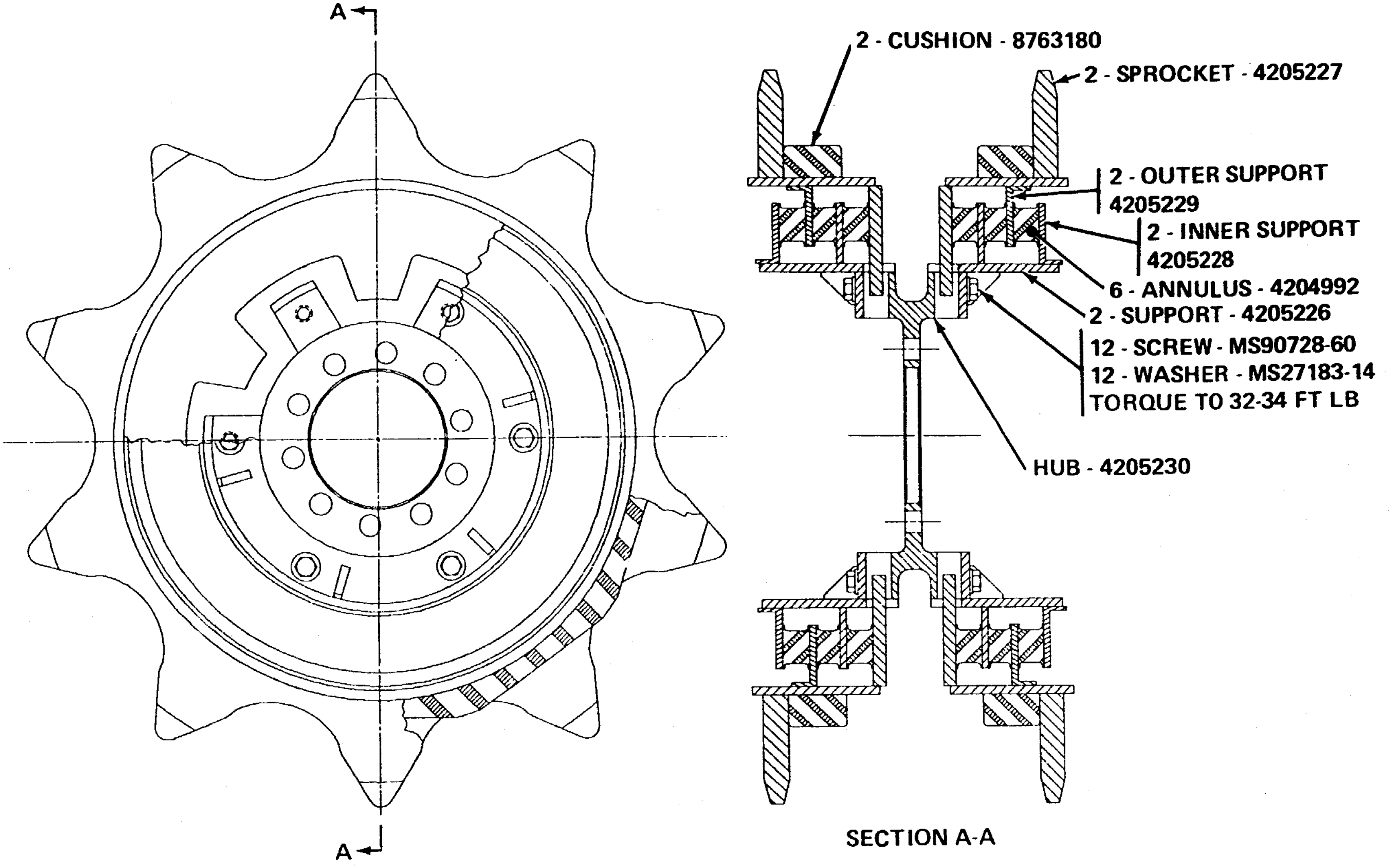
A
A
2 - CUSHION - 8763180
2 - SPROCKET - 4205227
2 - OUTER SUPPORT
4205229
2 - INNER SUPPORT
4205228
6 - ANNULUS - 4204992
2 - SUPPORT - 4205226
12 - SCREW - MS90728-60
12 - WASHER - MS27183-14
TORQUE TO 32-34 FT LB
HUB - 4205230
SECTION A-A

Figure 7.7 Sprocket Concept: Rubber in Shear.
This design chosen for Experimental Development and Test.

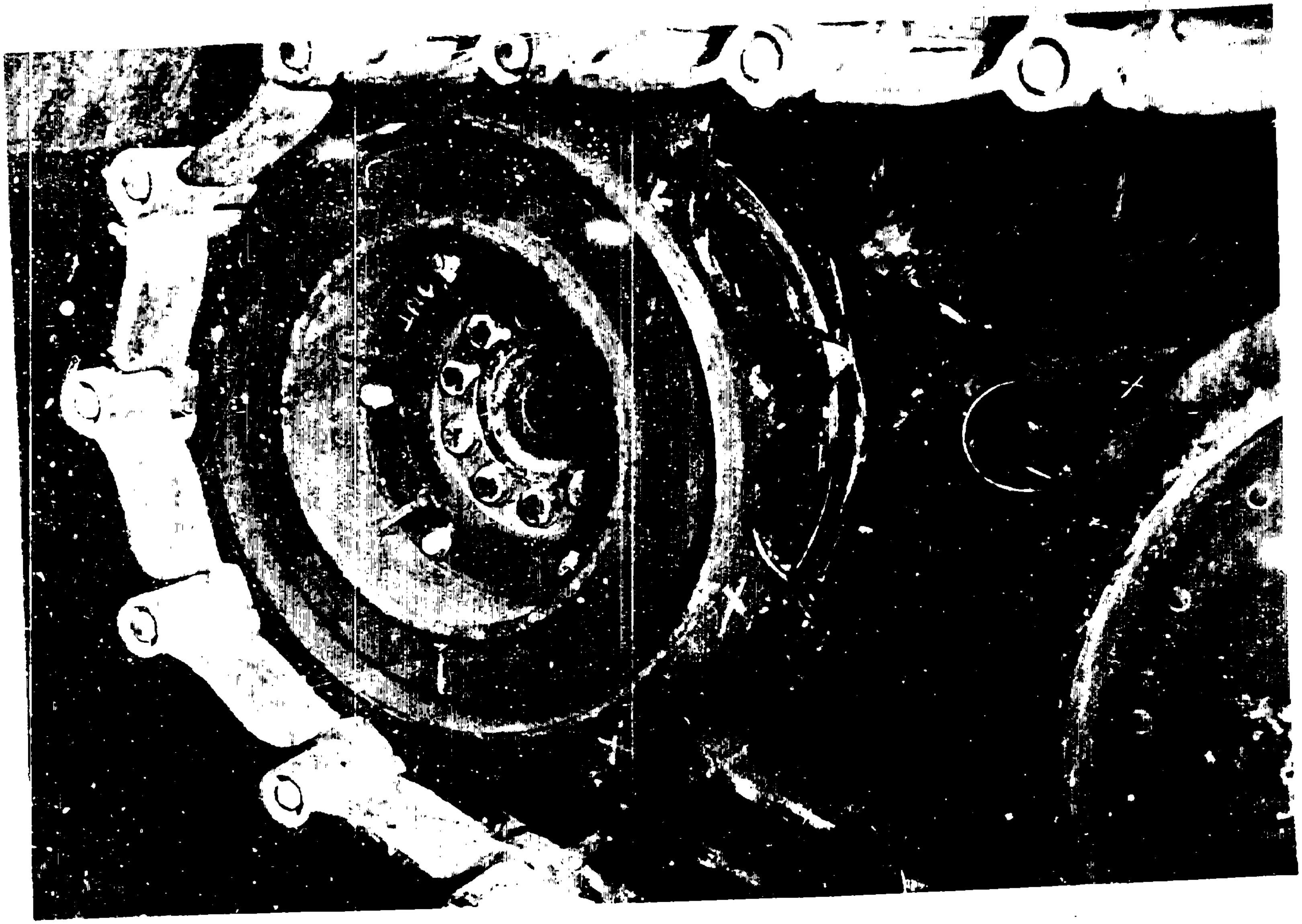

Figure 7.8 Experimental Sprocket Mounted on Test Stand.

Figure 7.9 shows the crew area A-weighted noise levels as a function of speed. This curve presents the best noise reduction obtained. The noise levels were not steady, but cyclic with track strand revolution. This unsteady noise level at constant speed was due to an unexpected metal-on-metal clatter which is discussed in Section 7.5.4. A-weighted noise reductions are 4 to 11 dB. For a sprocket to meet a goal of 92 dB(A) in the crew area, at least 11 dB(A) of additional noise reduction will be required. This is also true of the driver's area, Figure 7.10; at 30 mph the driver's compartment noise level is the same as in the crew space: 103 dB(A).

Figures 7.11 and 7.12 show octave band spectra of the standard and experimental sprockets. Noise levels are reduced by 1 to 11 dB between 63 and 8000 Hertz, and an average of 10 dB in the important 125, 250 and 500 Hertz octave bands. Considerable additional noise reduction will be required for the sprocket to be 7 dB below MIL-STD-1474 Category B. Achieving that degree of noise reduction is necessary for the entire vehicle to be below the Category B noise limits.

7.5.3 Exterior Noise Signature of the Experimental Sprocket

Exterior noise levels for the experimental and standard sprockets are shown in Figures 7.13 and 7.14. Because of the unexpected metal-on-metal clatter that was discovered, the exterior noise signature actually increased. The clatter was cyclic and closely associated with track strand revolution. When the track was run in reverse, however, this clatter was greatly reduced. The reduction in clatter may have been due to improved alignment of sprocket teeth caused by the orientation of the decagon sprocket cushion, or may have been due to a change in the complex dynamic interaction of the track with the sprocket. The cushion fit snugly to the outer hoop and maintained its original assembly position for forward speed operation. A 1.4 degree rotation was observed after reverse operation.

A detailed investigation of the clatter problem follows.

7.5.4. Experimental Sprocket Clatter

The unexpected metal-on-metal clatter that occurred with the experimental sprocket prevented achievement of the significant steady noise reductions which were predicted. Investigation of the problem included operational observations, dimensional and alignment comparisons, and detailed analysis of recorded noise data.

Initial test observations with a Strobotac and sound level meter provided no significant explanations. Interior noise level variations did not precisely follow the cyclic clatter throughout the octave bands. The track appeared to always align toward the outboard side of the sprocket. Correspondingly, each track shoe showed fresh wear marks in an inboard corner of the sprocket tooth cut-outs. This

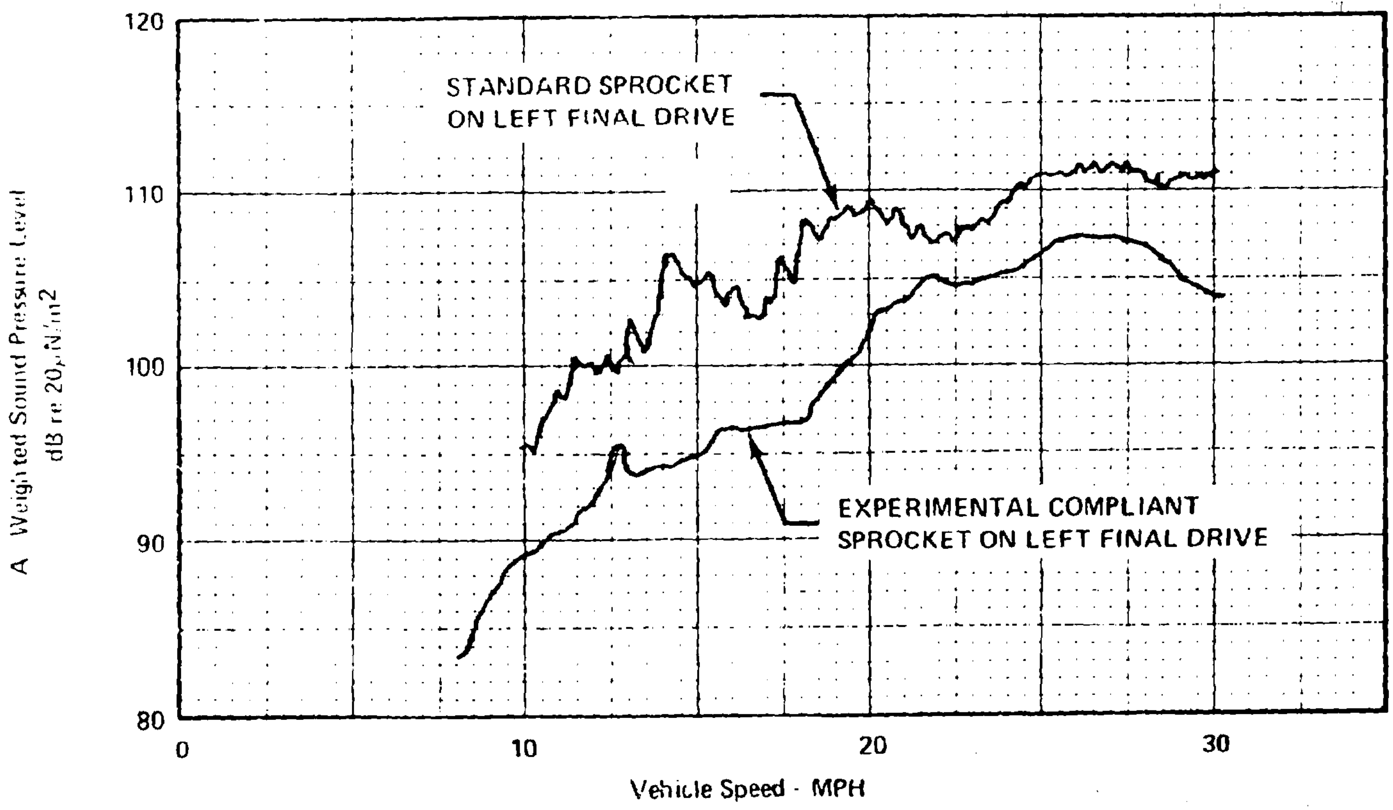

Figure 7.9 Noise Reduction in the Crew Compartment due to the Experimental Compliant Sprocket.

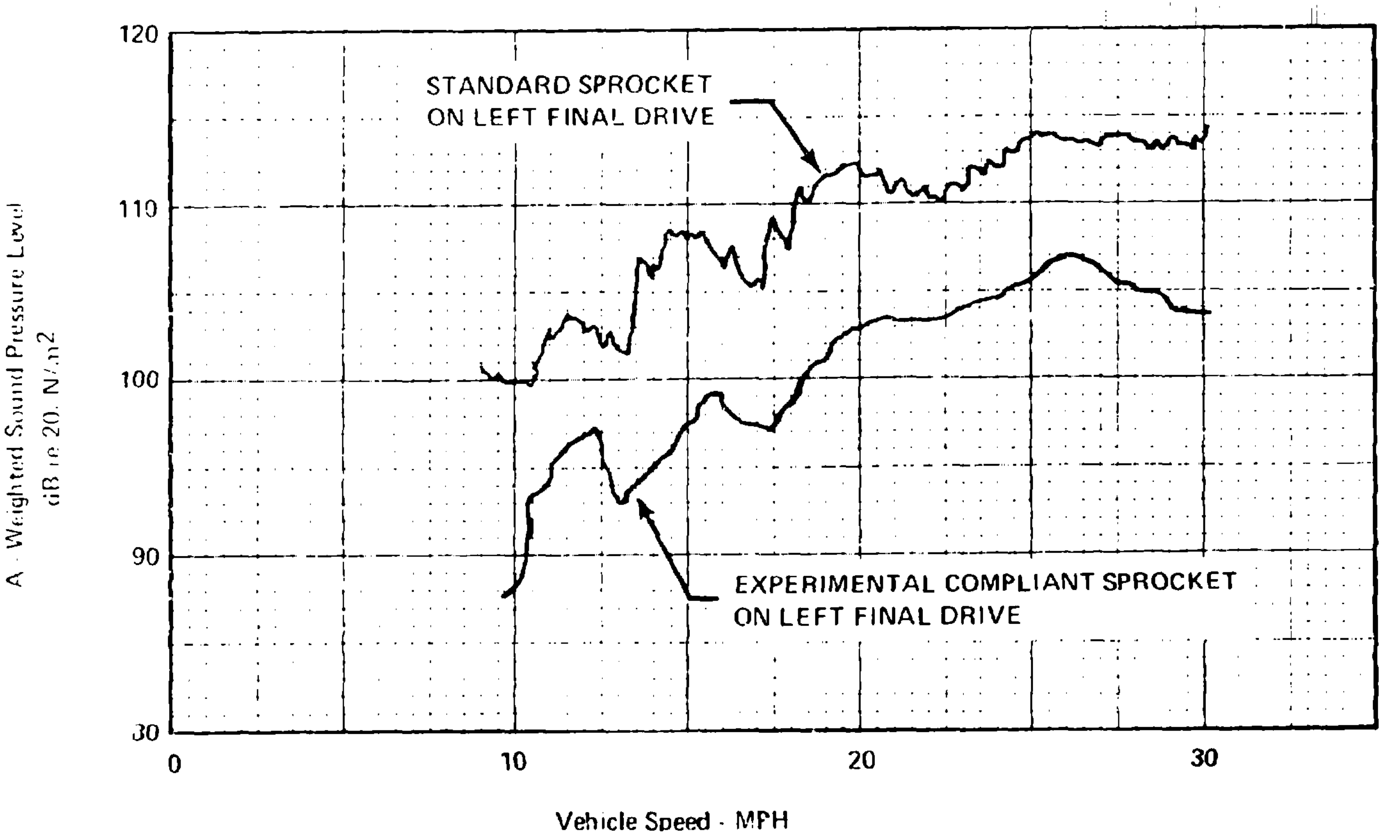

Figure 7.10 Noise Reduction in the Driver's Compartment Due to the Experimental Compliant Sprocket.

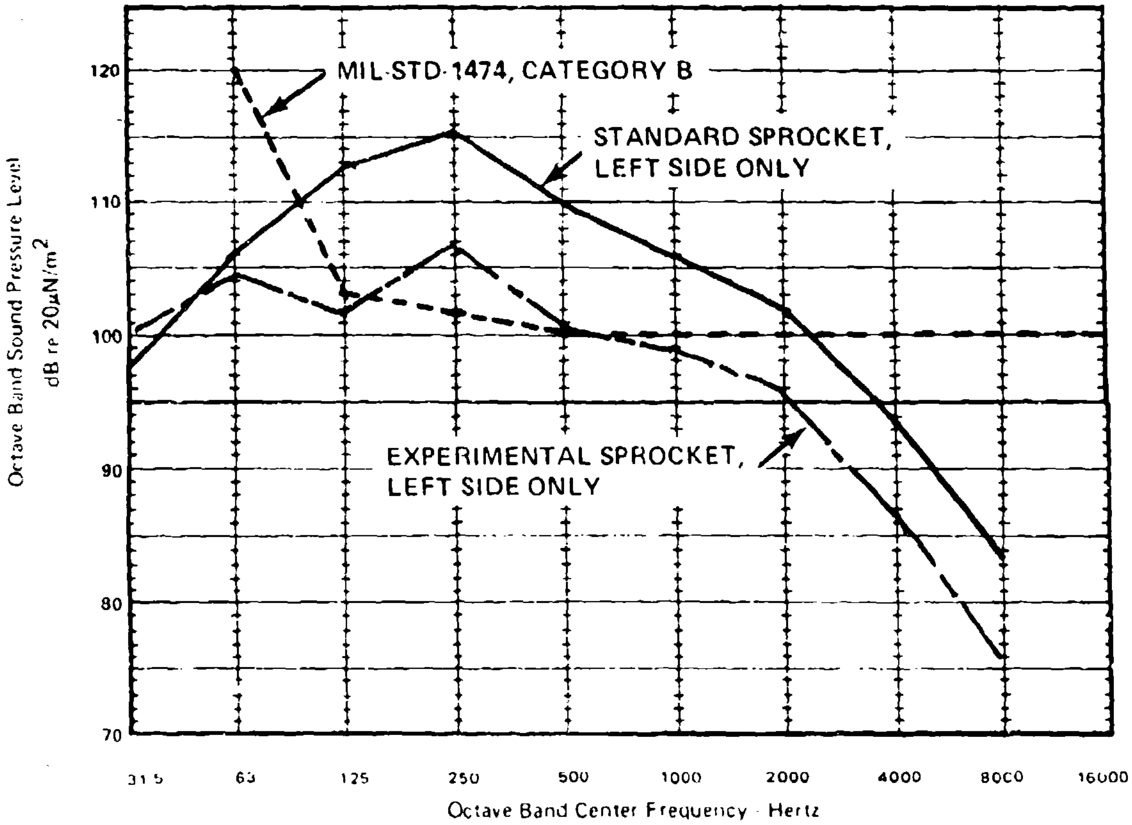

Figure 7.11 Crew Area Noise Spectra of Standard and Experimental Sprocket Wheels at 30 mph.

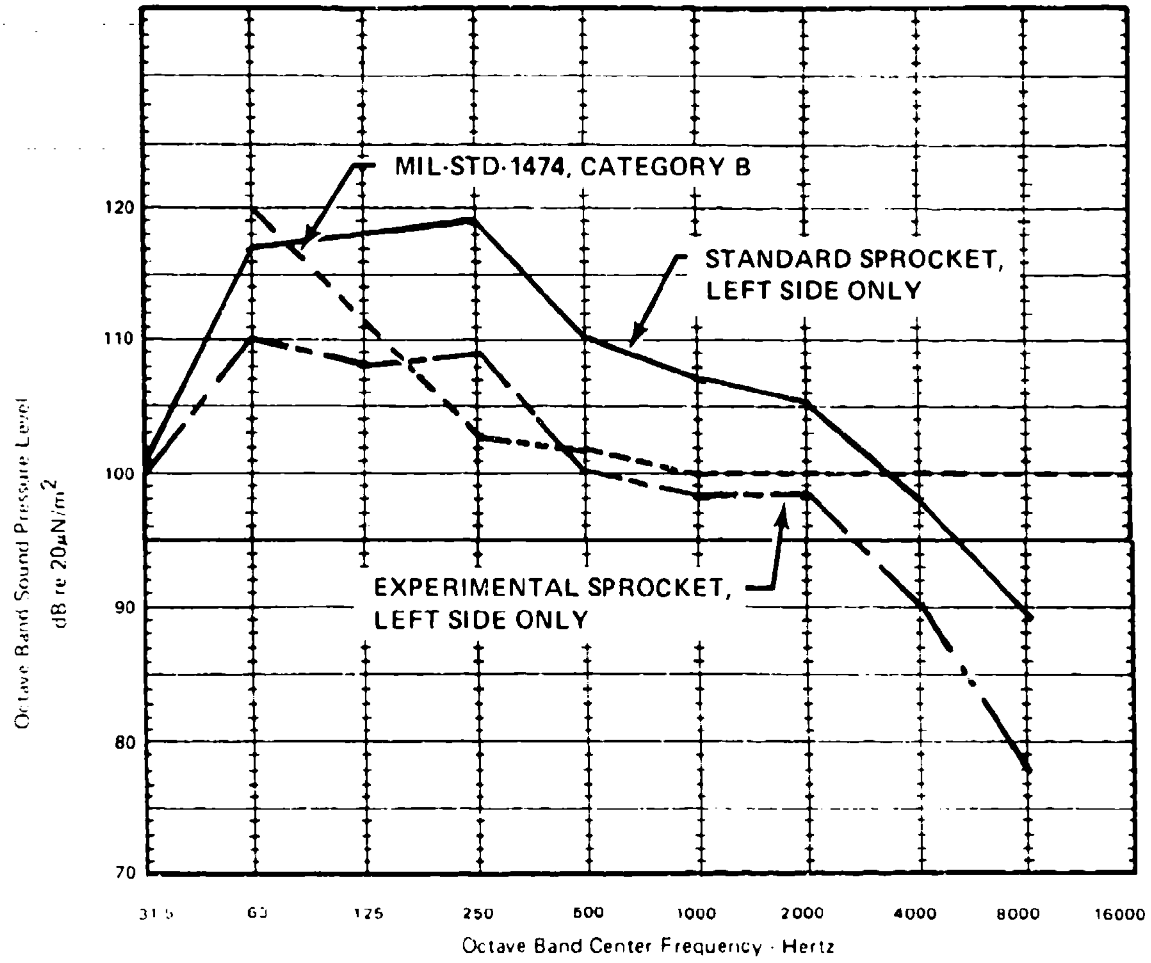

Figure 7.12 Driver's Compartment Noise Spectra of Standard and Experimental Sprokect Wheels at 30 mph.

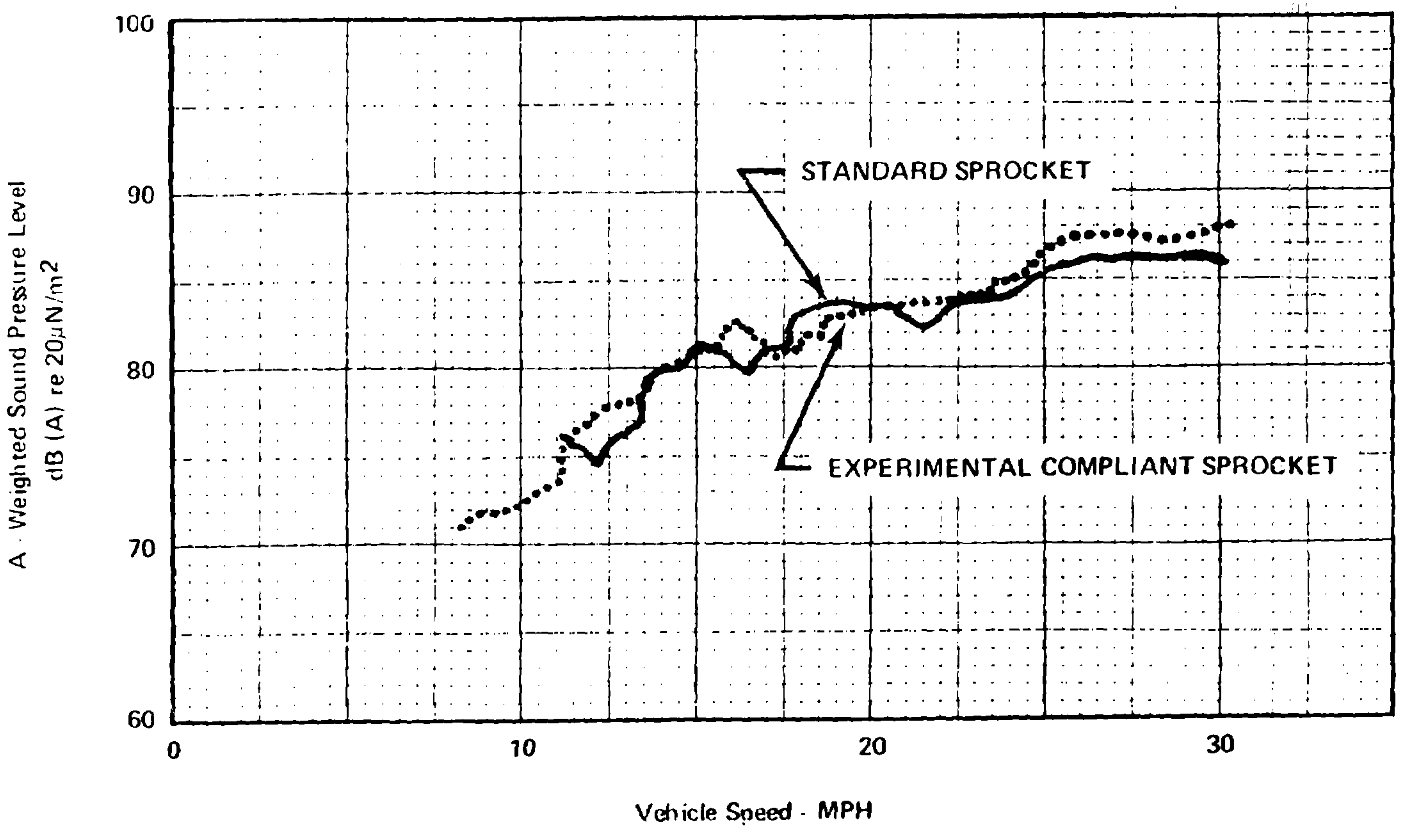

Figure 7.13 Exterior Noise Levels 25 Feet to the Right of the Vehicle Due to the Left Sprocket Only.

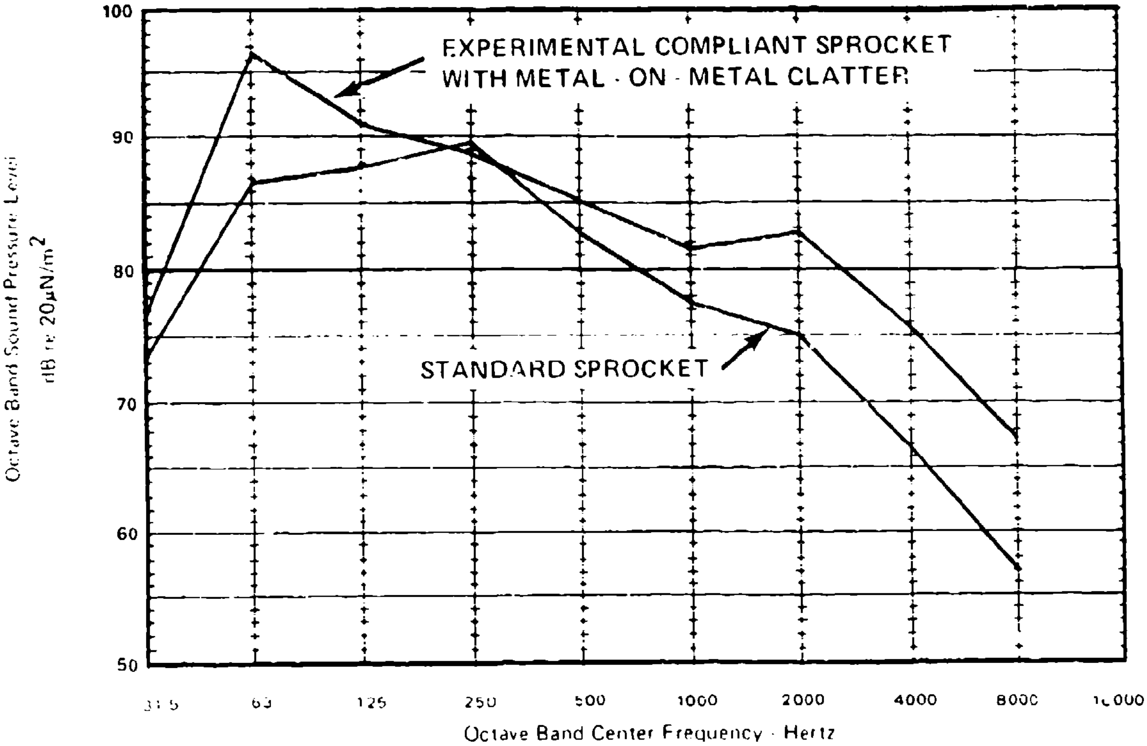

Figure 7.14 Exterior Noise Spectra at 30 mph due to the Left Sprocket Only. Measured 25 feet to the Right of the Hull.

indicates that both the side and driven edge of the sprocket teeth were in contact with the shoes. Wear on the inboard sides of both sprockets was evident. Some outboard sides were scraped whereas others were untouched. Finally, no significant torsional vibration was observed.

Dimensional measurements taken while the experimental sprocket was still mounted showed that assembled dimensions agreed closely with the standard sprocket. Also, misalignment with the track strand was only slight: 1/4 inch difference in offset from the hull between the test stand drive sprocket and the compliant sprocket under test. Systematic rotation of the experimental sprocket revealed that the teeth varied only .048 inch at the most in sideways offset. No significantly odd-shaped shoe or set of shoes was readily apparent on the track strand itself. Finally, disassembly of the experimental sprocket showed that no metal-to-metal contact was made at any point in the overload gear mechanism.

Analysis of the recorded data was conducted to evaluate the possibility of any consistent relationship between the clatter and a particular section of the track. Steady-state interior crew noise at 30-mph was plotted on time charts for both the experimental and standard sprockets. At 30-mph and with 57 track shoes per track strand, the following cycles are present:

0.114	seconds per sprocket revolution
0.65	seconds per track strand revolution
6.48	seconds per one sprocket tooth - one track shoe interaction

The noise-time charts showed a somewhat random cyclic noise level variation for the experimental sprocket. As previously discovered, this variation was not consistent throughout the noise spectrum. In some octave bands, cyclic sound pressure level variations corresponded to the one tooth - one shoe frequency (57 sprocket revolutions per ten track strand revolutions). This noise variation, however, accounted for only about thirty percent of the total variations apparent in a particular octave band time history. The association between the noise variation and track strand revolution was only observed during exterior listening tests.

In contrast to the experimental sprocket, high frequency time history plots for the standard sprocket revealed a definite cyclic variation of noise levels with each track strand revolution. Total variation of the magnitude of interior noise levels was about the same for the two types of sprocket wheels.

Since the analysis of recorded data was inconclusive, the experimental sprocket was reassembled and mounted on the test stand for more operational observation. Attention was focused on both the sprocket itself and the test stand system as a whole. A consistent sideways rolling motion of the test stand hull was discovered, which corresponded to twice the frequency of the track strand rotation. Both vertical and transverse nonsinusoidal wave motions of the track were observed to correspond to the track strand rotational frequency. The wave motions produce considerable axial and radial forces on the sprocket. Each track strand revolution included three waves, one of which produced a significantly stronger downward impulse. Thus, it appears that the test stand itself is producing strong impulses on the sprocket that are associated with the frequency of track strand revolution. Rocking of the test stand hull intensifies the axial forces on the sprocket teeth. Of course, the experimental sprocket is compliant in radial directions but relatively stiff in the axial direction, so side impacts are efficiently transmitted into the hull as interior noise.

Reasons for greater exterior clatter noise with the experimental sprocket, as opposed to the standard sprocket, are not fully understood. The increased compliance of the new sprocket may amplify the wave dynamics of the track strand and thereby cause greater clatter. The problem may also be due to the relatively low inertial mass of the experimental sprocket which might allow the sprocket to resonate.

Further testing will be performed on the experimental sprocket, including operation on paved track. The fact that two catenary track strands (upper and lower) are free to interact with no influence of the ground is not representative of actual vehicle operation. This and other test stand influences (vehicle rocking, etc.) must be eliminated for a meaningful evaluation of the experimental sprocket.

7.5.5 Durability

It was estimated that about 80 miles of free spinning test stand operation has been completed with the experimental sprocket. Most of this test service was at a track tension of 2500 lb, at 30 mph, and with some peculiar track dynamics occuring, as discussed in Section 7.5.4. No torque loads were included during these tests. No significant wear or damage was noted during this short service life except for that associated with the clatter problem. The sprocket tooth and track shoe wear patterns which occurred during the clatter may not continue after the peculiar track dynamics of the test stand are eliminated. Consequently, durability predictions for the compliant experimental sprocket are drawn from knowledge of the standard M113A1 sprocket performance record and from knowledge gained during the idler development program.

As with the prototype idler, the weakest part of the experimental sprocket is considered to be the rubber annuli. Results of the idler testing program can be extrapolated to predict that rubber annuli in this application will provide over 2,000 miles of service life if they are not subjected to severe damage caused by foreign objects. In the present design, hazard of damage from foreign objects is of concern at only two areas: (1) the exposed outer diameter of the exterior pair of annuli and (2) the partially exposed inner diameter of the inner pair of annuli, near the overload spline gear mechanism (Figure 7.7). All other surfaces of the rubber annuli are enclosed. The exposed outer diameters are expected to be self-purging. The second area, near the spline gear, will be exposed to small sized debris which may not be so readily purged. Future design studies should investigate this potential problem.

The next weakest link in the design is the rubber-to-steel bond. The experimental sprocket employed a cyanoacrylate adhesive, as did both the experimental and prototype idlers. No failures have occured with this sprocket and no points of possible failure initiation have been observed. However, vulcanizing is a preferable bonding method for production. Future design studies should investigate if the supports and rubber annuli could be vulcanized together in a separate subassembly. This would permit removal of the molds after vulcanization is complete, which is not possible with the present design.

The steel components of the experimental sprocket are expected to have a service life of well over 2000 miles of operation with the capability to withstand frequent overloading. Catastrophic failure of the rubber elements and continued failure mode operation could cause severe damage to the overload system. During normal compliant operation, only the sprocket teeth will be exposed to any significant wear. This component is made from the standard M113A1 sprocket which is a proven durable item. During overload operation, only limited wear will be experienced by the spline gear, even considering the sliding tooth action which results. This is because overload operation only transmits that component of an excessive torque or radial load to the spline gears which is not first taken up in the compliant elements. The long durability expectations for this sprocket under these conditions is further substantiated by the fact that the compliant sprocket wheel subassemblies are symmetrical and may be reversed to wear both faces of the sprocket and gear teeth equally. During failure mode operation, when the rubber rings fail completely, severely violent action will occur. A sliding, impacting load action will be experienced by not only the overload spline teeth but also by the sprocket teeth themselves. Single tooth loading will place high loads on the spline teeth which are designed with a factor of safety of only about two in this experimental configuration. Damage to the overload mechanism may render this system irrepairable, depending upon the duration and severity of failure mode operation.

Durability of the central area which provides clearance for the track guides is expected to be very good. Because the sprocket teeth maintain a lateral alignment of the track shoes, no contact between the track guide and sprocket will occur at this point. Foreign objects have less of a tendency to be drawn up into the sprocket than into the idler. Ingestion of foreign objects into the sprocket could normally only occur during reverse operation which is infrequent and slow, also the track guides would dislodge an object when forward operation is resumed. No cutouts are provided for debris in this area, because there are no structures in which foreign matter may become entangled.

7.6 Recommendations

The experimental sprocket design is considered capable of fulfilling all performance criteria, however, it is complex and does not fully meet the noise reduction goals. The complexity seems unavoidable with the present severely-restrictive size envelope. The limited noise reduction may be a problem of test conditions, and not necessarily the design itself. Consequently, recommendations for improvement include some additional testing with improved equipment.

There are two recommendations for improving the basic design of the experimental sprocket: (1) simplify and (2) toughen. A simpler design is needed to reduce initial cost, as well as improve reliability. The experimental design employs mild steel material designed, in some areas, with factors of safety of two. Future hardware may require harder or stronger designs. The overload spline gear mechanism, for example, is designed of mild steel using a factor of safety of about two. This is acceptable for experimentation but not for reliable failure mode operation. Other areas were similarily designed for expedient completion and with the knowledge that experimental operations would not be as severe as actual field use.

Before further testing is conducted, consideration should be given to the test stand. The significance of track strand misalignment, test hull instability, and track strand dynamics must be understood before more measurements are made.

Further, the experimental sprocket must be tested underway to determine the effects of the compliance on various vehicle manuevers, including high speed turns, pivot steering, hill climbing, etc. Sprocket tooth disengagement and/or track throwing are potential problems. Also, the dynamic effects on the upper track strand resulting from both a compliant idler and sprocket need to be investigated.

REFERENCES

1. Anatrol Corporation: "Interior Noise Control of the M113A1 Armored Personnel Carrier by Hull Damping." Anatrol Project No. 78067, Cincinnati, OH. Prepared for FMC Corporation, San Jose, CA., November 1979.

2. Bates, C.L., & Sparks, C.R.: "Development of Measurement Techniques for the Analysis of Tracked Vehicle Vibration and Noise." SWRI Project No. 04-1421, Contract DA 23-072-AMC-144(1), Southwest Research Institute, October 1964.

3. Beranek, L.L. (Ed): Noise and Vibration Control. Chapter 11, New York: McGraw-Hill Book Co., 1971.

4. Brown, R.: "Load-Deflection Tests of the Idler Paddles for the Experimental Compliant Idler Wheel." Test Report Lab No. 792282, FMC Corporation Central Engineering Laboratories, Santa Clara, CA, 09 April 1979.

5. Cybernet Services: "MRI/STARDYNE - Theoretical Manual", 1973, 1974.

6. Cybernet Services: "STARDYNE - Finite Element Demonstration Problems", 1973.

7. Department of Defense: "Military Standard Noise Limits for Army Materiel." MIL-STD-1474B(MI), Washington, DC 20301. (Obtain from the Naval Publications and Forms Center, 5801 Tabor Avenue, Philadelphia, PA 19120.)

8. Goodyear Tire & Rubber Company: Handbook of Molded and Extruded Rubber. (3rd ed.). Akron, Ohio 44316.

9. Hammond, S.: "M113A1 Idler Heat Rejection." Technical Report 3171, FMC Corporation, San Jose, CA, July 1977.

10. Hammond, S.: "Suspension Component Development for Reduced Noise," IR&D Data Sheet for Fiscal Year 1979, FMC Corporation, San Jose, CA.

11. Holland, H.H., Jr.: "Noise Levels in the Passenger Areas of a Standard and a Product Improved M113A1 Armored Personnel Carrier." Letter Report No. 124, U.S. Army Human Engineering Laboratory, Aberdeen Proving Ground, MD, October 1970.

12. Kasprik, J.E.: "AIFV Final Drive U-Joint Torque Test." Test Report 3579, FMC Corporation, San Jose, CA, 13 May 1980.

13. Kasprik, J.E.: "AIFV Initiation of Track Disengagement with Standard and Modified Idler Wheels." Technical Report 2982, FMC Corporation, San Jose, CA, 13 May 1980.

14. Kasprik, J.E.: "9600 Kilometer (6000 Mile) Durability and Performance of Hydrostatic Steer Differential System for M113 Family of Vehicles." Test Report 3465, FMC Corporation, San Jose, CA, March 1980.

15. Morse, R.M. and Ingard, V. Theoretical Acoustics, McGraw Hill Book Company (1967).

16. Norris, T.R., Hare, R.B., Galaitsis, A.G., & Garinther, G.R.: "Development of Advanced Concepts for Noise Reduction in Tracked Vehicles." Technical Memorandum 25-77, US Army Human Engineering Laboratory, Aberdeen Proving Ground, MD, August 1977.

17. Norris, T.R., Rentz, P.E., Galaitsis, A.G., Hare, R.B., Hammond, S.A., Garinther, G.R.: "Experimental Idler Design and Development of Hull Concepts for Noise Reduction in Tracked Vehicles." Technical Memorandum 8-79, U.S. Army Human Engineering Laboratory, Aberdeen Proving Ground, MD, June 1979.

18. Van Wyk, T.B.: Study of Track-Idler Engagement and Its Effect on Interior Noise. Technical Report 2976, FMC Corporation, San Jose, CA, April 1976.

19. Young, W.J.: "Rubber Tired Sprocket Hub (International Harvester Company Design) Effect on T141 Vehicle Vibration". Report 1201, Test and Development Department TE-20, Cadillac Motor Car Division, General Motors Corporation, Cleveland Tank Plant, March 11, 1954.

APPENDIX A

THEORY FOR HULL VIBRATIONAL RESPONSE AND INTERIOR SOUND LEVELS

The generalized theory for the prediction of the vibrational response of an arbitrarily-shaped structure bounding an enclosed cavity, and for the development of an acoustic field within the cavity, has been developed in various forms [A1,A2]. One such approach, termed the "power flow approach", has been developed by BBN [A3] and is summarized below in a form suitable to the present problem.

Figure A.1 shows the general situation of a distribution of excitation forces and radiated pressure fields which act on the structure as it vibrates. The structure is represented by its set of independent normal modes (uncoupled and orthogonal), so that the total displacement of the structure $w(\bar{x},\omega)$ at a point $\bar{x} = (x,y)$ on it is given by

$$w(\bar{x},\omega) = \sum_{r}^{\alpha} \bar{\xi}_r \psi_r(\bar{x}) \qquad (A.1)$$

where $\bar{\xi}_r = \bar{\xi}_r(\omega)$ is the displacement of the rth normal mode. The wall response to the forces and pressure fields acting is found as [A3]

$$w(\bar{x},\omega) = \int_{\bar{x}} G(\bar{x}/\bar{x}';\omega) \left[p^{\circ}(\bar{x}') - p_i(\bar{x}') \right] d\bar{x}' \qquad (A.2)$$

where the integration is over the structural surface area and the structure's Greens function is given by

$$G(\bar{x},\bar{x}';\omega) = \sum_{s} \frac{\psi_s(\bar{x})\psi_s(\bar{x}')}{M_s Y_s}$$

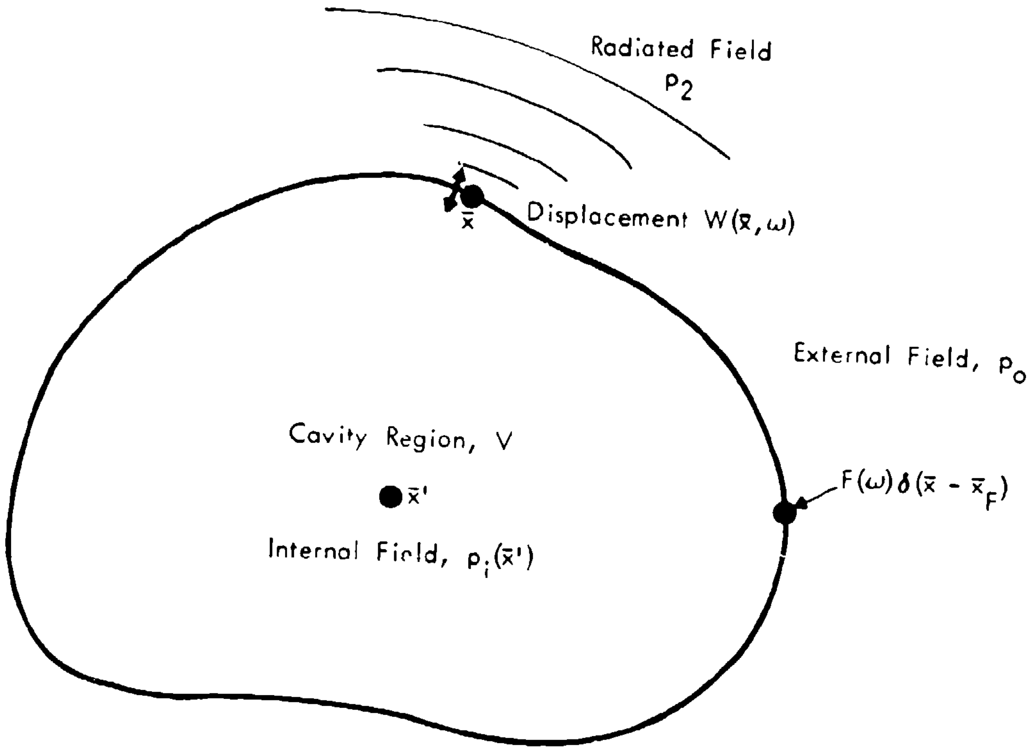
Radiated Field
p_2
$\bar{x}$
Displacement $W(\bar{x},\omega)$
External Field, p_o
Cavity Region, V
$\bar{x}'$
$F(\omega)\delta(\bar{x} - \bar{x}_F)$
Internal Field, $p_i(\bar{x}')$

Figure A.1 Cavity Nomenclature.

Here ψ_s, M_s and Y_s are the mode shape, generalized mass and admittance function for the sth structural mode.

$$Y_s = \omega_s^2 \left[1 - \left(\omega/\omega_s \right)^2 - i\eta_s \right]$$

The interior acoustic pressure field $p_i(\bar{x}')$ due to structural vibration is given by

$$\begin{aligned} p_i(\bar{x}') &= -\rho\omega^2 \int_{\bar{x}} G_p(\bar{x}/\bar{x}';\omega)\, w(\bar{x})\, d\bar{x} \\ &= -\rho\omega^2 \int_{\bar{x}} G_p(\bar{x},\bar{x}';\omega) \sum_s \psi_s(\bar{x})\xi_s\, d\bar{x} \end{aligned} \qquad (A.3)$$

where ρ is the density of the acoustic medium, and $G_p(\bar{x}/\bar{x}';\omega)$ is the cavity Green's function, defined by

$$G_p(\bar{x}/\bar{x}';\omega) = \sum_n \frac{\phi_n(\bar{x})\phi_n(\bar{x}')}{\iiint \phi_n^2(\bar{x})\, d\bar{x}\, (\bar{\lambda}_n^2 - k^2)}$$

Here $\phi_n(\bar{x})$ and $\bar{\lambda}_n$ are the cavity mode shape and eigenvalues while k is the acoustic wavenumber. The exterior force distribution consists of a point force of amplitude $F(\omega)$ at frequency ω located at $\bar{x} = \bar{x}_p$ and the radiated pressure field $p_o(\bar{x}')$, and is given by

$$p^o(\bar{x}') = F(\omega)\delta(\bar{x}'-\bar{x}_p) + p_o(\bar{x}') \qquad (A.4)$$

From Eq. (A.1), the modal response is found as

$$\sum_s \xi_s\psi_s(\bar{x}) = \int G(\bar{x},\bar{x}';\omega) \left[F(\omega)\delta(\bar{x}'-\bar{x}_p) + p_o(\bar{x}') - p_i(\bar{x}') \right] d\bar{x}'$$

Best Available Copy

Multiplying through by $m(\bar{x})\psi_r(\bar{x})$ and integrating over the structural area, leaves

$$M_r\xi_r = \int m(\bar{x})\psi_r(\bar{x}) \int G(\bar{x},\bar{x}';\omega)\Big[F(\omega)\delta(\bar{x}'-\bar{x}_F) + p_2(\bar{x}') - p_1(\bar{x}')\Big]\, d\bar{x}'d\bar{x} \qquad (A.5)$$

Multiplying Eqs. (A.3) and (A.4) by $\psi_r(\bar{x}')$ and integrating with respect to $\bar{x}'$ leads to an expression for the generalized force Γ^r on the rth mode due to, respectively, the interior acoustic field $\Gamma^r_{p_1}$, the point force Γ^r_F, and the radiated pressure field $\Gamma^r_{p_2}$; for example,

$$\Gamma^r_{p_1} = \int p_1(\bar{x}')\ \psi_r(\bar{x}')\ d\bar{x}'$$

$$= \sum_s \left[-\rho\omega^2 \int \psi_r(\bar{x}') \int G_p(\bar{x}/\bar{x}';\omega)\psi_s(\bar{x})d\bar{x}d\bar{x}' \right] \xi_s \qquad (A.6a)$$

or $$\Gamma^r_{p_1} = -\rho\omega^2 \sum_s I^{rs}\xi_s$$

where $$I_{rs} = \iint G_p(\bar{x},\bar{x}';\omega)\psi_r(\bar{x}')\psi_s(\bar{x}')d\bar{x}d\bar{x}' \qquad (A.6b)$$

is interior structural-acoustic coupling parameter

Similarly, $$\Gamma^r_F = F(\omega)\psi_r(\bar{x}_F) \qquad (A.7)$$

and $$\Gamma^r_{p_2} = \rho\omega^2 \sum_s J_{rs}$$

where $$J_{rs} = \iint G^o_p\ (\bar{x}/\bar{x}';\omega)\ \psi_r(\bar{x}')\psi_s(\bar{x})\ d\bar{x}d\bar{x}'$$

Best Available Copy

and $G_p^o(\bar{x}/\bar{x}';\omega)$ is the Green's function for the radiated pressure field. $\Gamma^r_{p_2}$ will be neglected from further analysis since its contribution is negligible in the present point force situation. Then, with $\Gamma^r = \Gamma^r_F + \Gamma^r_{p_1}$ and, on substitution of Eqs. (A.6) and (A.7) into Eq. (A.5), the modal response equation becomes

$$\left[-Y_r M_r + \rho\omega^2 I_{rr}\right]\xi_r + \rho\omega^2 \sum_{s\neq r} I_{rs}\xi_s = -\Gamma^r$$

or in matrix form,

$$\left[a_{rs}\right]\left\{\xi_s\right\} = \left\{-\Gamma^r\right\}$$

The solution is

$$\left\{\xi_r\right\} = \left[a_{rs}\right]^{-1}\left\{-\Gamma^s\right\} = \left[\bar{\alpha}_{rt}\right]\left\{-\Gamma^t\right\} \tag{A.8}$$

where

$$\left[\bar{\alpha}_{rt}\right] = \left\{-Y_r M_r + \rho\omega^2 \sum_s I_{rs}\right\}^{-1} \tag{A.9}$$

Then, the total structural displacement $W(\bar{x};\omega)$ is found from Eq. (A.1) as

$$\begin{aligned} W(\bar{x};\omega) &= -\sum_{r,t} \psi_r(\bar{x})\,\bar{\alpha}_{rt}\Gamma^t(\omega) \\ &= -\sum_r \psi_r(\bar{x})\bar{\alpha}_{rr}(\omega)\Gamma^r(\omega) \end{aligned} \tag{A.10}$$

on neglecting intermodal coupling terms which are generally small. Further, the acoustic effects will be negligible for the present structure in the sense that the acoustic reactance is much smaller than the structural reactance. Hence

$$\bar{\alpha}_{rr}(\omega) \simeq \left\{-Y_r M_r\right\}^{-1}$$

and η_r is the sum of the structural and external radiation loss factors, and the structural response becomes

$$w(\bar{x},\omega) = F(\omega) \sum_r \frac{\psi_r(\bar{x})\psi_r(\bar{x}_F)}{M_r Y_r} \tag{A.11a}$$

$$= |H(j\omega)| e^{-j\phi} \tag{A.11b}$$

which is a complex function.

The time average, mean square displacement at frequency ω

$$\overline{w^2(\bar{x},\omega)} = \tfrac{1}{2}\mathrm{Re}\left[w.w^*\right]$$

$$= \frac{F^2(\omega)}{2} \left\{ \sum_r \frac{\psi_r^2(\bar{x})\psi_r^2(\bar{x}_F)}{|Y_r|^2 M_r^2} + \mathrm{Re} \sum_r \sum_{\substack{s \\ r \neq s}} \frac{\psi_r(\bar{x})\psi_s(\bar{x})\psi_r(\bar{x}_F)\psi_s(\bar{x}_F)}{Y_r Y_s^* M_r M_s} \right\}$$

Thus the structural response depends on the spectrum of the excitation force, the mode shapes at both the point of application of the force and the observation point, and on the modal masses and admittance function. The output from the finite element program STARDYNE used in this study is in the form of Eq. (A.11b) i.e. providing results in terms of magnitude and phase. Point-to-point comparison of measured results with prediction tend to be inaccurate; better agreement is found by making space-averaged comparisons, where the average is performed over at least five representative positions on the structural element of interest.

As frequency increases above the fundamental structural (whole-body) modes, the number of modes accumulates rapidly with frequency. Certain structural elements may tend to respond more strongly (independently) than connected elements, and may tend to contribute most to the structural modal mass and hence kinetic energy at that resonance frequency. For example, as shown in other sections of this report, the M113 hull roof vibrates independently at about 65 Hz, contributing about 75% of the total modal mass for this mode. Further, in the one-third octave band centered on 160 Hz, F-E modeling predicts that the roof and floor respond more strongly than other hull elements, there being about 7 modes in this frequency band. An estimate for the space-averaged, mean-square displacement to a band-limited force excitation of mean-square force in $\Delta\omega$ of F_{Δ}^{2} for each of the major structural elements is of considerable interest and use in the evaluation of the effects of structural modifications on hull vibration response and the associated interior acoustic radiation.

The space-average, mean-square displacement, for an element A of the structure, averaged over a narrow frequency band containing several resonant modes $(r\varepsilon\Delta\omega)$, $\overline{w_{\Delta,A}^{2}}$, is found as

$$\overline{w_{\Delta,A}^{2}} = F_{\Delta}^{2} \sum_{r\varepsilon\Delta\omega} \frac{\left[\frac{1}{A}\int_{A} \psi_{r}^{2}(\bar{x})\,d\bar{x}\right] \psi_{r}^{2}(\bar{x}_{F})}{M_{r}^{2}} \bullet \frac{1}{\Delta\omega} \int_{\Delta\omega} |Y_{r}|^{-2}\,d\omega$$

$$= \frac{\pi}{2\omega^{3}} \bullet \frac{F_{\Delta}^{2}}{\Delta\omega} \sum_{r\varepsilon\Delta\omega} \frac{\left[\frac{1}{A}\int_{A} \psi_{r}^{2}(\bar{x})\,d\bar{x}\right] \psi_{r}^{2}(\bar{x}_{F})}{M_{r}^{2}\eta_{r}} \qquad (A.12)$$

Here the modal cross-coupling terms $(r \neq s)$ do not contribute to the response and the response is dominated by the resonant modal contributions. Further $\overline{w_{\Delta,A}^{2}}$ and F_{Δ}^{2} have units of $(\text{displacement})^{2}$ and $(\text{force})^{2}$ respectively.

STARDYNE calculates values of $\psi_r(\bar{x})$ at model nodes, so that on manipulation of the output files, the quantity in square braces [], which represents the degree of restraint provided by the remainder of the structure, can be calculated for each major structural element e.g. floor, roof, upper side plate, sponson. In detail, the calculation is found from

$$\frac{1}{A}\int_A \psi_r^2\,(\bar{x})d\bar{x} = \frac{1}{A}\sum_i \sum_{j\varepsilon A} \psi_r^2(i,j)\,A(j)$$

$$\simeq \frac{1}{A}\sum_{j\varepsilon A} \psi_r^2(3,j)\,A(j) \qquad (A.13)$$

where A(j) is the area associated with the j^{th} mode and where i and j represent the nodal coordinate directions and node number respectively, but only the coordinate normal to the surface (3) is important.

The contribution of structural elements to the total modal mass can be calculated as

$$M_{r,A} = \int_A m(\bar{x})\psi_r^2(\bar{x})d\bar{x} = \sum_i \sum_{j\varepsilon A} m(i,j)\psi_r^2(i,j)$$

$$\simeq \sum_{j\varepsilon A} m(3,j)\psi_r^2(3,j) \qquad (A.14)$$

where normal displacements are most important. Here M(i, j) is the modal mass of the j^{th} mode referred to the i^{th} coordinate direction.

At higher frequencies the element mode shapes will be essentially sinusoidal, and Eq. (A.14) reduces, using band-averaged concepts, to

$$\overline{w^2_{A,A}} = \frac{2\pi}{\omega} \bullet F_A^2 \bullet \frac{n_{r,A}(\omega)}{A^2 m_A^2} \bullet \frac{\overline{\psi_r^2\,(\bar{x}_F)}}{\bar{n}_r} \qquad (A.15)$$

where F_A^2 is the time-average, mean-square force input at $\bar{x}_F$ in band $\Delta\omega$. $n_{r,A}(\omega)$ is the modal density of the structural element of area A and surface density m_A, and where $\overline{\psi_r^2}(\bar{x}_F)$ and $\bar{\eta}_r$ are average values of $\psi_r^2(x_F)$ and $\bar{\eta}_r$ (assuming equal loss factors for each element). The relative energy levels between different structural elements is determined at high frequency by the element modal density, mass and area, while the coupling of the force to the structure is described by $\overline{\psi_r^2}(\bar{x}_F)$.

A reduction in response level will be produced as the force input, the modal density, and the modal displacement at the point of application of the force, are reduced.

Acoustic Power Radiated to Interior Acoustic Field

The time-averaged acoustic power being radiated due to the motion of the rth structural mode is given in terms of the modal radiation resistance by [A2].

$$W^r_{rad}(\omega) = R^r_{rad}(\omega_r)<v_r^2> \tag{A.16}$$

where $<v_r^2> = \omega^2<w_r^2>$, is the space-time average, mean-square velocity of the rth mode. If there are N modes in a frequency band of width $\Delta\omega$, the total time average power radiated is found by summing each modal contribution (assuming modes independent) i.e.

$$W_{rad}|_\Delta = \sum_{r\varepsilon\Delta\omega}^{N} R^r_{rad}(\omega)<v_r^2> \tag{A.17}$$

Assuming that equipartition of energy between the r modes applies, this reduces to

$$W_{\Delta} = v_{\Delta}^{2} \; \frac{1}{N} \sum_{r \varepsilon \Lambda\omega}^{N} R_{rad}^{r}\,(\omega)$$

$$= v_{\Delta}^{2} \bullet \overline{R_{rad}} \qquad (A.18)$$

where v_{Λ}^2 is the space-average, mean-square velocity of the radiating surface and $\overline{R}_{rad}$ is the band-averaged radiation resistance. Eq. (A.12) may be used to calculate v_{Λ}^2, and $\overline{R_{rad}}$ can be calculated using the methods of statistical energy analysis [A4]. Then, for an element A of structure, the band-limited radiated acoustic power (in watts) is found as

$$W_{\Lambda,A} = \omega^2 \overline{w^2}_{\Lambda,A} \bullet \overline{R_{rad,A}}$$

$$= \frac{\pi}{2} \frac{F_{\Lambda}^2}{\omega\Lambda\omega} \bullet \sum_{r\varepsilon\Lambda\omega} \frac{\left[\frac{1}{A}\int_{A} \psi_r^2(\bar{x})\,d\bar{x}\right] \psi_r^2(\bar{x}_F)}{M_r^2 \eta_r} \bullet \overline{R_{rad,A}} \qquad (A.19)$$

As before, using modal density relations and band-averaged expressions,

$$W_{\Lambda,A} = \frac{2\pi F_{\Lambda}^2}{\omega} \bullet \frac{n_{r,A}(\omega)}{m_A^2 A^2} \bullet \frac{\overline{\psi_r^2}(\bar{x}_F)}{\bar{\eta}_r} \bullet \overline{R_{rad,A}} \qquad (A.20)$$

It is clear that the power inflow depends on the magnitude of the force input, the radiation efficiency ($\sigma = R_{rad}/A\rho c$), modal density, loss factor and mass of the driven structure, as well as on the mode shapes at the point of application of the force Noise reductions will correspond to reductions in W_{Δ}, and can be related to changes in those quantities shown in Eqs. (A.19) and (A.20) on which W_{Λ} depends. For example, if $\psi_r^2(\bar{x}_F)$ can be reduced by a factor of 10, a 10dB noise reduction will be produced, all other parameters remaining fixed.

At those frequencies where several acoustic modes occur in the analysis band, the band-averaged radiation resistance will provide a good estimate for the structural-acoustic coupling.

Eqs. (A.15) for the band-averaged mean-square displacement $w^2_{\Delta\omega}(\omega)$ and (A.20) for the band-averaged acoustic power flow $W_{\Delta\omega}(\omega)$ incorporate statistical descriptors for the structure, as employed in Statistical Energy Analysis, but also includes a parameter $\bar{\Psi}^2_r(\bar{x}_p)$ which describes the coupling between the point force and the structural modal response. Values for $\bar{\Psi}^2_r(\bar{x}_p)$ are calculated from the finite element model for the hull structure in the present problem, (but may be compared to the coupling loss factor η_{12} used in Statistical Energy Analysis). Thus the detailed results from the hull modal analysis can be matched directly with statistical descriptors for the structure in calculation of the potential for vibration and noise reduction associated with various structural modifications.

REFERENCES

A1. Richards, E.J. and Mead, D.J. (Editors): "Noise and Acoustic Fatigue in Aeronautics" John Wiley & Son, Ltd. (London) 1968.

A2. Cremer, L., Heckl, M. and Ungar, E.E.: "Structure-borne Sound" Springer-Verlap (New York) 1973.

A3. Pope, L.D. and Wilby, J.F.: "Band-Limited Power Flow in Enclosures" *J. Acoustical Soc. Am.*, Vol. 67, March 1980, pp. 823-826.

A4. Lyon, R.H.: "Statistical Energy Analysis of Vibrating Systems." The MIT Press (Cambridge, Massachusetts) 1975.

APPENDIX B

STARDYNE Input and Output Data

Table B.1	STAR	Input Data
Table B.2	STAR	Output Data
Table B.3	DYNRE2	Input Data
Table B.4	DYNRE2	Output Data

Table B.1 STAR Input Data

```
             SSSSSSSS   SSSSSSSSSS   SSSSSSSS   SSSSSSSSS
            SSSSSSSSSS  SSSSSSSSSS  SSSSSSSSSS  SSSSSSSSSS
            SS       S      SS      SS      SS  SS      SS
  S    S    SS              SS      SS      SS  SS      SS       S    S
   S  S     SSSSSSSSS       SS      SS      SS  SSSSSSSSSS        S  S
SSSSSSSSSS   SSSSSSSSS      SS      SSSSSSSSSS  SSSSSSSSS       SSSSSSSSSS
   S  S             SS      SS      SSSSSSSSSS  SS   SS           S  S
  S    S    S       SS      SS      SS      SS  SS    SS         S    S
            SSSSSSSSSS      SS      SS      SS  SS     SS
             SSSSSSSS       SS      SS      SS  SS      SS
      **********************************************************
      *                  **  STAR       (R) **                  *
      *                  ** STARDYNE-3  (R) **                  *
      *                  ** MAR1080   LEVEL**                   *
      **********************************************************
      *   LATEST USER MANUAL  SEPT 1979                         *
      *                                                         *
      *                                                         *
      *   RUN DATE      MONDAY    .  JUN. 16, 1980              *
      *                 80/06/16.  DAY 168 OF 1980              *
      *   RUN TIME      13.17.34.                               *
      *                                                         *
      *    CYBERNET                     NOS 1      +48C         *
      *                                                         *
      *   (R) 1969 STARDYNE   SYSTEM  BY MECHANICS RESEARCH INC *
      *   (R) 1971 STARDYNE-2 SYSTEM  BY MECHANICS RESEARCH INC *
      *   (R) 1974 STARDYNE-3 SYSTEM  BY MECHANICS RESEARCH INC *
      *   (R) 1977 STARDYNE-3 SYSTEM  BY SYSTEM DEVELOPMENT CORP*
      **********************************************************


      **********************************************************
      *          S T A R D Y N E   B U L L E T I N S            *
      *                                                         *
      *     A STARDYNE INFORMATION BULLETIN IS AVAILABLE        *
      *   WHICH DESCRIBES IMPORTANT CHANGES CONCERNING THIS     *
      *   RELEASE LEVEL OF THE PROGRAM.  IN ORDER TO ACCESS     *
      *   THIS BULLETIN - ENTER THE FOLLOWING CONTROL CARDS..   *
      *    AT SCOPE 3.4                 AT NOS 1                *
      *                                                         *
      *    .                             .                      *
      *   APPLIC(STARBUL)              ATTACH(STARBUL/UN=LIBRARY)*
      *   REWIND(STARBUL)              REWIND(STARBUL)          *
      *   COPYSBF(STARBUL,A)           COPYSBF(STARBUL,A)       *
      *   REWIND(A)                    REWIND(A)                *
      *   COPYSBF(A,OUTPUT)            COPYSBF(A,OUTPUT)        *
      *    .                            .                       *
      **********************************************************
```

Table B.1 (cont.)

```
                                   *** STARDYNE 3.0      INPUT ***
          /------------------------------ CARD  IMAGE --------------------------------/
          1  4   8  12  16  20  24  28  32  36  40  44  48  52  56  60  64  68  72  76  80
          .  .   .   .   .   .   .   .   .   .   .   .   .   .   .   .   .   .   .   .   .
CARD NO   ****************************************************************************      CARD TYPE
      2   ELCTS       1  1 111011LNT      72                                                  ELCTS
      3    M113A1 HULL DYNAMIC MODEL - FMC CORPORATION                                        M113
      4   MATLG       1 ALUMINUM  10.2  E06      .33        .096   13.2 E-06                  MATLG
      5   MATLG       2WEIGHTLESS 10.2  E06      .33        .001   13.2 E-06                  MATLG
      6   END                                                                                 END
      7   NODEG     100 102   1 157.49    0.0      0.0    157.49   33.2      0.0              NODEG
      8   NODE 107          171.8            0.0              20.5                            NODE
      9   NODE 103          171.8           49.0              20.5                            NODE
     10   NODEG     104 106   1 171.8    33.2     20.5    171.8    12.5     20.5              NODEG
     11   NODEG     205 208   1 160.7    49.0     32.0    160.7    12.5     32.0              NODEG
     12   NODEG     306 309   1 148.8    49.0     43.5    148.8    12.5     43.5              NODEG
     13   NODEG     357 360   1 137.3    49.0     55.0    137.3    12.5     55.0              NODEG
     14   NODEGRP1 200 300 100 154.55    0.0      0.0    137.3     0.0      0.0              NODEG
     15   NODEGRP2 202 302   1 154.55   33.2      0.0    137.3    33.2      0.0              NODEG
     16   NODEGRP1 3001100 100 137.3     0.0      0.0      9.74    0.0      0.0              NODEG
     17   NODEGRP2 3021102   1 137.3    33.2      0.0      9.74   33.2      0.0              NODEG
     18   NODEG    12001202  1   0.0     0.0      0.0      0.0    33.2      0.0              NODEG
     19   NODEG     203 204   1 154.55   33.2     20.5    154.55   49.0     20.5              NODEG
     20   NODEG     303 304   1 137.3    33.2     20.5    137.3    49.0     20.5              NODEG
     21   NODEGRP1 3031103 100 137.3    33.2     20.5      9.74   33.2     20.5              NODEG
     22   NODEGRP2 3041104   1 137.3    49.0     20.5      9.74   49.0     20.5              NODEG
     23   NODEG    12031204  1  -2.31   33.2     20.5     -2.31   49.0     20.5              NODEG
     24   NODEG     310 412 102 137.3   12.5      0.0    121.36   12.5      0.0              NODEG
     25   NODE 305          143.55          49.0              32.0                            NODE
     26   NODEG     355 356   1 137.3    49.0     32.0    137.3    49.0     43.5              NODEG
     27   NODEGRP1 4051105 100 121.36   49.0     32.0      9.74   49.0     32.0              NODEG
     28   NODEGRP2 4061106   1 121.36   49.0     43.5      9.74   49.0     43.5              NODEG
     29   NODEG    12061207  1  -2.31   49.0     20.5     -6.20   49.0     55.0              NODEG
     30   NODEGRP1 4071207 100 121.36   49.0     55.0     -6.20   49.0     55.0              NODEG
     31   NODEGRP2 4101210   1 121.36   12.5     55.0     -6.20   12.5     55.0              NODEG
     32   NODEG    4111211 100 121.36    0.0     55.0     -6.20    0.0     55.0              NODEG
     33   NODEG    12121213  1  -7.61   34.41    32.0     -4.90   35.62    43.5              NODEG
     34   NODE1250             0.0           42.2              0.0                            NODE1
     35   NODE1251             1.0           42.2              0.0                            NODE1
     36   NODE1253             0.0           42.2              1.0                            NODE1
     37   END                                                                                 END
     38   RESTG      1001200 100101010                                                        RESTG
     39   RESTG      107        101010                                                        RESTG
     40   RESTG      4111211 100101010                                                        RESTG
     41   END                                                                                 END
     42   WGHT     1200    122.      122.      122.                                           WGHT
     43   WGHT     1201    243.      243.      243.                                           WGHT
     44   WGHT      903     82.       82.       82.                                           WGHT
     45   WGHT      904     82.       82.       82.                                           WGHT
     46   WGHT     1003     82.       82.       82.                                           WGHT
     47   WGHT     1004     82.       82.       82.                                           WGHT
     48   WGHT     1103     82.       82.       82.                                           WGHT
     49   WGHT     1104     82.       82.       82.                                           WGHT
     50   WGHT      811     11.2      11.2      11.2                                          WGHT
     51   WGHT      909     22.3      22.3      22.3                                          WGHT
     52   WGHT     1009     22.3      22.3      22.3                                          WGHT
     53   WGHT     1010     22.3      22.3      22.3                                          WGHT
     54   WGHT     1011     11.2      11.2      11.2                                          WGHT
```

Table B.1 (cont.)

```
                                  *** STARDYNE 3.0     INPUT ***
         /-------------------------------- CARD  IMAGE ---------------------------------/
         1  4   8  12  16  20  24  28  32  36  40  44  48  52  56  60  64  68  72  76  80
         *  *   *   *   *   *   *   *   *   *   *   *   *   *   *   *   *   *   *   *   *
CARD NO  ********************************************************************************  CARD TYPE
    109  QUADR     36     203     104     103     204                  .5                  QUADR
    110  QUADR     37  46 303 100 203 100 204 100 304 100                                  QUADR
    111  QUADR     47     204     304     305     205                1.75                  QUADR
    112  QUADR     48     304     404     405     355                                      QUADR
    113  QUADR     49  56 404 100 504 100 505 100 405 100                                  QUADR
    114  QUADR     57     305     355     356     306                                      QUADR
    115  QUADR     58     355     405     406     356                                      QUADR
    116  QUADR     59  66 405 100 505 100 506 100 406 100                                  QUADR
    117  QUADR     67     356     406     407     357                                      QUADR
    118  QUADR     68  75 406 100 506 100 507 100 407 100                                  QUADR
    119  QUADR     76  78 104   1 103   1 205   1 206   1             1.5                  QUADR
    120  QUADR     79  81 206   1 205   1 306   1 307   1                                  QUADR
    121  QUADR     82  84 307   1 306   1 357   1 358   1                                  QUADR
    122  QUADR     85  86 357   2 407   2 408   2 358   2                                  QUADR
    123  QUADR     87  90 407   1 507   1 508   1 408   1                                  QUADR
    124  QUADR     91  93 507   1 607   1 608   1 508   1                                  QUADR
    125  QUADR     94  96 607   1 707   1 708   1 608   1                                  QUADR
    126  QUADR     97 100 707   1 807   1 808   1 708   1                                  QUADR
    127  QUADR    101 102 807   1 907   1 908   1 808   1                                  QUADR
    128  QUADR    103 104 907   11007   11008   1 908   1                                  QUADR
    129  QUADR    105 1081007   11107   11108   11008   1                                  QUADR
    130  QUADR    109 1121107   11207   11208   11108   1                                  QUADR
    131  QUADR    113    1203    1204    1205    1212                                      QUADR
    132  QUADR    114    1212    1205    1206    1213                                      QUADR
    133  QUADR    115    1213    1206    1207    1208                                      QUADR
    134  QUADR    116     400     412     410     411                 .25                  QUADR
    135  QUADR    117     310     412     410     360                                      QUADR
    136  QUADR    118     101     102     104     105                 1.5                  QUADR
    137  END                                                                               END
    138  ENDGEOM                                                                           ENDGE
    139   LANCZOS MODAL EXTRACTION   ANTISYMMETRIC MODES                                    LANC
    140  DYNAMIC                                       .2   30     500   -.1               DYNAM
    141  ENDMODEL                                                                          ENDMO
```

Table B.2 STAR Output Data

```
*********************************************************************************************************
*********************************************************************************************************
            * T I M E   E S T I M A T E S   F O R   A   S T A T I C   A N A L Y S I S *                   *
                                                                                                         *
          ESTIMATED TIME       =   119.3        (DECIMAL)  +    54.2    PER LOAD CASE (FULL PROCESSING)  *
                                                     -OR-  +     3.7    PER LOAD CASE (DISP.VECTOR ONLY) *
                                                                                                         *
          TOTAL TIME  IF   1  LOAD CASE  =   180.4  (DECIMAL)  (FULL OUTPUT PROCESSING)                  *
          TOTAL TIME  IF   5  LOAD CASE  =   395.0  (DECIMAL)  (FULL OUTPUT PROCESSING)                  *
          TOTAL TIME  IF  10  LOAD CASE  =   665.4  (DECIMAL)  (FULL OUTPUT PROCESSING)                  *
                                                                                                         *
   **NOTE** ADD 0.18        PER (THERMALLY OR PRESSURE LOADED) QUADRILATERAL TO GENERATE CONSISTENT LOAD VECTOR *
   **NOTE** ADD 0.06   PER (INTERMEDIATELY LOADED) BEAM TO GENERATE EQUIV. LOAD VECTOR AND STRESS DISTRIBUTION *
                                                                                                         *
          STATIC MATRIX SIZE (DOF)  =   810                                                              *
          STATIC MATRIX BAND (DOF)  =    50                                                              *
*********************************************************************************************************
            * T I M E   E S T I M A T E S   F O R   A   D Y N A M I C   A N A L Y S I S *                 *
        LANCZOS AND INVITR MATRIX SIZES ARE THE SAME AS STATIC.                                          *
        HOR PARTITIONED MATRIX SIZES                                                                     *
          DEPENDENT MATRIX SIZE (DEPDOF) =   415                                                         *
          DEPENDENT MATRIX BAND          =    52                                                         *
          INDEPENDENT MATRIX SIZE (INDDOF) =   395                                                       *
   **WARNING** INVERSE ITERATION TIME IS VERY PROBLEM DEPENDENT.                                          *
                                                                                                         *
      ***************************************************************************************            *
      *              *              TOTAL TIME (DECIMAL) IF              *  ADDITIONAL TIME   *            *
      *              *                                                   *  IF        -OR-  IF *            *
      * NUMBER OF    *          EIGENVECTOR ONLY IS OUTPUT               *  COMPOSITE  * ALL POSSIBLE *   *
      *              *                *              *                   *  DAMPING IS *   OUTPUT IS  *   *
      * EIGENVECTORS *      LANCZOS   *   HOR/GUYAN  *       INVITR      *  COMPUTED ALSO* COMPUTED ALSO*  *
      *              *                *              *                   *  (ANY METHOD)*  (ANY METHOD)*  *
      ***************************************************************************************            *
      *        1     *        165.7   *     3012.9   *        217.4      *        34.2  *        51.0  *  *
      *        2     *        178.1   *     3017.8   *        318.8      *        68.3  *       101.9  *  *
      *        5     *        220.6   *     3032.5   *        623.2      *       170.8  *       254.9  *  *
      *       10     *        290.1   *     3057.0   *       1130.5      *       341.5  *       509.7  *  *
      *       25     *        523.4   *     3130.4   *       2652.5      *       853.9  *      1274.3  *  *
      *       50     *        960.3   *     3252.7   *       5189.1      *      1707.5  *      2548.6  *  *
      *       75     *       1465.9   *     3375.0   *       7725.7      *      2561.3  *      3822.8  *  *
      *      100     *       2092.6   *     3497.6   *      10262.3      *      3415.1  *      5097.1  *  *
      *      125     *       2780.3   *     3619.7   *      12798.9      *      4268.8  *      6371.4  *  *
      *      150     *       3548.5   *     3742.0   *      15335.5      *      5122.6  *      7645.7  *  *
*********************************************************************************************************
      * T I M E   S A V E D   I F   R E S T A R T   F I L E S   E N T E R E D *                          *
                                                                                                         *
       TAPE7      ANY METHOD                      TIME SAVED =       65.1                               *
       TAPE9      STATIC,LANCZOS,INVITR           TIME SAVED =       25.8                               *
       TAPE9      HOR                             TIME SAVED =        7.6                               *
       TAPE28     HOR                             TIME SAVED =      139.8                               *
                                                                                                         *
   **NOTE**  IF TAPE9 IS SUPPLIED FOR STATIC OR LANCZOS, THEN INCLUDE THE TAPE7 TIME SAVED ALSO.         *
*********************************************************************************************************
   **NOTE** TIME ESTIMATES ASSUME THAT INPUT IS ON TAPE2 AND THAT MAXIMUM OUTPUT OPTIONS ARE REQUESTED.   *
   **NOTE** ADD RENUMBERING AND/OR PLOT TIME TO ESTIMATES IF THEY ARE TO BE PERFORMED ON NEXT RUN.       *
   **NOTE** BEFORE CODING  TIME LIMIT , ADD  20  PERCENT TO TIME ESTIMATE.                               *
*********************************************************************************************************
```

Table B.2 (cont.)

```
****** EIGENVALUE SEARCH HAS BEEN COMPLETED ******

THE NUMBER OF EIGENVALUES EXTRACTED  =    10



** TIME SUMMARY FOR LANCZOS EIGENSOLUTION **

                                SPUCP     SPUIO
   TIME FOR   DECOMP            16.65      8.46
   TIME FOR   PREVEC              .01       .05
   TIME FOR   TRIDIAG          149.52    476.23
   TIME FOR   EIGVAL              .07       .37
   TIME FOR   EIGVEC              .54       .30
   TIME FOR   EXPAND            13.55     15.66
   TIME FOR   OUTPUT             4.73     78.33
   TOTAL LANCZOS TIME          182.02    578.93    760.95


                   **************************************************************************
                   *** ENTERING PHASE   7 *** RUN DATE = 80/06/16  TIME OF DAY 12.27.44 ***
                   **************************************************************************



**** POST-PROCESS FOR ELEMENT LOADS LINK ****
```

Table B.2 (cont.)

```
 .  .  .  .  .  .  .  .  .  .  .  .  .  .  .  .  .  .
            N O D A L    P O I N T    A C C E L E R    F O R C E S    FOR OUTPUT VECTOR    7
  NODE          Y1            Y2            Y3                   Y4           Y5           Y6
  100      0.             -.236347E+03  0.            0.              0.           0.
  101       .665109E+02   -.455811E+03  -.507652E+03  0.              0.           0.
  102       .115435E+03   -.307551E+03  -.676726E+03  0.              0.           0.
  103      -.109992E+03    .507531E+02  -.149470E+03  0.              0.           0.
  104      -.530125E+03    .113746E+03  -.684611E+03  0.              0.           0.
  105      -.310161E+03    .927979E+02  -.411756E+03  0.              0.           0.
  106      -.121536E+03    .779333E+02  -.208256E+03  0.              0.           0.
  107      0.              .335072E+02  0.            0.              0.           0.
  200      0.             -.179985E+03  0.            0.              0.           0.
  201       .346636E+02   -.244920E+03  -.259734E+03  0.              0.           0.
  202       .179321E+03   -.465253E+03  -.113882E+04  0.              0.           0.
  203      -.330163E+03    .238134E+03  -.526487E+03  0.              0.           0.
  204      -.139349E+03    .201124E+03  -.575274E+02  0.              0.           0.
  205      -.975609E+02    .869691E+02  -.160693E+03  0.              0.           0.
  206      -.237865E+03    .792956E+02  -.313038E+03  0.              0.           0.
  207      -.267222E+03    .824255E+02  -.359797E+03  0.              0.           0.
  208      -.109009E+03    .407399E+02  -.155852E+03  0.              0.           0.
  300      0.             -.201557E+03  0.            0.              0.           0.
  301       .470995E+02   -.271531E+03  -.297434E+03  0.              0.           0.
  302       .242901E+03   -.605114E+03  -.257038E+04  0.              0.           0.
  303      -.297322E+03    .372295E+03  -.138023E+04  0.              0.           0.
  304      -.142177E+03    .333691E+03   .555872E+02  0.              0.           0.
  305      -.613963E+02    .135734E+03   .170872E+02  0.              0.           0.
  306       .316513E+01    .686095E+02  -.270835E+02  0.              0.           0.
  307      -.827356E+02    .711827E+02  -.147183E+03  0.              0.           0.
  308      -.128261E+03    .685847E+02  -.215227E+03  0.              0.           0.
  309      -.670682E+02    .349515E+02  -.117592E+03  0.              0.           0.
  310       .285973E+02   -.256778E+03  -.599560E+02  0.              0.           0.
  355      -.655167E+02    .150328E+03   .540851E+02  0.              0.           0.
  356      -.832138E+01    .838144E+02   .622813E+02  0.              0.           0.
  357       .563315E+02    .347931E+02   .537067E+02  0.              0.           0.
  358      -.305433E+02    .974491E+02  -.156851E+03  0.              0.           0.
  359      -.564423E+00    .130994E+03  -.155352E+03  0.              0.           0.
  360      -.408320E+02    .433294E+02  -.132190E+03  0.              0.           0.
  400      0.             -.199591E+03  0.            0.              0.           0.
  401       .390131E+02   -.216830E+03  -.421245E+03  0.              0.           0.
  402       .188160E+03   -.485822E+03  -.304362E+04  0.              0.           0.
  403      -.217146E+03    .421759E+03  -.162987E+04  0.              0.           0.
  404      -.110782E+03    .365594E+03   .137376E+03  0.              0.           0.
  405      -.847547E+02    .790104E+02   .203557E+03  0.              0.           0.
  406      -.222436E+02   -.649707E+02   .203431E+03  0.              0.           0.
  407       .459466E+02    .145079E+03   .217225E+03  0.              0.           0.
  408      -.319733E+02    .311878E+03   .960341E+03  0.              0.           0.
  409      -.588662E+02    .328859E+03   .990143E+03  0.              0.           0.
  410      -.501927E+02    .194255E+03   .217409E+03  0.              0.           0.
  411      0.              .857925E+02  0.            0.              0.           0.
  412       .324600E+02   -.247699E+03  -.282659E+03  0.              0.           0.
  500      0.             -.158892E+03  0.            0.              0.           0.
  501       .741294E+02   -.233485E+03  -.541298E+03  0.              0.           0.
  502       .124888E+03   -.401983E+03  -.333670E+04  0.              0.           0.
  503      -.150359E+03    .452544E+03  -.186319E+04  0.              0.           0.
  504      -.765237E+02    .393376E+03   .159782E+03  0.              0.           0.
  505      -.657141E+02   -.249385E+03   .297398E+03  0.              0.           0.
  506      -.323105E+02   -.459344E+03   .360049E+03  0.              0.           0.
  507       .251647E+01    .158046E+03   .281689E+03  0.              0.           0.
  508      -.280435E+02    .152828E+03   .159236E+04  0.              0.           0.
  509      -.321659E+02    .149565E+03   .372873E+04  0.              0.           0.
  510      -.636420E+02    .277026E+03   .751799E+04  0.              0.           0.
  511      0.              .166370E+03  0.            0.              0.           0.
```

Table B.2 (cont.)

600	0.	-.148421E+03	0.	0.	0.	0.
601	.192008E+02	-.266125E+03	-.139160E+04	0.	0.	0.
602	.615779E+02	-.374192E+03	-.375339E+04	0.	0.	0.
603	-.756788E+02	.465932E+03	-.201003E+04	0.	0.	0.
604	-.282419E+02	.409756E+03	.228906E+03	0.	0.	0.
605	-.376261E+02	-.628740E+03	.335702E+03	0.	0.	0.
606	-.418619E+02	-.106822E+04	.344768E+03	0.	0.	0.
607	-.406183E+02	.166327E+03	.328904E+03	0.	0.	0.
608	-.406204E+02	.163982E+03	.377865E+04	0.	0.	0.
609	-.353309E+02	.164769E+03	.775671E+04	0.	0.	0.
610	-.622133E+02	.281666E+03	.150487E+05	0.	0.	0.
700	0.	-.128864E+03	0.	0.	0.	0.
701	-.511979E+01	-.207801E+03	-.133320E+04	0.	0.	0.
702	-.136505E+02	-.345800E+03	-.368934E+04	0.	0.	0.
703	-.611052E+01	.495328E+03	-.206201E+04	0.	0.	0.
704	.256470E+02	.438328E+03	.267504E+03	0.	0.	0.
705	-.376566E+01	-.853250E+03	.313345E+03	0.	0.	0.
706	-.580505E+02	-.131045E+04	.319256E+03	0.	0.	0.
707	-.525131E+02	.153492E+03	.302027E+03	0.	0.	0.
708	-.647363E+02	.153658E+03	.445161E+04	0.	0.	0.
709	-.456387E+02	.188747E+03	.863601E+04	0.	0.	0.
710	-.495603E+02	.300142E+03	.173563E+05	0.	0.	0.
711	0.	.131182E+03	0.	0.	0.	0.
800	0.	-.153590E+03	0.	0.	0.	0.
801	-.303722E+02	-.252665E+03	-.143821E+04	0.	0.	0.
802	-.522859E+02	-.386925E+03	-.376237E+04	0.	0.	0.
803	.676711E+02	.535619E+03	-.201354E+04	0.	0.	0.
804	.888721E+02	.467082E+03	.136300E+03	0.	0.	0.
805	.307641E+02	-.871444E+03	.210260E+03	0.	0.	0.
806	-.602615E+02	-.137113E+04	.215850E+03	0.	0.	0.
807	-.146645E+03	.108304E+03	.263063E+03	0.	0.	0.
808	-.518753E+02	.112781E+03	.441473E+04	0.	0.	0.
809	-.361170E+02	.882774E+02	.860466E+04	0.	0.	0.
810	-.116809E+02	.615689E+03	.407572E+04	0.	0.	0.
811	0.	.806416E+02	0.	0.	0.	0.
900	0.	-.161552E+03	0.	0.	0.	0.
901	-.465576E+02	-.257601E+03	-.115717E+04	0.	0.	0.
902	-.152361E+03	-.428730E+03	-.334071E+04	0.	0.	0.
903	.557347E+03	.251450E+04	-.784636E+04	0.	0.	0.
904	.673877E+03	.248950E+04	.770504E+02	0.	0.	0.
905	.610069E+02	-.687062E+03	.347923E+02	0.	0.	0.
906	-.677353E+02	-.120906E+04	.359036E+02	0.	0.	0.
907	-.192732E+03	.305050E+02	.377880E+02	0.	0.	0.
908	-.118852E+03	.346816E+03	.357317E+04	0.	0.	0.
909	-.675506E+02	.516653E+02	.120658E+05	0.	0.	0.
1000	0.	-.219990E+03	0.	0.	0.	0.
1001	-.715241E+02	-.358237E+03	-.556160E+03	0.	0.	0.
1002	-.236053E+03	-.536901E+03	-.202037E+04	0.	0.	0.
1003	.875256E+03	.267380E+04	-.675286E+04	0.	0.	0.
1004	.844650E+03	.262759E+04	-.650573E+03	0.	0.	0.
1005	.836439E+02	-.322722E+03	-.157778E+03	0.	0.	0.
1006	-.720105E+02	-.802675E+03	-.153354E+03	0.	0.	0.
1007	-.223119E+03	-.655764E+02	-.184636E+03	0.	0.	0.
1008	-.135710E+03	-.611860E+02	.232771E+04	0.	0.	0.
1009	-.114157E+03	-.132153E+03	.784112E+04	0.	0.	0.
1010	-.528127E+02	-.108772E+03	.553008E+04	0.	0.	0.

Table B.2 (cont.)

```
1011    0.            -.562128E+02  0.             0.          0.          0.
1100    0.            -.198944E+03  0.             0.          0.          0.
1101    -.565950E+02  -.305001E+03  -.267127E+03   0.          0.          0.
1102    -.218037E+03  -.506759E+03  -.186837E+04   0.          0.          0.
1103     .103003E+04   .262911E+04  -.524425E+04   0.          0.          0.
1104     .951830E+03   .257759E+04  -.193385E+04   0.          0.          0.
1105     .507482E+02   .168728E+03  -.425643E+03   0.          0.          0.
1106    -.654562E+02  -.268930E+03  -.441780E+03   0.          0.          0.
1107    -.237624E+03  -.156203E+03  -.435012E+03   0.          0.          0.
1108    -.146133E+03  -.146020E+03   .476282E+03   0.          0.          0.
1109    -.830819E+02  -.147594E+03   .153701E+04   0.          0.          0.
1110    -.375431E+02  -.147959E+03   .144749E+04   0.          0.          0.
1111    0.            -.755153E+02  0.             0.          0.          0.
1200    0.            -.153857E+04  0.             0.          0.          0.
1201    -.665508E+03  -.387663E+04   .704805E+04   0.          0.          0.
1202    -.135590E+03  -.375890E+03  -.569649E+03   0.          0.          0.
1203     .706656E+03   .657704E+03  -.115185E+04   0.          0.          0.
1204     .134576E+03   .364001E+03  -.320198E+03   0.          0.          0.
1205     .848267E+02   .316007E+03  -.563481E+03   0.          0.          0.
1206    -.563047E+02   .415535E+02  -.588546E+03   0.          0.          0.
1207    -.165272E+03  -.176285E+03  -.477721E+03   0.          0.          0.
1208    -.162726E+03  -.249456E+03  -.103201E+04   0.          0.          0.
1209    -.745906E+02  -.155405E+03  -.607738E+03   0.          0.          0.
1210    -.363904E+02  -.190485E+03  -.229169E+03   0.          0.          0.
1211    0.            -.548596E+02  0.             0.          0.          0.
1212     .196829E+03   .703175E+03  -.624847E+03   0.          0.          0.
1213     .118406E+03   .255831E+02  -.753835E+03   0.          0.          0.
1250    -.595321E-01  -.151677E+00  -.855957E+00   0.          0.          0.
1251    -.250719E-01  -.625771E-01  -.284875E+00   0.          0.          0.
1253    -.253162E-01  -.516691E-01  -.281075E+00   0.          0.          0.
```

Table B.2 (cont.)

```
   *   *   *   *   *   *   *   *   *   *   *   *   *   *   *   *   *   *
                  MODE SHAPE (EIGENVECTORS)
MODE NUMBER    7 .  FREQUENCY      =          62.671705     .  GENERALIZED WEIGHT =         237.28764
                              *MAXIMUM ROTATION    IS AT NODE   711 *DOF = 4 VALUE =   .760376E-01
                              *MAXIMUM TRANSLATION IS AT NODE   610 *DOF = 3 VALUE =   .100000E+01
            *********** TRANSLATIONS       ***********          *********** ROTATIONS (RADIANS) **********
 NODE          X1              X2              X3              X4              X5              X6
  100     0.000000000     -.037509336     0.000000000     -.001643166     0.000000000     -.000583618
  101      .005083432     -.037894837     -.038799826     -.003031877     -.000745908      .000401604
  102      .014769391     -.038414061     -.084525055     -.005266303     -.002223504     -.000396864
  103     -.016966096      .007828558     -.021667191      .001740203      .000534069     -.001349087
  104     -.035279025      .037503092     -.045559810      .000821920      .000572855      .000705101
  105     -.024744382      .007403327     -.032849519     -.001438678     -.000679423      .001508254
  106     -.011279791      .007239570     -.019328268     -.001617904     -.000255386      .001618979
  107     0.000000000      .006859360     0.000000000     -.000748460     0.000000000     -.000355936
  200     0.000000000     -.036430708     0.000000000     -.001025840     0.000000000     -.000275822
  201      .005191153     -.036671661     -.038899757     -.003112709      .000714199     0.000000000
  202      .014341798     -.037210110     -.091083856     -.005330198     -.002244399     -.000415659
  203     -.032190405      .023217716     -.090331051     -.001279305     -.001931387     -.001304470
  204     -.016798562      .024158901     -.006910128      .001165141     -.000658569     -.000716725
  205     -.007171215      .006392667     -.011811705      .001010502      .001082722     -.001168601
  206     -.020610269      .006862920     -.027121197      .000959235      .001369047     -.000959235
  207     -.023814541      .007345671     -.032064659     -.000170701      .000892174      .000170701
  208     -.019251070      .007261205     -.027778752     -.000309366      .000557658      .000309366
  300     0.000000000     -.030219565     0.000000000      .000496434     0.000000000     -.000325417
  301      .005225138     -.030123227     -.023012423     -.004512512     -.000259339     -.000466462
  302      .012208545     -.030414830     -.129194643     -.006019061     -.002058802     -.000355939
  303     -.026807133      .034735097     -.128775184     -.000828141     -.001889535     -.000556166
  304     -.015306801      .035925312      .005984547      .001992347      .000648165     -.000496614
  305     -.007792612      .017227760      .002168758      .000950876     0.000000000     -.000149792
  306      .000276655      .005996869     -.002360715      .000748580      .000687152     -.000448577
  307     -.007235667      .006225322     -.012871945      .000687374      .001047467     -.000687374
  308     -.011217129      .005992108     -.018822782      .000198087      .001225244     -.000188087
  309     -.011730968      .006095907     -.020568090      .000098685      .000957757     -.000098685
  310      .003402673     -.030131484     -.007035494     -.002712153      .000067610     -.000393984
  355     -.007541478      .017304778      .006225973      .001189373     0.000000000      .000220374
  356     -.000907373      .008091308      .006012541      .000458356     0.000000000      .000308310
  357      .005710564      .003475425      .005444474      .000632775     -.000201001     -.000635226
  358     -.001243072      .003966051     -.006385271      .001671506      .000295793      .000816850
  359     -.000322971      .005330891     -.007950572      .001119516      .000485882      .000507589
  360     -.005254246      .005575606     -.013149717      .000150833     -.000652777     -.000248751
  400     0.000000000     -.024681028     0.000000000     -.001333571     0.000000000     -.000242088
  401      .004783728     -.024985339     -.048545299     -.005652850     -.001955975     -.000304142
  402      .009828579     -.025544054     -.158987206     -.006082620     -.001673940     -.000264219
  403     -.021058742      .040960388     -.158289923     -.000694324     -.001676203     -.000243567
  404     -.012973701      .042474931      .015960447      .003725449      .000122181     -.000168135
  405     -.006858734      .006352017      .016467917      .002161810     0.000000000      .001287611
```

Table B.2 (cont.)

406	-.001799566	-.005249202	.016458116	-.000293699	0.000000000	.001712010
407	.003378224	.010658962	.015971470	-.001682279	.003141365	-.000296989
408	-.001138187	.011102252	.024188277	-.000930773	.006162493	-.000243643
409	-.002395525	.011708732	.035247178	.001093093	.009660176	-.000070131
410	-.003150371	.012192521	.013645791	.001780290	.009060444	.000060011
411	0.000000000	.013407435	0.000000000	.000693348	0.000000000	.000279128
412	.003273075	-.024976497	-.078501633	-.004005298	-.031644284	-.001229454
500	0.000000000	-.020714331	0.000000000	-.004293764	0.000000000	-.000211092
501	.003122006	-.021087773	-.086104969	-.005920929	-.002203475	0.000000000
502	.006799888	-.021859969	-.181792181	-.005813690	-.001178132	-.000191516
503	-.014696418	.043952201	-.160946581	-.000658541	-.001422480	-.000037567
504	-.026590284	.045702154	.023214059	.006652085	.000061642	.000309498
505	-.005715503	-.020172345	.024055975	.004209854	0.000000000	.002077622
506	-.002613542	-.040391057	.024270448	-.001149673	0.000000000	.002924511
507	.000213536	.013239443	.023898613	-.008267337	.000958775	.000245207
508	-.001787927	.013632591	.177723067	-.014018493	.010690904	0.000000000
509	-.002469271	.013341489	.332610798	-.008468843	.024670938	0.000000000
510	-.002902316	.012833397	.361088600	.010238654	.035554880	0.000000000
511	0.000000000	.011024636	0.000000000	.030268492	0.000000000	0.000000000
600	0.000000000	-.018453889	0.000000000	-.006511491	0.000000000	-.000085163
601	.001394575	-.018705308	-.106626524	-.005970229	-.000783517	-.000101654
602	.003216520	-.019545349	-.196058058	-.005118037	-.000808704	-.000089520
603	-.007679580	.045638851	-.195210116	-.000768716	-.000957974	-.000048013
604	-.003281050	.047487934	.026361235	.009855082	-.000107003	.000047654
605	-.003135425	-.050615037	.027477916	.006458626	0.000000000	.001724467
606	-.003386107	-.081391420	.027886055	-.001942734	0.000000000	.002401799
607	-.003448194	.014111763	.027735566	-.016115121	.000367355	.008323203
608	-.003623426	.014827533	.337063586	-.031418716	.007408103	0.000000000
609	-.003151594	.014897744	.691915340	-.028222698	.015575088	0.000000000
610	-.003268713	.014783471	1.000000000	-.036243263	.015494738	0.000000000
700	0.000000000	-.017766850	0.000000000	-.007098740	0.000000000	.000016347
701	-.000446300	-.018044740	-.116218134	-.006109405	-.000117737	0.000000000
702	-.000743715	-.019658024	-.201004855	-.004937368	-.000018614	.000021220
703	-.000593489	.048109235	-.200258540	-.001033614	-.000290297	-.000138849
704	.003444291	.049994125	.024107089	.011874783	-.000308409	-.000167967
705	-.000304598	-.069017916	.025345917	.007922652	0.000000000	.000652539
706	-.004113214	-.106003392	.025824083	-.002536241	0.000000000	.000975659
707	-.007849115	.013022755	.025624983	-.019817444	-.000976054	.000237478
708	-.005774620	.013706672	.397039025	-.035993626	.000465152	0.000000000
709	-.004016835	.013892994	.770350657	-.019742669	-.000095727	0.000000000
710	-.002260127	.013697536	.791507535	.023800621	-.016436621	0.000000000
711	0.000000000	.013634660	0.000000000	.076037590	0.000000000	0.000000000
800	0.000000000	-.019098554	0.000000000	-.006958870	0.000000000	.000140691
801	-.002327165	-.019359603	-.110197731	-.005915000	.000449789	.000148289
802	-.004829751	-.020211012	-.196527316	-.004929223	.000593124	.000137373
803	.006591506	.052406754	-.195589241	-.001520771	.000360957	-.000257348
804	.010324877	.054264101	.015834905	.012377259	-.000578241	-.000337581
805	.002490373	-.070485626	.017007530	.008388846	0.000000050	-.000441378
806	-.004872539	-.110908469	.017459716	-.002434829	0.000000000	-.000274130
807	-.012441887	.009188905	.017273403	-.019740619	-.000461736	.000297541
808	-.008195638	.010060294	.353803311	-.036717226	-.000615923	0.000000000
809	-.004295626	.010495383	.785533371	-.021712244	.009558350	0.000000000
810	-.002059764	.010835372	.717299736	.036197491	.006425078	0.000000000

Table B.2 (cont.)

```
 811    0.000000000    .010854667   0.000000000    .067732355   0.000000000   0.000000000
 900    0.000000000   -.022273762   0.000000000   -.006058814   0.000000000    .000260107
 901   -.044356183   -.022455653   -.130872681   -.005476537    .001143158   0.000000000
 902   -.058845878   -.023358837   -.182010431   -.065106536    .001219658    .000246343
 903    .013826459    .058201903   -.181615650   -.012232698    .001128883   -.000252966
 904    .016232566    .059753965    .001877663    .011384823   -.000693327   -.000410198
 905    .004934742   -.055575275    .002814291    .007902427   0.000000000   -.001511850
 906   -.005478591   -.057717865    .003227717   -.001523255   0.000000000   -.001629964
 907   -.016352045    .002622381    .003203512   -.017517397   -.001102423    .000273498
 908   -.010601885    .003093654    .354415170   -.037372584   -.005564768   0.000000000
 909   -.004668307    .003549861    .829382676   -.046814285   -.010862741   0.000000000
1000    0.000000000   -.027214339   0.000000000   -.004443408   0.000000000    .000346214
1001   -.025510946   -.027448422   -.176328062   -.004675490    .001817747    .000381251
1002   -.012330232   -.028045014   -.157769529   -.005428557    .001928045    .000357139
1003    .020352563    .061851040   -.157230683   -.002848686    .001500362   -.000136118
1004    .020341374    .063307724   -.016634717    .009747238   -.000368805   -.000311017
1005    .006765813   -.026104383   -.015597267    .006251599   0.000000000   -.002275035
1006   -.005824809   -.064922966   -.015640039   -.000192450   0.000000000   -.002750541
1007   -.018930154   -.005567713   -.015665183   -.010540585   -.001598587    .000129975
1008   -.012105614   -.005457924    .207279704   -.022357239   -.010541420   0.000000000
1009   -.006579385   -.005887770    .445456075   -.012045358   -.024875180   0.000000000
1010   -.003605661   -.007195165    .777571110    .020271632   -.021133400   0.000000000
1011    0.000000000   -.006762817   0.000000000    .003106124   0.000000000   0.000000000
1100    0.000000000   -.003712990   0.000000000   -.001421255   0.000000000    .003432636
1101   -.010646593   -.001447528   -.028511456   -.003374861    .004805357   0.000000000
1102   -.014638181   -.003798661   -.125178723   -.006146446    .003217232    .003312604
1103   [illegible]   [illegible]   [illegible]   [illegible]   [illegible]   [illegible]
[illegible]   [illegible]   [illegible]   [illegible]   [illegible]   [illegible]   [illegible]
1106   -.005457764   -.022576788   -.037255475    .001373675   0.000000000   -.002615989
1107   -.002269374   -.013324091   -.377183263   -.002586450   -.001716410   -.001315564
1108   -.013335354   -.013292938    .542485422   -.003834776   -.003346523   0.000000000
1109   -.007483456   -.013166865    .136747363   -.005610856   -.016656468   0.000000000
1110   -.007733674   -.013016946    .127776366    .008055815   -.013130315   0.000000000
1111    0.000000000   -.013070270   0.000000000    .011261642   0.000000000   0.000000000
1200    0.000000000   -.037882387   0.000000000    .036188892   0.000000000   0.000000000
1201   -.006587964   -.038375309    .330178860   -.003122719    .008101351    .009425746
1202   -.015309758   -.036433349   -.103565649   -.006528818    .002177365   0.000000000
1203    .025698282    .058007706   -.056527115   -.006354977    .009373151    .000202020
1204    .022795100    .061625157   -.054212755    .002652087   -.001528678    .000635608
1205    .006438408    .033038857   -.058054050    .002509658   -.001347049    .000009970
1206   -.005546929    .004053696   -.087581340    .002392324   -.000851336   -.008655559
1207   -.020680502   -.022272350   -.069356568    .002741549   -.000847187   -.009405215
1208   -.013878169   -.021275018   -.098015724    .001132250   -.006065749    .000871333
1209   -.007736511   -.020268409   -.063037568   -.003863265   -.009328128    .002025216
1210   -.003723591   -.015491012   -.023445311   -.002681922   -.006757787    .000037345
1211    0.000000000   -.019153855   0.000000000   -.001621593   0.000000000    .000374931
1212    .021185561    .033678727   -.092545182    .032858750   -.000534745    .000210479
1213    .013916445    .007053887   -.088597289    .002296580   -.000527550    .001480374
1250   -.016827593   -.036437619   -.162659813   -.006525871    .002177368    .001820152
1251   -.016827594   -.036231590   -.164975682   -.006525871    .002177370    .000202029
1253   -.014653625   -.025937748   -.162699316   -.006525870    .002177368    .000202029

MODAL PARTICIPATION FACTOR (X1) =  -1.6040642E-02    GEN.WT. TIMES MODAL PART. FACT. (X1) =  -3.8062475E+00
MODAL PARTICIPATION FACTOR (X2) =  -2.6751445E-11    GEN.WT. TIMES MODAL PART. FACT. (X2) =  -6.3477082E-09
MODAL PARTICIPATION FACTOR (X3) =   5.1711464E-01    GEN.WT. TIMES MODAL PART. FACT. (X3) =   1.2270491E+02
```

Best Available Copy

Table B.3 DYNRE2 Input Data

```
                    SSSSSSSSS    SS      SS   SS      SS   SSSSSSSSS    SSSSSSSSSS    SSSSSSSS
                    SSSSSSSSSS    SS    SS    SSS     SS   SSSSSSSSSS   SSSSSSSSSS   SSSSSSSSSS
  S    S            SS      SS     SS  SS     SS S    SS   SS      SS   SS           S       SS     S    S
   S  S             SS      SS      SSSS      SS SS   SS   SS      SS   SS                   SS      S  S
SSSSSSSSSS          SS      SS       SS       SS  SS  SS   SSSSSSSSSS   SSSSSS              SS    SSSSSSSSSS
   S  S             SS      SS       SS       SS  SS  SS   SSSSSSSSS    SSSSSS             SS        S  S
  S    S            SS      SS       SS       SS   SS SS   SS   SS      SS                SS          S    S
                    SS      SS       SS       SS    S SS   SS    SS     SS               SS
                    SSSSSSSSSS       SS       SS     SSS   SS     SS    SSSSSSSSSS   SSSSSSSSSS
                    SSSSSSSSS        SS       SS      SS   SS      SS   SSSSSSSSSS   SSSSSSSSSS

****************************************************************
*                   **    DYNRE2  (R) **                        *
*                   ** STARDYNE-3 (R) **                        *
*                   **  MAR 10/ODLEVEL**                        *
****************************************************************
*  LATEST USER MANUAL  SEPT 1979                                *
*                                                               *
*                                                               *
*  RUN DATE      MONDAY    , JUN. 16, 1980                      *
*                80/06/16.  DAY 168 OF 1980                     *
*  RUN TIME      20.13.46.                                      *
*                                                               *
*   CYBERNET                    NOS 1      #453                 *
*                                                               *
*  (R) 1968 STARDYNE   SYSTEM  BY MECHANICS RESEARCH INC        *
*  (R) 1971 STARDYNE-2 SYSTEM  BY MECHANICS RESEARCH INC        *
*  (R) 1974 STARDYNE-3 SYSTEM  BY MECHANICS RESEARCH INC        *
*  (R) 1977 STARDYNE-3 SYSTEM  BY SYSTEM DEVELOPMENT CORP       *
****************************************************************

****************************************************************
*          S T A R D Y N E   B U L L E T I N S                  *
*                                                               *
*    A STARDYNE INFORMATION BULLETIN IS AVAILABLE               *
*  WHICH DESCRIBES IMPORTANT CHANGES CONCERNING THIS            *
*  RELEASE LEVEL OF THE PROGRAM.  IN ORDER TO ACCESS            *
*  THIS BULLETIN - ENTER THE FOLLOWING CONTROL CARDS..          *
*   AT SCOPE 3.4                  AT NOS 1                      *
*   .                              .                            *
*  APPLIC(STARBUL)                ATTACH(STARBUL/UN=LIBRARY)    *
*  REWIND(STARBUL)                REWIND(STARBUL)               *
*  COPYBF(STARBUL,A)              COPYBF(STARBUL,A)             *
*  REWIND(A)                      REWIND(A)                     *
*  COPYSBF(A,OUTPUT)              COPYSBF(A,OUTPUT)             *
*   .                              .                            *
****************************************************************

***********************************************************
* NOTICE - THE NEW STARDYNE USERS MANUAL IS AVAILABLE.    *
*          THE VERSION DATE = SEPTEMBER 1, 1979           *
*          PLEASE CONTACT YOUR SALES REPRESENTATIVE..     *
***********************************************************
```

Table B.3 (cont.)

```
                         *****  INPUT DATA CARDS  *****
           /------------------------------ CARD  IMAGE ------------------------------/
           1    6    12   17   22   27   32   37   42   47   52   57   62   67   72      80
           .    .    .    .    .    .    .    .    .    .    .    .    .    .    .       .
CARD NO    ********************************************************************************
        1  STARTZ                         0         0   10.       250.
        2          3600         0                            4.        2
        3  END
        4  MODES                          1
        5             .        14 .05
        6            14        30 .010
        7  END
        8  PLOT                 2                   1
        9                    1251         1         6      1253         3         6
       10                    1252         1         6      1250         3         6
       11                    1262         1         6      1262         3         6
       12                    1263         3         6      1021         3         6
       13  END
       14  FORCE                               1.000     1.000
       15  DRIVER               1                   4
       16                    1250         1      1290         3
       17  END
       18  ALL DONE

                 (END OF INPUT FOR MODEL NO.    1)
```

Table B.4 DYNRE2 Output Data

```
XXXXX HEADER XXXXXX(DRIVE                   :                                      )XXXXXXXXX

          DRIVE POINT LIST
              FORCE

          JOINT        LOCAL
           NO.         D.O.F.
          1253            1
          1253            3

XXXXXXXXXXXXXXXXXXXXX(END

XXXXX HEADER XXXXXX(ALL DONE                                                       )XXXXXXXXX


*****************************************************************************************
*****************************************************************************************


          M113A1 HULL DYNAMIC MODEL - FMC CORPORATION

 MAX NODE NO. =  1253, NO. NODES =   148, DOF PER NODE =  6, NO. OF DOF =   888, G =  .38640E+03

   1 T-VERS = (81/16/1612.11.43MAR1161 )

TAPE+ HEADER=(ELELOADS 1253    6   30    1    6 0 1 0 0 0 0 0 0 0 0 0 0 0 0 0)

                    27 MODES (EIGENVECTORS) HAVE BEEN SELECTED.
 MODE         NATURAL FREQUENCY              GENERALIZED WEIGHT              DAMPING
  NO.            (CPS)         (RAC/SEC)        (WEIGHT)             (MASS)  COEFFICIENT

    1      .199575E+02     .125397E+03     .182045E+04     .471132E+01     .500000E-01
    2      .413072E+02     .259541E+03     .327894E+03     .848598E+00     .500000E-01
    3      .531549E+02     .333982E+03     .133354E+04     .345119E+01     .500000E-01
    4      .626717E+02     .393778E+03     .237288E+03     .614099E+00     .500000E-01
    5      .743567E+02     .467197E+03     .235454E+03     .609354E+00     .500000E-01
    6      .849132E+02     .533526E+03     .628948E+03     .162771E+01     .500000E-01
    7      .987767E+02     .620632E+03     .742360E+03     .192124E+01     .500000E-01
    8      .111572E+03     .701030E+03     .285227E+03     .738165E+00     .500000E-01
    9      .115074E+03     .723055E+03     .185913E+03     .481134E+00     .500000E-01
   10      .129461E+03     .813429E+03     .185303E+03     .479563E+00     .500000E-01
   11      .150552E+03     .945947E+03     .133629E+03     .345832E+00     .180000E-01
   12      .156269E+03     .981870E+03     .854754E+03     .221210E+01     .180000E-01
   13      .167407E+03     .105185E+04     .418609E+03     .108336E+01     .180000E-01
   14      .179656E+03     .112881E+04     .929516E+03     .240558E+01     .180000E-01
   15      .190222E+03     .119520E+04     .336355E+03     .870484E+00     .180000E-01
   16      .197885E+03     .124335E+04     .116083E+03     .300423E+00     .180000E-01
   17      .209486E+03     .131625E+04     .241445E+03     .624858E+00     .180000E-01
   18      .209516E+03     .131643E+04     .304881E+03     .789030E+00     .180000E-01
   19      .219252E+03     .137760E+04     .212094E+03     .548896E+00     .180000E-01
   20      .222061E+03     .139525E+04     .444196E+03     .114957E+01     .180000E-01
   21      .230501E+03     .144828E+04     .460238E+03     .119101E+01     .180000E-01
   22      .236943E+03     .148876E+04     .701317E+03     .181500E+01     .180000E-01
   23      .245926E+03     .154520E+04     .165466E+03     .428223E+00     .180000E-01
   24      .250264E+03     .157245E+04     .158848E+03     .411098E+00     .180000E-01
   25      .252513E+03     .158659E+04     .186725E+03     .484195E+00     .180000E-01
   26      .258358E+03     .162332E+04     .116939E+03     .302636E+00     .180000E-01
   27      .261247E+03     .164147E+04     .149514E+03     .386942E+00     .180000E-01

                     END OF INPUT DATA
```

Table B.4 (cont.)

```
***** POINT-TO-POINT TRANSFER FUNCTIONS *****  M113A1 HULL DYNAMIC MODEL - FMC CORPORATION                    *****

*** COMPUTE GENERALIZED FORCES *** FCTRS ***

MAX CORE FOR THIS OVERLAY =0000000000000072146


                         GENERALIZED (MODAL) FORCE COMPONENTS

MODE NO.        X1              X2              X3              THETA 1         THETA 2         THETA 3

     1   -.281693E-01   0.              0.              0.              0.              0.
     2   -.376313E-02   0.              0.              0.              0.              0.
     3   -.393522E-01   0.              0.              0.              0.              0.
     4   -.274031E-01   0.              0.              0.              0.              0.
     5   -.336577E-02   0.              0.              0.              0.              0.
     6    .229075E-01   0.              0.              0.              0.              0.
     7    .531431E-01   0.              0.              0.              0.              0.
     8   -.356274E-01   0.              0.              0.              0.              0.
     9    .442774E-01   0.              0.              0.              0.              0.
    10   -.930981E-01   0.              0.              0.              0.              0.
    11    .126423E+00   0.              0.              0.              0.              0.
    12    .172362E+00   0.              0.              0.              0.              0.
    13   -.119446E+00   0.              0.              0.              0.              0.
    14    .655441E-01   0.              0.              0.              0.              0.
    15    .499866E-01   0.              0.              0.              0.              0.
    16   -.206375E+00   0.              0.              0.              0.              0.
    17   -.215591E-01   0.              0.              0.              0.              0.
    18   -.679984E-01   0.              0.              0.              0.              0.
    19   -.206981E+00   0.              0.              0.              0.              0.
    20   -.769359E-01   0.              0.              0.              0.              0.
    21    .476293E-01   0.              0.              0.              0.              0.
    22   -.621229E-01   0.              0.              0.              0.              0.
    23    .727049E-01   0.              0.              0.              0.              0.
    24   -.111769E+00   0.              0.              0.              0.              0.
    25    .135011E-01   0.              0.              0.              0.              0.
    26   -.454099E-02   0.              0.              0.              0.              0.
    27    .311039E-01   0.              0.              0.              0.              0.


*** COMPUTE FREQUENCIES *** AMPS ***

MAX CORE FOR THIS OVERLAY =0000000000000000057766



  LIST OF OUTPUT / PLOT FREQUENCIES.  LOWER LIMIT =    .10000000E+02, UPPER LIMIT =    .25000000E+03

         1      .17755281E+02
         2      .19957500E+02
         3      .22159720E+02
         4      .30532369E+02
         5      .39105017E+02
         6      .41307237E+02
         7      .42523190E+02
         8      .47231[illegible]E+02
         9      .51932[illegible]E+02
        10      .53154[illegible]E+02
        11      .541365[illegible]E+02
        12      .5771329[illegible]
```

Table B.4 (cont.)

```
*************************************************************
*                                                           *
* EXCITING FREQUENCY NUMBER   2 (         19.957563 CPS)    *
*                                                           *
*************************************************************


************ DISPLACEMENT PHASE ANGLES
*************(THIS IS THE PHASE ANGLE BY WHICH THE MAXIMUM DISPLACEMENT LAGS THE EXCITATION)
*************(THESE VALUES HAVE BEEN REFERENCED TO THE PHASE ANGLE OF THE DRIVEN NODAL/DOF.      .84659670E+02 DEG.)

JOINT         X1               X2               X3             THETA 1          THETA 2          THETA 3
          PHASE ANGLE      PHASE ANGLE      PHASE ANGLE      PHASE ANGLE      PHASE ANGLE      PHASE ANGLE

 1001     .671154E+00      .428694E+01     -.174465E+03     -.174284E+03     -.177066E+03     -.179367E+03
 1019    -.174036E+03     -.174648E+03     -.174463E+03     -.180287E+03     -.184376E+03     -.846597E+02
 1202    -.1[illegible]27[illegible]    .370896E+01     -.175191E+03      .679215E+00     -.180637E+03     -.179555E+03
 1250     0.               .370894E+01     -.174431E+03      .679205E+00     -.180637E+03     -.179556E+03
 1251    -.594655E-06      .372309E+01     -.174372E+03      .679205E+00     -.180637E+03     -.179556E+03
 1253     .364628E-01      .379911E+01     -.174431E+03      .679211E+00     -.180637E+03     -.179556E+03

ACCELERATION TRANSFER FUNCTIONS, SINUSOIDAL EXCITATION FREQUENCY =    .199575E+02 HERTZ
EXCITATION APPLIED TONODE  NUMBER      1250. DOF      1. DRIVING FORCE =    .100000E+01

JOINT         X1               X2               X3             THETA 1          THETA 2          THETA 3
          ACCELERATION     ACCELERATION     ACCELERATION     ACCELERATION     ACCELERATION     ACCELERATION

 1001     .152296E-01      .160546E+00      .161989E+00      .743964E-02      .213726E-02      .914782E-03
 1019     .309969E-01      .186270E+00      .273831E+00      .118301E-02      .819446E-03     0.
 1202     .304616E-01      .183799E+00      .274122E+00      .474365E-02      .216225E-02      .793598E-03
 1250     .376037E-01      .183860E+00      .231587E+00      .474367E-02      .216225E-02      .793597E-03
 1251     .376037E-01      .183867E+00      .229437E+00      .474367E-02      .216225E-02      .793597E-03
 1253     .354416E-01      .179366E+00      .231597E+00      .474067E-02      .216225E-02      .793597E-03

  MAXIMUM X1 =      .37603734E-01  AT NODE 1251
  MAXIMUM X2 =      .18626973E+00  AT NODE 1019
  MAXIMUM X3 =      .27412177E+00  AT NODE 1202
  MAXIMUM X4 =      .74396423E-02  AT NODE 1001
  MAXIMUM X5 =      .21622472E-02  AT NODE 1202
  MAXIMUM X6 =      .91478219E-03  AT NODE 1001
```

Table B.4 (cont.)

```
FREQUENCY RESPONSE HISTORY, JOINT1251, DIRECTION   1

ACCELERATION TRANSFER FUNCTIONS.

  FREQUENCY (HZ)   PHASE ANGLE   ACCELERATION   ACCEL. IN G S      FREQUENCY (HZ)   PHASE ANGLE   ACCELERATION   ACCEL. IN G S

 1  .177553E+02   .180000E+03   .156232E-01   .40425E-04    48   .161838E+03   .180000E+03   .752892E+00   .19464E-02
 2  .199575E+02   .180000E+03   .376037E-01   .97318E-04    49   .166250E+03   .180000E+03   .624558E+00   .16163E-02
 3  .221597E+02   .180000E+03   .140907E-01   .36466E-04    50   .167407E+03   .180000E+03   .690381E+00   .10872E-02
 4  .366324E+02   .180000E+03   .278867E-02   .72171E-05    51   .168671E+03   .180000E+03   .698524E+00   .18078E-02
 5  .391350E+02   .180000E+03   .119780E-01   .30999E-04    52   .173532E+03   .180000E+03   .400293E+00   .10359E-02
 6  .413472E+02   .180000E+03   .152188E-01   .39386E-04    53   .178393E+03   .180000E+03   .395857E+00   .10245E-02
 7  .425293E+02   .180000E+03   .173120E-01   .44803E-04    54   .179656E+03   .180000E+03   .450962E+00   .11078E-02
 8  .472311E+02   .180000E+03   .298218E-01   .77179E-04    55   .180746E+03   .180000E+03   .473259E+00   .12248E-02
 9  .513328E+02   .180000E+03   .567507E-01   .14687E-03    56   .184939E+03   .180000E+03   .323946E+00   .83837E-03
10  .531549E+02   .180000E+03   .571539E-01   .14793E-03    57   .189132E+03   .180000E+03   .236308E+00   .61156E-03
11  .541365E+02   .180000E+03   .491539E-01   .12721E-03    58   .190222E+03   .180000E+03   .234367E+00   .60654E-03
12  .579133E+02   .180000E+03   .170368E-01   .44091E-04    59   .191093E+03   .180000E+03   .230368E+00   .59619E-03
13  .616910E+02   .180000E+03   .139683E-01   .36151E-04    60   .194463E+03   .180000E+03   .238357E+00   .61687E-03
14  .626717E+02   .180000E+03   .143126E-01   .37036E-04    61   .197794E+03   .180000E+03   .419173E+00   .10848E-02
15  .636770E+02   .180000E+03   .141945E-01   .36736E-04    62   .198665E+03   .180000E+03   .456506E+00   .11814E-02
16  .685142E+02   .180000E+03   .202950E-01   .52523E-04    63   .199618E+03   .180000E+03   .465044E+00   .12035E-02
17  .731514E+02   .180000E+03   .302354E-01   .78249E-04    64   .203281E+03   .180000E+03   .329541E+00   .85285E-03
18  .743567E+02   .180000E+03   .329858E-01   .85334E-04    65   .206944E+03   .180000E+03   .256980E+00   .66506E-03
19  .755441E+02   .180000E+03   .357921E-01   .92604E-04    66   .207896E+03   .180000E+03   .265912E+00   .68818E-03
20  .801124E+02   .180000E+03   .475562E-01   .12385E-03    67   .208063E+03   .180000E+03   .268223E+00   .69416E-03
21  .846818E+02   .180000E+03   .601342E-01   .15552E-03    68   .208766E+03   .180000E+03   .277631E+00   .71851E-03
22  .858682E+02   .180000E+03   .620282E-01   .16059E-03    69   .209349E+03   .180000E+03   .285791E+00   .73963E-03
23  .871997E+02   .180000E+03   .641756E-01   .16609E-03    70   .209516E+03   .180000E+03   .287443E+00   .74390E-03
24  .923225E+02   .180000E+03   .832522E-01   .21546E-03    71   .210520E+03   .180000E+03   .292866E+00   .75793E-03
25  .974452E+02   .180000E+03   .101236E+00   .26220E-03    72   .214384E+03   .180000E+03   .388700E+00   .10060E-02
26  .987787E+02   .180000E+03   .967515E-01   .25039E-03    73   .218247E+03   .180000E+03   .785647E+00   .20332E-02
27  .100497E+03   .180000E+03   .883421E-01   .22852E-03    74   .219252E+03   .180000E+03   .873282E+00   .22600E-02
28  .105175E+03   .180000E+03   .782032E-01   .20233E-03    75   .219541E+03   .180000E+03   .890207E+00   .23038E-02
29  .110525E+03   .180000E+03   .100125E+00   .25912E-03    76   .220656E+03   .180000E+03   .918614E+00   .23774E-02
30  .111572E+03   .180000E+03   .105412E+00   .27280E-03    77   .221771E+03   .180000E+03   .902423E+00   .23355E-02
31  .112216E+03   .180000E+03   .107085E+00   .27714E-03    78   .222661E+03   .180000E+03   .893288E+00   .23118E-02
32  .113723E+03   .180000E+03   .113456E+00   .29357E-03    79   .222931E+03   .180000E+03   .856918E+00   .22177E-02
33  .115430E+03   .180000E+03   .120847E+00   .31276E-03    80   .226261E+03   .180000E+03   .670679E+00   .17357E-02
34  .115974E+03   .180000E+03   .121935E+00   .31557E-03    81   .229630E+03   .180000E+03   .555773E+00   .14383E-02
35  .117675E+03   .180000E+03   .128422E+00   .33236E-03    82   .230501E+03   .180000E+03   .542137E+00   .14030E-02
36  .122667E+03   .180000E+03   .165722E+00   .42869E-03    83   .231165E+03   .180000E+03   .533081E+00   .13794E-02
37  .128166E+03   .180000E+03   .204727E+00   .52983E-03    84   .233722E+03   .180000E+03   .505155E+00   .13073E-02
38  .123401E+03   .180000E+03   .211467E+00   .54469E-03    85   .236279E+03   .180000E+03   .535928E+00   .13870E-02
39  .131637E+03   .180000E+03   .220138E+00   .56972E-03    86   .236943E+03   .180000E+03   .549677E+00   .14226E-02
40  .140127E+03   .180000E+03   .353132E+00   .91390E-03    87   .237870E+03   .180000E+03   .561832E+00   .14540E-02
41  .148377E+03   .180000E+03   .771961E+00   .19992E-02    88   .241435E+03   .180000E+03   .518914E+00   .13429E-02
42  .150552E+03   .180000E+03   .953117E+00   .24667E-02    89   .245000E+03   .180000E+03   .478152E+00   .12375E-02
43  .151142E+03   .180000E+03   .100432E+01   .26005E-02    90   .245526E+03   .180000E+03   .480669E+00   .12440E-02
44  .153411E+03   .180000E+03   .137294E+01   .35529E-02    91   .246774E+03   .180000E+03   .483237E+00   .12506E-02
45  .155006E+03   .180000E+03   .189366E+01   .49749E-02    92   .248095E+03   .180000E+03   .499092E+00   .12937E-02
46  .156269E+03   .180000E+03   .191038E+01   .49456E-02    93   .249816E+03   .180000E+03   .528382E+00   .13674E-02
47  .157418E+03   .180000E+03   .173758E+01   .44971E-02

      LINEAR PLOT OF [illegible]

1.411
1.555
```

Table B.4 (cont.)

FREQUENCY RESPONSE HISTORY, JOINT1009, DIRECTION 3

ACCELERATION TRANSFER FUNCTIONS.

	FREQUENCY (HZ)	PHASE ANGLE	ACCELERATION	ACCEL. IN G S		FREQUENCY (HZ)	PHASE ANGLE	ACCELERATION	ACCEL. IN G S
1	.177553E+02	.397821E+01	.602177E-01	.15597E-03	48	.161838E+03	-.168868E+03	.507142E+00	.13125E-02
2	.199575E+02	.553731E+01	.173831E+00	.44987E-03	49	.166258E+03	-.143995E+03	.306563E+00	.79442E-03
3	.221597E+02	.827576E+01	.837558E-01	.21676E-03	50	.167407E+03	-.147902E+03	.295804E+00	.76554E-03
4	.306324E+02	.152412E+03	.317937E-01	.82349E-04	51	.168671E+03	-.154396E+03	.283921E+00	.73478E-03
5	.391055E+02	.176071E+03	.289465E-01	.74913E-04	52	.173532E+03	-.151996E+03	.218623E+00	.56579E-03
6	.413072E+02	-.173785E+03	.259525E-01	.67165E-04	53	.178393E+03	-.100058E+03	.179498E+00	.46452E-03
7	.425432E+02	-.175676E+03	.224252E-01	.58036E-04	54	.179656E+03	-.938560E+02	.151259E+00	.39146E-03
8	.472311E+02	.173947E+03	.249322E-01	.64576E-04	55	.180746E+03	-.961404E+02	.119959E+00	.31045E-03
9	.519328E+02	-.172264E+03	.376128E-01	.97342E-04	56	.184939E+03	-.121189E+03	.762531E-01	.19734E-03
10	.531549E+02	-.163252E+03	.394365E-01	.10214E-03	57	.189132E+03	-.759811E+02	.881934E-01	.22824E-03
11	.541365E+02	-.146796E+03	.385429E-01	.99714E-04	58	.190222E+03	-.527627E+02	.844758E-01	.21862E-03
12	.579133E+02	-.749353E+02	.483394E-01	.12523E-03	59	.191093E+03	-.350060E+02	.771408E-01	.19964E-03
13	.616940E+02	.238735E+02	.106218E+00	.27489E-03	60	.194443E+03	.247874E+02	.515807E-01	.13328E-03
14	.626727E+02	.472631E+02	.119394E+00	.30896E-03	61	.197794E+03	.399851E+02	.748582E-01	.19373E-03
15	.638770E+02	.761455E+02	.121646E+00	.31482E-03	62	.198665E+03	.403602E+02	.888796E-01	.23002E-03
16	.685142E+02	.142834E+03	.884593E-01	.22893E-03	63	.199618E+03	.413259E+02	.103319E+00	.26739E-03
17	.731514E+02	.152121E+03	.893552E-01	.23125E-03	64	.203281E+03	.533774E+02	.142019E+00	.36754E-03
18	.743567E+02	.155302E+03	.994233E-01	.25730E-03	65	.206944E+03	.841621E+02	.196559E+00	.50869E-03
19	.755441E+02	.160961E+03	.113134E+00	.29311E-03	66	.207896E+03	.927089E+02	.217156E+00	.56200E-03
20	.801124E+02	-.176435E+03	.136611E+00	.35355E-03	67	.208063E+03	.940241E+02	.220997E+00	.57194E-03
21	.840604E+02	-.146735E+03	.165679E+00	.42878E-03	68	.208766E+03	.984846E+02	.236262E+00	.61144E-03
22	.858682E+02	-.135767E+03	.159454E+00	.41266E-03	69	.209349E+03	.102120E+03	.252314E+00	.65299E-03
23	.871997E+02	-.124587E+03	.141550E+00	.36635E-03	70	.209516E+03	.102976E+03	.256656E+00	.66422E-03
24	.923225E+02	-.124695E+03	.107416E+00	.27797E-03	71	.210522E+03	.108164E+03	.285274E+00	.73829E-03
25	.974452E+02	-.117235E+03	.204130E+00	.52842E-03	72	.214384E+03	.141665E+03	.485573E+00	.12567E-02
26	.987767E+02	-.106932E+03	.230342E+00	.59612E-03	73	.218247E+03	.159495E+03	.924682E+00	.23929E-02
27	.100037E+03	-.953225E+02	.244533E+00	.63295E-03	74	.219252E+03	.160820E+03	.106609E+01	.27590E-02
28	.105175E+03	-.249726E+02	.250022E+00	.64708E-03	75	.219541E+03	.161235E+03	.110662E+01	.28639E-02
29	.110252E+03	.315977E+02	.285971E+00	.74059E-03	76	.220656E+03	.163904E+03	.125829E+01	.32564E-02
30	.111572E+03	.447175E+02	.290167E+00	.75095E-03	77	.221771E+03	.169216E+03	.138841E+01	.35932E-02
31	.112016E+03	.493806E+02	.290137E+00	.75103E-03	78	.222081E+03	.171017E+03	.141456E+01	.36609E-02
32	.113722E+03	.665551E+02	.285812E+00	.73968E-03	79	.222931E+03	.177106E+03	.146640E+01	.37950E-02
33	.115430E+03	.829349E+02	.277235E+00	.71749E-03	80	.226281E+03	-.156117E+03	.142026E+01	.36756E-02
34	.115674E+03	.871305E+02	.274216E+00	.70964E-03	81	.229630E+03	-.121381E+03	.129424E+01	.33495E-02
35	.117275E+03	.997556E+02	.261671E+00	.67720E-03	82	.230501E+03	-.112223E+03	.122590E+01	.31728E-02
36	.122667E+03	.127154E+03	.201312E+00	.52099E-03	83	.231165E+03	-.106059E+03	.116852E+01	.30189E-02
37	.128265E+03	.137494E+03	.183346E+00	.47450E-03	84	.233722E+03	-.872619E+02	.103247E+01	.26720E-02
38	.129401E+03	.138823E+03	.164359E+00	.42536E-03	85	.236279E+03	-.620625E+02	.106615E+01	.27592E-02
39	.131637E+03	.145579E+03	.192759E+00	.49886E-03	86	.236943E+03	-.548963E+02	.105508E+01	.27305E-02
40	.140072E+03	.165951E+03	.224223E+00	.58029E-03	87	.237871E+03	-.455163E+02	.100867E+01	.26104E-02
41	.148377E+03	.156601E+03	.354365E+00	.91709E-03	88	.241435E+03	-.171024E+02	.705061E+00	.18260E-02
42	.150552E+03	.149591E+03	.559253E+00	.14468E-02	89	.245000E+03	.987194E+01	.562329E+00	.14553E-02
43	.151142E+03	.152072E+03	.640287E+00	.16571E-02	90	.245926E+03	.186443E+02	.554508E+00	.14352E-02
44	.153411E+03	.166843E+03	.957466E+00	.24779E-02	91	.246374E+03	.233047E+02	.552429E+00	.14297E-02
45	.155680E+03	.174910E+03	.125626E+01	.32512E-02	92	.248095E+03	.439070E+02	.539833E+00	.13971E-02
46	.158209E+03	.176346E+03	.126225E+01	.32667E-02	93	.249816E+03	.660604E+02	.501478E+00	.12978E-02
47	.157418E+03	.178845E+03	.113382E+01	.29343E-02					

LINEAR PLOT OF [illegible] RESPONSES

```
1.460   *         *         *         *         *         *         *         *         *         A *       *
1.425                                                                                             A A
1.3[illegible]
```

APPENDIX C

STARDYNE Input and Output Data

Revised Hull Model

Table C.1 STAR Input Data
Table C.2 STAR Output Data
Table C.3 DYNRE2 Input Data
Table C.4 DYNRE2 Output Data

Table C.1 STAR Input Data

```
           SSSSSSSS  SSSSSSSSSS   SSSSSSSS   SSSSSSSS
          SSSSSSSSSS SSSSSSSSSS  SSSSSSSSSS  SSSSSSSSSS
          SS      S      SS      SS      SS  SS      SS
  S   S   SS             SS      SS      SS  SS      SS
   S S    SSSSSSSSS      SS      SS      SS  SSSSSSSSSS
SSSSSSSSSSS SSSSSSSSS    SS      SSSSSSSSSS  SSSSSSSSS
   S S           SS      SS      SSSSSSSSSS  SS   SS
  S   S   S      SS      SS      SS      SS  SS    SS
          SSSSSSSSSS     SS      SS      SS  SS     SS
           SSSSSSSS      SS      SS      SS  SS      SS

**************************************************************
*                    ** STAR        (R)  **                  *
*                    ** STARDYNE-3 (R)   **                  *
*                    ** AUG0180  C LEVEL **                  *
**************************************************************
*   LATEST USER MANUAL   SEPT 1977                           *
*                                                            *
*                                                            *
*   RUN DATE      FRIDAY   ,  SEP. 26, 1980                  *
*                 80/09/26.  DAY 270 OF 1980                 *
*   RUN TIME      22.47.50.                                  *
*                                                            *
*    CYBERNET                     NOS 1        4.60          *
*                                                            *
*   (R) 1968 STARDYNE   SYSTEM  BY MECHANICS RESEARCH INC    *
*   (R) 1971 STARDYNE-2 SYSTEM  BY MECHANICS RESEARCH INC    *
*   (R) 1974 STARDYNE-3 SYSTEM  BY MECHANICS RESEARCH INC    *
*   (R) 1977 STARDYNE-3 SYSTEM  BY SYSTEM DEVELOPMENT CORP   *
**************************************************************


**************************************************************
*           S T A R D Y N E    B U L L E T I N S             *
*                                                            *
*      A STARDYNE INFORMATION BULLETIN IS AVAILABLE          *
*   WHICH DESCRIBES IMPORTANT CHANGES CONCERNING THIS        *
*   RELEASE LEVEL OF THE PROGRAM.  IN ORDER TO ACCESS        *
*   THIS BULLETIN - ENTER THE FOLLOWING CONTROL CARDS..      *
*    AT SCOPE 3.4                AT NOS 1                    *
*     .                          .                           *
*   APPLIC(STARBUL)             ATTACH(STARBUL/UN=LIBRARY)   *
*   REWIND(STARBUL)             REWIND(STARBUL)              *
*   COPYBF(STARBUL,A)           COPYBF(STARBUL,A)            *
*   REWIND(A)                   REWIND(A)                    *
*   COPYSBF(A,OUTPUT)           COPYSBF(A,OUTPUT)            *
*     .                          .                           *
**************************************************************
```

Table C.1 (cont.)

```
                              *** STARDYNE 3.0      INPUT ***
         /------------------------------ CARD  IMAGE  ------------------------------/
         1  4   8  12  16  20  24  28  32  36  40  44  48  52  56  60  64  68  72  76  80
         .  .   .   .   .   .   .   .   .   .   .   .   .   .   .   .   .   .   .   .   .
CARD NO  ..............................................................................   CARD TYPE
     2   PLOTS       1   1 1110115C420    72                                                PLOTS
     3    HELSAT HULL DYNAMIC MODEL NO.2                                                     ALL3
     4   MATLG       1 ALUMINUM  10.2  E06      .33       .098    13.2 E-06                  MATLG
     5   MATLG       2WEIGHTLESS 10.2  E06      .33       .001    13.2 E-06                  MATLG
     6   END                                                                                 END
     7   NODE 010          3.0            35.2            3.0                                NODE
     8   NODE 020          5.0            36.2            0.0                                NODE
     9   NODE 030         -1.205          38.2            6.833                              NODE
    10   NODE 040          5.0            36.2            6.833                              NODE
    11   NODEG      100  103   1    0.0     0.0      0.0      0.0     33.2      0.0          NODEG
    12   NODEGRD1 200  203   1    5.0     0.0      0.0      5.0     33.2      0.0            NODEG
    13   NODEGRD2 400  403 100   22.0     0.0      0.0     22.0     33.2      0.0            NODEG
    14   NODEGRD1 400  403   1   22.0     0.0      0.0     22.0     33.2      0.0            NODEG
    15   NODEGRD2 600  603 100   48.667   0.0      0.0     48.667   33.2      0.0            NODEG
    16   NODEG      650  653   1   62.0     0.0      0.0     62.0     33.2      0.0          NODEG
    17   NODEGRD1 700  703   1   75.333   0.0      0.0     75.333   33.2      0.0            NODEG
    18   NODEGRD2 900  903 100  102.0     0.0      0.0    102.0     33.2      0.0            NODEG
    19   NODEGRD1 900  903   1  102.0     0.0      0.0    102.0     33.2      0.0            NODEG
    20   NODEGRD211001103 100  134.0     0.0      0.0    134.0     33.2      0.0             NODEG
    21   NODEGRD1 204  206   1    5.0    33.2      6.833    5.0     33.2     20.5            NODEG
    22   NODEGRD2 404  406 100   22.0    33.2      6.833   22.0     33.2     20.5            NODEG
    23   NODEGRD1 404  406   1   22.0    33.2      6.833   22.0     33.2     20.5            NODEG
    24   NODEGRD2 604  606 100   54.0    33.2      6.833   54.0     33.2     20.5            NODEG
    25   NODEGRD1 704  706   2   70.0    33.2     10.25    70.0     33.2     20.5            NODEG
    26   NODEGRD211041106 100  134.0    33.2     10.25   134.0     33.2     20.5             NODEG
    27   NODEG      104  106   1   -1.205  33.2      6.833   -3.615  33.2     20.5           NODEG
    28   NODEG      117  119   1   -1.205  27.2      6.833   -3.615  27.2     20.5           NODEG
    29   NODEGRD1 107  110   1   -3.615  49.0     20.5     -9.70    49.0     55.0            NODEG
    30   NODEGRD2 407  410 100   22.0    49.0     20.5     22.0     49.0     55.0            NODEG
    31   NODEGRD1 407  410   1   22.0    49.0     20.5     22.0     49.0     55.0            NODEG
    32   NODEGRD211071110 100  134.0    49.0     20.5    134.0     49.0     55.0             NODEG
    33   NODEGRD1 110  116   1   -9.70   49.0     55.0     -9.70     0.0     55.0            NODEG
    34   NODEGRD2 410  416 100   22.0    49.0     55.0     22.0      0.0     55.0            NODEG
    35   NODEGRD1 410  416   1   22.0    49.0     55.0     22.0      0.0     55.0            NODEG
    36   NODEGRD211101116 100  134.0    49.0     55.0    134.0      0.0     55.0             NODEG
    37   NODEG      120  121   1   -5.642  38.1     32.0     -5.642   27.2     32.0           NODEG
    38   NODEG      122  123   1   -7.670  38.1     43.5     -7.670   27.2     43.5           NODEG
    39   NODEG      716  816 100   63.0     0.0     55.0     93.0      0.0     55.0          NODEG
    40   NODEG      715  815 100   70.5    12.990   55.0     86.5     12.990   55.0          NODEG
    41   NODEG      9151115 100  102.0    11.067   55.0    134.0     11.067   55.0           NODEG
    42   NODEG     10131063  50  106.933  22.133   55.0    129.067   22.133   55.0           NODEG
    43   NODEG     10111111 100  118.0    33.2     55.0    134.0     33.2     55.0           NODEG
    44   NODEG     10121014   2  110.175  29.958   55.0    110.175   14.308   55.0           NODEG
    45   NODEG      9141113 199  102.0    15.0     55.0    134.0     22.133   55.0           NODEG
    46   NODEGRD112001203   1  157.5     0.0      0.0    157.5     33.2      0.0             NODEG
    47   NODEGRD212081211   4  168.5     0.0     20.5    168.5     33.2     20.5             NODEG
    48   NODEG     12121220   4  168.5    49.0     20.5    145.5     49.0     43.5           NODEG
    49   NODEGRD112131217   4  157.0     0.0     32.0    145.5      0.0     43.5             NODEG
    50   NODEGRD212151219   1  157.0    33.2     32.0    145.5     33.2     43.5             NODEG
    51   END                                                                                 END
    52   RESTG      1001200 100101010                                                        RESTG
    53   RESTG      650        101010                                                        RESTG
    54   RESTG     12041208   4101010                                                        RESTG
```

Table C.1 (cont.)

```
                                   *** STARDYNE 3.0      INPUT ***
         /------------------------------- CARD  IMAGE  -----------------------------------/
         1  4    8   12   16   20   24   28   32   36   40   44   48   52   56   60   64   68   72   76   80
         .  .    .    .    .    .    .    .    .    .    .    .    .    .    .    .    .    .    .    .    .
CARD NO  *********************************************************************************        CARD TYPE
    55   RESTG      116 916 100101010                                                              RESTG
    56   END                                                                                       END
    57   WGHT       100     122.        122.        122.                                           WGHT
    58   WGHT       102     243.        243.        243.                                           WGHT
    59   WGHT       106      61.         61.         61.                                           WGHT
    60   WGHT       107      61.         61.         61.                                           WGHT
    61   WGHT       206      61.         61.         61.                                           WGHT
    62   WGHT       207      61.         61.         61.                                           WGHT
    63   WGHT       306      61.         61.         61.                                           WGHT
    64   WGHT       307      61.         61.         61.                                           WGHT
    65   WGHT       406      61.         61.         61.                                           WGHT
    66   WGHT       407      61.         61.         61.                                           WGHT
    67   WGHT       716      22.3        22.3        22.3                                          WGHT
    68   WGHT       715      44.7        44.7        44.7                                          WGHT
    69   WGHT       815      44.7        44.7        44.7                                          WGHT
    70   WGHT       816      22.3        22.3        22.3                                          WGHT
    71   WGHT       416      10.3        10.3        10.3                                          WGHT
    72   WGHT       415      20.6        20.6        20.6                                          WGHT
    73   WGHT       414      20.6        20.6        20.6                                          WGHT
    74   WGHT       413      10.3        10.3        10.3                                          WGHT
    75   WGHT       513      10.3        10.3        10.3                                          WGHT
    76   WGHT       613      10.3        10.3        10.3                                          WGHT
    77   WGHT       614      20.6        20.6        20.6                                          WGHT
    78   WGHT       615      20.6        20.6        20.6                                          WGHT
    79   WGHT       616      10.3        10.3        10.3                                          WGHT
    80   WGHT      1011      29.4        29.4        29.4                                          WGHT
    81   WGHT      1012      19.6        19.6        19.6                                          WGHT
    82   WGHT      1013      19.6        19.6        19.6                                          WGHT
    83   WGHT      1014      19.6        19.6        19.6                                          WGHT
    84   WGHT      1015      29.4        29.4        29.4                                          WGHT
    85   WGHT      1113      39.2        39.2        39.2                                          WGHT
    86   END                                                                                       END
    87   BEAMG        1    5 103 100 203 100 100    1    1                                         BEAMG
    88   BEAMG        6    7 603  50 653  50 100    1    1                                         BEAMG
    89   BEAMG        8   12 703 100 803 100 100    1    1                                         BEAMG
    90   BEAMG       13   15 100   1 101   1 504    1    2                                         BEAMG
    91   BEAMG       16   18 400   1 401  11200     1    3                                         BEAMG
    92   BEAMG       19   21 600   1 601  11200     1    3                                         BEAMG
    93   BEAMG       22   24 700   1 701  11200     1    3                                         BEAMG
    94   BEAMG       25   27 900   1 901  11200     1    4                                         BEAMG
    95   BEAMG       26   301100  11101   11200     1    3                                         BEAMG
    96   BEAMG       31   34 112   1 113   1 616    1    5                                         BEAMG
    97   BEAMG       35      716     715     616    1    5                                         BEAMG
    98   BEAMG       36      715     815     916    1    5                                         BEAMG
    99   BEAMG       37      815     816     916    1    6                                         BEAMG
   100   BEAMG       38   43 910   1 911   11010    1    7                                         BEAMG
   101   BEAMG       44   471011   11012   11013    1    5                                         BEAMG
   102   BEAMG       48     1015    1063    1013    1    6                                         BEAMG
   103   BEAMG       49     1063    1013    1013    1    6                                         BEAMG
   104   BEAMG       50   55 100 100 200 100 103    1   12                                         BEAMG
   105   BEAMG       59     1100    1200     103    1   13                                         BEAMG
   106   BEAMG       60      204     203     103    2   14                                         BEAMG
   107   BEAMG       61       10     103     304    2    7                                         BEAMG
   108   BEAMG       62       20     203     616    2   10                                         BEAMG
```

Table C.1 (cont.)

```
                                         *** STARDYNE 3.0     INPUT ***
               /----------------------------------- CARD  IMAGE --------------------------------------/
               1  4   8  12  16  20  24  28  32  36  40  44  48  52  56  60  64  68  72  76  80
               *  *   *   *   *   *   *   *   *   *   *   *   *   *   *   *   *   *   *   *   *
CARD NO        ****************************************************************************************    CARD TYPE
    109  BEAMG         63        30        104       406   2  11                                           BEAMG
    110  BEAMG         64        40        204       606   2  12                                           BEAMG
    111  END                                                                                               END
    112  BPROP1         1  14.69      126.28      90.86       80.04                                        BPROP
    113  BPROP1         2   7.50        3.86      41.87        1.41                                        BPROP
    114  BPROP1         3   1.57        0.03      14.60        4.09                                        BPROP
    115  BPROP1         4   1.92        0.04      37.25        4.09                                        BPROP
    116  BPROP1         5   6.61        4.73      40.15        1.67                                        BPROP
    117  BPROP1         6   3.75        1.75       7.81        0.70                                        BPROP
    118  BPROP1         7   5.50        8.59      41.11        6.83                                        BPROP
    119  BPROP1         8   3.75        1.75       7.81        0.70                                        BPROP
    120  BPROP1         9   5.52        4.84      20.58       11.12                                        BPROP
    121  BPROP1        10   5.52        4.84      22.52       31.60                                        BPROP
    122  BPROP1        11   5.52        4.84      23.92       13.14                                        BPROP
    123  BPROP1        12   5.52        4.84      21.11       35.77                                        BPROP
    124  BPROP1        13   0.79        0.02       7.30        2.05                                        BPROP
    125  BPROP1        14   0.11        0.11       3.11        0.11                                        BPROP
    126  END                                                                                               END
    127  TRIA6          1      112       111       122        1  1  1.5                                    TRIA6
    128  TRIA6          2      603       653       604              1.25                                   TRIA6
    129  TRIA6          3      653       703       704              1.25                                   TRIA6
    130  TRIA6          4     1109      1220      1110              1.75                                   TRIA6
    131  END                                                                                               END
    132  QUAD8          1      102       103       104       117        1    1  1.5          2             QUAD8
    133  QUAD8          2      117       104       105       118                                           QUAD8
    134  QUAD8          3      118       105       106       119                                           QUAD8
    135  QUAD8          4      119       106       120       121                                           QUAD8
    136  QUAD8          5      121       120       122       123                                           QUAD8
    137  QUAD8          6      123       122       112       113                                           QUAD8
    138  QUAD8          7      106       107       108       120                                           QUAD8
    139  QUAD8          8      120       108       109       122                                           QUAD8
    140  QUAD8          9      122       109       110       111                                           QUAD8
    141  QUAD8         10   14 100 100 200 100 201 100 101 100            1.125                            QUAD8
    142  QUAD8         15   16 600  50 650  50 651  50 601  50                                             QUAD8
    143  QUAD8         17   21 700 100 800 100 801 100 701 100                                             QUAD8
    144  QUAD8         22   26 101 100 201 100 202 100 102 100                                             QUAD8
    145  QUAD8         27   28 601  50 651  50 652  50 602  50                                             QUAD8
    146  QUAD8         29   33 701 100 801 100 802 100 702 100                                             QUAD8
    147  QUAD8         34   38 102 100 202 100 203 100 103 100                                             QUAD8
    148  QUAD8         39   40 602  50 652  50 653  50 603  50                                             QUAD8
    149  QUAD8         41   45 702 100 802 100 803 100 703 100                                             QUAD8
    150  QUAD8         46   50 103 100 203 100 204 100 104 100            1.25                             QUAD8
    151  QUAD8         51   55 104 100 204 100 205 100 105 100                                             QUAD8
    152  QUAD8         56      604       653       704       605                                           QUAD8
    153  QUAD8         57   60 703 100 803 100 804 100 704 100                                             QUAD8
    154  QUAD8         61     1103      1203      1207      1104                                           QUAD8
    155  QUAD8         62   66 105 100 205 100 206 100 106 100            1.75                             QUAD8
    156  QUAD8         67      605       704       706       606                                           QUAD8
    157  QUAD8         68   71 704 100 804 100 806 100 706 100            1.25                             QUAD8
    158  QUAD8         72     1104      1207      1211      1106                                           QUAD8
    159  QUAD8         73   82 106 100 206 100 207 100 107 100            0.50                             QUAD8
    160  QUAD8         83     1106      1211      1212      1107                                           QUAD8
    161  QUAD8         84   93 107 100 207 100 208 100 108 100            1.75                             QUAD8
    162  QUAD8         94     1107      1212      1216      1108                                           QUAD8
```

Table C.1 (cont.)

```
                                   *** STARDYNE 3.3      INPUT ***
          /-------------------------------- CARD  IMAGE ---------------------------------/
          1  4   8  12  16  20  24  28  32  36  40  44  48  52  56  60  64  68  72  76  80
          .  .   .   .   .   .   .   .   .   .   .   .   .   .   .   .   .   .   .   .   .
CARD NO   ................................................................................   CARD TYPE
    163   QUAD8     95 104 108 100 208 100 209 100 109 100                                   QUAD8
    164   QUAD8    105    1108    1216    1220    1109                                       QUAD8
    165   QUAD8    106 115 109 100 209 100 210 100 110 100                                   QUAD8
    166   QUAD8    116 125 110 100 210 100 211 100 111 100        1.50                       QUAD8
    167   QUAD8    126 134 111 100 211 100 212 100 112 100                                   QUAD8
    168   QUAD8    135    1011    1111    1113    1063                                       QUAD8
    169   QUAD8    136 144 112 100 212 100 213 100 113 100                                   QUAD8
    170   QUAD8    145    1063    1113    1115    1015                                       QUAD8
    171   QUAD8    146 148 113 100 213 100 214 100 114 100                                   QUAD8
    172   QUAD8    149 152 613 100 713 100 714 100 614 100                                   QUAD8
    173   QUAD8    153 155 114 100 214 100 215 100 115 100                                   QUAD8
    174   QUAD8    156 159 614 100 714 100 715 100 615 100                                   QUAD8
    175   QUAD8    160 162 115 100 215 100 215 100 116 100                                   QUAD8
    176   QUAD8    163 164 615 200 715 200 716 200 616 200                                   QUAD8
    177   QUAD8    165 1671200   11204   11205   11201   1                                   QUAD8
    178   QUAD8    168 1701204   11208   11209   11205                                       QUAD8
    179   QUAD8    171 1731213   11209   11210   11214   1                                   QUAD8
    180   QUAD8    174 1761217   11213   11214   11216                                       QUAD8
    181   QUAD8    177 1781115  -21217   11216   11113  -2                                   QUAD8
    182   QUAD8    179    1111    1219    1220    1110                                       QUAD8
    183   QUAD8    180     900     901     915     915            0.25                       QUAD8
    184   QUAD8    181     901    1001    1015     915                                       QUAD8
    185   END                                                                                END
    186   ENDGEOM                                                                            ENDGE
    187    LANCZOS MODAL EXTRACTION  REFINED HULLMODEL ANTISYMMETRIC MODES                    LANC
    188   DYNAMIC                                       42  53     300  -.1                  DYNAM
    189   ENDMODEL                                                                           ENDMO
```

Table C.2 STAR Output Data

```
*****************************************************************************************************
*****************************************************************************************************
*                 * T I M E   E S T I M A T E S   F O R   A   S T A T I C   A N A L Y S I S *       *
*                                                                                                   *
*                 ESTIMATED TIME      =   209.5        (DECIMAL)  *    81.2   PER LOAD CASE (FULL PROCESSING) *
*                                                        -OR-     *     5.0   PER LOAD CASE (DISP.VECTOR ONLY) *
*                                                                                                   *
*                 TOTAL TIME   IF    1  LOAD CASE  =    304.3  (DECIMAL)  (FULL OUTPUT PROCESSING)  *
*                 TOTAL TIME   IF    5  LOAD CASE  =    629.9  (DECIMAL)  (FULL OUTPUT PROCESSING)  *
*                 TOTAL TIME   IF   10  LOAD CASE  =   1027.4  (DECIMAL)  (FULL OUTPUT PROCESSING)  *
*                                                                                                   *
*     **NOTE** ADD 0.18         PER (THERMALLY OR PRESSURE LOADED) QUADRILATERAL TO GENERATE CONSISTENT LOAD VECTOR *
*     **NOTE** ADD 0.06   PER (INTERMEDIATELY LOADED) BEAM TO GENERATE EQUIV. LOAD VECTOR AND STRESS DISTRIBUTION *
*                                                                                                   *
*                 STATIC MATRIX SIZE (DOF)  =  1203                                                 *
*                 STATIC MATRIX BAND (DOF)  =   129                                                 *
*****************************************************************************************************
*                * T I M E   E S T I M A T E S   F O R   A   D Y N A M I C   A N A L Y S I S *      *
*            LANCZOS AND INVITR MATRIX SIZES ARE THE SAME AS STATIC.                                *
*        *WARNING* MAX NODE NO  OR  DYNAMIC DOF  TOO LARGE  FOR  HQR  ANALYSIS.                     *
*     **WARNING** INVERSE ITERATION TIME IS VERY PROBLEM DEPENDENT.                                 *
*                                                                                                   *
*        *****************************************************************************************  *
*        *               *             TOTAL TIME (DECIMAL) IF             *  ADDITIONAL TIME      *  *
*        *               *                                                 *  IF        -OR-  IF   *  *
*        * NUMBER OF     *          EIGENVECTOR ONLY IS OUTPUT             *  COMPOSITE  * ALL POSSIBLE *  *
*        *               *                 *              *                *  DAMPING IS *  OUTPUT IS  *  *
*        * EIGENVECTORS  *      LANCZOS    *   HQR/GUYAN  *     INVITR     * COMPUTED ALSO* COMPUTED ALSO*  *
*        *               *                 *              *                *  (ANY METHOD)* (ANY METHOD)*  *
*        *****************************************************************************************  *
*        *         1     *         293.7   *        0.0   *        382.2   *      51.1   *      76.2  *  *
*        *         2     *         316.5   *        0.0   *        568.9   *     102.2   *     152.5  *  *
*        *         5     *         397.6   *        0.0   *       1129.0   *     255.4   *     381.2  *  *
*        *        10     *         538.2   *        0.0   *       2062.5   *     510.8   *     762.3  *  *
*        *        25     *        1054.5   *        0.0   *       4863.0   *    1276.9   *    1905.8  *  *
*        *        50     *        2211.6   *        0.0   *       9530.4   *    2553.8   *    3811.7  *  *
*        *        75     *        3764.0   *        0.0   *      14197.9   *    3830.7   *    5717.5  *  *
*        *       100     *        5576.0   *        0.0   *      18865.4   *    5107.7   *    7623.4  *  *
*        *       125     *        7996.0   *        0.0   *      23532.8   *    6384.6   *    9529.2  *  *
*        *       150     *       10562.7   *        0.0   *      28200.3   *    7661.5   *   11435.0  *  *
*****************************************************************************************************
*        * T I M E   S A V E D   I F   R E S T A R T   F I L E S   E N T E R E D *                  *
*                                                                                                   *
*        TAPE7     ANY METHOD                     TIME SAVED =      111.9                           *
*        TAPE9     STATIC,LANCZOS,INVITR          TIME SAVED =       67.9                           *
*        TAPE9     HQR                            TIME SAVED =        0.0                           *
*        TAPE28    HQR                            TIME SAVED =        0.0                           *
*                                                                                                   *
*     **NOTE**  IF TAPE9 IS SUPPLIED FOR STATIC OR LANCZOS, THEN INCLUDE THE TAPE7 TIME SAVED ALSO.  *
*****************************************************************************************************
*     **NOTE** TIME ESTIMATES ASSUME THAT INPUT IS ON TAPE2 AND THAT MAXIMUM OUTPUT OPTIONS ARE REQUESTED. *
*     **NOTE** ADD RENUMBERING AND/OR PLOT TIME TO ESTIMATES IF THEY ARE TO BE PERFORMED ON NEXT RUN. *
*     **NOTE** BEFORE CODING  TIME LIMIT , ADD  20  PERCENT TO TIME ESTIMATE.                       *
*****************************************************************************************************
```

Table C.2 (cont.)

```
            LANCZOS MODAL EXTRACTION  REFINED HULLMODEL ANTISYMMETRIC MODES

                          M O D A L   E X T R A C T I O N   D A T A

                                                                                    --- M O D A L   W E I G H T S ---
MODE   EIGENVALUE       NATURAL                 GENERALIZED    MAX TRANSLATION    (GEN. WGT. * PARTICIPATION FACTORS**2)
 NO    (OMEGA**2 )     FREQUENCY     PERIOD       WEIGHT       NODE-DOF  VALUE          X1             X2             X3


  1   -.137568E-04       -.001       0.0000      3145.49       210-2    1.0000      13.14368     4638.00735      208.23380      12.0
  2   -.617524E-05       -.000       0.0000      3057.69      1203-2    1.0000      70.60863      413.58053     2476.49220      12.0
  3    .140561E-03        .002     529.3623      2178.24      1211-2    1.0000    1037.39054        5.53460      155.07019      12.0
  4    71137.2          42.449        .0236      1632.37       121-3    1.0000      52.27819         .00000      793.04426      12.0
  5    119834.          55.095        .0182      293.755      1217-3    1.0000      74.05392         .00000      477.83959      12.0
  6    176902.          66.940        .0149      191.536       513-3    1.0000        .90923         .00000        5.89476      12.0
  7    206535.          72.330        .0138      715.551      1217-3    1.0000       9.94232         .00000      106.60840      12.0
  8    292218.          86.035        .0116      90.9340      1213-1    1.0000     140.00204         .00000        3.03341      12.0
  9    314989.          89.324        .0112      130.294       414-3    1.0000       4.32891         .00000        9.91946      12.0
 10    419327.         103.062        .0097      1732.60       904-3    1.0000     155.24525         .00000       27.39351      12.0
 11    510074.         113.668        .0088      967.574       806-2    1.0000      41.65783         .00000        2.03292      12.0
 12    718454.         134.902        .0074      174.534       513-3    1.0000       4.08065         .00000       50.92993      12.0
 13    .102820E+07     161.384        .0062      584.794      1213-1    1.0000       1.12250         .00000       14.42944      12.0
 14    .107945E+07     165.356        .0060      703.504      1213-1    1.0000     199.36722         .00000        2.02755      12.0
 15    .115845E+07     171.300        .0058      305.418       513-3    1.0000      54.12520         .00000         .02284      12.0
 16    .119889E+07     174.265        .0057      316.101       513-3    1.0000        .06847         .00000        3.96806      12.0
 17    .137256E+07     186.460        .0054      175.159       513-3    1.0000       1.88195         .00000        1.56549      12.0
 18    .157609E+07     199.807        .0050      275.642      1012-3    1.0000     191.70674         .00000       36.45601      12.0
 19    .171842E+07     208.634        .0048      156.504      1213-3    1.0000      22.00415         .00000       19.24922      12.0
 20    .179578E+07     213.337        .0047      485.470       408-2    1.0000      10.90907         .00000        2.00928      12.0
 21    .185695E+07     216.880        .0046      101.992       121-1    1.0000      65.40265         .00000         .51886      12.0
 22    .210604E+07     230.969        .0043      221.377       121-1    1.0000       3.35402         .00000         .02240      12.0
 23    .217824E+07     234.895        .0043      379.777       121-1    1.0000     428.07457         .00000        2.27610      12.0
 24    .235461E+07     244.219        .0041      106.383       121-1    1.0000     112.66265         .00000        9.19716      12.0
 25    .249946E+07     251.619        .0040      400.887       615-3    1.0000      86.92832         .00000         .17256      12.0
 26    .261512E+07     257.375        .0039      410.666       801-3    1.0000     612.34816         .00000        4.16041      12.0
 27    .265749E+07     259.451        .0039      312.776      1008-2    1.0000       4.26714         .00000       24.18750      12.0
 28    .278092E+07     265.408        .0038      142.259       121-1    1.0000      81.59104         .00000        3.32971      12.0
 29    .294327E+07     273.046        .0037      115.843       501-3    1.0000     166.12637         .00000         .86188      12.0
 30    .315699E+07     282.785        .0035      171.303       501-3    1.0000       4.29417         .00000        5.17309      12.0
 31    .324554E+07     286.724        .0035      204.111       121-1    1.0000      43.29610         .00000        2.39615      12.0
 32    .344953E+07     295.597        .0034      1663.42       708-2    1.0000      83.25653         .00000       18.66659      12.0
 33    .348557E+07     297.137        .0034      49.9514       601-3    1.0000        .00346         .00000        7.38764      12.0

                  THE FOLLOWING ARE APPROX. EIGENVALUES  FOR WHICH MODES WERE NOT REQUESTED.

 34    .360197E+07     302.058                                                                                                12.0
 35    .399177E+07     317.982                                                                                                12.0
 36    .412578E+07     323.276                                                                                                12.0
 37    .426556E+07     328.707                                                                                                12.0
 38    .447716E+07     336.761                                                                                                12.0
 39    .455350E+07     339.620                                                                                                12.0
 40    .473174E+07     346.203                                                                                                12.0
 41    .505377E+07     357.790                                                                                                12.0
 42    .525094E+07     364.702                                                                                                12.0
 43    .536616E+07     368.682                                                                                                12.0
 44    .597117E+07     388.911                                                                                                11.7
 45    .614149E+07     394.418                                                                                                10.0
 46    .625792E+07     398.139                                                                                                 9.1
 47    .631828E+07     400.055                                                                                                 8.6
 48    .670769E+07     412.196                                                                                                 7.0
 49    .686755E+07     417.082                                                                                                 6.7
 50    .713789E+07     425.211                                                                                                 5.5
 51    .732465E+07     430.744                                                                                                 4.0
```

Table C.2 (cont.)

```
  *     *     *     *     *     *     *     *     *     *     *     *     *     *     *     *     *     *
                      MODE SHAPE (EIGENVECTOR)
MODE NUMBER     9 .  FREQUENCY      =         89.323973      ,  GENERALIZED WEIGHT =          130.29389
                                   *MAXIMUM ROTATION     IS AT NODE    416 *DOF = 4 VALUE =   .895910E-01
                                   *MAXIMUM TRANSLATION IS AT NODE    414 *DOF = 3 VALUE =   .100090E+01
              *********** TRANSLATIONS         ***********          ********** ROTATIONS (RADIANS) **********
 NODE              X1                X2                X3                X4                X5                X6
  10          .009799087        .041277151       -.003125769        .003087086       -.000266241       -.000117729
  20          .009970670        .040581020       -.003670419        .002733470       -.000199151       -.000162046
  30          .007911492        .018570620        .003151676        .003784228        .000035956        .000045297
  40          .006909716        .019560475       -.000335993        .003365958       -.000131827        .000239323
 100         0.000000000        .042959066       0.000000000       -.003777471       0.000000000       -.000351571
 101          .003442542        .042445029       -.037296065       -.002550371       -.000887197       -.000251577
 102          .006574669        .041730831       -.047329277        .001163272       -.000796293       -.000462694
 103          .009210461        .041277110       -.018561200        .003087086       -.000266241       -.000117718
 104          .008137993        .018570602       -.015769458        .003784224        .000035956        .000045305
 105          .007860477       -.008939247       -.015446649        .003611100       -.000276656        .000753279
 106          .008091006       -.032647814       -.018304466        .002345256        .001305550        .002153175
 107         -.010058706       -.035602659       -.026618015       -.000105645       -.000169588        .000639277
 108         -.008182845       -.032647278       -.028185466        .000004783        .000008795       -.000890457
 109         -.006628998       -.029288834       -.029588249       -.000070494        .000648596       -.000611277
 110         -.008243786       -.020382431       -.031312672       -.000679190       -.000080224        .000405059
 111         -.006658802       -.020422928       -.025141990       -.000379720       -.005228382        .001822891
 112         -.005962063       -.020118358       -.019936608       -.001202098       -.014019669        .000324249
 113         -.003963465       -.019924435       -.009769692       -.001301506       -.021606298        .000802087
 114         -.002894974       -.020069617       -.000284333       -.000861408       -.023179357       -.000037630
 115         -.001548501       -.020180556        .002894403        .000058023       -.014617007        .000233163
 116         0.000000000       -.020227536       0.000000000        .000495123       0.000000000        .000167837
 117          .008087069        .019091000       -.035509510        .000139333        .000425863       -.000758163
 118          .012462992       -.009210546       -.035778199       -.000032732        .000679642        .000185624
 119          .020332226       -.030344151       -.027146214       -.000447947        .002384778        .001364240
 120          .015355481       -.033796338       -.020269078        .001324899        .001474423        .004499924
 121          .063930994       -.034438455       -.008514478       -.000772110        .004411572        .004942147
 122          .030182239       -.029063684       -.017429076        .000525625        .000340519        .006441453
 123          .097535129       -.028564549        .001010521        .003472393       -.000674181        .008370295
 200         0.000000000        .041247667       0.000000000       -.003349401       0.000000000       -.000318608
 201          .003502990        .041104331       -.033111632       -.002288021       -.000977451       0.000000000
 202          .006642498        .040778835       -.042213076        .000950587       -.001265070       0.000000000
 203          .009160451        .040580960       -.017337776        .002733473       -.000199151       -.000162040
 204          .008106335        .019560455       -.017165764        .003365959       -.000131627        .000239326
 205          .008347862       -.003980154       -.017018533        .003342196       0.000000000        .000557196
 206          .008070014       -.026526330       -.016332866        .003313977       -.000079735        .000683996
 207         -.009840074       -.026532556       -.030060839        .002562452        .000739201        .000900414
 208         -.008176366       -.051919855       -.029941400        .001869930       0.000000000       -.002760010
 209         -.006951377       -.057758155       -.029517040       -.000325853       0.000000000       -.004330531
 210         -.007642018       -.017793845       -.029234670       -.006499989       -.000524933       -.000917040
 211         -.006694874       -.017928741        .059669803       -.013704973       -.009066841       0.000000000
 212         -.005553381       -.018097499        .178498516       -.013856705       -.021171032       0.000000000
 213         -.004408817       -.018269913        .269374926       -.006860657       -.029872714       0.000000000
 214         -.003022036       -.018428875        .272438430        .005638172       -.030283785       0.000000000
 215         -.001578315       -.018493562        .177039979        .017793666       -.019095792       0.000000000
 216         0.000000000       -.016493501       0.000000000        .022644637       0.000000000       0.000000000
 300         0.000000000        .038918884       0.000000000       -.002471460       0.000000000       -.000247865
 301          .003477732        .038911612       -.024691131       -.001678191       -.001113826       0.000000000
 302          .006636297        .038914760       -.032201468        .000472492       -.001205264       0.000000000
 303          .009295058        .038902474       -.016372745        .002087240       -.000059511       -.000227434
 304          .008631628        .021833276       -.016580799        .002842781       0.000000000        .000238539
 305          .008134673        .001207601       -.015637336        .002978958       0.000000000        .000720293
 306          .007871939       -.013126562       -.016773603        .002504802        .000282131        .001091649
 307         -.001384537       -.016321621       -.031303204        .005003808        .000816243        .006994136
 308         -.003396053       -.072076951       -.030597675        .004995605       0.000000000       -.001515553
```

Table C.2 (cont.)

309	-.007344149	-.092068724	-.035274634	-.001042933	0.000000000	-.002957394
310	-.007378121	-.016172201	-.029752429	-.013431500	.000394600	-.000519200
311	-.006011434	-.015171805	.145476275	-.028273074	-.006222306	0.000000000
312	-.005635524	-.016364393	.360255142	-.028559466	-.016403677	0.000000000
313	-.004745849	-.016618088	.576005860	-.014700996	-.027351367	0.000000000
314	-.003273239	-.016784944	.607408745	.012049524	-.035164134	0.000000000
315	-.001555262	-.016756320	.394040171	.039770609	-.023985152	0.000000000
316	0.000000000	-.016740628	0.000000000	.051599601	0.000000000	0.000000000
400	0.000000000	.036719001	0.000000000	-.001694372	0.000000000	-.000287924
401	.003433375	.036745081	-.016958017	-.001206252	-.000703906	-.000310717
402	.006639667	.036793982	-.023964367	.000018451	-.000749662	-.000269103
403	.009524631	.036793964	-.015942347	.001414775	-.000056263	-.000261961
404	.008860619	.023971300	-.016042029	.002226325	0.000000000	.000190992
405	.008260455	.007697172	-.016143979	.002440439	0.000000000	.000211622
406	.007768250	-.003558558	-.016153870	.002303728	.001067525	.001210242
407	-.010034169	-.009198500	-.032467571	.006363209	-.000748498	.000685533
408	-.003551955	-.075975961	-.032270274	.004978210	0.000000000	.000750216
409	-.007607753	-.102664672	-.031686536	-.001260406	0.000000000	.000673070
410	-.006671760	-.014677207	-.030717755	-.017397352	-.002988269	.000050661
411	-.006637348	-.015054947	.189634492	-.035974117	-.005882599	0.000000000
412	-.006343441	-.015131798	.491952663	-.045974255	-.000493113	0.000000000
413	-.005396399	-.015174667	.799942734	-.039064530	-.007075260	0.000000000
414	-.003220718	-.014887106	1.000000000	.007425189	-.047916535	0.000000000
415	-.001611068	-.014816436	.685523171	.065465666	-.036589566	0.000000000
416	0.000000000	-.014811551	0.000000000	.084591007	0.000000000	0.000000000
500	0.000000000	.033053075	0.000000000	-.001175116	0.000000000	-.000281272
501	.003440567	.033071769	-.012334621	-.000908368	-.000302780	0.000000000
502	.006779760	.033100057	-.018655130	-.000169562	-.000398506	0.000000000
503	.009966929	.033062244	-.014771966	.000839492	-.000121266	-.000293649
504	.008995240	.026521282	-.014536039	.000482694	0.000000000	.000126945
505	.008022210	.016906215	-.014430762	.001194025	0.000000000	.000666467
506	.007280569	.010951451	-.014324443	.001097915	-.000696462	.001174794
507	-.007406629	.010506300	-.035085629	.004564668	.000302053	.001745449
508	-.008202311	-.037191460	-.035332245	.003599648	0.000000000	.003630863
509	-.007942057	-.058777607	-.035209629	-.000314918	0.000000000	.004745739
510	-.006757197	-.014782733	-.034737676	-.008655671	.004666979	.000605769
511	-.007240240	-.014967652	.076846648	-.018316680	.013455305	0.000000000
512	-.006958229	-.015158986	.235939326	-.022212970	.027776469	0.000000000
513	-.007251608	-.015308116	.419229677	-.026570574	.038793674	0.000000000
600	0.000000000	.029008740	0.000000000	-.000794114	0.000000000	-.000321777
601	.003523047	.029011921	-.008173029	-.000626618	-.000281546	-.000316995
602	.007017616	.029010560	-.012974072	-.000210937	-.000417557	-.000312608
603	.010435949	.028965723	-.012632997	.000262352	-.000202950	-.000320108
604	.008580848	.027536512	-.011427649	-.000176713	0.000000000	.000504383
605	.007222863	.028413348	-.011471912	-.000111343	0.000000000	.002460379
606	.005918236	.029115232	-.011295866	-.000168505	-.000923630	.000939233
607	-.006755233	.028942905	-.036954666	-.000009868	.000188628	.001393535
608	-.006923531	.026488717	-.037652559	.000318563	0.000000000	.003747661
609	-.008011977	.017414140	-.038114541	.001362114	0.000000000	.004609635
610	-.008455098	-.014895966	-.038340815	.005961663	.000676158	.000777673
611	-.008466763	-.015147489	-.108540865	.011680098	.007995968	0.000000000
612	-.008085507	-.015450014	-.196503138	.012992070	.018331551	0.000000000
613	-.007476446	-.015810608	-.297022055	.016757134	.024402594	0.000000000
614	-.005630235	-.016606858	-.425270501	-.000713276	.000442409	0.000000000
615	-.003038998	-.017163059	-.306356956	-.027592247	-.005002763	0.000000000
616	0.000000000	-.017617694	0.000000000	-.041043465	0.000000000	0.000000000
650	0.000000000	.024547513	0.000000000	-.000504945	0.000000000	0.000000000
651	.003638075	.024543030	-.004943394	-.000397653	-.000297567	0.000000000
652	.007278679	.024535839	-.008189339	-.000171132	-.000432697	0.000000000
653	.010979956	.024496516	-.009425959	-.000098247	-.000308524	-.000349146
700	0.000000000	.014715541	0.000000000	.000058107	0.000000000	-.000345767
701	.003752514	.014726201	.000321122	-.000034576	-.000030623	-.000340213
702	.0075341[illegible]	.014697414	-.000106473	-.000215613	-.000071156	-.000335096

Table C.2 (cont.)

703	.011351404	.019681604	-.004269713	-.000356723	-.000440093	-.000373151
704	.007394684	.029915584	-.006497245	-.001136537	0.000000000	.000013000
706	.003705225	.040675909	-.055155199	-.001111307	-.000005339	.000490555
707	-.002169274	.040646354	-.035584447	-.002906750	-.000093168	.000482351
708	-.004883719	.067102313	-.036525033	-.001584345	0.000000000	.001281236
709	-.007978066	.062876467	-.037062550	.002739692	0.000000000	.001286404
710	-.011267394	-.012744721	-.037252392	.012509968	-.000333684	.000269120
711	-.010180473	-.013032084	-.178735448	.021828566	.000630786	0.000000000
712	-.009043903	-.013112775	-.343149633	.019675339	.001181099	0.000000000
713	-.007569215	-.013036755	-.458329094	.005121341	.000550754	0.000000000
714	-.005838668	-.012692356	-.463631935	-.010769176	-.002388815	0.000000000
715	-.005048641	-.012389294	-.411666350	-.021194455	-.002276523	.000236035
716	0.000000000	-.014411955	0.000000000	-.038416447	0.000000000	.000420351
800	0.000000000	.014637601	0.000000000	.001234656	0.000000000	-.000432714
801	.003905631	.014526317	.010232204	.000540160	-.000758040	0.000000000
802	.007697583	.014574931	.009814638	-.000574266	-.000657757	0.000000000
803	.011672827	.014575862	.002401842	-.000524938	-.000569759	-.000388022
804	.006373166	.026827425	.000949838	-.001493264	0.000000000	-.000305952
806	.000908065	.042428040	.001312840	-.001635324	-.000340262	-.000218448
807	.003143415	.042284584	-.029704742	-.002712283	-.000452311	-.000424040
808	-.002588091	.067028867	-.030595949	-.001209098	0.000000000	-.001060694
809	-.008103354	.058768337	-.030950224	.003014576	0.000000000	-.001549997
810	-.014062243	-.008673093	-.030853177	.009549062	-.002715465	-.000112738
811	-.011940254	-.008975877	-.131823203	.014214575	-.006059367	0.000000000
812	-.010041183	-.009119352	-.239989742	.011630603	-.011651743	0.000000000
813	-.008163299	-.009189022	-.305143433	.003881910	-.015919226	0.000000000
814	-.006095737	-.009448998	-.294982561	-.006476520	-.016866197	0.000000000
815	-.005334122	-.009529058	-.257971999	-.010396720	-.015921512	.000260831
816	0.000000000	-.007372870	0.000000000	-.017223214	0.000000000	.000461831
900	0.000000000	.008710012	0.000000000	.001695162	0.000000000	-.000399588
901	.003895103	.009273967	.015510322	.000806010	.000649702	-.000365961
902	.007812507	.009347173	.015642495	-.000403353	.000258913	-.000346602
903	.011775640	.009402176	.010521756	-.000532018	-.000618756	-.000383923
904	.005506939	.019570308	.010412517	-.001354714	0.000000000	-.000575405
906	-.001154826	.034602796	.010613050	-.001611534	-.000361789	-.000737532
907	.007804992	.034286870	-.019654903	-.001047784	-.000732641	-.000909869
908	-.000503671	.042760207	-.020336173	.000025212	0.000000000	-.001740018
909	-.008181695	.030142472	-.020541051	.002286568	0.000000000	-.001677002
910	-.016240849	-.003723246	-.020415957	.002687071	-.001659601	.000203706
911	-.013613910	-.004034290	-.040516969	.002048047	-.004298168	.000350473
912	-.011072519	-.004145310	-.052585227	.000681609	-.007943901	.000292972
913	-.008794850	-.004102868	-.050920614	-.001142931	-.010548389	.000247907
914	-.006535840	-.003839952	-.032196179	-.002539150	-.010416751	.000273268
915	-.005303789	-.003621030	-.022297930	-.002365771	-.009246513	.000359629
916	0.000000000	-.003798381	0.000000000	-.001676452	0.000000000	.000497845
1000	0.000000000	.003399633	0.000000000	-.002037684	0.000000000	-.000298054
1001	.004147910	.003263849	-.013861639	.000365132	.000226795	.001627390
1002	.007759405	.003293034	.005998274	.002163374	-.000079569	0.000000000
1003	.011687596	.003337336	.020510881	.000028793	-.000637413	-.000375045
1004	.004937512	.008689997	.020586355	-.000925328	0.000000000	-.000705843
1006	-.002245893	.019993782	.020641610	-.001313685	-.000603817	-.001075570
1007	.011191554	.019649675	-.006650602	.000043492	-.000970892	-.001112151
1008	.001142708	.017984517	-.007133643	.000501129	0.000000000	-.001378450
1009	-.008306761	.008871291	-.007115513	.001017715	0.000000000	-.000991495
1010	-.017625884	.000908382	-.006714230	-.000317167	-.000517634	.000246110
1011	-.012379612	.000792290	.017741761	-.002042086	-.002411379	.000268320
1012	-.010657639	-.001737893	-.002762745	-.001723129	-.004231595	.000370274
1013	-.003146174	-.002592257	-.008142676	-.001115416	-.005686653	.000249577
1014	-.006896350	-.001546786	.011796071	-.001006810	-.001500666	.000119740
1015	-.007566928	.000658369	.024407999	.001134052	-.002999999	.000256551
1063	-.011376372	.003330267	.056097070	-.001613552	-.001564042	.000228735
1100	0.000000000	-.002618514	0.000000000	.000821118	0.000000000	-.000344724
1101	.003719503	-.002578091	.004796440	.001000048	-.000080965	-.000356845

Table C.2 (cont.)

```
 1102        .007755931    -.002591931     .021630245     .001051669    -.000934494    -.000339460
 1103        .011459329    -.002584090     .030646606     .000531936    -.000636044    -.000365371
 1104        .004699444    -.003183014     .030950033    -.000334234    0.000000000    -.000687437
 1106       -.002692956     .001445157     .031232260    -.000495088    -.000184484    -.001327349
 1107        .013603084     .001086722     .007832252     .000141378    -.001199311    -.001101321
 1108        .001973161    -.000737632     .007843474     .000155748    0.000000000    -.001070676
 1109       -.008644027    -.002117707     .008135140    -.000112996    0.000000000    -.000666092
 1110       -.018585324     .005204607     .008332945    -.001302156    -.001069981     .000109464
 1111       -.013122400     .004441442     .037658079    -.002323765    -.000060008     .000229946
 1113       -.010502728     .003594590     .055559106    -.000471694     .001882135     .002629611
 1115       -.011677346     .003249587     .065675906    -.006759034     .008598967    -.006334357
 1200       0.000000000    -.011159505    0.000000000     .001441538    0.000000000    -.000469969
 1201        .003408066    -.011130364     .014605937     .001371725    -.000260573    -.000392330
 1202        .007564615    -.010594642     .029631541     .001430676    -.000424251    -.000124517
 1203        .011188570    -.010408591     .045126090     .000749659    -.000595548    -.000339400
 1204       0.000000000    -.027059378    0.000000000     .000299810    0.000000000     .000559738
 1205       -.001976926    -.026835105     .017557483     .000272434    -.001560683     .000507727
 1206        .000095265    -.026749192     .033167127     .000264012    -.000421692     .000649253
 1207        .004495244    -.026867906     .046374733     .001475683    -.000277253    -.000683627
 1208       0.000000000    -.042365506    0.000000000     .002427773    0.000000000     .004524967
 1209       -.042706223    -.042576817     .038583098     .004700261    -.010190165    -.000670257
 1210       -.020897257    -.042549205     .045192379    -.000484912    -.003397917    -.001345604
 1211       -.001244874    -.042373142     .051000528     .000218411    -.001656544    -.001487521
 1212        .015730309    -.042390416     .044661366    -.000423508    -.000649967    -.001088050
 1213       -.305341677    -.027222619    -.209410000     .014960911    -.006388002    -.014960911
 1214       -.109167067    -.027159317    -.035751032     .006734558    -.005014576    -.006734558
 1215       -.028702367    -.027004252     .022192057     .002451165    -.001647704    -.002451165
 1216        .002340435    -.026403229     .032002521     .000038214    -.001379628    -.001322969
 1217       -.275407234    -.011709200    -.183176743     .013812190     .010434320    -.013812190
 1218       -.094087267    -.011393273    -.022282762     .065849673     .007145345    -.005849673
 1219       -.023755304    -.011629734     .021213946     .001492667     .001530214    -.001492667
 1220       -.009117014    -.011584666     .014447352    -.000415165    -.000720156    -.001105038

MODAL PARTICIPATION FACTOR (X1) =  -1.8227503E-01     GEN.WT. TIMES MODAL PART. FACT. (X1) =  -2.3749373E+01
MODAL PARTICIPATION FACTOR (X2) =  -5.0825349E-10     GEN.WT. TIMES MODAL PART. FACT. (X2) =  -6.6222327E-08
MODAL PARTICIPATION FACTOR (X3) =  -2.7591925E-01     GEN.WT. TIMES MODAL PART. FACT. (X3) =  -3.5950599E+01
```

Table C.3 DYNRE2 Input Data

```
                         SSSSSSSSS   SS      SS  SS      SS  SSSSSSSSS   SSSSSSSSSS   SSSSSSSS
                         SSSSSSSSSS   SS    SS   SSS     SS  SSSSSSSSSS  SSSSSSSSSS  SSSSSSSSSS
                         SS      SS    SS  SS    SSSS    SS  SS      SS  SS          S       SS
     S   S               SS      SS     SSSS     SS SS   SS  SS      SS  SS                  SS   S   S
      S S                SS      SS      SS      SS  SS  SS  SSSSSSSSSS  SSSSSS            SSS     S S
  SSSSSSSSSS             SS      SS      SS      SS   SS SS  SSSSSSSSS   SSSSSS           SS    SSSSSSSSSS
      S S                SS      SS      SS      SS    SSSS  SS   SS     SS              SS        S S
     S   S               SS      SS      SS      SS     SSS  SS    SS    SS             SS        S   S
                         SSSSSSSSSS      SS      SS      SS  SS     SS   SSSSSSSSSS  SSSSSSSSSS
                         SSSSSSSSS       SS      SS      SS  SS      SS  SSSSSSSSSS  SSSSSSSSSS

**************************************************************
*                 **    DYNRE2   (R)  **                     *
*                 ** STARDYNE-3  (R)  **                     *
*                 ** ADD 01/001 LEVEL **                     *
**************************************************************
*  LATEST USER MANUAL  SEPT 1979                             *
*                                                            *
*                                                            *
*  RUN DATE      FRIDAY    , OCT.  3, 1980                   *
*                80/10/03,  DAY 277 OF 1980                  *
*  RUN TIME      13.47.15.                                   *
*                                                            *
*   CYBERNET          .           NOS 1       4800           *
*                                                            *
*  (R) 1970 STARDYNE    SYSTEM  OF MECHANICS RESEARCH INC    *
*  (R) 1971 STARDYNE-2  SYSTEM  OF MECHANICS RESEARCH INC    *
*  (R) 1974 STARDYNE-3  SYSTEM  OF MECHANICS RESEARCH INC    *
*  (R) 1977 STARDYNE-3  SYSTEM   BY SYSTEM DEVELOPMENT CORP  *
**************************************************************


**************************************************************
*          S T A R D Y N E    B U L L E T I N S              *
*                                                            *
*     A STARDYNE INFORMATION BULLETIN IS AVAILABLE           *
*   WHICH DESCRIBES IMPORTANT CHANGES CONCERNING THIS        *
*   RELEASE LEVEL OF THE PROGRAM.  IN ORDER TO ACCESS        *
*   THIS BULLETIN - ENTER THE FOLLOWING CONTROL CARDS..      *
*    AT SCOPE 3.4              AT NOS 1                      *
*     .                         .                            *
*   ATTACH(STARBUL)            ATTACH(STARBUL/UN=LIBRARY)    *
*   REWIND(STARBUL)            REWIND(STARBUL)               *
*   COPYCF(STARBUL,A)          COPYCF(STARBUL,A)             *
*   REWIND(A)                  REWIND(A)                     *
*   COPYSBF(A,OUTPUT)          COPYSBF(A,OUTPUT)             *
*     .                         .                            *
**************************************************************


**********************************************************
* NOTICE - THE NEW STARDYNE USERS MANUAL IS AVAILABLE.   *
*          THE VERSION DATE IS SEPT 1979                  *
*          PLEASE CONTACT YOUR SALES REPRESENTATIVE ..    *
**********************************************************
```

Table C.3 (cont.)

```
                              *****  INPUT DATA CARDS  *****
          /--------------------------- CARD  COLUMN ------------------------------/
          1    7    12   17   22   27   32   37   42   47   52   57   62   67   72       80
          *    *    *    *    *    *    *    *    *    *    *    *    *    *    *        *
CARD NO.  ****************************************************************************
   1  START                           1         0    20.       300.
   2             3600      0                              0
   3  END
   4  MODES                           1
   5              4        5  .170
   6              6        6  .122
   7              7        7  .102
   8              8        8  .079
   9              9        9  .065
  10             10       10  .050
  11             11       11  .042
  12             12       12  .032
  13             13       13  .025
  14             14       14  .023
  15             15       15  .022
  16             16       16  .021
  17             17       17  .019
  18             18       18  .017
  19             19       21  .016
  20             22       23  .014
  21             24       27  .013
  22             26       29  .012
  23             30       31  .011
  24             32       33  .010
  25  END
  26  PLOT                 3              6
  27                      20          1   6    20        3        6
  28                      30          1   6    30        3        6
  29                      40          1   6    40        3        6
  30                     313          3   6   313        3        6
  31  END
  32  XTRA
  33                 20.0      22.5      25.0      27.5      30.0      32.5
  34                 35.0      37.5      40.0      42.5      45.0      47.5
  35                 50.0      52.5      55.0      57.5      60.0      62.5
  36                 65.       67.5      70.       72.5      75.       77.5
  37                 80.       82.5      85.       87.5      90.       92.5
  38                 95.       97.5     100.      102.5     105.      107.5
  39                110.      112.5     115.      117.5     120.      122.5
  40                125.      127.5     130.      132.5     135.      137.5
  41                140.      142.5     145.      147.5     150.      152.5
  42                155.      157.5     160.      162.5     165.      167.5
  43                170.      172.5     175.      177.5     180.      182.5
  44                185.      187.5     190.      192.5     195.      197.5
  45                200.      202.5     205.      207.5     210.      212.5
  46                215.      217.5     220.      222.5     225.      227.5
  47                230.      232.5     235.      237.5     240.      242.5
  48                245.      247.5     250.      252.5     255.      257.5
  49                260.      262.5     265.      267.5     270.      272.5
  50                275.      277.5     280.      282.5     285.      287.5
  51                290.      292.5     295.      297.5     300.
  52  END
```

Table C.3 (cont.)

```
                                          ***** INPUT DATA CARDS *****
          /-------------------------------- CARD IMAGE --------------------------------/
          1    7     12    17    22    27    32    37    42    47    52    57    62    67    72     80
          *    *     *     *     *     *     *     *     *     *     *     *     *     *     *      *
CARD NO   ************************************************************************************
     53   FORCE                                  1.000       1.000
     54   DRIVER                 1                       4
     55                          20          1           20          3           30          4
     56                          30          3           40          1           40          3
     57   END
     58   ALL DONE

                    (END OF INPUT FOR MODEL NO.   1)
```

Table C.3 (cont.)

```
         JOINT        LOCAL
          NO.        D.O.F. NO.
           20            1
           20            3
           30            1
           30            3
           40            1
           40            3

XXXXXXXXXXXXXXXXXXXXXXEND

XXXXX MEM. OF XXXXXXXX(ALL DONE                                                     $XXXXXXXXX



****************************************************************************************************
****************************************************************************************************



          INITIAL HULL DYNAMIC MODEL NO.2

 MAX NODE NO. =  1220, NO. NODES =   215, DOF PER NODE =  6, NO. OF DOF =  1314, G =  .38640E+03

   1 TAPE5 = (E2709/2022.47.50AJ0061EC )

TAPE4 HEADER=(ELEDOADS 1220     6    33     1     0 0 1 0 0 0 0 0 0 0 0 0 0 0 0 0)

                                33 MODES (EIGENVECTORS) HAVE BEEN SELECTED.
 MODE         NATURAL FREQUENCY               GENERALIZED WEIGHT               DAMPING
  NO.            (CPS)         (RAD/SEC)         (WEIGHT)             (MASS)    COEFFICIENT

    1      .424491E+02    .266716E+03    .103257E+04    .402497E+01    .170000E+00
    2      .550794E+02    .346070E+03    .243755E+03    .700216E+00    .170000E+00
    3      .669401E+02    .420597E+03    .191530E+03    .495654E+00    .122000E+00
    4      .723296E+02    .454461E+03    .715651E+03    .185209E+01    .102000E+00
    5      .866346E+02    .543572E+03    .909543E+02    .235386E+00    .700000E-01
    6      .897324E+02    .563823E+03    .138379E+03    .358127E+00    .650000E-01
    7      .103062E+03    .647555E+03    .173820E+04    .449844E+01    .500000E-01
    8      .113668E+03    .714199E+03    .987574E+03    .255583E+01    .420000E-01
    9      .134902E+03    .847617E+03    .179534E+03    .464634E+00    .320000E-01
   10      .161384E+03    .101400E+04    .504794E+03    .130640E+01    .250000E-01
   11      .165356E+03    .103896E+04    .703504E+03    .182066E+01    .250000E-01
   12      .171300E+03    .107632E+04    .305418E+03    .790419E+00    .220000E-01
   13      .174265E+03    .109494E+04    .318101E+03    .823243E+00    .210000E-01
   14      .186460E+03    .117156E+04    .175100E+03    .453158E+00    .190000E-01
   15      .199607E+03    .125343E+04    .275692E+03    .713490E+00    .170000E-01
   16      .208634E+03    .131089E+04    .155504E+03    .402442E+00    .160000E-01
   17      .213337E+03    .134044E+04    .465470E+03    .120463E+01    .160000E-01
   18      .216880E+03    .136270E+04    .101962E+03    .263877E+00    .160000E-01
   19      .230969E+03    .145122E+04    .221377E+03    .572922E+00    .140000E-01
   20      .234895E+03    .147589E+04    .379777E+03    .982860E+00    .140000E-01
   21      .244219E+03    .153447E+04    [illegible]    [illegible]    .130000E-01
   22      .251619E+03    .158097E+04    .400537E+03    .103659E+01    .130000E-01
   23      .257375E+03    .161713E+04    .410556E+03    .106252E+01    .130000E-01
   24      .259451E+03    .163018E+04    .312770E+03    .809447E+00    .130000E-01
   25      .265408E+03    [illegible]    [illegible]    [illegible]    .120000E-01
   26      .278046E+03    [illegible]    [illegible]    [illegible]    .120000E-01
   27      [illegible]    [illegible]    [illegible]    [illegible]    .110000E-01
   28      [illegible]    [illegible]    [illegible]    [illegible]    [illegible]
   29      [illegible]    [illegible]    [illegible]    [illegible]    [illegible]
   30      [illegible]    [illegible]    [illegible]    [illegible]    [illegible]
```

Table C.4 DYNRE2 Output Data

```
FREQUENCY RESPONSE HISTORY, JOINT     , DIRECTION   1

ACCELERATION TRANSFER FUNCTIONS.

    FREQUENCY (HZ)   PHASE ANGLE    ACCELERATION   ACCEL. IN G S        FREQUENCY (HZ)   PHASE ANGLE    ACCELERATION   ACCEL. IN G S

 1   .200000E+02    .180000E+03    .246443E-02    .63779E-05      51   .145000E+03    .180000E+03    .258569E+00    .66918E-03
 2   .225000E+02    .180000E+03    .317120E-02    .82070E-05      52   .147500E+03    .180000E+03    .307295E+00    .79528E-03
 3   .250000E+02    .180000E+03    .399235E-02    .10332E-04      53   .150000E+03    .180000E+03    .372250E+00    .96338E-03
 4   .275000E+02    .180000E+03    .494150E-02    .12789E-04      54   .152500E+03    .180000E+03    .463437E+00    .11994E-02
 5   .300000E+02    .180000E+03    .603530E-02    .15619E-04      55   .155000E+03    .180000E+03    .599077E+00    .15504E-02
 6   .325000E+02    .180000E+03    .726243E-02    .18795E-04      56   .157500E+03    .180000E+03    .806724E+00    .20878E-02
 7   .350000E+02    .180000E+03    .866270E-02    .22419E-04      57   .160000E+03    .180000E+03    .105795E+01    .27380E-02
 8   .375000E+02    .180000E+03    .100567E-01    .26027E-04      58   .162500E+03    .180000E+03    .106061E+01    .27449E-02
 9   .400000E+02    .180000E+03    .111542E-01    .28867E-04      59   .165000E+03    .180000E+03    .866094E+00    .22414E-02
10   .425000E+02    .180000E+03    .116515E-01    .30154E-04      60   .167500E+03    .180000E+03    .673797E+00    .17438E-02
11   .450000E+02    .180000E+03    .118906E-01    .30773E-04      61   .170000E+03    .180000E+03    .517285E+00    .13387E-02
12   .475000E+02    .180000E+03    .125582E-01    .32500E-04      62   .172500E+03    .180000E+03    .449866E+00    .11642E-02
13   .500000E+02    .180000E+03    .137880E-01    .35683E-04      63   .175000E+03    .180000E+03    .412030E+00    .10663E-02
14   .525000E+02    .180000E+03    .153400E-01    .39700E-04      64   .177500E+03    .180000E+03    .334487E+00    .86565E-03
15   .550000E+02    .180000E+03    .170578E-01    .44145E-04      65   .180000E+03    .180000E+03    .254561E+00    .65880E-03
16   .575000E+02    .180000E+03    .190275E-01    .49243E-04      66   .182500E+03    .180000E+03    .206545E+00    .53454E-03
17   .600000E+02    .180000E+03    .214243E-01    .55446E-04      67   .185000E+03    .180000E+03    .197582E+00    .51134E-03
18   .625000E+02    .180000E+03    .242941E-01    .62873E-04      68   .187500E+03    .180000E+03    .206416E+00    .53420E-03
19   .650000E+02    .180000E+03    .274717E-01    .71097E-04      69   .190000E+03    .180000E+03    .167376E+00    .43317E-03
20   .675000E+02    .180000E+03    .304397E-01    .78777E-04      70   .192500E+03    .180000E+03    .166648E+00    .43128E-03
21   .700000E+02    .180000E+03    .320530E-01    .82953E-04      71   .195000E+03    .180000E+03    .262206E+00    .67857E-03
22   .725000E+02    .180000E+03    .310717E-01    .80413E-04      72   .197500E+03    .180000E+03    .467378E+00    .12096E-02
23   .750000E+02    .180000E+03    .284450E-01    .73615E-04      73   .200000E+03    .180000E+03    .663814E+00    .17179E-02
24   .775000E+02    .180000E+03    .268036E-01    .69367E-04      74   .202500E+03    .180000E+03    .580013E+00    .15011E-02
25   .800000E+02    .180000E+03    .274540E-01    .71051E-04      75   .205000E+03    .180000E+03    .433881E+00    .11229E-02
26   .825000E+02    .180000E+03    .299251E-01    .77446E-04      76   .207500E+03    .180000E+03    .346904E+00    .89779E-03
27   .850000E+02    .180000E+03    .333406E-01    .86285E-04      77   .210000E+03    .180000E+03    .313224E+00    .81062E-03
28   .875000E+02    .180000E+03    .369823E-01    .95710E-04      78   .212500E+03    .180000E+03    .329210E+00    .85199E-03
29   .900000E+02    .180000E+03    .406056E-01    .10509E-03      79   .215000E+03    .180000E+03    .365367E+00    .94557E-03
30   .925000E+02    .180000E+03    .448740E-01    .11613E-03      80   .217500E+03    .180000E+03    .372796E+00    .96479E-03
31   .950000E+02    .180000E+03    .503576E-01    .13033E-03      81   .220000E+03    .180000E+03    .335465E+00    .86818E-03
32   .975000E+02    .180000E+03    .566357E-01    .14657E-03      82   .222500E+03    .180000E+03    .284299E+00    .73576E-03
33   .100000E+03    .180000E+03    .645028E-01    .16693E-03      83   .225000E+03    .180000E+03    .241020E+00    .62376E-03
34   .102500E+03    .180000E+03    .735953E-01    .19046E-03      84   .227500E+03    .180000E+03    .201194E+00    .52068E-03
35   .105000E+03    .180000E+03    .845793E-01    .21889E-03      85   .230000E+03    .180000E+03    .172205E+00    .44567E-03
36   .107500E+03    .180000E+03    .975614E-01    .25249E-03      86   .232500E+03    .180000E+03    .149804E+00    .38769E-03
37   .110000E+03    .180000E+03    .111649E+00    .28895E-03      87   .235000E+03    .180000E+03    .149245E+00    .38624E-03
38   .112500E+03    .180000E+03    .115913E+00    .29998E-03      88   .237500E+03    .180000E+03    .131755E+00    .34098E-03
39   .115000E+03    .180000E+03    .962230E-01    .24902E-03      89   .240000E+03    .180000E+03    .107501E+00    .27821E-03
40   .117500E+03    .180000E+03    .729001E-01    .18866E-03      90   .242500E+03    .180000E+03    .122837E+00    .31790E-03
41   .120000E+03    .180000E+03    .675056E-01    .17490E-03      91   .245000E+03    .180000E+03    .164064E+00    .42461E-03
42   .122500E+03    .180000E+03    .749906E-01    .19407E-03      92   .247500E+03    .180000E+03    .229024E+00    .59271E-03
43   .125000E+03    .180000E+03    .872690E-01    .22585E-03      93   .250000E+03    .180000E+03    .391727E+00    .10138E-02
44   .127500E+03    .180000E+03    .101679E+00    .26314E-03      94   .252500E+03    .180000E+03    .486400E+00    .12588E-02
45   .130000E+03    .180000E+03    .117601E+00    .30435E-03      95   .255000E+03    .180000E+03    .414732E+00    .10733E-02
46   .132500E+03    .180000E+03    .134168E+00    .34723E-03      96   .257500E+03    .180000E+03    .484688E+00    .12544E-02
47   .135000E+03    .180000E+03    .149099E+00    .38587E-03      97   .260000E+03    .180000E+03    .647897E+00    .16768E-02
48   .137500E+03    .180000E+03    .165943E+00    .42946E-03      98   .262500E+03    .180000E+03    .593489E+00    .15359E-02
49   .140000E+03    .180000E+03    .189915E+00    .49150E-03      99   .265000E+03    .180000E+03    .494625E+00    .12801E-02
50   .142500E+03    .180000E+03    .220475E+00    .57059E-03     100   .267500E+03    .180000E+03    .422709E+00    .10940E-02
```

*U.S. GOVERNMENT PRINTING OFFICE: 1981-0-720-037/5637